

PREPARATION, CHARACTERIZATION AND PERFORMANCE STUDIES OF POLYETHERIMIDE BASED MEMBRANES FOR WATER PURIFICATION

Thesis

Submitted in partial fulfillment of the requirements for the degree of
DOCTOR OF PHILOSOPHY

by

RAGHAVENDRA SEETHARAMA HEBBAR



**DEPARTMENT OF CHEMISTRY
NATIONAL INSTITUTE OF TECHNOLOGY KARNATAKA,
SURATHKAL, MANGALORE – 575025**

September, 2017

DECLARATION

I hereby *declare* that the thesis entitled “**Preparation, characterization and performance studies of polyetherimide based membranes for water purification**” which is being submitted to the National Institute of Technology Karnataka, Surathkal in partial fulfillment of the requirements for award of the Degree of *Doctor of Philosophy* is a *bonafide report of the research work carried out by me*. The material contained in this thesis has not been submitted to any University or Institution for the award of any degree.

Reg. No. 135062CY13F03,
Raghavendra Seetharama Hebbar
Department of Chemistry

Place: NITK, Surathkal

Date:

CERTIFICATE

This is to *certify* that the thesis entitled “**Preparation, characterization and performance studies of polyetherimide based membranes for water purification**” submitted by **Raghavendra Seetharama Hebbar (Register No. 135062CY13F03)** as the record of the research work carried out by him is accepted as the *Research Thesis* submission in partial fulfillment of the requirements for the award of degree of **Doctor of Philosophy**.

Dr. Arun M. Isloor
Research Guide

Chairman- DRPC

ACKNOWLEDGEMENTS

I would like to express my deep sense of gratitude to my research supervisor, Dr. Arun M. Isloor, Associate Professor, Department of Chemistry, NITK, Surathkal, for giving me an opportunity to pursue my research work under his guidance. Without his direction and persistence, this thesis would not have been possible.

I acknowledge my thanks to NITK, Surathkal for providing the institute fellowship and financial support necessary for the completion of my doctoral work.

My sincere gratitude is due to my RPAC members, Prof M. B Saidutta of Chemical Engineering and Prof D. Krishna Bhat, Head, Department of chemistry, for their timely assessment and evaluation of my research progress. Their valuable inputs at various stages of my work have contributed immensely in giving the final shape to my research work.

I thank the present Head of the Department, Prof D. Krishna Bhat and former Heads of the Department, Prof. B. Ramachandra Bhat and Prof. A. Chitharanjan Hegde for providing moral support throughout my work. I am also thankful to Prof. A. V. Adhikari, Prof. A. Nithyananda Shetty, Dr. D. Udayakumar, Dr. Darshak R. Trivedi and Dr. Sib Sankar Mal, Dr. Bineesh, Dr. Saikant Dutta and Dr. Debashree Chakraborty for their encouragement and support.

I would like to convey my grateful appreciation to Prof. K. Narayan Prabhu, Prof. Udupa and Prof. Udaya Bhat (Department of Metallurgical and Materials Engineering, NITK) for allowing me to avail the instrumentation facility whenever required. I am very thankful to Dr. K. Ananda Poornaprajna Institute of Scientific Research, Bangalore for anti-biofouling analysis of the membranes. A special thanks to Prof. A. F. Ismail, Advanced Membrane Technology Research Center (AMTEC), Universiti Teknologi Malaysia, Malaysia for permitting me to carry out a part of my research work in his laboratory.

I, truly appreciate the support extended by my research group at NITK, including Dr. Rajesh, Dr. Garudachari, Dr. Ganesh, Dr. Seema, Dr. Rashmi, Dr. Harikrishna, Ms. Irfana, Mr. Chandrashekar Nayak and Mr. G P Syed Ibrahim. I am greatly thankful to all my friends at NITK, for making my stay during research days a fun filled and cherishable one.

I am grateful to the non-teaching staff, Mrs. Shamila Nandini, Mrs. Deepa, Mrs. Sharmila, Mr. Pradeep, Mr. Prashanth, Mr. Harish, and Mr. Santosh for their timely co-operation with laboratory and analysis work.

I am highly indebted to my parents, my beloved sister and brother in law for their everlasting faith in me which has been the backbone of my hard work and patience. Finally, I extend my gratitude to all those who have contributed directly or indirectly towards the completion of this work.

Thank you.

Raghavendra Seetarama Hebbar

ABSTRACT

Membrane based separation has sustained its efficiency over other traditional techniques of water purification. Significant research has been carried out in this area, still the abundant scope of membrane technology has driven many scientists to further explore the field. The current research work is one such attempt to study the influence of organic and inorganic nanomaterials in the polymeric membranes.

This research work is focused on modification of polyetherimide membrane by the addition of organic and inorganic additives to improve the physiochemical properties and its performance. The various additives employed in this work includes citric acid, ascorbic acid, activated bentonite, poly (4-styrenesulfonate) modified bentonite, polydopamine coated HNTs, amine functionalized HNTs, poly(m-aminophenol) coated HNTs and carboxylated Fe₂O₃ nanoparticles. The properties and performance of the membranes was analyzed by cross sectional morphology, surface hydrophilicity, water uptake capacity, porosity, surface topography studies, permeation properties and antifouling ability. The self-cleaning ability of the membranes was determined by evaluating the flux recovery ratio. The water purification ability of the membranes was assessed in terms of hazardous heavy metal ion rejection, humic acid removal and dye removal applications.

The PEI membrane with 4 wt. % activated bentonite dosage showed maximum rejection of 69.3 %, 76.2 % and 82.5 % for 250 ppm of Cd (II), Ni (II) and Cu (II) ion solutions respectively. The 3 wt. % polydopamine modified HNTs in the membrane showed resistance to microbial growth with FRR of 74.5 % and reversible fouling ratio of 60.7 %. The membrane comprising of bentonite clay bearing the poly (4-styrenesulfonate) brushes showed 80.5 % (Pb²⁺) and 74.6 % (Cd²⁺) respectively, during PEUF. The hollow fiber membrane with 2 wt. % of poly (m-aminophenol) coated HNTs exhibited the water flux of 104.9 Lm⁻¹h⁻¹ and only 9.6 % of irreversible fouling with more than 90.3 % of flux recovery. These membranes also showed rejection of 97 % and 94 % for the hazardous reactive red 102 and reactive black 5 dyes respectively.

Keywords: *membrane, hydraulic permeation, nanocomposites, heavy metal ion and hollow fiber.*

CONTENTS

CHAPTER 1

1.1 GLOBAL SCENARIO	01
1.2 KEY DEVELOPMENTS OF MEMBRANE TECHNOLOGY	02
1.3 MEMBRANE DEFINITION AND CLASSIFICATION	03
1.3.1 Pressure driven membranes	04
1.4 FUNDAMENTAL ASPECTS OF MEMBRANES AND MEMBRANE PROCESSES	05
1.4.1 Membrane transport mechanism	05
1.4.2 Factors affecting the performance	06
1.4.3 Advantages of membrane processes	07
1.4.4 Membrane fouling and prevention	08
1.5 MEMBRANE MATERIALS	09
1.5.1 Polyetherimide as membrane material	12
1.6 MEMBRANE PREPARATION	13
1.7 BASIC TERMINOLOGIES USED IN MEMBRANE TECHNOLOGY	16
1.8 APPLICATIONS OF MEMBRANE TECHNOLOGY	18
1.9 LITERATURE SURVEY	20
1.10 SCOPE OF THE WORK	26
1.11 OBJECTIVES	27

CHAPTER 2

PREPARATION AND CHARACTERIZATION OF POLYETHERIMIDE/HYDROLYZED PIAM BLEND NANOFILTRATION MEMBRANE FOR ANTIFOULING AND SALT REJECTION APPLICATION	
2.1 EXPERIMENTAL PART	32
2.1.1 Materials	32
2.1.2 Preparation of blend Membranes	33
2.2 MEMBRANE CHARACTERIZATION	33
2.2.1 FTIR analysis	33
2.2.2 Ion exchange capacity	33
2.2.3 Membrane morphology	33

2.2.4 Water uptake and contact angle measurement	33
2.2.5 Permeation properties	34
2.2.6 Porosity of the membrane	34
2.2.7 Antifouling properties	35
2.2.8 Salt rejection studies	35
2.3. RESULTS AND DISCUSSIONS	35
2.3.1 FTIR analysis	35
2.3.2 Ion exchange Capacity	36
2.3.3 Water swelling and contact angle measurement	37
2.3.4 Morphology of the membrane	37
2.3.5 Permeation and antifouling properties	38
2.3.6 Salt rejection study	40
2.4 CONCLUSIONS	42

CHAPTER 3

MORPHOLOGY AND ANTIORGANIC FOULING BEHAVIOUR OF THE POLYETHERIMIDE MEMBRANE MODIFIED WITH HYDROPHILIC ORGANIC ACIDS AS ADDITIVES

3.1 MATERIALS AND METHODS	45
3.1.1 Materials	45
3.1.2 Preparation of Membranes	45
3.2 MEMBRANE CHARACTERIZATION	46
3.2.1 AFM analysis	46
3.2.2 Viscosity measurement	46
3.2.3 Antifouling properties	46
3.2.4 Humic acid rejection study	47
3.3 RESULTS AND DISCUSSIONS	47
3.3.1 ATR-IR spectroscopy	47
3.3.2 Water uptake and contact angle	48
3.3.3 Rheological properties of the casting solutions	49
3.3.4 Effect of additive on morphology of the membrane	49
3.3.5 AFM analyses of membrane	51

3.3.6 Water permeability	53
3.3.7 Antifouling performance against BSA	54
3.3.8 Antifouling performances against HA	56
3.4 CONCLUSIONS	57

CHAPTER 4

PREPARATION AND EVALUATION OF HEAVY METAL REJECTION PROPERTIES OF POLYETHERIMIDE/POROUS ACTIVATED BENTONITE CLAY NANOCOMPOSITE MEMBRANE

4.1 EXPERIMENTAL PART	63
4.1.1 Materials	63
4.1.2 Activation of bentonite clay	63
4.1.3 Preparation of composite membrane	63
4.2 CHARACTERIZATION AND PERFORMANCE STUDY	64
4.3 RESULTS AND DISCUSSION	65
4.3.1 Chemical composition of bentonite clay	65
4.3.2 Porosity and contact angle	65
4.3.3 Morphology of the membranes	66
4.3.4 Pure water flux	68
4.3.5 Hydraulic resistance of membranes	69
4.3.6 Heavy metal ion rejection study	69
4.4 CONCLUSIONS	72

CHAPTER 5

FUNCTIONALIZATION OF POLYETHERIMIDE MEMBRANE WITH BENTONITE CLAY GRAFTED WITH POLY (4-STYRENESULFONATE) BRUSHES AS EFFECTIVE REMOVAL OF HAZARDOUS HUMIC ACID AND HEAVY METAL IONS

5.1 MATERIALS AND METHODS	76
5.1.1 Materials	76
5.1.2 Grafting of sodium4-styrenesulfonate brushes onto bentonite clay	76
5.1.3 Preparation of Membranes	77
5.3 RESULTS AND DISCUSSIONS	78

5.3.1 FTIR analysis	78
5.3.2 Contact angle measurement	81
5.3.3 Water uptake capacity	82
5.3.4 Porosity of the membrane	83
5.3.5 Membrane morphology	83
5.3.6 Permeation properties	85
5.3.7 Antifouling properties	86
5.3.8 Humic acid rejection properties	88
5.3.9 Heavy metal ion rejection	90
5.4 CONCLUSIONS	91

CHAPTER 6

FABRICATION OF POLYDOPAMINE FUNCTIONALIZED HALLOYSITE NANOTUBE/POLYETHERIMIDE MEMBRANES FOR HEAVY METAL REMOVAL

6.1 MATERIALS AND METHODS	97
6.1.1. Materials	97
6.1.2 Preparation of Modified HNTs	97
6.1.3. Preparation of composite membrane	98
6.2 CHARACTERIZATION AND PERFORMANCE STUDY	98
6.3 RESULTS AND DISCUSSIONS	99
6.3.1 TEM analysis	99
5.3.2 FTIR analysis	100
6.3.3 Hydrophilicity of membranes	101
6.3.4 Porosity of the membrane	102
6.3.5 Morphological study	102
6.3.6 Permeation properties	103
6.3.7 Membrane hydraulic resistance	104
6.3.8 Antifouling performance of the membrane	105
6.3.9 Heavy metal ion rejection study	106
6.3.10 Antimicrobial activity of membranes	107
6.4 CONCLUSION	108

CHAPTER-7

FABRICATION OF POLYETHERIMIDE NANOCOMPOSITE MEMBRANE WITH AMINE FUNCTIONALISED HALLOYSITE NANOTUBES FOR EFFECTIVE REMOVAL OF CATIONIC DYE EFFLUENTS

7.1 MATERIALS AND METHODS	112
7.1.1 Materials	112
7.1.2 Preparation of modified HNTs	112
7.1.3 Membrane preparation	112
7.2 CHARACTERIZATION OF MHNTs AND MEMBRANE	113
7.2.1 Dye Removal Studies	113
7.3 RESULTS AND DISCUSSIONS	114
7.3.1 Characterization of MHNTs	114
7.3.2 Porosity and Contact angle of membrane	115
7.3.3 Zeta potential measurement	116
7.3.4 Membrane morphology	117
7.3.5 Permeation properties	120
7.3.6 Dye removal studies	120
7.3.6.1 Effect of pH of dye solution	121
7.3.6.2 Effect of contact time	122
7.3.6.3 Adsorption Isotherms	123
7.4 CONCLUSIONS	125

CHAPTER 8

EFFICIENT TREATMENT OF HAZARDOUS REACTIVE DYE EFFLUENTS THROUGH ANTIFOULING POLYETHERIMIDE HOLLOW FIBER MEMBRANE EMBEDDED WITH FUNCTIONALISZD HALLOYSITE NANOTUBES

8.1 MATERIALS AND METHODS	131
8.1.1. Materials	131
8.1.2 Modification of HNTs	131
8.1.3 Preparation of hollow fiber (H.F) membranes	132
8.2 CHARACTERIZATION AND PERFORMANCE STUDY	133
8.2.1 Zeta Potential analysis	134

8.2.2 Permeation analysis	134
8.2.3 Reactive dye rejection study	134
8.3 RESULTS AND DISCUSSIONS	135
8.3.1 FTIR analysis	135
8.3.2 TEM analysis	136
8.3.3 Contact angle and surface energy analysis	136
8.3.4 Zeta potential analysis	137
8.3.4 Porosity and water content	138
8.3.5 Membrane morphology	138
8.3.6 Permeation properties	140
8.3.7 Antifouling properties of the membranes	140
8.3.8 Reactive dye rejection.	142
8.3.8.1 Effect of pressure	143
8.3.8.2 Effect of operating time	143
8.4. CONCLUSIONS	144

CHAPTER 9

PREPARATION AND CHARACTERIZATION OF FUNCTIONALIZED IRON OXIDE NANOPARTICLES INCORPORATED POLYETHERIMIDE HOLLOW FIBER MEMBRANE FOR HUMIC ACID REJECTION APPLICATION

9.1. MATERIALS AND METHODS	148
9.1.1 Materials	148
9.1.2 Modification of iron oxide nanoparticles	148
9.1.3 Preparation of hollow fiber membrane	149
9.2 CHARACTERIZATION OF NANOCOMPOSITE HOLLOW FIBER MEMBRANE	150
9.2.1 Membrane characterization	150
9.3. RESULT AND DISCUSSIONS	151
9.3.1 Characterization of iron oxide nanoparticles	151
9.3.2 Membrane morphology and properties	153
9.3.3 Zeta potential analysis	156
9.3.4 Permeations and antifouling study	156

9.3.5 Anti-biofouling properties of membrane	157
9.3.6 Humic acid removal study	158
9.3.6.1 Relative flux rate	159
9.3.6.5 Effect of feed solution pH	160
9.3.6.3 Effect of ionic strength	160
9.4. CONCLUSIONS	161
CHAPTER 10	
SUMMARY AND CONCLUSIONS	
10.1 SUMMARY OF THE WORK	163
10.2 CONCLUSIONS	167
LIST OF PUBLICATIONS AND CONFERENCES ATTENDED	169
REFERENCES	173
BIODATA	

List of figures

Fig.1.1 Graphical representation of distribution of water on earth	01
Fig.1.2 Schematic representation of membrane separation process	04
Fig.1.3 Classification of the membranes based on average pore size	05
Fig.1.4 Molecular transport mechanisms through membranes	06
Fig.1.5 Schematic representation of fouling on membrane surface	08
Fig.1.6 Structures of some commonly used polymers in membrane preparation	10
Fig.1.7 Chemical structure of polyetherimide (PEI) polymer	12
Fig.1.8 Schematic representation of membrane preparation by phase inversion method.	14
Fig.1.9 Schematic representation of a film/bath interface in the coagulation bath.	15
Fig.1.10 Schematic representation of the lab scale filtration set up	17
Fig.1.11 Comparison of A) Ideal pore structure and B) Real pore structure in asymmetric membranes	18
Fig.1.12 Cross-section of PEI hollow fiber membranes from different dope (AA) solutions	21
Fig.1.13 Structure of PEI indicating possible positions for sulfonic acid groups to occupy upon sulfonation	22
Fig.1.14 Influence PEG on cross-section structure of the PEI membranes	23
Fig.1.15 Schematic representation of the physical interaction between polyacrylonitrile and carboxylated polyetherimide in PAN/CPEI blend membranes	25
Fig.1.16 Variation in hydrophilicity of hybrid PEI membrane	25
Fig.1.17 Variation in contact angle with different additive dosage	26
Fig.2.1 Permeation behaviour of blend membranes during the different filtration conditions	30
Fig.2.2 Permeability and BSA protein rejection of blend membrane	31
Fig.2.3 Percentage salt rejection of a) before hydrolysis of PIAM and b) after hydrolysis of PIAM	32
Fig.2.4 Schematic representation of hydrolysis of PIAM	33
Fig. 2.5 FTIR spectra of (a) before hydrolysis of PIAM and (b) after hydrolysis of PIAM	36
Fig. 2.6 Schematic representation of contact angles of (a) PM-1, (b) PM-2, (c) PM-3 and (d) PM-4	37

Fig.2.7 Cross sectional SEM images of (a) PM-1, (b) PM-2, (c) PM-3, (d) PM-4 membranes and (f) surface image of PM4 membrane	38
Fig.2.8 Pure water flux of membranes at 4 bar pressure	39
Fig.2.9 Time dependent flux of PEI/ hydrolyzed PIAM membranes at 4 bar TMP during three different conditions	40
Fig. 2.10 Electrolyte rejection study of membranes at 0.4MPa pressure	41
Fig. 2.11 Pressure dependent electrolyte rejection of PM-4 membrane	41
Fig 3.1. Effects of FM concentration on the viscosity of the casting solution	43
Fig.3.2 Effect of acrylic acid and HEMA in the casting solution on flux stability of membranes during milk filtration at long time	44
Fig 3.3 FT-IR spectra of prepared membranes	48
Fig.3.4 Cross sectional and magnified cross sectional SEM images of a, A) PMA-0, b, B) PMA-1, c, C) PMA-2 and d, D) PMA-3 membrane	50
Fig.3.5 Two and three dimensional AFM surface images of a, A) PMA-0, b, B) PMA-1, c, C) PMA-2 and d, D) PMA-3 membrane	52
Fig.3.6 Pure water flux of the membranes with 0.2MPa pressure	53
Fig.3.7 Flux variation of membranes during three different filtration conditions	54
Fig.3.8 Contact angle and FRR of the prepared membranes	54
Fig.3.9 Flux ratio during the humic acid solution filtration	56
Fig.3.10 Humic acid rejection by prepared membranes	56
Fig.3.11 Photographic image of (a) feed humic acid solution and b,c and d are the permeate of PMA-1, PMA-2 and PMA-3 membranes	56
Fig.4.1 Diagrammatic sketch of the structure of bentonite clay	60
Fig.4.2 Immobilization of bentonite into membrane matrix	61
Fig.4.3 Effect of bentonite additive dosage on water flux of polysulfone nanocomposite membrane	62
4.4 Schematic representation of β -cyclodextrin modification of bentonite	62
Fig.4.5 EDX analysis of bentonite clay a) before acid activation b) after acid activation	65
Fig.4.6 Aluminium and silicon mapping of PBM-4 membrane	67
Fig.4.7 Cross sectional SEM images of a) PBM-0, b) PBM-1, c) PBM-2, d) PBM-3, e) PBM-4, and f) Magnified cross sectional image of PBM-4 membrane	67

Fig.4.8 Time dependent pure water fluxes of membranes at 0.3 MPa TMP	68
Fig.4.9 Pressure dependent pure water fluxes of membranes	69
Fig.4.10 Variation of nickel rejection with different initial feed concentration (pH= 4±0.5)	70
Fig.4.11 Variation of cadmium rejection with different initial feed concentration (pH= 4±0.5)	70
Fig.4.12 Variation of copper rejection with different initial feed concentration (pH= 4±0.5)	71
Fig.4.13 Elemental mapping of a) cadmium b) nickel c) copper after rejection study of PBM-4 and virgin membranes	72
Fig.4.14 Rejection of heavy metal ions at different pH values for PBM-4 membrane	73
Fig.5.1 Comparison of sorption of (a) Cu (II) and (b) 2,4-dichlorophenol individually and simultaneously onto humic acid modified bentonite.	74
Fig.5.2 Poly (vinylidene fluoride) (PVDF) membranes with covalently immobilized hyperbranched polymers	75
Fig.5.3 Schematic representation of preparation of HNTs-poly (NASS)	75
Fig.5.4 Synthetic route for the modified bentonite	77
Fig.5.5 FT-IR spectrum of a) bentonite b) modified bentonite	79
Fig 5.6 EDX analysis of a) bentonite and b) modified bentonite	80
Fig.5.7 TGA analysis of a) bentonite and b) modified bentonite	80
Fig.5.8 TEM and FESEM images of bentonite	81
Fig.5.9 XRD analysis of a) bentonite and b) modified bentonite	81
Fig.5.10 Contact angle and surface energy of the membranes	82
Fig.5.11 Time dependent contact angle of the membranes	82
Fig.5.12 Cross sectional SEM images of the a) PEM-0, b) PEM-1, c) PEM-2 and d) PEM-3 membranes.	84
Fig.5.13 Elemental mapping of a) silicon and b) aluminium of PEM-3 membrane	84
Fig.5.14 Three dimensional AFM images of a) PEM-0, b) PEM-1, c) PEM-2 and d) PEM-3 membranes.	85
Fig.5.15 Time dependent pure water of the membranes.	86
Fig.5.16 Pure water fluxes of the membranes after BSA protein solution filtration	87

Fig.5.17 Flux recovery ratio and flux of prepared membranes	87
Fig.5.18 Fouling resistance behaviour of prepared membranes	88
Fig.5.19 Photographic image of a) HA solution in the feed, b), c) and d) are permeate of PEM-1, PEM-2 and PEM-3 membranes respectively	89
Fig.5.20 Relative flux ratio during HA filtration	89
Fig.5.21 Humic rejected by the membranes at 0.3MPa TMP	89
Fig.5.22 Heavy metal ion rejected by the PEM-3 membrane	90
Fig.5.23 Elemental mapping of PEM-3 membrane after the heavy metal ion filtration	91
Fig 6.1 Chemical structure of halloysite nanotube	93
Fig.6.2 Schematic representation of preparation silver doped HNTs	94
Fig.6.3 Schematic representation of preparation of dextran grafted HNTs	94
Fig.6.4 Preparation process of HNTs-MPC via reverse atom transfer radical polymerization	95
Fig.6.5 Schematic representation of preparation of sulfonated HNTs	95
Fig.6.6 Rejection behavior of NF membrane with different electrolyte solutions	96
Fig.6.7 Schematic representation of polymerization of dopamine	98
Fig.6.8 TEM images of a) HNTs and b) MHNTs	100
Fig.6.9 FTIR spectrum of the HNTs and MHNTs	100
Fig.6.10 Contact angle and water uptake capacity of the membranes	101
Fig.6.11 Digital photography of the top surface of a) HMM-0 b) HMM-1 c) HMM-2 and d) HMM-3 membranes	101
Fig.6.12 Cross sectional SEM images of the a) HMM-0, A) magnified HMM-0, b) HMM-1, c) HMM-2, d) HMM-3 and D) magnified HMM-3	103
Fig.6.13 Elemental mapping of silicon and aluminium on HMM-2 membrane	103
Fig 6.14 Time dependent pure water flux of the membranes	104
Fig.6.15 Pressure dependent pure water fluxes of membranes	105
Fig.6.16 Flux versus time for membranes at 0.3 MPa during three conditions	105
Fig.6.17 Elemental mapping of lead and cadmium after the UF experiment	107
Fig.6.18 Interaction of heavy metal ion with MHNTs	107
Fig.6.19 Representative agar plates showing a) few colonies of <i>Staphylococcus aureus</i> , b) complete inhibition of <i>Candida albicans</i> .	108

Fig.6.20 A) colonies of <i>Candida albicans</i> around the control strip and no colonies on the HMM-1 (B) and HMM-2 (C) membrane strip respectively.	108
Fig.7.1 Schematic representation of adsorption of Cr (IV) to modified HNTs	110
Fig. 7.2 Schematic representation of chemical modification of HNTs	110
Fig.7.3. Schematic representation of chemical modification of HNTs and PVDF membrane	111
Fig.7.4 Chemical modification of HNTs by AEAPTMS	112
Fig 7.5. FTIR spectra of x) AEAPTMS, b) raw HNTs, c) MHNTs-1 and c) MHNTs-2	113
Fig.7.6. TEM and EDX analysis of a) HNTs and b) MHNTs	114
Fig.7.7 TGA analysis of HNTs and modified HNTs	114
Fig.7.8 Contact angle and surface energy of the prepared membranes	116
Fig.7.9 Zeta potential measurement of prepared membranes	117
Fig.7.10 Cross sectional and magnified cross sectional SEM images of a) MHM-0, b) MHM-1, c) MHM-2, d) MHM-3 membranes	118
Fig.7.11 Three dimensional AFM images of a) MHM-0, b) MHM-1, c) MHM-2, d) MHM-3 membranes.	119
Fig.7.12 Time dependent pure water flux of the membranes	120
Fig.7.13 Photographic image of a) MB and b) Rh.B before adsorption and after adsorption	121
Fig.7.14 Effect of pH on the dye removal capacity	122
Fig.7.15 Schematic representation of mechanism of interaction of dye molecules with the MHNTs	122
Fig.7.16 Dye removal efficiency as a function of time for a) MB and b) Rh.B	123
Fig.7.17 Variation in amount of a) MB and b) Rh.B dye adsorbed on the membrane.	124
Fig.8.1 Permeation rate and dye rejection capacity of the H.F membrane	128
Fig.8.2 Effect of dye concentration on permeation and rejection rate of H.F membrane.	129
Fig.8.3 Photos of (a) solutions and (b) membranes before and after dye permeating	130
Fig.8.4. Self-polymerization of m-aminophenol over the HNTs	132
Fig.8.5 Schematic representation of the hollow fiber membrane fabrication system	133
Fig.8.6 FTIR spectrum of the HNTs and PHNTs	135
Fig.8.7 TEM and EDX analysis of a) HNTs and b) modified HNTs	136

Fig.8.8 Contact angle and surface energies of the prepared membranes	137
Fig.8.9 Zeta potential measurements of prepared nanocomposite H.F membrane	137
Fig.8.10 Porosity of the prepared nanocomposite hollow fiber membrane	138
Fig.8.11 Cross sectional images of both magnified cross sectional SEM images of a) PMM-0, b) PMM-1, c) PMM-2 and PMM-3 membranes	139
Fig.8.12 Elemental mapping analysis on cross sectional PMM-3 membrane	140
Fig.8.13 Permeation and permeability of prepared membranes	140
Fig.8.14 Time dependent water flux of the prepared H.F membranes with three different filtration conditions	141
Fig.8.15 FRR and BSA protein rejection of nanocomposite H.F membranes	141
Fig.8.16 Total fouling phenomena of prepared nanocomposite H.F membranes	142
Fig.8.17 Photographic image of a) reactive red 120, b) reactive black 5 dye before and after dye rejection	142
Fig.8.18 Effect of transmembrane pressure on the rejection of reactive dyes	143
Fig.8.19 Time dependent flux study of reactive dye solutions	144
Fig.9.1 Schematic representation of humic acid adsorption a) without and b) with Ca^{2+}	146
Fig.9.2 Schematic representation of preparation of GO-TiO ₂ nanocomposite	146
Fig.9.3 Normalized flux decline during the humic acid filtration	147
Fig. 9.4 Schematic representation of chemical modification of Fe ₂ O ₃ nanoparticles.	149
Fig .9.5 FTIR spectrum of a) Fe ₂ O ₃ nanoparticles and b) modified Fe ₂ O ₃ nanoparticles.	152
Fig.9.6 X-ray diffraction patterns of a) Fe ₂ O ₃ nanoparticles and b) modified Fe ₂ O ₃ nanoparticles	152
Fig.9.7 a) average particle size distribution and b) FESEM images of modified Fe ₂ O ₃	152
Fig.9.8 EDX analysis of a) Fe ₂ O ₃ nanoparticles and b) modified Fe ₂ O ₃ nanoparticles	153
Fig.9.9 Zeta potential analysis of a) Fe ₂ O ₃ nanoparticles and b) modified Fe ₂ O ₃ nanoparticles	153
Fig.9.10 SEM images of the a) IOM-0, b) IOM-1, c) IOM-2 and d) IOM-3 H.F membranes	154
Fig.9.11 Contact angle analysis of prepared membranes	155
Fig.9.12 Zeta potential analysis of prepared nanocomposite hollow fiber membrane	156
Fig.9.13 Time dependent water flux at different filtration environments	157

Fig.9.14 FRR and BSA protein rejection of prepared membranes	157
Fig.9.15 Biofouling analysis a) microbial growth on whatman filter paper strip (as control), and membrane incubated with b) <i>Mycobacterium smegmatis</i> , c) <i>Staphylococcus aureus</i> d) <i>Escherichia coli</i> colonies.	158
Fig.9.16 Humic acid rejection coefficients of the hollow fiber membranes	159
Fig.9.17 Time dependent relative flux of prepared membranes	159
Fig.9.18 Effect of feed solution pH on normalized permeation rate	160
Fig.9.19 Effect of ionic strength of feed solution on normalized hydraulic permeation	161
Fig.10.1 Pure water flux of (L/m ² h) of prepared flat sheet membranes	
Fig.10.2 Pure water flux of (L/m ² h) of prepared hollow fiber membranes	
Fig.10.3 Contact angles (in degrees) of prepared membranes	
Fig.10.4 FRR values of prepared membranes	

List of tables

Table.1.1 Driving forces for the membrane separation	04
Table 1.2 Preparation methods of some commonly used polymers	11
Table 1.3 The advantage and disadvantages of polymers employed in membrane technology	16
Table 2.1 Composition and properties of the membranes	36
Table 3.1 Composition of casting solution	46
Table 3.2 The properties of the membranes	49
Table 3.3 The roughness parameters of the membranes	53
Table 3.4 Filtration and antifouling performance of the membranes	55
Table 4.1 Composition of casting solutions	64
Table 4. 2- EDX analysis results of elemental compositions for acid treated and untreated bentonite clay	65
Table 4.3- Physical properties of membranes	66
Table-5.1-Composition of casting solutions	77
Table-5.2 -Elemental composition of the bentonite and modified bentonite	80
Table-5.3- Properties of the prepared membranes.	83
Table-5.4 -Roughness parameters of the membranes	85
Table-6.1 - Composition of the casting solution	98
Table-6.2 Properties of the prepared membranes	102
Table-6.3 - Filtration and antifouling performances of the membranes	106
Table -6.4 -The reusability study for the heavy metal ion rejection	107
Table 7.1 Chemical composition of the nanocomposite membrane	113
Table-7.2 Properties of prepared membranes	116
Table -7.3 Roughness parameters of the prepared membranes	119
Table -7.4 Adsorption isotherm parameters of MB and Rh.B dyes on nanocomposite membrane	124
Table-8.1. Casting solution composition	132
Table 8.2 -Spinning conditions of PEI/PHNTs H.F membranes.	133
Table-9.1 Composition of casting solution	150

Table -9.2 Spinning parameters of nanocomposite H.F membranes	150
Table-9.3 The physical properties of prepared nanocomposite H.F membranes	155

ABBREVIATIONS

MF	Microfiltration
UF	Ultrafiltration
NF	Nanofiltration
RO	Reverse osmosis
MWC	Molecular Weight Cut off
PEI	Poly(etherimide)
PVDF	Polyvinylidene fluoride
EIPS	Evaporation induced phase separation
VIPS	Vapor induced phase separation
TIPS	Thermally induced phase separation
NIPS	Non-solvent induced phase separation
CA	Acetate cellulose
PA	Polyamide
NMP	N-methyl-2-pyrrolidone
DMAc	Dimethylacetamide
DMF	Dimethylformamide
SPEI	Sulfonated polyetherimide
AA	Acetic acid
CSA	Chlorosulfonic acid
SPEEK	sulfonated poly(ether ether ketone)
SEM	scanning electron microscopy
Br PVP	brominated polyvinylpyrrolidone
PWF	pure water flux
CPEI	Carboxylated polyetherimide
PAN	polyacrylonitrile
LCP	linearized cloud point
NPHCs	N-phthaloyl chitosan
FTIR	Fourier transform infrared
PVP	polyvinylpyrrolidone
BSA	bovine serum albumin

MMMs	mixed matrix membrane
PIAM	poly(isobutylene-alt-maleic anhydride)
IEC	ion exchange capacity
WCA	water contact angle
PVA	poly (vinyl alcohol)
FM	formamide
HEMA	2-hydroxyethylmethacrylate
NSCS	N-succinyl chitosan
AFM	Atomic force microscopy
FRR	flux recovery ratio
EDX	energy dispersive X-ray
TMP	transmembrane pressure
HNTs	halloysite nanotubes
TEPA	tetraethylenepentamine
MPS	3-(methacryloxy)propyltrimethoxysilan
XRD	X-ray diffraction
PEUF	polymer enhanced ultrafiltration
TEM	Transmission electron microscopy
MPC	2-methacryloyloxyethyl phosphorylcholine
PDA	polydopamine
MWCNTs	multiwalled carbon nanotubes
AAS	Atomic Absorption Spectrometer
AEAPTMS	N- β -(aminoethyl)- γ -aminopropyltrimethoxy silane
H.F	Hollow fiber
NOM	natural organic matter
PES	Polyethersulfone

CHAPTER 1
INTRODUCTION

Abstract : This chapter gives a detailed information about the ongoing research in the field of membrane technology. It includes the challenges of global water crisis, history, growth and applications of membrane technology. It also includes the preparation and characterization of membrane along with the technologies used in membrane based separation process.

1.1 GLOBAL SCENARIO

Water is an indispensable source for the life on the Earth. It is estimated that, there is sufficient amount of fresh water available for all present and foreseeable human needs, provided it is evenly distributed around the world. This sadly is not the case since, fresh water accounts for only 3% share of all the water present on the earth. Out of which, 68% of the fresh water is trapped in the form of frozen polar ice caps and 30% of the fresh water is trapped deep beneath the earth which are inaccessible for human needs. Only available fresh water source for human consumption are groundwater, lakes and rivers, that are found in less percentage (Fig. 1.1). The amount of water on earth is virtually unchanged throughout the ages for which the life exist on the earth and will continue to remain so, till the population will touch upon 8 billion by 2030 as per the current estimation (Shannon *et al.* 2008). Water obtained from naturally occurring source is sufficient to cater our needs if resourcefully utilized. The demand for water has been growing at an alarming rate than the human population itself. It is estimated that, during 20th century, the world population increased fourfold, while the amount of fresh water consumption during this time increased about nine times indicating higher demand than supply. The rise in population implies increased industrialization, rapid urbanization, agricultural activities and household activities which are directly associated with the increased water consumption.

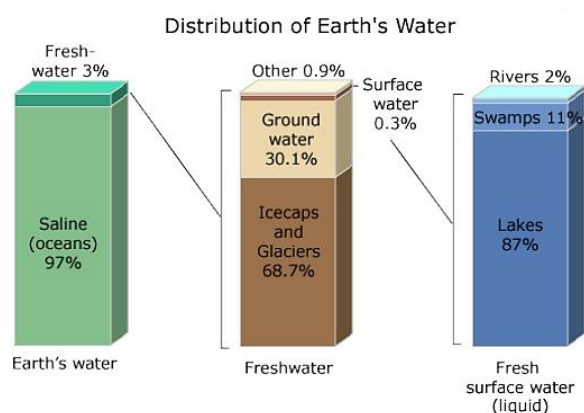


Fig.1.1 Graphical representation of distribution of water on earth (Source: Rice University and the Houston Museum of Natural Science)

Also contamination of available fresh water source is making the water scarcity a serious concern. Often the water sources near industries like textile, painting, ceramics, glass, mining and battery manufacturing are considered to be the main source of contaminations. Particularly, in humans, accumulation of hazardous heavy metals like lead, copper, chromium, iron, zinc and mercury causes kidney damage, nervous system failure and bone damage, in addition to other serious ailments. Waste water discharge is a primary source of heavy metal contaminations into the environment. The development of new technology for the removal of heavy metal ions from aqueous solution remains an important scientific challenge.

As mentioned above, the scarcity of pure and safe drinking water has reached an alarming stage and an instant action to curb this problem is necessary. There are many processes such as distillation, evaporation, extraction and coagulation that are in practice of water purification in earlier days. These processes consume more energy and hence increase the operational cost. The contaminated water should be purified substantially to meet stringent environmental quality standards. Therefore, one has to look at the newer alternatives which should be energy efficient and effective in water purification. For this purpose, pressure driven membrane based water purification is the best option for the effective water purification system.

1.2 KEY DEVELOPMENTS OF MEMBRANE TECHNOLOGY

The literature on studies of membranes and discovery of osmosis process dates back to the eighteenth century. Nollet has the distinction of being the first researcher to identify the role of semipermeable membrane and pressure in osmosis. Later, Thomas Graham carried systematic studies to understand the mass transport through semipermeable membranes. Pfeffer prepared the first synthetic semipermeable membranes by precipitation of cupric ferrocyanide in a thin layer of porous porcelain for the investigation of osmosis. The Fick's law of diffusion provides a theoretical model for the understanding of osmotic phenomena and mass transport through the membranes (Baker 2004). These early studies in membrane science reasonably describe the basic phenomenon with theoretical justification.

Over the years, membranes and membrane based separation process has been developed as an efficient separation technique from a mere laboratory experiment. It is now of industrial significance with appreciated technical and commercial impact. Presently, membranes are being employed in an array of fields ranging from the desalination of sea

water to cleaning industrial effluents, from fractionating macromolecular solutions in food and drug industry to the removal of urea and other toxins from blood stream by dialysis in artificial kidneys, from controlled release of drugs in medical treatment to immobilize catalyst in order to bring about effective chemical transformation, and also to separate gas and vapors in petrochemical processes, etc. Thus, with membrane based industry growing at a rate of 10 % per year, the use of membrane processes will most likely to extend far beyond its present level by designing new membranes possessing better chemical, thermal, and mechanical properties with improved fouling resistance which are capable of providing more selective and energy efficient carrier- facilitated transport.

By upgrading the synthetic asymmetric membrane for the separation of salt from seawater at the University of California, Loeb and Sourirajan (1962) have inspired significant development in the field of membrane science and technology. Production of potable water is a key area where membrane based separation processes have recently been introduced (Singh 2006). The popularity of the membrane technology in environmental applications is due to the present scare of potential shortage of fresh water and stringent environmental regulations. Meanwhile, the rapid development in polymer science over the recent years has also aided the widespread use of membrane technology.

1.3 MEMBRANE DEFINITION AND CLASSIFICATION

In the broadest sense, “membrane acts as a selective barrier, allowing some particles or species to pass through, but not others”. A membrane can be homogeneous or heterogeneous, symmetric or asymmetric in structure, solid or liquid; it may be neutral or charged, or dipolar. The mass transport through a membrane may either be caused by convection or by diffusion process induced by a gradient in electric field, pressure, temperature or concentration (Baker 2004). The schematic representation of membrane separation process is illustrated in fig. 1.2. All materials which are intended to be used as membranes have a characteristic selective restriction for the passage of different molecules.

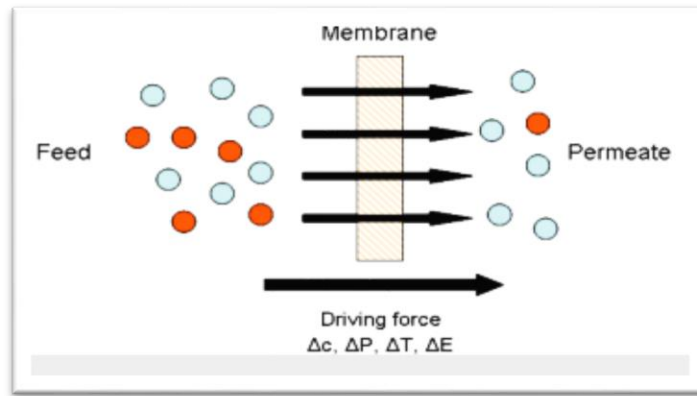


Fig.1.2 Schematic representation of membrane separation process

Classification of membranes based on the driving force to achieve the separation is given as following.

Table.1.1 Driving force for the membrane separation

Driving force	Membrane process
Pressure gradient	Reverse osmosis, Microfiltration, Nanofiltration, and Ultrafiltration.
Concentration gradient	Evaporation, Gas separation, Dialysis, Vapour permeation, and Liquid membranes.
Electrical potential gradient	Electrodialysis membrane, and Electrophoretic membrane
Temperature gradient	Membrane distillation

Pressure driven membrane separation processes, electrodialysis and gas separation are industrially implemented and are generally considered as proven technology. The current work will focus on pressure driven membrane separations, no further details will be given on the other techniques.

1.3.1 Pressure driven membranes

The four pressures driven membranes are distinguished in practice (Mulder 1996), namely

a) *Microfiltration (MF) membranes*: These membranes are used for separation of fine particles of upto 100nm from solutions. The transmembrane pressure is maintained within 1 to 50 psig (pound-force per square inch gauge) which is a unit of pressure relative to the

surrounding atmosphere (1 psig = 6.894×10^3 Pascal, 1 atm = 14.696 psig). Most MF membranes arrests particles by sieving mechanism. (Mulder 1996)

b) Ultrafiltration (UF) membranes: UF membranes retain macromolecules such as proteins while allowing smaller molecules to pass through it and are mostly asymmetric in nature. The separation mechanism in UF is size exclusion. However, the physicochemical interactions between solutes, membrane, and operating conditions may impact the process significantly. Usual transmembrane pressure applied in UF ranges from 10 to 100 psig.

c) Nanofiltration (NF) membranes: NF membranes allow small molecules like salts to pass through but retain larger molecules like sugar, peptides and hormones. The transmembrane pressure in NF ranges from 40 to 200 psig. Mostly the construction of NF membranes are composite i.e. asymmetric like UF membranes. (Mulder 1996)

d) Reverse osmosis (RO) membranes: RO membranes are deemed as ultimate membranes among the membrane technology owing to their restricted permeability. It allows only water molecules to go through but retain all dissolved substances present in the feed. In a typical RO process, water travels from the side having higher solute concentration to the lower solute concentration side of the membrane. This is reverse of what happens in osmosis hence the name of the process. The normal transmembrane pressure range in RO is from 200 to 300 psig. (Mulder 1996)

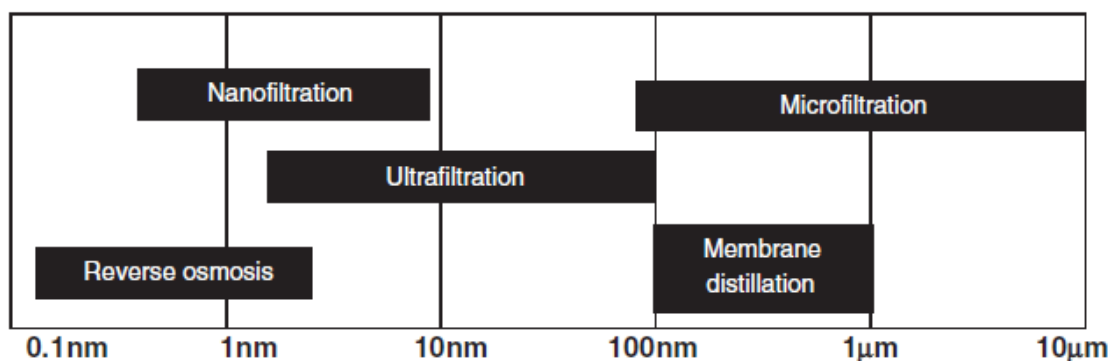


Fig.1.3 Classification of the membranes based on average pore size (Mulder 1996)

1.4 FUNDAMENTAL ASPECTS OF MEMBRANES AND MEMBRANE PROCESSES

1.4.1 Membrane transport mechanism

As discussed earlier, separations in membrane processes are the result of variation in the transport rates of different molecules through the membrane. The rate of transport is governed by the driving force or the forces acting on different components, their mobility,

and concentration gradient across the membrane. The mobility of species is mainly determined by their size and the physical properties of the membrane interphase (Baker 2004). The transport of substance through membrane is a non-equilibrium process. It is typically expressed by the Fick's law of diffusion which correlates the flux of species with the concentration gradient. It is mathematically expressed as,

$$J_i = -D_i \frac{dc_i}{dx} \quad (1.1)$$

Where ' J_i ' ($\text{g}/\text{cm}^2 \text{ s}$) is the transport rate (or flux) of constituent ' i ' and ' dc_i/dx ' is the concentration gradient of ' i ' constituent. The term ' D_i ' is the diffusion coefficient (cm^2/s) which is a measure of the mobility of the individual molecules. The negative sign indicates the diffusion is down the concentration gradient. Fig.1.4 represents the molecular transport mechanisms through membranes. In diffusion-controlled separation processes, the membranes are made very thin to obtain large concentration gradient across the membrane thereby achieving good flux.

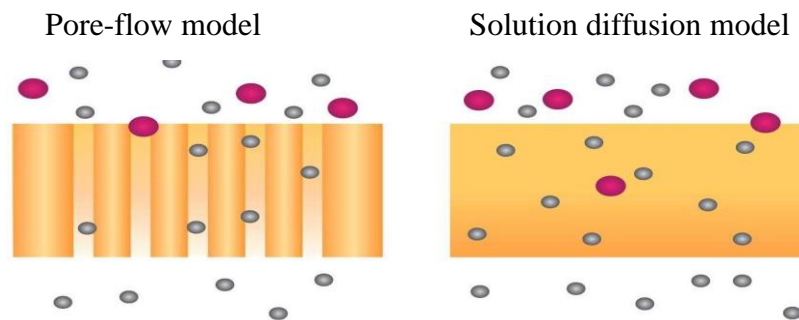


Fig.1.4 Molecular transport mechanisms through membranes (Source: CO2CRC Limited)

Pressure-driven mass transfer is the basis of the asymmetric membranes and most commonly used to describe the flow in porous medium. The basic equation encompassing this type of transport phenomenon is Darcy's law, which can be stated as

$$J_i = K_{ci} \frac{dp}{dx} \quad (1.2)$$

Where ' dp/dx ' is the pressure gradient present in the porous medium, ' c_i ' is the concentration of component ' i ' in the medium and ' K ' is a coefficient revealing the nature of the medium. In general, fluxes of convective-pressure-driven membranes are high compared with those obtained by simple diffusion process (Baker 2004).

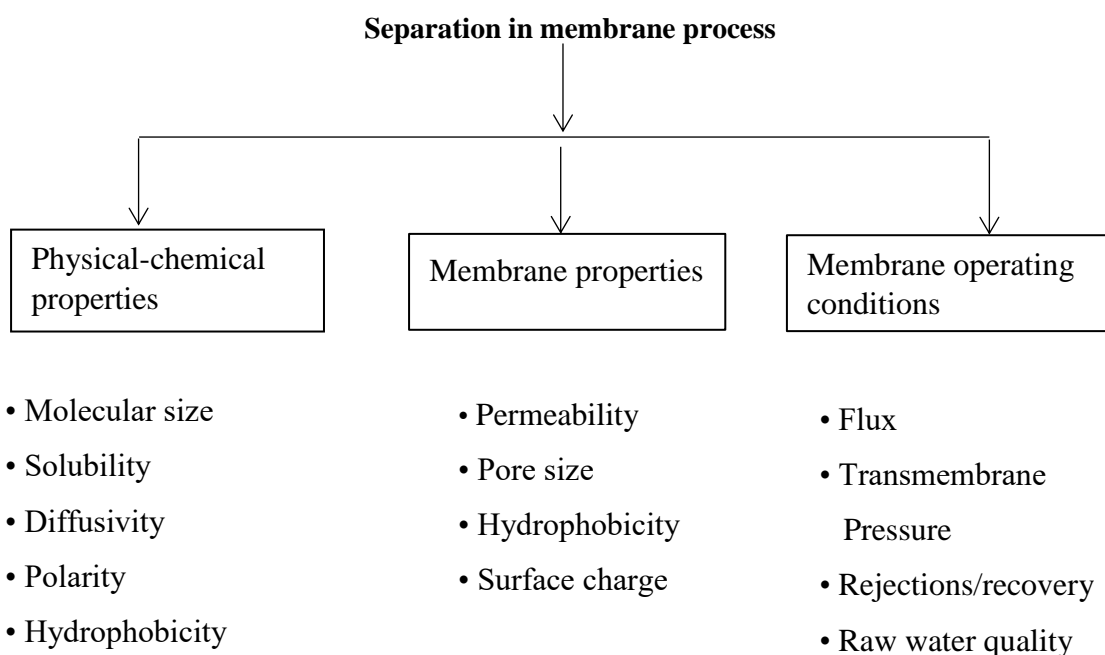
1.4.2 Factors affecting the performance

The performance or efficiency of membrane as the filter in water purification application can be influenced by various parameters. The flux and selectivity are the

important factors of the membrane decided by the physicochemical properties, operation condition and morphological features. The flux can be defined as “Volume of permeate passing through membrane per unit area and unit time.” This is expressed using SI unit as $\text{m}^3/\text{m}^2 \text{ s}$ or $\text{L}/\text{m}^2 \text{ h}$. The selectivity of the membrane towards a mixture is generally expressed as retention factor. It is given by

$$R = 1 - \frac{C_p}{C_f} \quad (1.3)$$

Where ‘ C_f ’ is the concentration of solute in feed and ‘ C_p ’ is concentration of solute in the permeate. The selectivity of the membrane can also be expressed in terms of exclusion limit or "cut-off" of the membrane, and is normally stated as MWC (Molecular Weight Cut off, Unit: Dalton). MWC is the minimum molecular weight of the compound which is retained by the membrane to 90 %. In addition to the pore size the selectivity largely depends on the separation process, the composition and electrochemical properties of the membranes (Mulder 1996). Generally, factors that affect the membrane performance is given below



1.4.3 Advantages of membrane processes

Membrane systems present more economical advantages over conventional systems. Specific criteria of the membrane system are listed as following:

1. This technology is applicable to wide range of separation process compared to traditional methods. The system can be operated in combination with the conventional methods or as stand alone method.

2. Membrane process are energy efficient because separation occurs without any phase change.
3. Separation can be carried out under moderate conditions.
4. Separation phenomenon is done physically and it is environmentally green.

Limitation of membrane process:

1. Long term reliability of membranes is still an ongoing research.
2. Membranes are sensitive towards **concentration polarization**, chemical interaction with feed constituents and **fouling**.
3. Membranes often have poor mechanical stability and can easily rupture due to malfunction in the operating procedure, or concentration polarization with solute precipitation at the membrane surface.

1.4.4 Membrane fouling and prevention

Fouling can be described as deposition of filtered particles, colloids, macromolecules, salts, etc., on the surface of the membrane or inside the pores (Fig.1.5). Fouling can reduce the membrane flux either temporarily or permanently depending on its type. While the initial flux reduction by temporarily fouled membrane can be recovered either by washing the membrane or by applying back-pressures, but it cannot be restored in case of the permanent fouling of the membrane. The fouling is a result of the interaction between the surface of the membrane and the foulants, which consists of inorganic, organic, and biological substances (Rana and Matsuura 2010). This is a severe problem for membranes which are used in pressure-driven processes such as RO, NF, UF, and MF because of decrease in efficiency and life time of the membrane material.

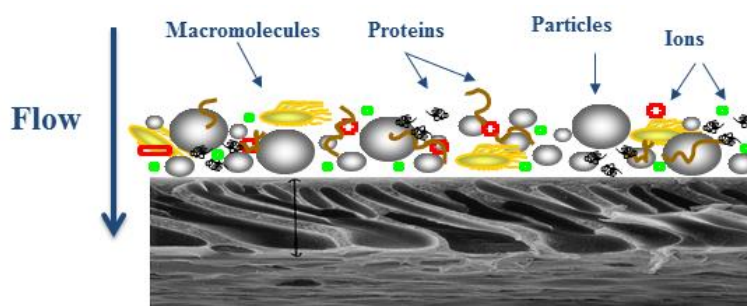


Fig.1.5 Schematic representation of membrane surface fouling

The fouling prevention is one of the important parameters in membrane separation process. Hence to minimise the fouling, proper selection of membrane, appropriate pre-treatment of the process fluid, and optimization of operating design and other conditions are required. Some of the factors that reduce the fouling are listed as follows

- a) *Hydrophilicity*: It is usually accepted that hydrophilic membranes shows better fouling resistance because most foulants like proteins are hydrophobic in nature. This can be achieved by chemical modification and other methods.
- b) *Surface Charge*: It is commonly known that the repulsive interaction between the co-ions in the feed solution and charge on the surface of the membrane prevent the solute deposition on the membrane surface, thereby reducing the fouling.
- c) *Surface Roughness*: The flux through a membrane increases with the increase of surface roughness of the membrane, as it increases the area available for the transport through the membrane. However, the interaction between colloidal particles with the rough surface is also enhanced, i.e, the colloidal particles preferentially accumulate over the pores of the rough membrane. As a result, pores become completely blocked and fouling is more intensive. This can be prevented by reducing surface roughness.

Significant progress has been made in recent years in membrane technology. There have been widespread research in reverse osmosis for desalination of seawater, in developing membranes which not only significantly improve the overall performance but also show better chemical and thermal stability and are less sensitive towards operational errors.

1.5 MEMBRANE MATERIALS

The choice of a membrane material for a particular membrane separation is not arbitrary, but is dependent on its properties which are essential for membrane fabrication process. The following important material properties need to be considered during their selection as an interphase

- a) Film forming property of the material is important since it decides the formation of cohesive film due to attractive interactions between chain segments of the polymer.
- b) The mechanical strength of the material involves film strength and film flexibility to withstand high operating pressures of the process.

c) Chemical stability is essential in order to sustain extreme pH and other chemical conditions. The feed solution may contain a number of harsh components like cleaning agents or chlorinated compounds which are capable of altering the membrane morphology or property. Chemical resistance towards such agents forms an important membrane property.

d) Requirement of thermal stability of the membranes depend mainly on the application. The glass transition temperature, 'T_g' indicates the physicothermal stability of the membrane. 'T_g' of the membrane material should be higher than that of the process temperature in order to ensure overall integrity of the membrane structure.

e) A fine balance of hydrophobicity and hydrophilicity ensures better membrane performance in terms of flux, rejection and fouling.

Polymers have achieved an vital place in membrane technology and are being used in a broad range of applications. The key property of the polymer that is exploited is the ability of polymers to exhibit different morphological features with proper selectivity and flux. The behaviour of a polymer to act as a membrane requires several qualification such as good film forming ability, Thermal stability, mechanical strength and chemical resistivity (Baker 2004). In addition to this, hydrophilicity and hydrophobicity of the material also plays an important role during the performance.

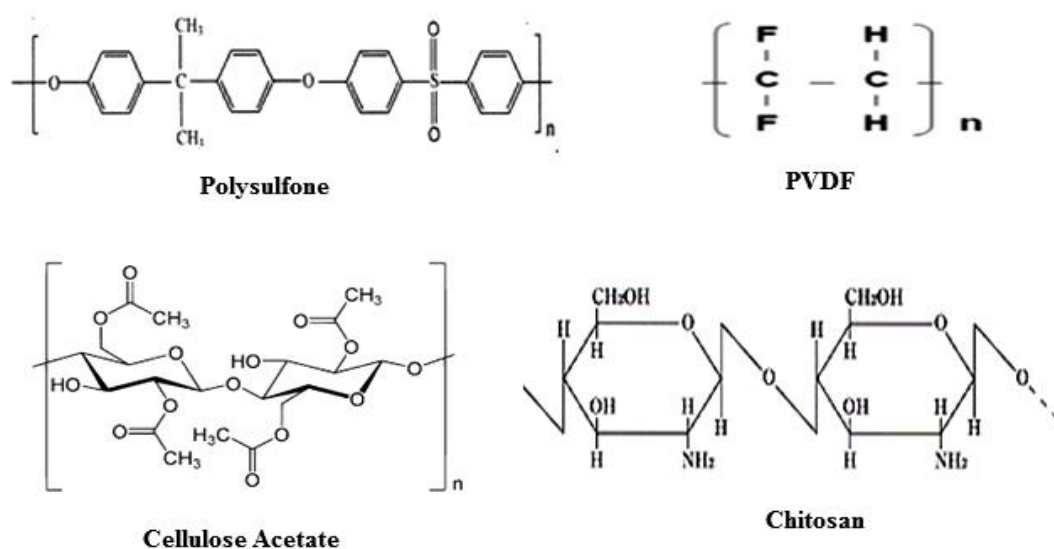


Fig.1.6 Structures of some commonly used polymers in membrane preparation

The materials used to prepare the MF and UF membranes are almost the same, however they will be prepared maintaining different conditions to attain different

morphological structures. Typical MF and UF membrane materials are poly (vinylidene fluoride), polysulfone, poly (acrylonitrile) and poly (acrylonitrile)-poly (vinyl chloride) copolymers, poly (ether sulfone), polyetherimide. In addition to this membranes can also prepared by using blends of several polymer materials, such as cellulose acetate, cellulose nitrate, chitosan etc. Choosing the right material is very crucial and is dependent on the applications and the operating conditions.

Table 1.2 Preparation methods of some commonly used polymers

Polymer	Membrane preparation method	Reference
Polysulfone	Non-solvent induced Phase Inversion	(Holda <i>et al.</i> 2013, Zhao <i>et al.</i> 2014)
Polyacrylonitrile	Thermally induced Phase Inversion	(Jung 2004)
PVDF	Non-solvent induced Phase Inversion	(Li <i>etal.</i> 2010, Pezeshk and Narbaitz 2012)
Cellulose esters	Non-solvent and thermally induced phase inversion	(Chen <i>et al.</i> 2004, Waheed <i>et al.</i> 2014)
Cellulose nitrate	Non-solvent induced Phase inversion	(Sun <i>et al.</i> 2007, Uragami <i>et al.</i> 1976)
PVC	Non-solvent induced Phase inversion	(Xu and Xu 2002)
polycarbonate	Track etched	(Tracey and Davis 1994)
polypropylene	Extrusion	(Saffar <i>et al.</i> 2014)
Polystyrene	Thermally induced phase separation	(Gao <i>et al.</i> 2000)
PEES	Non-solvent induced Phase inversion	(Maheswari <i>et al.</i> 2013)
Polyethersulfone	Non-solvent induced Phase inversion	(Hwang <i>et al.</i> 1996)
Polyetherimide	Non-solvent induced Phase inversion	(Xu <i>et al.</i> 2003)

1.5.1 Polyetherimide as a membrane material

Among high performance polymers, poly(etherimide) (PEI) continues to attract attention as the material of choice for membrane preparation. The aromatic imide unit provides excellent mechanical and thermal properties. It has a good film forming capacity and chemical resistance over a wide range of pH, while the flexible ether linkages provide good process ability. Its outstanding characteristics have resulted in it being extensively employed as industrial films, coatings, adhesives, and mouldings at high temperatures. The chemical structure of PEI is presented in Fig.1.7. It is a versatile and well-known specific engineering polymer that consists of repeated phenyl groups, imide groups, ether linkages, and angular bonds between aromatic rings (Nagendran *et al.* 2008). The aromatic imide units of PEI are responsible for high-performance characteristics such as high mechanical strength, thermal stability, and chemical resistance, while the flexible ether linkages provide good process ability (Kim *et al.* 2002).

In general, a kind of material does not possess all the excellent properties required for membranes. As for PEI, its application for aqueous phase is limited by hydrophobicity. Therefore, polymers may need some modification to improve their performance for specific applications. Currently there are two methods for surface modification of PEI membrane. First, sulfonation of the chemical structure, which improves the hydrophilicity of PEI membrane with a controlled level of sulfonation. Secondly, modification of surface can be achieved by physical adsorption (that is, coating) or blending of hydrophilic polymer onto the surface of the PEI membrane, followed by the crosslinking of this thin coating layer. Hence, it is expected that the separation tendency of top layer and supporting layer can be significantly reduced as the result of the increased affinity via hydrophilic binding polymer.

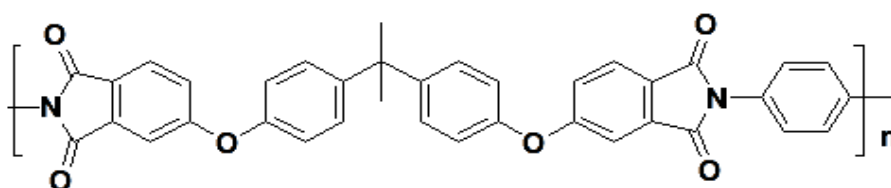
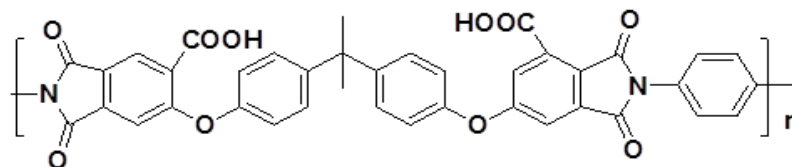


Fig.1.7 Chemical structure of polyetherimide (PEI) polymer

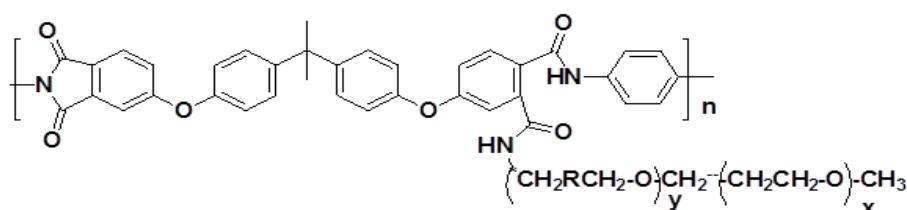
A few attempts have been made to enhance the hydrophilicity of PEI membranes. (Chinpa *et al.* 2010) modifying PEI by attaching poly (ethylene glycol) to the membrane. (S.Senthilkumar *et al.* 2013) synthesised carboxylated PEI using butyl lithium in presence

of dry ice. Bianca et al prepared sulfonated PEI. Few examples of chemical modification of PEI are given below.

1. Carboxylated PEI



2. PEI modified with poly (ethylene glycol)



1.6 MEMBRANE PREPARATION

Synthetic membranes can be prepared from a large number of materials. Depending on the requirement of a particular separation process, it is possible to modify the available polymers by adopting the necessary membrane preparation techniques. Some of them are listed below,

- ❖ Sintering
- ❖ Stretching
- ❖ Vapor deposition
- ❖ Solution casting
- ❖ Track etching
- ❖ **Phase inversion**

Most of the commercially available membranes are obtained by phase inversion process which results in the formation of asymmetric membranes characterized by dense top layer followed by porous sub-layer. Solvent containing single polymer solution is transformed in a controlled manner into a two phase system namely, polymer-rich solid phase which forms the membrane structure and solvent-rich/polymer lean liquid phase which forms the liquid filled membrane pores (Jansen *et al.* 2005).

- ❖ **Evaporation induced phase separation (EIPS):** The polymer solution is made from a relatively volatile solvent and a less volatile non solvent. The evaporation of the solvent from the dope solution results in precipitation.
- ❖ **Vapor induced phase separation (VIPS):** The polymer solution is exposed to an atmosphere containing non-solvent (typically water), absorption of non-solvent from atmosphere leads to demixing/precipitation.
- ❖ **Thermally induced phase separation (TIPS):** The polymer solution is cast at an elevated temperature, cooling leads to demixing/precipitation. This technique is generally applied for a polymer having poor solubility where the wet phase inversion approach is not feasible. The substance used in this process acts as a latent solvent, i.e. it acts as a solvent at elevated temperatures but plays the role of non-solvent on cooling.
- ❖ **Non-solvent induced phase separation (NIPS):** The polymer solution is immersed in a non-solvent coagulation bath (typically water); demixing and precipitation occur due to egress of solvent from polymer solution and ingress of non-solvent (from coagulation bath) into the casting solution. Solvent-non-solvent exchange occurs faster at the interface and hence, the polymer precipitates faster at the surface giving a dense structure than the underlying substrate. Schematic representation of membrane preparation by phase inversion method is presented in Fig.1.8.

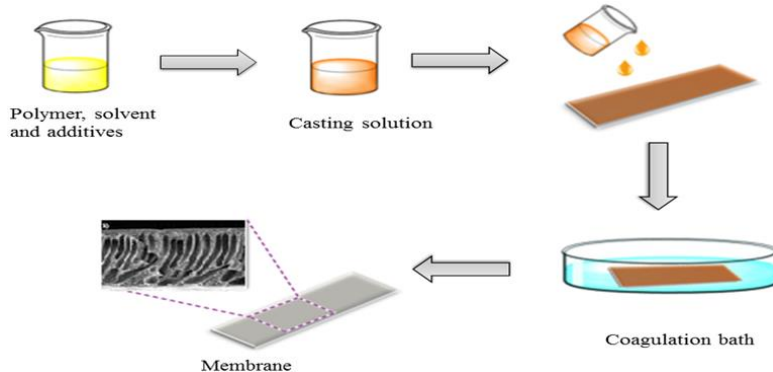


Fig.1.8 Schematic representation of membrane preparation by phase inversion method

Phase separation or Non-solvent induced phase separation is a process where a polymer solution is cast on a suitable support, then immersed in a coagulation bath containing a non-solvent, where an exchange of solvent and non-solvent takes place and the membrane is formed. Schematic presentation of processes after polymer solution immersion in a non-solvent bath is shown in Fig1.9. The solvent diffuses into the coagulation bath (at a flux = J_2) whereas the non-solvent will diffuse into the cast film (at a flux = J_1). After a certain time the exchange of solvent and non-solvent proceeds until the

solution becomes thermodynamically unstable and demixing takes place. A solid polymeric film finally is obtained with an asymmetric structure. Usually at $J_2 \gg J_1$ “skin” UF membranes with pore size of 10–300 Å are obtained, while at $J_2 = J_1$ mainly MF membranes with pore size of 0.2–0.5 μm are fabricated. Isotropic acetate cellulose (CA) RO membranes via immersion precipitation by Loeb and Sourirajan was one of the most critical break throughs in desalination. Today, extensive knowledge exists on how to ‘tailor’ the membrane’s pore structure including its cross-section morphology by the selection of polymer, solvents and non-solvents, additives, precipitation time, bath temperature and other parameters during immersion precipitation. For example, different casting conditions and post-treatments were proposed to improve the water flux and salt rejection of the CA membranes.

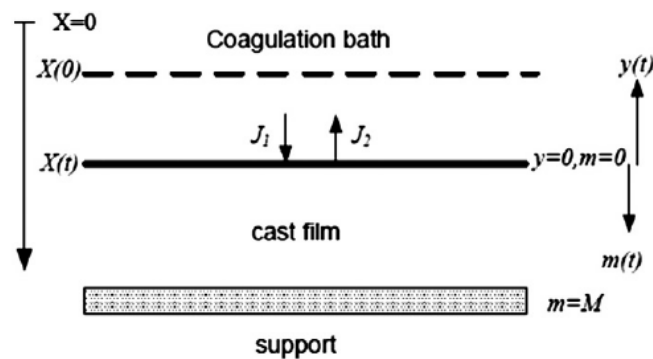


Fig.1.9 Schematic representation of a film/bath interface in the coagulation bath

Apart from the chemical nature of a casting polymer, the concentration of the polymer is very important in membrane fabrication via immersion precipitation. Increasing polymer concentration in the casting solution produces membranes with low porosity and pore size. The main polymers used in membrane formation and their advantages and disadvantages are presented in Table 1.3.

Table 1.3 The merits and demerits of polymers employed in membrane technology

Polymer	Advantages	Disadvantages
Cellulose acetate	<ul style="list-style-type: none"> • Hydrophilicity • Flexibility in fabrication • Low cost 	<ul style="list-style-type: none"> • Low thermal resistance (< 30 °C) • Low chemical resistance, pH range (2–8)
PS and PES	<ul style="list-style-type: none"> • High thermal resistance (up to 75 °C) • Wide pH tolerances (1–13) • Good chlorine resistance • Flexibility in membrane fabrication (wide range of pore size) • High mechanical characteristics 	<ul style="list-style-type: none"> • Low operating pressure limits • Hydrophobicity • Poor resistance to chlorine
PVDF	<ul style="list-style-type: none"> • High mechanical strength and chemical resistance • High thermal stability (up to 75 °C) • High mechanical characteristics 	<ul style="list-style-type: none"> • Hydrophobicity
Polyamide (PA)	<ul style="list-style-type: none"> • Wide pH tolerance • High thermal stability • High mechanical properties 	<ul style="list-style-type: none"> • Poor chlorine resistance
PEI	<ul style="list-style-type: none"> • Wide pH tolerance • High thermal stability • High mechanical properties 	<ul style="list-style-type: none"> • Hydrophobicity

1.7 BASIC TERMINOLOGIES USED IN MEMBRANE TECHNOLOGY

The commonly encountered terms in membrane separation process are summarized below.

- ❖ **Flux:** The permeability or productivity of the membrane is one of the parameters that quantify a membrane performance. It is expressed in terms of flux and is defined as the amount of water passing through a unit area of a membrane in unit time. Schematic representation of the lab scale filtration set up is presented in Fig.1.10.

$$J_w = \frac{Q}{\Delta t A}$$

Where, J_w is expressed in L/m²h and ' Q ' is the amount of water collected for Δt (h) time duration using a membrane of area ' A ' (m²).

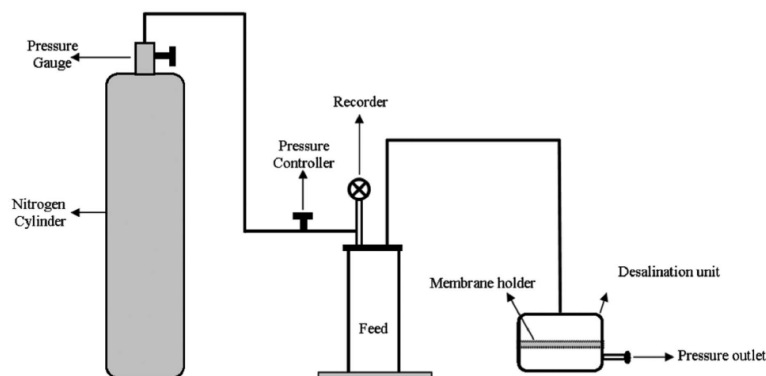


Fig.1.10 Schematic representation of the lab scale filtration set up

The flux of the membrane is primarily governed by pore size distribution, pore tortuosity and thickness of the membrane. Lower permeability translates increased capital cost due to larger membrane area and hence more energy input. The concentration polarization caused by the components present in the feed solution also influences the water flux.

- ❖ **Solute Rejection:** The selectivity of the membrane towards the solute is expressed in terms of rejection. It is given by

$$\%R = \left(1 - \frac{C_p}{C_f}\right) \times 100$$

Where ' C_f ' and ' C_p ' (mg mL⁻¹) are the concentration of the solute, dye or protein molecules in the feed and permeate respectively

- ❖ **Swelling:** The water uptake capacity of the membrane is expressed as

$$\% \text{ uptake} = \left(\frac{W_w - W_d}{W_d}\right) \times 100$$

Where ' W_w ' and ' W_d ' are the weights of wet membrane and dry membrane respectively. The water uptake property of the membrane reflects the bulk hydrophilic nature of the membrane which is a very essential parameter that affects its permeability and antifouling property.

❖ **Porosity:** Porosity of a membrane is defined as the ratio of the pore volume to geometrical volume. It is given as

$$\varepsilon = \frac{W_w - W_d}{A \times l \times d_w}$$

Where 'ε' is the porosity of membrane, 'W_w' is the weight of wet sample (g), 'W_d' is the weight of dry sample (g), 'd_w' is the density of pure water (0.998 g/cm³), 'A' is the area of membrane in wet state (cm²) and 'l' is the thickness of membrane in wet state (cm).

❖ **Membrane fouling:** Major problem encountered in membrane separation process is membrane fouling which results in flux decline and eventually affects the performance of the membrane over a period of time. This process refers to the formation of cake or blockage of membrane pores by feed solution constituents that are retained by the membrane (Fig. 1.11). This leads to an accumulation of retained material and to a depletion of the permeating components in the boundary layers adjacent to the membrane surface.

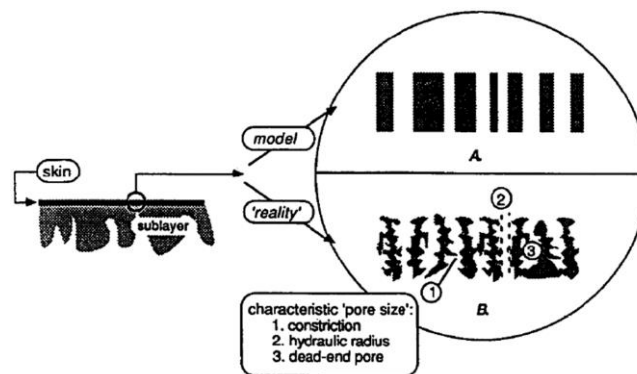


Fig.1.11 Comparison of A) Ideal pore structure and B) Real pore structure in asymmetric membranes

1.8 APPLICATIONS OF MEMBRANE TECHNOLOGY

Bearing in mind the increasing demand for potable drinking water in the years to come, there will be a need for energy-efficient and affordable processes for the production of high quality water. Since membrane processes have proved to be an economic and energy efficient tool, the market for membrane is bound to increase exponentially. The market of the by far largest commercial membrane process, the 'artificial kidney' alone accounts for turnover of about US \$ 1 billion (Ulbricht 2006).

Apart from purification of water and desalination, membranes are used as a separation tool in various other fields which are summarized below,

RO applications

- ❖ Desalination Industry – Potable water production from sea water and brackish water.
- ❖ Ultra-pure water – In semiconductor industry
- ❖ Municipal wastewater treatment.
- ❖ High purity water – In pharmaceuticals, beverages and medical usage
- ❖ Chemical process industries – Effluent water reuse, Water/ organic separation, organic liquid mixture separation.

NF applications

- ❖ Cleaning up of contaminated ground water
- ❖ Treatment of effluents containing heavy metals and oil
- ❖ Water softening
- ❖ Food processing

UF and MF process applications

a) Concentration

- ❖ Proteins - enzymes, milk proteins, egg white
- ❖ Starch and pectin
- ❖ Yeast production
- ❖ As pretreatment for NF & RO processes

b) Effluent treatment

- ❖ Oily waste water – from washing operations
- ❖ Bleach effluents – pulp and paper industry
- ❖ Leather and tanning effluents

c) Clarification

- ❖ Sugar refining – removal of polysaccharides, proteins, colloidal impurities
- ❖ Sterile filtration of biological – removal of bacteria and viruses
- ❖ Fruit juices and wine purification

d) Water treatment

- ❖ RO pre-treatment

- ❖ Potable water – removal of bacteria and viruses

Pervaporation

- ❖ Removal of organics from water
- ❖ Organic/organic separation
- ❖ Water removal from organic liquids

Gas separation

- ❖ Oxygen nitrogen separation
- ❖ Separation of organic vapors from air
- ❖ Biogas processing removal of acid gases from light hydrocarbons

1.9 LITERATURE SURVEY

A significant amount of research has been conducted in the field of water treatment using membrane technology. Membranes play a key role in membrane based water treatment processes and improvement of the membranes with novel materials can greatly affect the membrane performance. Among high performance polymers, PEI continues to attract attention as the material of choice for membrane preparation. The brief literature survey is given below.

Kim *et al.* (2002) reported the synthesis of integrally skinned asymmetric PEI nanofiltration membranes by phase inversion process. The casting solution consist of DMF as a solvent and 1,4-dioxane as a cosolvent with water as non solvent in the coagulation bath. It shows that,the low miscibility of 1,4-dioxane with coagulant (water) resulted in reducing the membrane pore size and molecular weight cutoff values of asymmetric membranes could be controlled by changing the amount of 1,4-dioxane in the casting solution.

Xu *et al.* (2003) prepared ultrafiltration hollow fiber membrane from PEI with a wet spinning method. They investigated the effects of DMAc as a solvent additive in internal coagulant and acetic acid (AA) as a nonsolvent additive in dope solution on the morphologies and performances of the membranes. With the increase of acetic acid ratio, the pure water flux of the membrane increased about four times, and the solute retention showed a slight decrease.

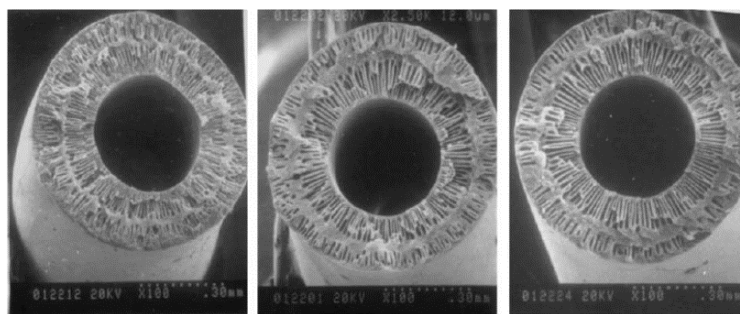
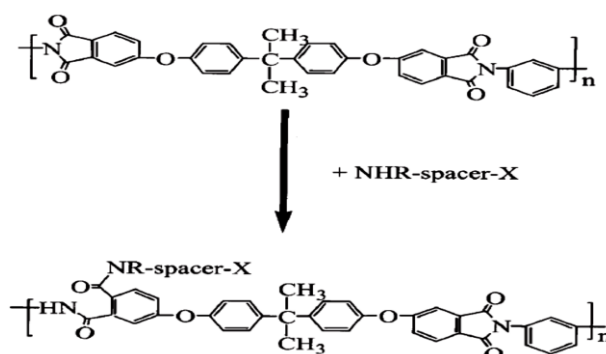


Fig.1.12 Cross-section of PEI hollow fiber membranes from different dope (AA) solutions.

Albrecht *et al.* (2003) reported the amination of PEI membranes using di- and multivalent amines. They used wet chemical method to functionalise the PEI. According to them, the carbonyl group of the imide ring reacts with the nucleophilic amine group of the modifier forming one amide group, maintaining the macromolecular structure and generating an additional second amide group bearing the amine group or amine groups. The modification results in a strong influence on the contact angle and morphology of the modified membrane.



Scheme 1.1 Schematic reaction for the change in function of PEI membrane.

Shen *et al.* (2004) reported the preparation of SPEI /PEI blend membranes. PEI was sulfonated by chlorosulfonic acid (CSA) in 1,2-dichloroethane solvent. Membranes were fabricated from SPEI/PEI blends with different ratios. The morphologies of the blend membranes were examined by scanning electron microscopy. The contact-angle data of the membranes showed the enhanced hydrophilicity of the blend membrane because of the sulfonate group on the SPEI molecular backbone.

Bowen *et al.* (2005) reported the preparation of PEI and sulfonated poly(ether ether ketone) (SPEEK) blend membranes. SPEEK was used to improve the hydrophilic properties and permeability of the PEI membrane. With the increase of SPEEK from 3% to 6% in the casting solution, water permeability increased from $24.0 \pm 2.1 \times 10^{-11}$ to $36.6 \pm$

$3.0 \times 10^{-11} \text{ m s}^{-1} \text{ N}^{-1}$. Further, SEM cross-sectional images of the membranes showed a top layer with a sponge-type structure and a support layer with a finger-like structure.

Tao *et al.* (2006) studied the phenomenon PEI membrane formation by the non-solvent system. PEI membrane was prepared by immersion precipitation process by using the *N*-methyl-2-pyrrolidone (NMP) – methylene chloride (MC) cononsolvent as the coagulation medium. The scanning electron microscopy (SEM), showed a typically asymmetrical structure consisting of a thin and dense skin layer, sponge morphology in the cross-section and porous bottom surface. This was due to two solvents serving as a cononsolvent system during the membrane formation by replacing the traditional solvent–nonsolvent pair.

Albrecht *et al.* (2007) have done modification of poly(ether imide) membranes with brominated polyvinylpyrrolidone(Br PVP). The PEI membranes were first aminated with poly(ethylene imine) (Pei) and then coated with BrPVP. The results revealed that PVP layer on the membrane prepared from a high molecular weight BrPVP was resistant against washing out with aqueous solutions. The separation profiles of ultrafiltration PEI membranes can be tailored by the amination and subsequent coating with BrPVP according to the requirements of the application.

Nagendran *et al.* (2008) investigated removal of heavy metal ions such as Ni (II), Cu (II), Cd (II) and Zn (II) by use of CA/ SPEI blend membrane and polyethyleneimine as the complexing agent. SPEI was carried out by chlorosulfonic acid (Figure 1.13). Inclusion of SPEI in the polymer blend increased the permeability and water uptake of the CA membrane. However, the blend membranes showed lower heavy metal removal than neat CA membrane which was attributed to formation of larger pores by addition of hydrophilic SPEI. The observed rejection was in the order Cu (II) > Ni (II) > Zn (II) > Cd (II) which was based on the size of the metal chelate.

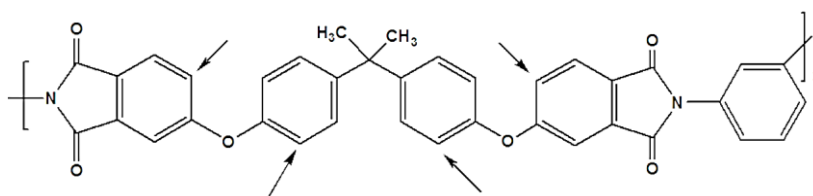
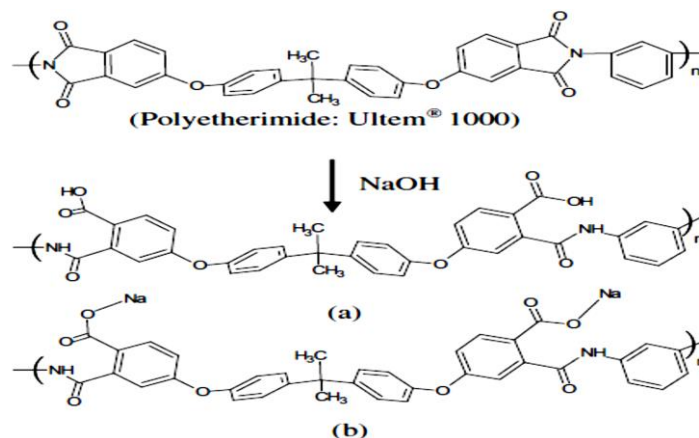


Fig.1.13 Structure of PEI indicating possible positions for sulfonic acid groups to occupy upon sulfonation (Pinto *et al.* 2007)

Kim *et al.* (2009) studied the effects of chemical transition of PEI membranes having an integrally skinned asymmetric structure. The PEI membranes were prepared from an NMP/water system by using the phase inversion process. To estimate the effects of chemical transition on the skin layer of the prepared asymmetric PEI membranes, oxidizing treatment was carried out by using aqueous sodium hydroxide solution. The results showed that the overall prepared membranes exhibited an asymmetric structure composed of a dense skin layer and a porous sub-layer of finger-like type.



Scheme 1.2. Schematic representation of chemical structures of PEI after oxidizing reaction: (a) polyamic acid, (b) sodium salt of polyamic acid.

Chen *et al.* (2010) investigated the effect of PEG additives on properties and morphologies of PEI membranes prepared by phase inversion method. Membranes prepared by changing the ratio of PEG to PEI, were characterized by SEM observations, measurements of water flux and γ -globin rejection. The thermodynamic and kinetic properties of the membrane-forming system were studied through viscosity.

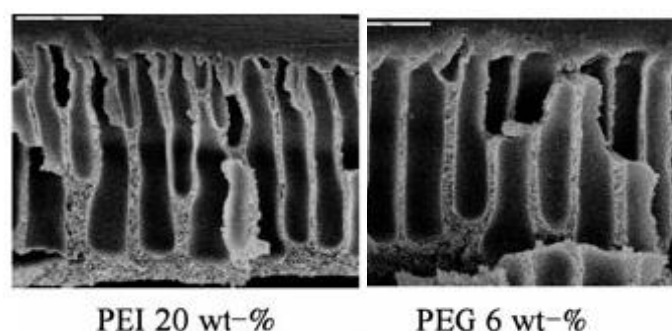
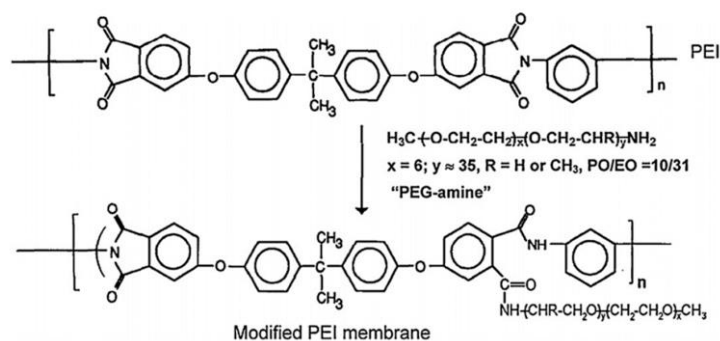


Fig.1.14 Influence PEG on cross-section structure of the PEI membranes

Chinpa *et al.* (2010) reported the simple approach for attaching poly(ethylene glycol) chains onto the surface of asymmetric ultrafiltration PEI membranes. An amino

terminated poly(propylene oxide)/poly(ethylene oxide) block copolymer (PEG-amine) was used as a surface modifying agent. They investigated the effects of the PEG-amine concentration (2 and 10 wt%), modification time (0.5, 1, 3, and 5 h) and treatment temperature on the morphology, hydrophilicity, permeability, and anti-fouling property of the membrane.



Scheme 1.3 Schematic reaction for the change in function of PEI membrane using PEG amine.

Sultan *et al.* (2011) studied the effect of sulfonated poly (ether ether ketone) and PEI blend membranes on viscosity, rheology and morphological properties. The membranes were prepared in five different weight ratios using DMAc as solvent. Cannon–Fenske viscometer was used to study the viscoelastic parameters of the salt-free polyelectrolyte blends and the data obtained was fitted in Fuoss–Strauss equation. The results revealed that storage modulus (G') and dynamic viscosity (η) of the blends varies significantly as compared to pure SPEEK and PEI.

Senthilkuma *et al.* (2013) studied biocompatibility and separation performance of carboxylated PEI incorporated polyacrylonitrile membranes. PEI was carboxylated by activating the PEI backbone with n-butyllithium and subsequent treatment with dry carbon dioxide. This carboxylated form of PEI (CPEI) was then used as the hydrophilic modification agent for the preparation of biocompatible polyacrylonitrile (PAN) hemodialysis membranes. The results revealed that hydrophilicity, permeation rate, molecular weight cut off and protein adsorption resistance of the PAN/CPEI blend membranes were found to be improved considerably as compared to the pure PAN membranes.

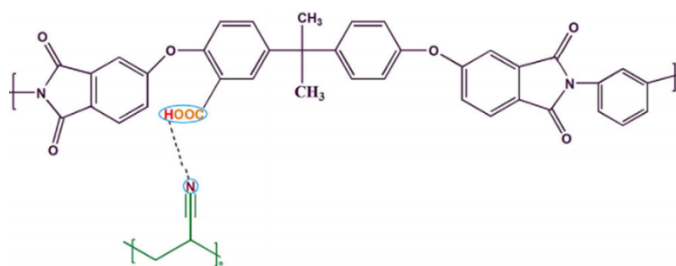


Fig.1.15 Schematic representation of the physical interaction between polyacrylonitrile and carboxylated polyetherimide in PAN/CPEI blend membranes

Bakeri *et al.* (2014) reported the analysis of PEI/NMP /non- solvent phase separation behaviour. The phase separation behaviour of the PEI casting dope was investigated for different types of coagulants and non-solvent additives. Cloud point data were obtained by the titration method on the ternary PEI/solvent/coagulant. The results revealed that, when water, methanol, ethanol, glycerol, and acetic acid were used as the coagulants, the experimental cloud point data fit the LCP relation very well. The slopes of the LCP relation for all the coagulants are greater than unity, as expected from the theory.

Thuyavan *et al.* (2015) studied the effect of incorporation of TiO_2 -sulfonated polymer embedded PEI membranes for effective desalination application. The hybrid membranes were characterized by attenuated total reflection Fourier transform infrared (FTIR) spectroscopy, contact angle and SEM. The modified membrane exhibited a higher flux of $44.75 \text{ L/m}^2 \text{ h}$ and lesser contact angle value of 61.38° . The filtration experiment of three different electrolytes (NaCl , Na_2SO_4 and MgSO_4) with varying concentrations from 50 to 500 mg/L.

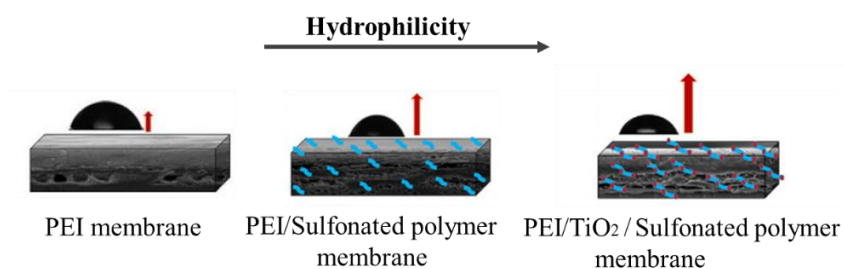


Fig.1.16 Variation in hydrophilicity of hybrid PEI membrane.

Sumisha *et al.* (2015) prepared the functionalized titanate nanotube–PEI nanocomposite membrane for enhanced salt rejection capacity under low pressure nanofiltration. The neat and mixed matrix membrane (MMMs) was prepared using PEI as a polymeric material and nanomaterials such as TiO_2 particles (TP), as-synthesized

hydrogen trititanate nanotubes (pTNT), N-doped TiO₂NT (N-TNT) and Cu-doped H₂Ti₃O₇NT) employed as hydrophilic additives. Interestingly, the salt rejection performance of monovalent (NaCl) and divalent (K₂SO₄ and CaCl₂) ions in the single salt mixture were found to increase in the same order. The salt rejection performance of PEI/Cu-TNT was found in the decreasing order: K₂SO₄ (80%) < NaCl (75%) < CaCl₂ (45%).

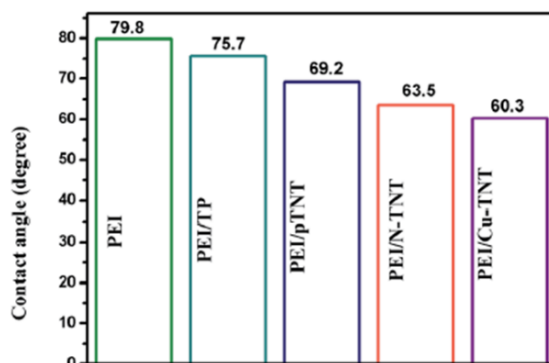


Fig.1.17 Variation in contact angle with different additive dosage.

Wu *et al.* (2016) reported the in-situ preparation of PEI /amino functionalized silica (SiO₂-NH₂) mixed matrix membranes for application in enzyme separation applications. The obtained crosslinked PEI/SiO₂-NH₂ mixed matrix membranes (MMMs) had good solvent resistance. Lysozyme (LZ) adsorption capacity had a maximum value at pH 11 and adsorption equilibrium was achieved in 24 h for both MMMs and crosslinked MMMs.

Mansourizadeh *et al.* (2017) investigated the structure of PEI and polyvinylidene fluoride (PVDF) hollow fiber membranes developed by formulation of the polymer solutions and regulating spinning parameters. The prepared membranes were characterized in terms of morphology, overall porosity, gas permeation, collapsing pressure, wetting resistance and mass transfer resistance. The PEI and PVDF membrane forms finger-like and sponge-like structure, respectively. Both membrane showed good surface porosity due to enhancement of phase inversion by addition of glycerol to the spinning solutions.

1.10 SCOPE OF THE WORK

It is evident from the literature survey that, use of PEI as membrane material has attracted many researchers worldwide for its expanding utility in the field of membrane separation technology. Keeping in view the advantages offered by this material, research is in progress to overcome their existing drawbacks by some suitable modifications in order to make them an ideal membrane material. The possibility of enhancing the membrane

properties in terms of hydrophilicity, porosity, morphology and other physicochemical properties may help in large scale utilization of this material in the near future.

1.11 OBJECTIVES

1. To modify and characterize the nanoparticles with hydrophilic functional groups.
2. To prepare the flat sheet and hollow fiber PEI membranes by incorporating organic, inorganic and nano additives.
3. To determine the modified PEI membrane properties in terms of its water uptake capacity, porosity, zeta potential, and contact angle measurement. Morphological properties are to be studied SEM, AFM, EDX and Elemental mapping analyses.
4. To investigate the performance of the PEI membrane in terms of hydraulic permeation, protein rejection, anti-fouling, and anti-biofouling properties.
5. To study rejection efficacy of modified PEI membranes in terms of toxic heavy metal ions, humic acids and dye removal ability.

CHAPTER 2

PREPARATION AND CHARACTERIZATION OF POLYETHERIMIDE/ HYDROLYZED PIAM BLEND NANOFILTRATION MEMBRANE FOR ANTIFOULING AND SALT REJECTION APPLICATION

Abstract: This chapter deals with the preparation of PEI:hydrolyzed PIAM blend nanofiltration membrane via phase inversion method. The modified membranes were studied in terms of hydrophilicity, water uptake capacity, permeation and antifouling properties. The rejection efficacy of monovalent and multivalent electrolyte were investigated and results are discussed in detail.

In recent years NF membranes have attracted an increasing attention because of their valuable application in water purification. They display separation characteristics in the intermediate range of RO and UF. The NF membranes have created great interest worldwide because of several advantages such as low-operation pressure, high-permeation and high rejection of electrolytes (Hilal *et al.* 2004). One of the most widely accepted model for transport of electrolyte solution through the NF membrane is the Donnan effect, which explains the dependency of charge density on the membrane surface. The charged membranes can be obtained by incorporating suitable functional groups such as carboxylic acid (-COOH), sulfonic acid (-SO₃H), amine (-NH₂) etc. Hence, the type of charge and charge density are important parameter for these membranes (Childress *et al.* 2000, Bruggen *et al.* 2008). To prepare a high performance membrane, a suitable secondary polymer or additive is commonly used, as it extends an effective and convenient way to control the membrane properties.

From the literature it was observed that, PEI membranes have been effectively used for desalination, water treatment, pervaporation, oil–water separation, gas separation, proton-exchange membrane and other applications (Swier *et al.* 2006). However, the extensive usage of PEI membrane in aqueous medium is restricted due to its hydrophobic nature. The hydrophobic membrane suffers from fouling which affect the membrane performance for a prolonged period of time. Thus, preparation of antifouling membrane remains as one of the crucial objective while fabricating new membranes. For this purpose, making membranes more hydrophilic serves as one of the important tool to reduce fouling. Imparting hydrophilicity to the membranes can be achieved by a number of techniques such as blending, tailor made polymers, polymer grafting, incorporation of inorganic oxides, etc. Amongst these, polymer blending is the simplest method to achieve enhanced membrane performance.

Polymer blending has been extensively used to obtain new kind of membrane materials with properties lying between those of pure components. Blending not only alters the properties of the materials, but also have a significant effect on permiselectivity and

permeability of the membrane. The desired properties and good rejection rate in a membrane can be obtained by preparing the membrane via multicomponent polymer blend system (Bowen *et al.* 2005). PEI with cellulose acetate, sulfonated polyphenylsulfone and sulfonated poly(ether ether ketone) constitutes the miscible pairs of blend membranes comprising of considerable changes in membrane properties and performance. Asymmetric and dense membrane can be achieved from homogeneous blend of various polymers. However, properties of such a polymer blend depend on the compatibility and miscibility of the individual polymers as well as on the method of preparation (Shu *et al.* 2008), (Shen *et al.* 2004).

Kim *et al.* (2002) described the fabrication method for uncharged and integrally skinned PEI membrane via dry/ wet phase separation technique. The prepared asymmetric NF membrane exhibited hydraulic permeation rate of 1.27 ton/m² per day with high rejection value of 83 % for PEG 600. Similarly, Bowen *et al.* (2005) reported the fabrication of PEI/ sulfonated poly(ether ether ketone) blend membranes for UF applications. The blend membrane exhibited superior hydrophilicity and higher hydrodynamic permeation rate compared to pristine PEI membrane. Further, applicability of the PEI membranes was illustrated by Nagendran *et al.* (2008). They reported the fabrication of PEI/Cellulose acetate blend membranes for ultrafiltration applications. The resultant blend membranes showed a considerable improvement in antifouling and permeation properties.

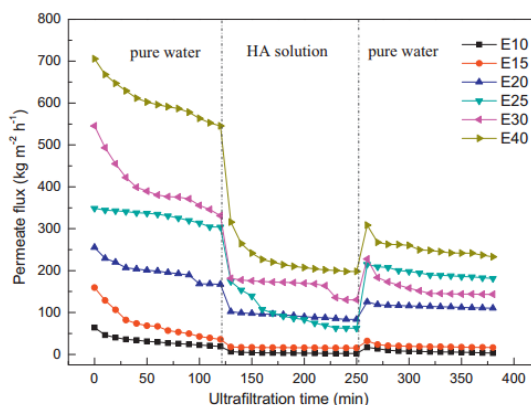


Fig.2.1 Permeation behaviour of blend membranes during the different filtration conditions (Hwang *et al.* 2011)

Hwang *et al.* (2011) reported the preparation of PEI/polyphenylsulfone blend membrane for water treatment applications. They stated that, morphology, hydrophilicity, surface roughness and surface charge were mainly dependent on blending ratio of the polymers. The antifouling and permeation properties of blend membrane can also be

tailored by altering the blending ratio. The permeation behaviour of blend membranes during the different filtration conditions is given Fig.2.1.

Liu *et al.* (2014) reported the preparation of PEI/ sulfonated poly (ether ether ketone) blend membranes. The blend membrane resulted in higher ion exchange capacity (IEC), proton conductivity, water uptake and hydrophilicity. The presence of sulfonated groups in the blend membrane facilitate the transport of water molecules through the membrane leading to higher membrane permeation rate. In addition to this, negatively charged $-\text{SO}_3\text{H}$ group in the membrane aids to form the hydration layer on the membrane thereby reducing the membrane-fouling propensity.

Harsha *et al.* (2015) illustrated the fabrication of blend membrane by using sulfonated PEI and aminated PEI with pristine PEI. The resultant membrane showed higher water uptake capacity, change in morphological feature and hydrophilicity compared to pristine PEI membrane.

Govardhan *et al.* (2017) reported the preparation of PEI/polyethersulfone blend hollow fiber membranes via phase separation method for the purification of surface water. The resultant membrane exhibited the permeability of $250 \text{ L/m}^2 \text{ h}$ with turbidity rejection of 99.65 %. Along with higher permeability, the blend membrane exhibited superior antifouling properties with BSA rejection of 94.2 %. The water permeability and BSA rejection are provided in Fig.2.2.

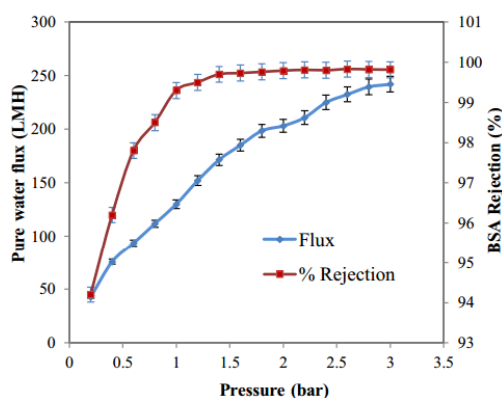


Fig.2.2 Permeability and BSA protein rejection of blend membrane (Govardhan *et al.* 2017)

The poly(isobutylene-alt-maleic anhydride) (PIAM) is another polymer material, which has commonly been used for the preparation NF membranes. PIAM comprises of an aliphatic chain with a repeating anhydride group, which can be easily hydrolysed to give carboxylic functionality. It is well known that, incorporation of carboxylic acid groups not only results in the enhancement of the hydrophilic nature but also imparts charge on the membrane surface. Padaki *et al.* (2011) studied the applicability of PIAM and polysulfone

blend membrane for desalination process before and after alkali treatment. These membranes were also tested for salt rejection, flux and water-swelling studies. The results clearly indicate that the salt rejection and flux was less before alkali treatment. However, alkali treatment has resulted in hydrolysis of the anhydride bonds to form the acid groups, which resulted in the formation of nanopores on the membranes (Fig.2.3). Among the tested salt solutions, Na_2SO_4 showed maximum salt rejection, because of the Donnan effect. Higher the concentration of PIAM, higher was the salt rejection and flux due to an increased surface charge.

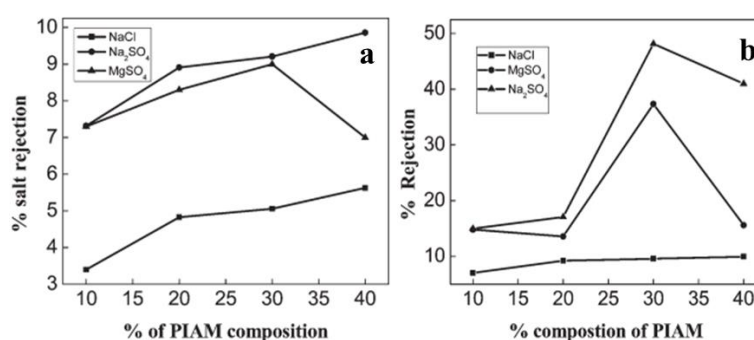


Fig.2.3 Percentage salt rejection of a) before hydrolysis of PIAM and b) after hydrolysis of PIAM (Padaki *et al.* (2011))

In this chapter, fabrication of PEI/ hydrolysed PIAM blend membranes were carried out via phase inversion method with different blend composition. The properties of the blend membrane were evaluated in terms of hydrophilicity, ion exchange capacity (IEC), pure water flux (PWF) and antifouling property. The salt rejection behavior of the membrane was investigated by using 1000 ppm electrolyte solutions of sodium chloride, sodium sulphate and magnesium sulphate.

2.1 EXPERIMENTAL PART

2.1.1 Materials

PEI ($M_w = 35,000\text{Da}$), PIAM ($M_w = 3,000\text{Da}$) were purchased from Sigma Aldrich (India). N-methyl-2-pyrrolidone (NMP) of analytical-grade purity was obtained from Merck, India. BSA was purchased from Central Drug House (CDH), New Delhi, India. 1000 ppm solutions of Na_2SO_4 , MgSO_4 , NaCl were used as feed solutions for rejection studies. The concentration of feed and permeate solutions were measured using EQ-660A conductivity meter (Equiptronics, India).

2.1.2 Preparation of blend membranes

The PEI and PIAM blend membranes with different compositions were prepared by phase inversion method. Both PEI and PIAM were dried in vacuum over 10 h at 80 °C before use. The polymers with desired ratio were dissolved in NMP at 60 °C for 16 h on a hot plate to get a clear homogenous solution. The solution was kept at same temperature for at least 6 h to remove any trapped air bubbles. The homogenous polymer solution was then casted over the glass plate using doctor's blade. The casted film was immersed in a non-solvent (water) bath. Later the membrane was dipped in 0.1% NaOH solution for 20 h at room temperature in order to hydrolyze the anhydride group of PIAM (Fig.2.4). The hydrolyzed membranes were washed with distilled water several times to remove all the traces of the sodium hydroxide solution until washing solution reaches neutral pH and dried before further analysis.

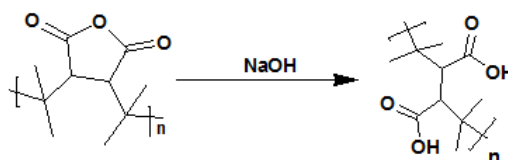


Fig.2.4 Scheme for the hydrolysis of PIAM

2.2 MEMBRANE CHARACTERIZATION

2.2.1 FTIR analysis

The hydrolysis of anhydride to acid group of PIAM was determined by taking IR spectrum of membrane before and after hydrolysis. FTIR spectra were recorded using Avatar 360 IR spectrophotometer in the range of 4000-400 cm^{-1} . The changes in the characteristic peaks of spectra are discussed in results and discussion.

2.2.3 Membrane morphology

The cross-section image of the membrane was taken with JEOL JSM-6380LA SEM instrument. Before commencing the analysis, membrane samples were dried and then fractured cryogenically in liquid nitrogen. By using sputtering device, samples were smeared with gold in order to obtain conductance.

2.2.4 Water uptake, contact angle measurement and ion exchange capacity

The water content of the membrane was determined by dipping the membranes (2 cm^2) in water for 24 h and weighed after pressing with blotting paper. Then wet membranes were placed in a vacuum oven at 70 °C for 45 h and the dry weights were determined (Kumar *et al.* 2013). The percentage water content was calculated using equation (2.1)

$$\% \text{ uptake} = \left(\frac{W_w - W_d}{W_d} \right) \times 100 \quad (2.1)$$

Where ' W_w ' and ' W_d ' are the sample weights after swelling for 24 h under wet and dry conditions respectively. For each membrane, five samples were examined and the average values are reported.

The hydrophilic property of the membrane was analyzed by the water contact angle (WCA) measurement. It was measured using FTA-200 Dynamic contact angle analyzer according to the sessile droplet method. In order to minimize the experimental errors, the WCA measurement of each sample was measured five times and average value is reported.

Ion exchange capacity (IEC) of the membrane was measured by using conventional titration method. The membrane in H^+ form was immersed in a 2 M NaCl solution for 24 h to replace H^+ with Na^+ completely. The remaining solution was then titrated against 0.01 M of NaOH, using phenolphthalein indicator. The IEC value was calculated using equation

$$IEC(\text{mmol/g}) = \frac{0.01 \times 1000 \times V}{W_d}$$

Where, ' V ' is the volume of NaOH solution consumed for titration (L) and ' W_d ' is the weight of the dry membrane sample (g).

2.2.5. Permeation properties

The performance of the membranes was analyzed using a self-constructed dead end filtration cell at room temperature. The membrane with an effective area of 5 cm^2 was dipped in distilled water for 24 h before starting the permeation experiment. Initially each membrane was compacted at 0.5 MPa for about 1 h and then it was reduced to 0.4 MPa to obtain the pure water flux (' J_{w1} ', $L/m^2 \text{ h}$). Then the flux was measured for every 10 min interval. The pure water flux (PWF), ' J_w ' was calculated using equation (2.2)

$$J_w = \frac{Q}{\Delta t A} \quad (2.2)$$

Where ' J_w ' is expressed in $L/m^2 \text{ h}$ and ' Q ' is the amount of water collected for ' Δt ' (h) time duration using a membrane of area ' A ' (m^2).

2.2.6. Porosity of the membrane

The overall porosity (ε) was determined by gravimetric method (Liao *et al.* 2012), as defined in the equation (2.3)

$$\varepsilon = \frac{W_1 - W_2}{A \times l \times d_w} \quad (2.3)$$

Where ' W_1 ' is weight of the wet membrane, ' W_2 ' is weight of the dry membrane, ' A ' is the membrane effective area (m^2), ' d_w ' is the water density (0.998 g/cm^3) and ' l ' is the membrane thickness (m).

2.2.7. Antifouling properties

The antifouling property of the membranes was determined using reported procedure as in literature (Oh *et al.* 2009). Briefly, the PWF of the membrane was determined ' J_{w1} ' (L/m^2h) at 0.4 MPa TMP. Antifouling property of membrane was investigated by considering Bovine Serum Albumin (BSA) as a model protein. The BSA solution was prepared with concentration of 0.8 g/L and passed through the membrane for 80 min. After BSA filtration, membrane was thoroughly washed with pure water for 15 minutes and again PWF, ' J_{w2} ' (L/m^2h) was measured. Finally, the antifouling property of membrane was determined by flux recovery ratio (FRR) using the equation (2.4)

$$FRR(\%) = \frac{J_{w2}}{J_{w1}} \times 100 \quad (2.4)$$

2.2.8. Salt rejection studies

The salt rejection performance of all membranes was carried out by using self-constructed dead end filtration cell. The feed solutions of NaCl, Na_2SO_4 and $MgSO_4$ with concentration of 1000 ppm were used for the rejection study. The feed solution was filled into a feed tank and pressurized as required using a nitrogen cylinder. Then permeate was collected for a particular interval of time and the concentration of the solution was measured in terms of conductivity. Then percentage of salt rejection was determined by using equation (2.5).

$$\%R = \left(1 - \frac{C_p}{C_f}\right) \times 100 \quad (2.5)$$

Where ' C_p ' and ' C_f ' are concentrations of permeate and feed respectively. In order to minimize the experimental error, the salt rejection experiment was carried out three times for each membrane and the average value reported.

2.3. RESULTS AND DISCUSSIONS

2.3.1 FTIR analysis

The FTIR spectrum confirms the conversion of anhydride functionality to acid groups after hydrolysis (Fig.2.5). As shown in Fig.2.5, (b) showed broad -OH stretching at 3481cm^{-1} and carboxylic carbonyl stretching at 1724 cm^{-1} . Before hydrolysis, PM1 membrane showed spectral peaks at 1855 cm^{-1} and 1772 cm^{-1} which corresponds to anhydride carbonyl group stretching.

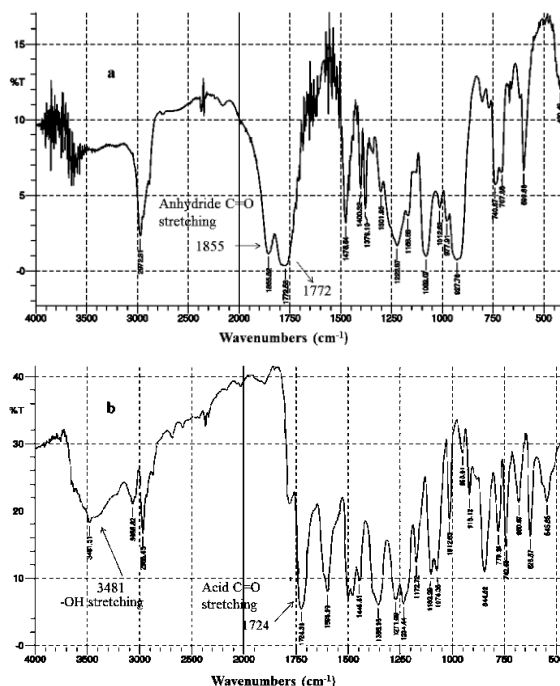


Fig. 2.5 FTIR spectra of (a) before hydrolysis of PIAM and (b) after hydrolysis of PIAM

2.3.2 Ion exchange Capacity

The IEC value of membranes signifies the bulk charge present on the membrane surface and thus confirms the presence of carboxylic acid. Since the percentage of hydrolysed PIAM was less than that of PEI, the IEC of all the membranes was low. The measured IEC values are given in Table 2.1. The membrane PM-4 showed highest IEC value of 0.877 mmol/g , whereas the membrane PM-1 showed least IEC value of 0.519 mmol/g . This is attributed to the content of hydrolysed PIAM in the membranes. As the content of hydrolysed PIAM in the membranes increases from PM-1 to PM-4, the carboxylic acid groups on the membrane surface available for ion exchange also increases, hence the IEC also increases.

Table 2.1 Composition and properties of the membranes.

Membrane code	Composition PEI:Hydrolysed PIAM	Water uptake (%)	IEC (mmol/g)
PM-1	95:5	59	0.519
PM-2	90:10	62	0.649
PM-3	85:15	69	0.784
PM-4	80:20	78	0.877

2.3.3 Water uptake capacity and contact angle measurement

In order to understand the hydrophilicity of prepared membranes, water uptake capacity and contact angle measurements were performed. The obtained contact angle results were presented in Fig.2.6. It was noticed that, PM-1 exhibits the highest contact angle of 56.39 °, corresponding to the lowest hydrophilicity among the prepared blend membranes, whereas PM-4 showed a contact angle of 43.08 °. This clearly indicated that, an increased content of hydrolysed PIAM enhanced the hydrophilicity of the membrane. Water swelling behavior of the membranes is displayed in Table 2.1. It can be noticed that, uppermost water uptake observed was 78.8 % and the minimum was 59.1%. The membrane with highest percentage of hydrolysed PIAM exhibited maximum water uptake which provides an evidence for the fact that the increase in number of carboxylic group enhances the hydrophilic nature of the membrane.

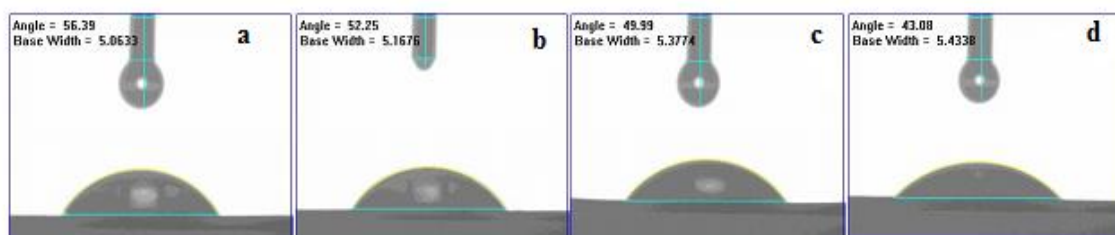


Fig. 2.6 Digital images of contact angles of (a) PM-1, (b) PM-2, (c) PM-3 and (d) PM-4.

2.3.4 Morphology of the membrane

Cross-sectional SEM images of the blend membranes are shown in Fig. 2.7. The morphology of blend membranes were found to be very similar to that of asymmetric membranes which consists of a top skin layer and a sublayer with finger like substructure. In the prepared blend membranes, as there is an increase in the concentration of hydrolysed PIAM, there was a considerable change in the morphology of the membranes. This may be due to the secondary force of interaction between dicarboxylic acid, nitrogen and oxygen

of the imide group of PEI. The complex formation thereby causes a decrease in polymer chain flexibility (Wienk *et al.* 1996). This may be attributed to the change in the morphology as well as membrane properties. Also the stability of PEI and acid complex is stronger if the interaction between the acid and the water in the coagulation bath is lower i.e. when solubility of dicarboxylic acid in water is less (Matsuda 1991). This was supported by the lower solubility of hydrolysed PIAM in water. This may cause the delayed phase separation process, as a result polymer precipitates slowly and thus creates spongy like structure. These parameters may cause the visible changes in the morphological features of the blend membranes.

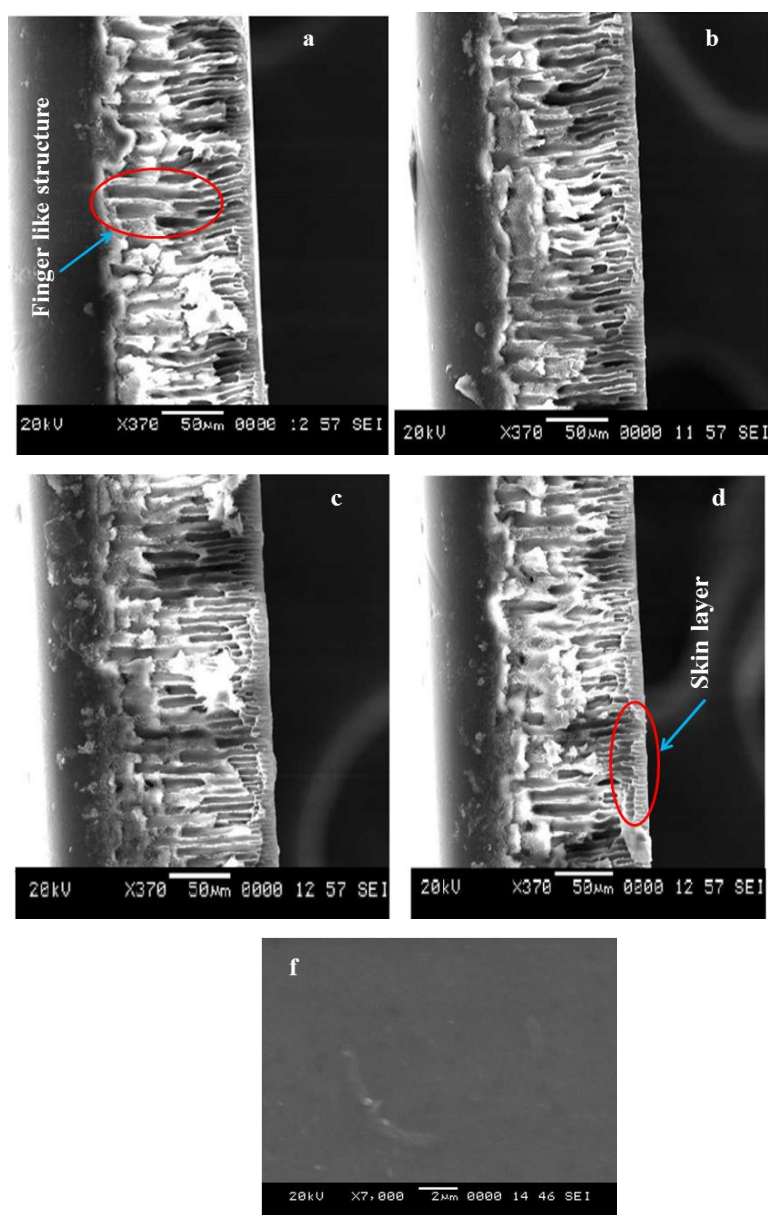


Fig.2.7 Cross sectional SEM images of (a) PM-1, (b) PM-2, (c) PM-3, (d) PM-4 membranes and (f) surface image of PM4 membrane.

2.3.5 Permeation and antifouling properties

The filtration experiments were conducted to investigate the permeability and antifouling property of the membranes. Fig.2.8 represents the pure water flux of the blend membranes at 4-bar pressure. PM-4 shows maximum PWF of 11.8 L/m²h compared to other membranes. This is due to the presence of more number of hydrophilic –COOH groups in the membrane, which resulted in good interaction between the acid and water molecules (Bakeri *et al.* 2010).

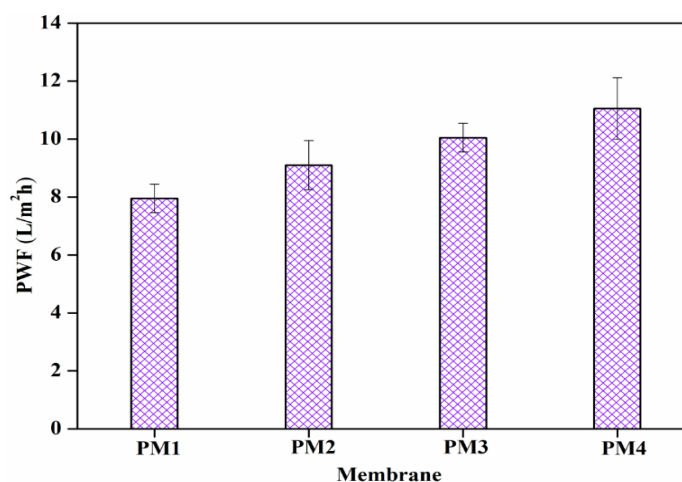


Fig.2.8 Pure water flux of membranes at 0.4 MPa pressure

Membrane fouling deteriorates the membrane performance, resulting in flux decline, membrane degradation and also affects the membrane properties. Fouling occurs due to the adsorption and deposition of particulates on the membrane surface and also in the pores (Rana *et al.* 2010). Fig.2.9 shows the flux of the prepared blend membranes performed at 4 bar pressure under different environments i.e before BSA filtration, during BSA filtration and after BSA filtration. The initial flux decline of all blend membranes is due to the mechanical deformation (Wang *et al.* 2006). During the BSA rejection study there was flux decline due to adsorption or deposition of protein molecules on the membrane surface (Huisman *et al.* 2000). The prepared membranes are hydrophilic in nature, therefore they show lesser affinity towards protein binding. In addition to this, presence of hydrophilic –COOH functional groups impart the negative charge on the membrane which repels negatively charged BSA molecules at neutral pH (isoelectric point of BSA molecules at neutral pH is around 4.5–5.0, therefore the protein is negatively charged at neutral pH). The estimation of flux recovery ratio (FRR) is the best method for analyzing the antifouling properties of the membranes. FRR value was highest for PM-4 membrane i.e. 73 % indicating good reversible nature of membrane.

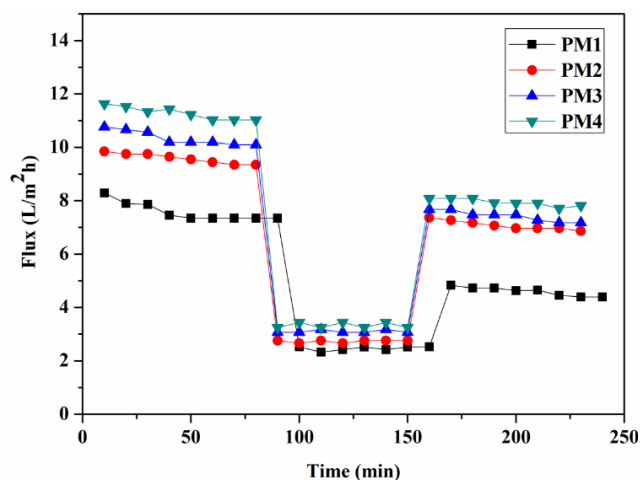


Fig.2.9 Time dependent flux of PEI/ hydrolyzed PIAM membranes at 0.4 MPa TMP during three different conditions.

2.3.6 Salt rejection study

All the membranes were subjected to electrolyte rejection study at 4 bar pressure (Fig. 2.10). The rejections of different membranes are in the order of $\text{Na}_2\text{SO}_4 > \text{MgSO}_4 > \text{NaCl}$. The PM-4 membrane showed maximum rejection of sodium sulphate up to 77 % with higher content of hydrolyzed PIAM. Generally, this trend of rejection in NF membrane can be explained on the basis of Donnan effect and size exclusion mechanism. When a membrane comes in contact with an electrolytic solution, it acquires charge by certain phenomena like adsorption of ions from the solutions or dissociation of surface functional groups (Wang *et al.* 2005). The presence of $-\text{COOH}$ groups on the membrane back bone makes it negatively charged. When such a membrane comes in contact with the electrolyte solution, the membrane will have higher concentration of oppositely charged ions (counter-ions) on the surface than in the solution, whereas the concentration of co-ions (ions having same charge as that of the membrane) will be higher in the solution than on the membrane. This difference in concentration of the ions gives rise to the potential difference between the membrane and the solution at their interface. Thus in order to maintain the electrochemical equilibrium between solution and membrane, equal number of counter ions are repelled by the membrane surface (Bruni *et al.* 2008).

Also it was observed that, rejection of electrolytes decrease to 52 %, 39 %, 10 % of sodium sulphate, magnesium sulphate and sodium chloride respectively with increase in pressure up to 10 bar (Fig.2.11). With increase in TMP, convective transport of the electrolyte through the NF membrane dominates over diffusive and electrostatic repulsion

resulting an enhanced permeate salt concentration and decline of rejection (Peeters *et al.* 1998).

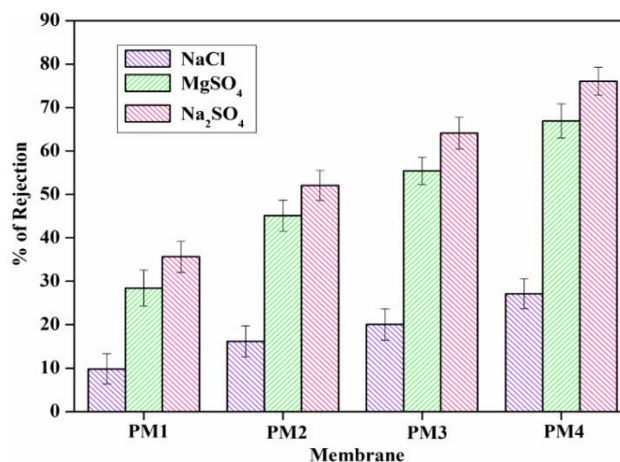


Fig. 2.10 Electrolyte rejection study of membranes at 0.4 MPa pressure

The higher rejection of the MgSO₄ and Na₂SO₄ over NaCl can be explained on the basis of charge density. The order of rejection, SO₄²⁻ > Cl⁻ is due to the higher anion charge density of SO₄²⁻ in MgSO₄ and Na₂SO₄ than that of Cl⁻ in NaCl. As a result, the anion repulsion forces become progressively weaker. Also rejection of the membrane depends on the electrostatic interaction between ion and membrane surface. The higher rejection of Na₂SO₄ over MgSO₄ is due to the increasing order of cation positive charge density Na⁺ > Mg²⁺. Hence the attraction forces acting on the cations Mg²⁺ and Na⁺ become progressively stronger and higher affinity of Na⁺ ions towards -COOH group of the membrane than Mg²⁺ contributes to the higher rejection (Kumar *et al.* 2013).

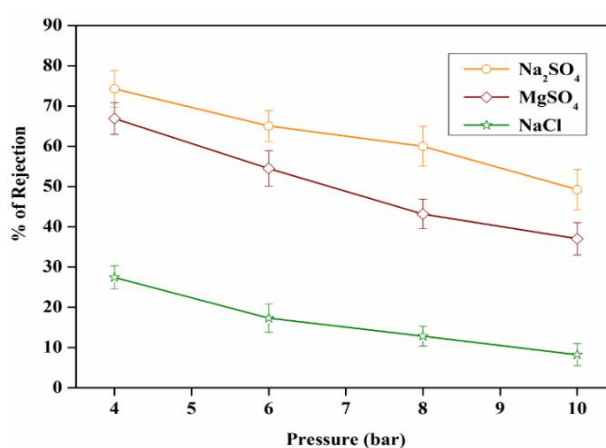


Fig. 2.11 Pressure dependent electrolyte rejection of PM-4 membrane

2.4 CONCLUSIONS

In the present work, PEI/hydrolyzed PIAM blend membranes were prepared by phase inversion method with different compositions. The presence of dicarboxylic acid due to hydrolysed PIAM in the membrane increased the hydrophilicity of the membranes and reduced the pore size of the membranes. PM-4 membrane showed highest pure water flux of 11.8 L/m² h with lowest pressure and maximum FRR value up to 73 %. Also the membranes being negatively charged, showed good rejection for electrolytes. Of all the membranes, membrane PM-4 showed maximum rejection for electrolytes and exhibited rejection in the order of Na₂SO₄ > MgSO₄ > NaCl at lowest pressure. In conclusion, the presence of dicarboxylic group greatly affected the morphology of the membranes enhancing hydrophilicity, flux, rejection and antifouling properties of the blend membranes.

CHAPTER 3

**MORPHOLOGY AND ANTIORGANIC FOULING
BEHAVIOUR OF THE POLYETHERIMIDE MEMBRANE
MODIFIED WITH HYDROPHILIC ORGANIC ACIDS AS
ADDITIVES**

Abstract: In continuation of the research work to improve the physicochemical properties and rejection performance of the membranes, an effort has been made to utilise hydrophilic organic acids as additives. In this chapter effect of organic acids in the membrane morphology, contact angle, permeation and antifouling behaviour were studied in detail. The humic acid rejection and relative flux decline were also investigated and reported.

In order to improve the polymer membrane performance, many methods have been employed in contemporary scenario. It includes polymer modification, blending and surface modification. Among these methods, addition of hydrophilic additive into the membrane matrix is also an effective technique to improve the performance. In this regard, many organic additives have been tried to improve membrane properties and performance. Initially, Chuang et al. (2000) reported the role of acetic acid (AA) as an additive in the formation of poly (vinyl alcohol) (PVA) membranes. The results revealed that, the AA additive exerts strong impact on the morphology and other properties of the membrane. Kim et al. (2003) reported the effect of an additive on the pore size of the polysulfone membrane by the phase inversion method. The results revealed that γ -butyrolactone additive increased the pore size of the membrane because of its higher miscibility with water than NMP.

Zhang et al. (2011) investigated the influence of formamide (FM) additive on physicochemical properties and permeation behavior of PEI membrane. With the increase of FM concentration, the casting solution becomes thermodynamically unstable and easier to cause casting solution demixing, however the precipitation rate decreases because of the increased viscosity of the casting solution (Fig.3.1). Moreover, the structure and morphology strongly depends on the concentration of FM in the casting solution.

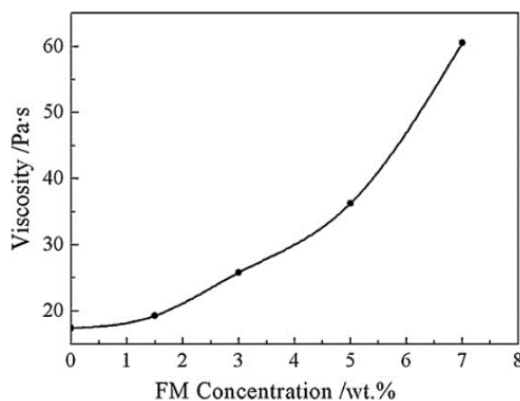


Fig 3.1. Effects of FM concentration on the viscosity of the casting solution. (Zhang et al. 2011).

Rahimpour et al. (2011) used hydrophilic monomer as an additive to enhance the surface properties and performance of nano-porous polyethersulfone membranes. Acrylic acid or 2-hydroxyethylmethacrylate (HEMA) was used as additive in casting solution while preparing the polyethersulfone membrane via phase inversion method. The mixture of water (80 vol. %) and 2-propanol (IPA, 20 vol. %) was employed as gelation media. The experimental results showed that, the protein rejection and milk water permeation were improved at these conditions (Fig.3.2).

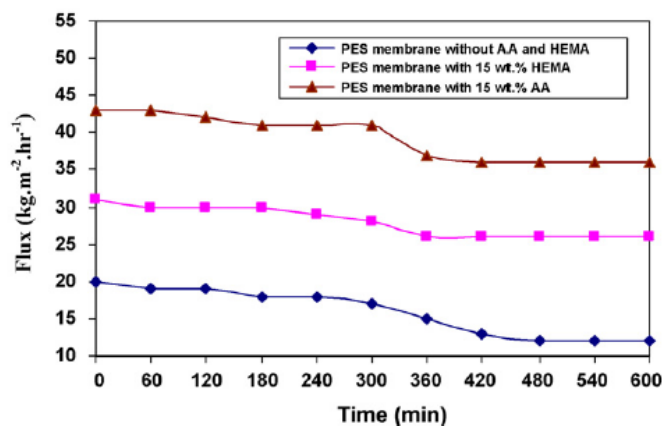


Fig.3.2 Effect of acrylic acid and HEMA in the casting solution on flux stability of membranes during milk filtration at long time. (Rahimpour et al. 2011)

Ghaemi et al. (2012) investigated the influence of low molecular weight organic acids such as ascorbic acid, citric acid and maleic acid additives on membrane properties and permeability. They showed that, membrane with these acids exhibited higher water flux, permeation and rejection compared to pristine polysulfone membrane. The water contact angle measurements proved that, the hydrophilicity of polysulfone membrane strongly increases by increasing the concentration of additives in the casting solution.

Kumar et al. (2013) prepared novel N-succinyl chitosan (NSCS) derivative containing a terminal phosphonic acid functional group as an additive. The polysulfone/NSCS blend membranes showed enhanced hydrophilicity and permeation fluxes compared to the pristine polysulfone membrane. The maximum flux recovery ratio (FRR) of 70 % was observed by the polysulfone /NSCS blend membrane with 20 % NSCS content. The modified membranes exhibited an improved hydrophilicity and antifouling properties as compared to pristine polysulfone membrane.

Lopes et al. (2014) investigated the effect of hyaluronic acid on cellulose acetate membrane properties and performance. After the immobilisation of hyaluronic acid into the membrane matrix, thermal stability, surface roughness and hydrophilicity changed

significantly. The hyaluronic acid can strongly interact with membrane thereby changing the membrane properties.

Sharma and Purkait (2016) reported the influence of racemic and enantiomeric effect of tartaric acid on polysulfone membrane for the removal of crystal violet dye. The resultant membrane showed the higher hydrophilicity, porosity and hydrodynamic permeation compared to pristine polysulfone membrane. From the literature, it was observed that the presence of low molecular weight organic additives offers an effective and convenient way to enhance the membrane performance with high permeability and antifouling properties.

This chapter emphasizes the effect of low molecular weight organic additive in the casting solution on the resultant membrane morphology and permeation properties. Ascorbic acid, citric acid and maleic acid containing different functional groups were used as additives and their influence on the casting solution were analysed by viscosity measurements. The characteristics of the resultant membrane were investigated in terms of water uptake capacity, water contact angle measurement, surface roughness, morphological features and permeation properties. Further, the organic antifouling behaviour of the membrane was estimated by using BSA and humic acid as model foulants.

3.1 MATERIALS AND METHODS

3.1.1 Materials

Additives such as ascorbic acid, citric acid and maleic acid were procured from Merck, India. Humic acid was obtained from Himedia, India. The polyvinylpyrrolidone (PVP) was purchased from Sigma Aldrich, India.

3.1.2 Preparation of Membranes

PEI membranes were prepared with various low molecular weight organic acids as additives. The membrane has been prepared according to the procedure given in chapter-2, Section 2.1.2. In brief, desired quantities of ratio of PEI and PVP (pore forming agent) were dissolved in the desired volume of NMP at 60°C. The obtained homogeneous solution was casted over the glass plate and gently immersed in water bath for the phase inversion. The detailed composition of the casting solution is presented in Table 3.1.

Table 3.1 Composition of casting solution

Membrane	Additive	PEI (wt. %)	NMP (wt. %)	PVP (wt. %)	Additive (wt. %)
PMA-0	-	18	80	2.0	-
PMA-1	Ascorbic acid	18	79	2.0	1.0
PMA-2	Maleic acid	18	79	2.0	1.0
PMA-3	Citric acid	18	79	2.0	1.0

3.2 MEMBRANE CHARACTERIZATION

3.2.1. AFM analysis

Atomic force microscopy (AFM) was used to examine the changes in the topography and surface roughness of the prepared membranes after the addition of low molecular weight organic acid as additives. Images of the dry samples were taken using Anova SPM Atomic Force Microscope. A small piece of the membranes (almost 1 cm²) were cut and glued on a glass substrate and images were taken.

3.2.2. Viscosity measurement

The Brookfield DV-III Ultra (USA) instrument was used to measure the viscosity of the casting solution. The viscosity was determined by using cup/cone geometry at 90/s shear rate, 22 rpm and 45 °C.

3.2.3 Antifouling properties

The antifouling behaviour of all prepared membranes was analyzed using the reported procedure as in literature (Seema et al. 2014). In brief, each membrane was subjected to compaction for an initial 30 min at 0.3 MPa. Then the pressure was reduced to 0.2 MPa and PWF of the membrane was determined ' J_{w1} ' (L/m²h) at 0.2 MPa TMP. The BSA solution was prepared with concentration of 0.8 g/L and passed through the membrane for 80 minutes. After BSA filtration, membrane was thoroughly washed with distilled water for 20 minutes and again PWF, ' J_{w2} ' (L/m²h) was measured. Finally, the antifouling performance of the membrane was calculated in terms of flux recovery ratio (FRR) using the equation.

$$FRR(\%) = \left(\frac{J_{w2}}{J_{w1}} \right) \times 100 \quad (3.1)$$

Generally, higher FRR signifies a better antifouling behaviour of the membranes. Also, in order to examine the fouling processes, following studies were carried out.

The total protein fouling (R_t) produced by the membrane after BSA filtration was calculated by equation.

$$R_t(\%) = \left(\frac{J_{w1} - J_p}{J_{w1}} \right) \times 100 \quad (3.2)$$

The flux loss caused from both reversible and irreversible protein fouling (R_r and R_{ir}), were calculated using equation

$$R_r(\%) = \left(\frac{J_{w2} - J_p}{J_{w1}} \right) \times 100 \quad (3.3)$$

$$R_{ir}(\%) = \left(\frac{J_{w1} - J_{w2}}{J_{w1}} \right) \times 100 \quad (3.4)$$

3.2.4 Humic acid rejection study

Humic acid rejection behaviour of PEI membranes was carried out with the 50 mg/L humic acid solution in the feed tank. In order to study the relative flux of the membrane, the PWF was evaluated before investigating the humic acid resistance behaviour of the membrane. The flux decline was measured in terms of relative fluxes.

The humic acid rejection efficiency of the membrane was tested by the filtration experiments. The concentration of humic acid solution in the feed tank and permeate solutions was measured by a UV-Vis spectrometer at a wavelength of 254 nm. The humic acid rejection efficiency of the membrane was determined by using equation

$$\%R = \left(1 - \frac{C_p}{C_f} \right) \times 100 \quad (3.5)$$

Where ' C_f ' and ' C_p ' (mg mL^{-1}) are the concentration of the humic acid in the feed and permeate respectively.

3.3 RESULTS AND DISCUSSIONS

3.3.1 ATR-IR spectroscopy

The incorporation of low molecular weight organic acids as additives in the PEI membrane was confirmed by IR spectrum. Fig 3.3 shows IR stretching bands at 1725 cm^{-1} and 1782 cm^{-1} related to -C=O symmetric and asymmetric stretching respectively. Also, the presence of broad peak around $3000\text{--}3400 \text{ cm}^{-1}$ corresponds to the stretching of -O-H functional groups of the additives.

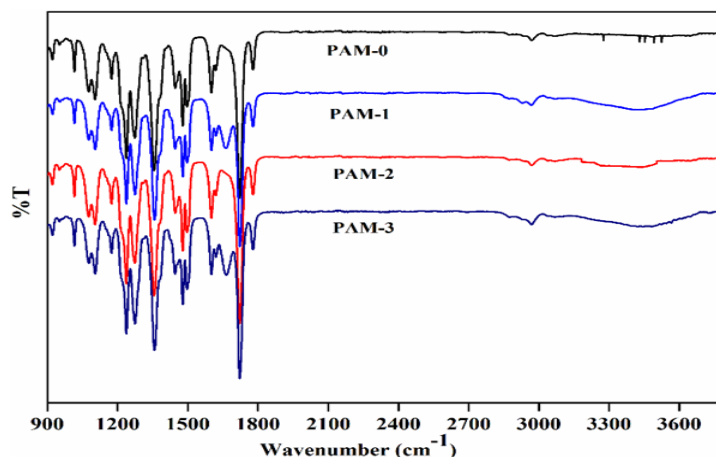


Fig 3.3 FT-IR spectra of prepared membranes

3.3.2 Water uptake and contact angle

The water uptake capacity of any membrane primarily depends on two parameters, firstly on the number of hydrophilic sites present in membrane matrix and secondly, on the morphology i.e., the presence of macrovoids in the membrane sub-layer (Ganesh et al. 2013). It can be noticed from the results presented in the Table 3.2 that all the membranes are having a higher water uptake capacity compared to PMA-0 membrane. PMA-3 membrane exhibited a maximum of 76.5 %, since citric acid offers more hydrophilicity than other additives. SEM images showed that the presence of these acids in the casting solution caused an increased formation of macrovoids in the membrane sublayer. Due to this, membrane can hold more water molecules and thus increases the overall water uptake capacity.

Contact angle of the membranes were measured by the sessile drop method. The presence of additives showed a decreasing trend of contact angle in the order of PMA-0 > PMA-1 > PMA-2 > PMA-3. In general, the smaller contact angle corresponds to the membrane with more hydrophilic nature. The pristine PEI membrane showed higher contact angle of 79.4°, whereas membrane with citric acid as an additive possessed contact angle of 68.8°. The significant change in the surface hydrophilicity of the membranes after addition of these additives into the PEI casting solution can be attributed to the presence of hydrophilic functional groups. Citric acid consists of three ionisable hydrogen atoms and it easily forms strong dipole interaction ($-\text{COO}^- \cdots \text{H}$) with water molecules. This mechanism helps to hold the water molecules on the surface of the membranes.

Table 3.2 Properties of the membranes

Membrane	Membrane thickness (μm)	Water uptake (%)	Viscosity (mPa.s)	Contact angle ($^{\circ}$)
PMA-0	121	58	270	79
PMA-1	123	72	490	75
PMA-2	120	69	382	73
PMA-3	122	76	650	68

3.3.3 Rheological properties of the casting solutions

The rheology of the casting solution has major influence on the exchange rate of non-solvent and solvent during the phase inversion and thus, it can be utilized as an important parameter to change the precipitation kinetics and consequently, the formation of resulting membrane morphology (Rahimpour et al. 2010). The additive showed an increase in viscosity of the casting solution (Table 3.2) and high viscosity of the casting solution decreases the diffusional exchange rate of the non-solvent (water) and solvent (NMP) during the membrane formation process. This can contribute to delayed demixing and consequently formation of thinner skin layer and larger macrovoids in the sub-layer.

3.3.4 Effect of additive on morphology of the membrane

The SEM was employed to study the morphological changes in membranes, which plays a significant role in performance and selectivity of the membranes. During membrane preparation, casted polymer film was gently immersed in a coagulation bath containing water as non-solvent. Upon immersion, non-solvent (water) entused inward into the cast film from the coagulation bath. This enforced a remarkable change in the driving force across cast film. At the same time, the polymer rich phase allowed water molecule (non - solvent) to equilibrate between the internal and external phases of polymer film before significant outward diffusion of NMP (solvent) molecules. Hence, the influx of water molecule was predominantly high as compared to the out flux of NMP. This is because of the large diffusion coefficient of tiny water molecules compared to that of the much bulkier organic solvent molecule (Rajesh et al. 2011). From Fig 3.4, it is clear that, all the prepared membranes have typical asymmetric structures, which consists of the thin skin layer and the porous sub layer. Further the effect of low molecular weight organic additives such as citric acid, ascorbic acid and maleic acid was studied. The changes in the morphology with different additives discussed below.

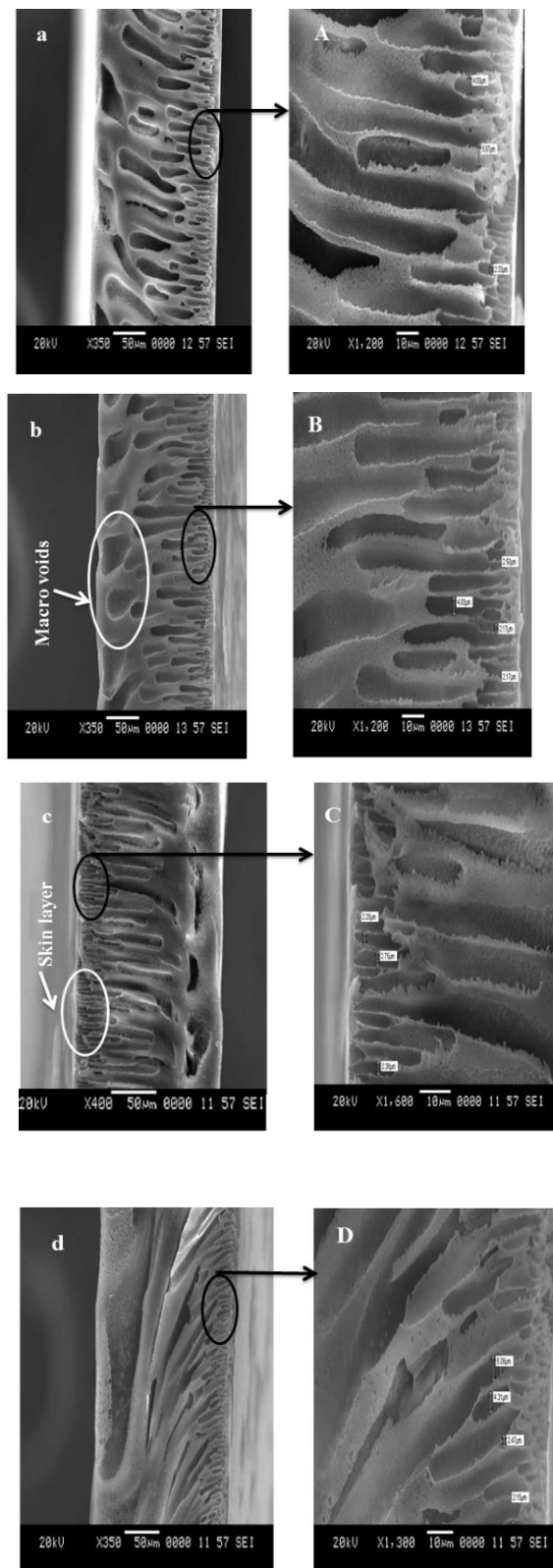


Fig.3.4 Cross sectional and magnified cross sectional SEM images of a, A) PMA-0, b, B) PMA-1, c, C) PMA-2 and d, D) PMA-3 membrane

3.3.4.1. Citric acid

There is formation of asymmetric structures with thinner skin layer thickness in PMA-3 compared to PMA-0 membranes (Fig.3.4 (d)). The induced changes in membrane morphology may be due to the interaction between components in the casting solution. The addition of citric acid into the casting solution may result in the formation of the secondary intermolecular force of interaction with the polymer chains. Different types of secondary forces such as hydrogen bonding, dipole interaction and dispersion forces reduces interaction among polymer chains. In addition, due to the hydrophilic nature of the citric acid, there is possibility for the formation of hydrogen bonds with solvent (NMP) molecule also (Ghaemi et al. 2012). Both the phenomenon exhibited decreased outflow rate of solvent (NMP) and increased inflow rate of non-solvent (water), which resulted in delayed demixing in the coagulation bath. Therefore, the growth of skin layer is reduced and formation of finger-like pores (or macrovoid in the sub layer is improved).

3.3.4.2 Ascorbic acid

The change in the morphological features like decline of skin layer thickness and formation of macrovoids in the sub-layer can be described in the same way as in the case of citric acid. (a) Decrease in the interactions between polymer chains due to the formation of secondary intermolecular force of interaction between ascorbic acid and polymer chains. (b) Increase in the inflow of water molecule (non-solvent) and decrease in the solvent (NMP) outflow because of the hydrophilic nature of ascorbic acid (c). Also, there may be formation of hydrogen bonding between solvent and ascorbic acid (Ghaemi et al. 2012). Eventually, the rate of demixing affects the membrane formation with a thinner top-layer thickness and formation of macro-voids in the sub-layer compared to the pristine PEI membrane

3.3.4.3 Maleic acid

Maleic acid is a dicarboxylic acid employed as another additive in the preparation of PEI casting solution. The change in the morphological features compared to the neat PEI membrane can be explained similarly as above.

3.3.5 AFM analyses of membrane

AFM analysis was carried out, to further explore the influence of these additives on surface topology and roughness parameters of the PEI membrane. Fig.3.5 illustrates the representative two and three dimensional topological images of all prepared membranes. The results for roughness parameters, for PEI and modified membranes are presented in Table 3.3. All the membranes showed lower surface roughness compared to pristine PEI

membrane i.e M-0. The maximum mean roughness (R_a) and route mean square roughness (R_q) value showed by M-0 membrane was 11.5 nm and 14.3 nm respectively. Membrane with citric acid as an additive showed decrease in mean roughness around 48 % with the maximum feature heights (R_{max}) of 61.5 nm compared to other membranes. This observation is particularly important since smoother surface shows less adsorption of organic molecules to reduce the organic fouling (Wandera et al. 2011).

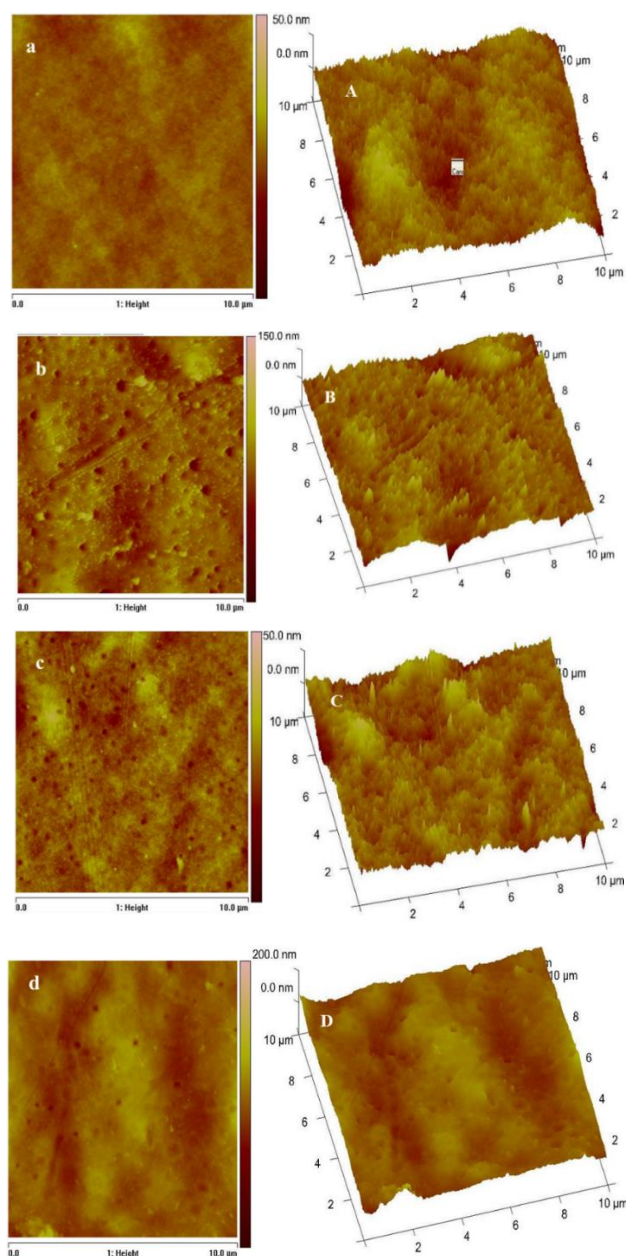


Fig.3.5 Two and three dimensional AFM surface images of a, A) PMA-0, b, B) PMA-1, c, C) PMA-2 and d, D) PMA-3 membrane

Table 3.3 Roughness parameters of the membranes

Membrane	Image surface area (μm^2)	Surface area Difference (%)	Roughness		
			R_a (nm)	R_q (nm)	R_{max} (nm)
PMA-0	101	0.53	11.5	14.3	108
PMA-1	101	1.45	10.4	14.0	177
PMA-2	100	0.91	6.05	7.93	102
PMA-3	101	0.58	5.55	7.0	61.5

3.3.6 Water permeability

The filtration experiments have been conducted to investigate the permeability and antifouling property of the membranes. Fig.3.6 represents the PWF of the membranes. The pristine PEI membrane showed a minimum of $133 \text{ L m}^{-2}\text{h}^{-1}$ and membranes with citric acid as an additive showed maximum PWF of $242 \text{ L m}^{-2}\text{h}^{-1}$. Remarkable changes in the performance of the membranes were obtained after the addition of organic acids as additives as they induce changes on the hydrophilicity and permeation properties of the membranes. The citric and malic acids having three and two carboxylic acid functional groups respectively, which impart the negative charge on the membranes. The carbonyl groups bonded to $-\text{OH}$ in carboxylic acid moieties have electrophilic character. Hence, carboxylic acids undergo dissociation easily and form the carboxylate anion. Ascorbic acid molecules are not able to properly ionize their $-\text{OH}$ functional groups because they do not have linked carbonyl groups. But it contains number of hydroxyl groups and one ionisable hydrogen atom in its structure, which induce the hydrophilicity to the membranes.

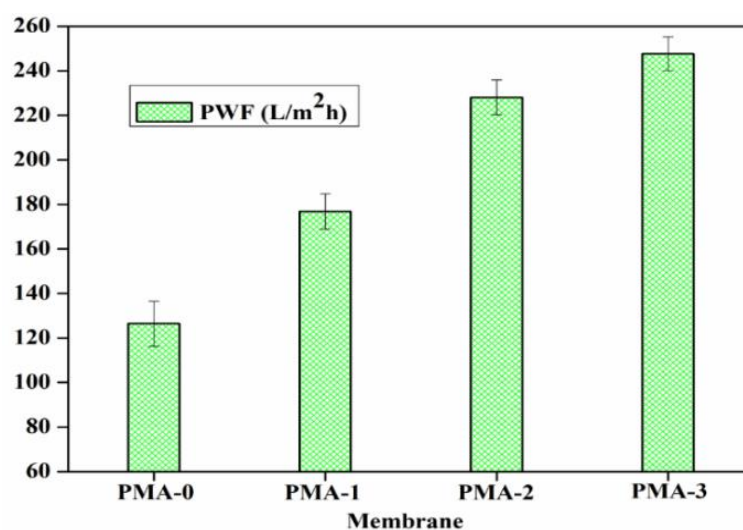


Fig.3.6 Pure water flux of the membranes with 0.2 MPa pressure

3.3.7 Antifouling performance against BSA

The antifouling properties of the membranes with and without additives (organic acids) were investigated by measuring the pure water flux recovery after membrane fouled by the 800 ppm of BSA solution. Fig.3.7 showed the pure water flux before, during and after BSA filtration. Water fluxes of the fouled membranes were measured after thorough washing with distilled water. The FRR of the prepared membranes are described in Table 3.4. The higher FRR value indicates a better antifouling property for the membrane. The pristine membrane exhibit lower flux recovery ratio of 21.4 % and membrane with citric acid as additive showed maximum FRR of 71.6 %. This specifies the high antifouling property of the modified membranes induced by the low molecular weight organic acids. The observed trend of FRR is matched by hydrophilicity of the membranes (Fig.3.8). Hydrophilic surface can adsorb water molecules and form a water layer, which reduces the adsorption of protein and other fouling agents (Fan et al. 2001, Rana and Matsuura 2010).

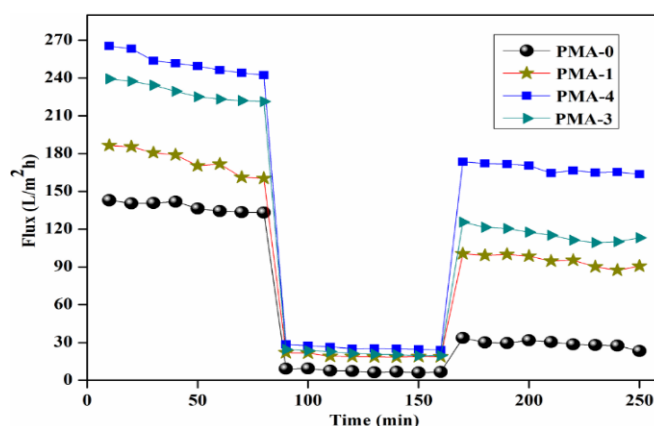


Fig.3.7 Flux variation of membranes during three different filtration conditions

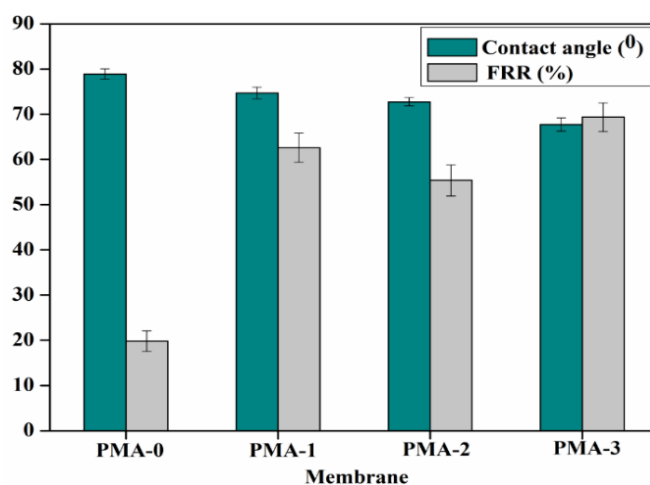


Fig.3.8 Contact angle and FRR of the prepared membranes

In general, the membrane fouling can be categorized as hydraulically irreversible and reversible. In hydraulically irreversible fouling, the fouling agents are strongly attached to the membrane and it can only be cleaned by chemical treatment. In case of hydraulically reversible fouling, the foulants are loosely bound to the membrane and it can easily be removed by backwashing (Lee et al. 2008). Table-3.4 represents the hydraulically reversible (R_r), hydraulically irreversible fouling ratio (R_{ir}) and total fouling ratio (R_t) for the membranes. From the results, it was clear that all the modified membranes exhibited higher hydraulic reversibility in the order of PMA-3 > PMA-1 > PMA-2 > PMA-0. The hydraulic reversible fouling ratio of the membrane was considerably increased from 14.5 % to 65.7 % for the membrane with citric acid as the additive. These results demonstrate that the membrane with organic acids as additives show a remarkable change in the pure water flux, hydrophilicity and antifouling property.

Table 3.4 Filtration and antifouling performance of the membranes

Membrane code	Permeate Flux ($L m^{-2}h^{-1}$)			FRR and Fouling recovery (%)			
	J_{w1}	J_p	J_{w2}	FRR	R_t	R_r	R_{ir}
PMA-0	133.1	9.2	28.6	21.4	93.0	14.5	78.6
PMA-1	160.5	11.5	96.8	60.3	92.8	53.1	39.7
PMA-2	223.8	12.1	118.5	52.9	94.5	47.5	47.1
PMA-3	242.3	14.2	173.5	71.6	94.1	65.7	28.4

3.3.8 Antifouling performances against humic acid

To further investigate the humic acid rejection and antifouling property of prepared membranes, the filtration experiments were carried out at 0.2 MPa TMP with 5 mg/L initial concentration in the feed tank. Fig.3.9 represents the relative fluxes of the membranes. It clearly showed that the rate and extent of fouling reduced significantly after the addition of additives. Rapid flux decline was observed at the beginning of each filtration experiment. The adsorption of humic acid is considered as the first step in membrane fouling and is strongly influenced by on the physicochemical properties of both membranes and foulants, especially the affinity of foulants towards the membrane material (Shao et al. 2011). A maximum resistance against fouling was observed for the PAM-3 membrane with humic acid rejection up to 84.7 % (Fig.3.10). This is corresponding to the low contact angle (higher hydrophilicity) and other surface parameters. Humic acid fouling is dominated by its adsorption on the membrane surface. In addition to this, these additives impart the

negative charges to the membrane which reduces adsorption of humic acid on the membrane surface due to the electrostatic repulsion between humic acid molecules and the membrane surface (Hamid et al. 2011). The photographic images of humic acid rejection was presented in Fig.3.11.

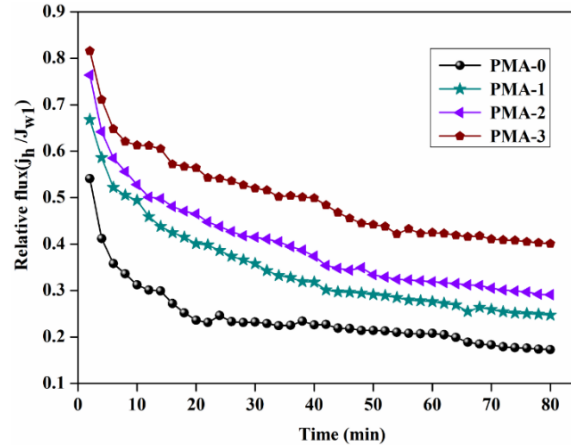


Fig.3.9 Flux ratio during the humic acid solution filtration

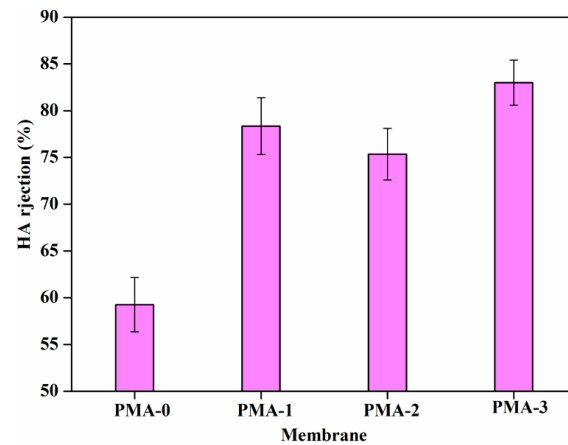


Fig.3.10 Humic acid rejection by prepared membranes

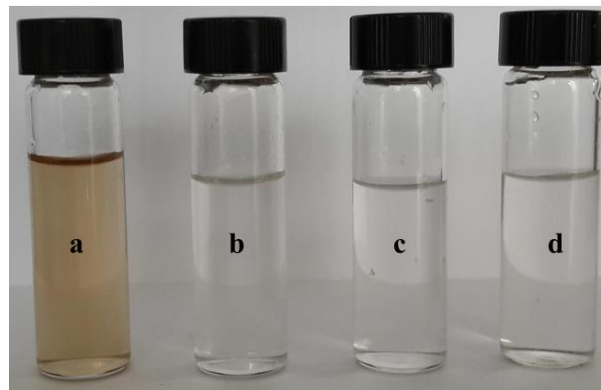


Fig.3.11 Photographic image of (a) feed humic acid solution and b, c and d are the permeate of PMA-1, PMA-2 and PMA-3 membranes

3.4 CONCLUSIONS

Presence of low molecular weight organic acids in the casting solution imparts a strong influence on morphology and antifouling properties of PEI membrane. The rheology of the casting solution was changed dramatically after addition of additive and highly influenced the membrane morphological features. The water uptake capacity and water contact angle measurements confirmed the enhanced hydrophilicity of the membranes for all the organic acid additives. Permeation experiments showed an enhanced water flux of $242.3 \text{ L m}^{-2}\text{h}^{-1}$ with FRR of 72 %. Humic acid rejection study showed that modified membrane having rejection efficiency up to 86 %. Overall, the performance of the membranes revealed that the prepared membranes with citric acid offered a higher efficiency compared to maleic acid and ascorbic acid.

CHAPTER 4

PREPARATION AND EVALUATION OF HEAVY METAL REJECTION PROPERTIES OF POLYETHERIMIDE/POROUS ACTIVATED BENTONITE CLAY NANOCOMPOSITE MEMBRANE

Abstract: *The work presented in this chapter is an attempt to address the improved permeation and heavy metal ion removal from aqueous solution. For this purpose, activated bentonite clay was used as additive in PEI nanocomposite membrane. In this chapter, copper, nickel and cadmium rejection were studied with different experimental condition and results are discussed in detail.*

Possessing an undesirable property of being non-biodegradable and environmentally persistent, the heavy metals constitute the most hazardous environments pollutants in nature. Even the lower concentrations of these pollutants accumulated in an organism's tissue causes severe and fatal damage to the health due to its extreme toxicity. The industries such as metal plating facilities, mining operations, fertilizers and pesticide industries, tanneries, batteries and paper industries are the ones which discharge heavy metals into the environment in the name of the industrial sewage (Fu and Wang 2011, Khin *et al.* 2012, Azimi *et al.* 2016). Toxic heavy metals draw the attention of scientists for the purification attempts of waste water consisting of cadmium, nickel, zinc, copper, mercury, chromium and lead. In particular, copper has very important role in animal metabolism (Zhu *et al.* 2014). The intake of unnecessary copper into the body can cause severe health concerns like vomiting, cramp, convulsion and even death. Presence of nickel beyond the permissible limit can cause severe harm to lungs, kidney and disorders such as skin dermatitis, pulmonary fibrosis and gastrointestinal distress. And importantly it is also a known carcinogen. Cadmium has been categorized by the U.S. Environmental Protection Agency as a potential human carcinogen. Cadmium exposes human to severe health risks. Prolonged exposure of cadmium brings about kidney dysfunction and high levels of exposure will result in death (Park *et al.* 2007). These examples illustrate the havoc of heavy metal accumulation in the body; thus, it is necessary to eliminate these metal ions from the consumable water.

Polymer- clay nanocomposite membranes put forward a very promising result in the above mentioned needs. These are the mixed matrix material consisting of a polymer with uniformly dispersed clay nanoparticles. They offer better separation properties of membranes because of them acquiring properties of both organic and inorganic materials with good permeability, selectivity, mechanical strength, thermal stability and chemical resistance (Choudalakis and Gotsis 2009). The strong interactions between the polymer chains and the clay mineral platelets make them significant in the field of membrane science (Zanetti *et al.* 2000).

Though there are several clay materials available for this purpose, smectic clays are commonly used in the preparation of nanocomposite membranes such as bentonite, hectorite, montmorillonite (MMT) and synthetic mica. Structurally bentonite clay is made up of two basic building blocks, the aluminium octahedral sheets and the silica tetrahedral sheets (Fig.4.1). A single unit cell consists of one aluminium octahedral sheet sandwiched between two tetrahedral silica sheets (Liu *et al.* 2016). These silicate layers have a slight negative charge that is compensated by exchangeable cations in the intermediate layers. The charge is so weak that the cations (Na^+ , Mg^{2+} or Ca^{2+} ions) can be adsorbed with an associated hydration shell. The cations held in this pattern in the clay can be easily replaced by ion exchange. Bentonite clay with this structure along with polymer can be considered as an important technique to produce nanocomposite material (Bohnhoff and Shackelford 2013). It is very interesting to note that the addition of even less than 10 wt. % of clay material into the polymer makes a lot of difference in the properties like hydrophilicity, adsorption capacity and permeability.

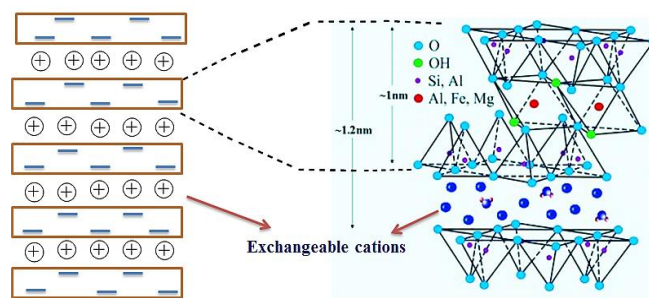


Fig.4.1 Diagrammatic sketch of the structure of bentonite clay.

The effect of aluminium pillared bentonite clay for the rejection of cobalt (II) from aqueous solution was reported by Manohar *et al.* (2006). The resultant membrane showed the maximum rejection of 99.8 % and 87.0 % which took place at pH 6.0 from an initial concentration of 10.0 and 25.0 mg l^{-1} respectively. Further, Eren *et al.* (2009) demonstrated the applicability of MnO_2 doped bentonite for removal of lead (Pb) from water. The study revealed that, adsorption of Pb by the bentonite clay was influenced by pH and ionic strength of the solution. The presence of bentonite in the composite significantly influence the adsorption of Pb by increasing the active adsorption site in the intercalation layers.

Ma *et al.* (2012) reported polysulfone/ organomodified montmorillonite nanocomposite membrane with dimethyl acetamide as the solvent, water as a non-solvent and PEG 400 as the pore forming additive. The report revealed that addition of clay was

responsible for the increase in porosity and permeability (from $0.095 \text{ Lm}^{-2} \text{ s}^{-1}$, 0 wt % clay to $0.106 \text{ Lm}^{-2} \text{ s}^{-1}$, 6 wt % clay).

Jose *et al.* (2014) investigated the influence of bentonite on poly(vinyl alcohol) nanocomposite membrane properties and its performance. The schematic representation of intercalation of bentonite into the membrane matrix was presented in Fig.4.2. They stated that the presence of 5 wt. % of bentonite in the membrane matrix exhibited higher mechanical strength and permeation compared to pristine membrane.

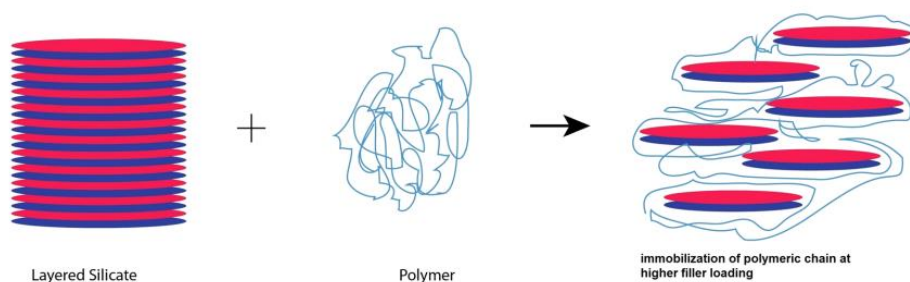


Fig.4.2 Immobilization of bentonite into membrane matrix. (Jose *et al.* 2014)

Kiran *et al.* (2015) illustrated the effect of bentonite in polymer membrane for the effective removal of hazardous effluents from wastewater. The inclusion of bentonite resulted in increased membrane hydrophilicity, mechanical strength, porosity, morphology and permeation. They reported that, the higher hydraulic permeation of $52.3 \text{ L/m}^2 \text{ h}$ was obtained for modified membrane and lower flux of $41.50 \text{ L/m}^2 \text{ h}$ for unmodified membrane. Kumar *et al.* (2015) also reported the fabrication of polysulfone/ bentonite nanocomposite UF membrane for oil water separation. The nanocomposite membrane resulted in porosity enhancement of 29 % with increase in number of straight pores and 25 % improvement in hydrophilicity. The effect of bentonite additive dosage on water flux of polysulfone nanocomposite membranes are presented in Fig.4.3.

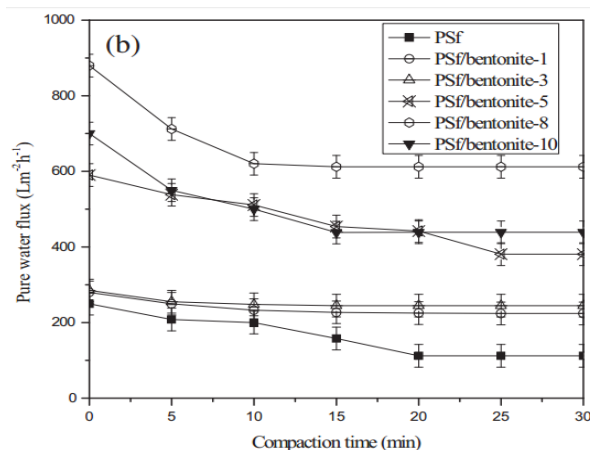


Fig.4.3 Effect of bentonite additive dosage on water flux of polysulfone nanocomposite membrane (Kiran *et al.* 2015)

Kumar *et al.* (2016) employed the polymer grafted bentonite as hydrophilic additive to improve the membrane performance. After the inclusion of modified bentonite, pure water flux of the membrane increases to $> 400 \text{ Lm}^{-2} \text{ h}^{-1}$ at 100 kPa transmembrane pressure. Heydari *et al.* (2016) reported the modification of bentonite with polymerization of β -cyclodextrin (Fig.4.4). The modified bentonite was used as hydrophilic additive to enhance the membrane performance. They reported that the polymer/clay nanocomposites showed higher removal capacity for Co^{2+} , Cu^{2+} and Zn^{2+} ions in comparison with pristine polymer membrane. The selectivity order could be given as $\text{Zn}^{2+} > \text{Cu}^{2+} > \text{Co}^{2+}$.

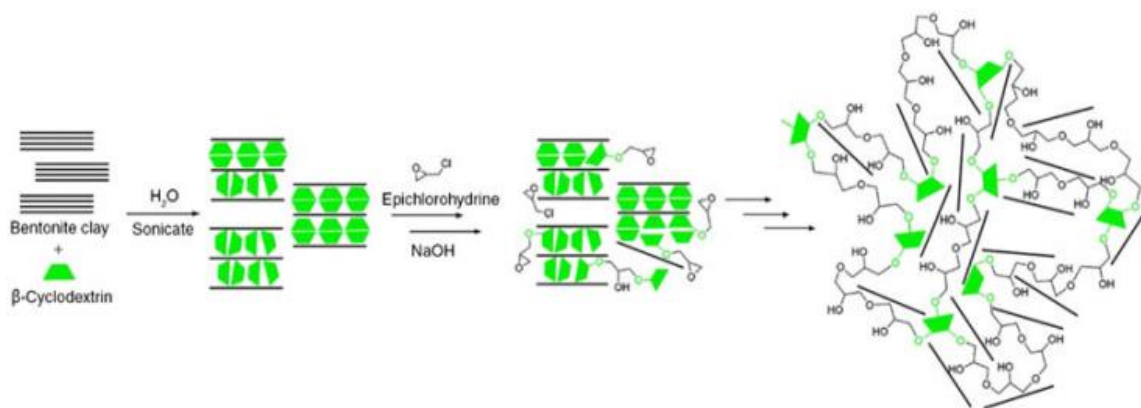


Fig.4.4 Schematic representation of β -cyclodextrin modification of bentonite (Heydari *et al.* 2016)

In this chapter, PEI/ activated bentonite clay nanocomposite membranes were prepared by phase inversion method using PEG 1000 as pore former. The variation in morphology and hydrophilicity of the membranes with different amount of additive dosage was determined by SEM and contact angle analyzer. The presence of bentonite clay and its uniform distribution in polymer matrix was confirmed by energy dispersive X-ray analysis

(EDX) and elemental analyses. The performance of these membranes was analyzed in terms of water flux, porosity, membrane hydraulic resistance and heavy metal ion rejection study.

4.1 EXPERIMENTAL PART

4.1.1 Materials

Polyethylene glycol (Mw =1000), analytical grade copper nitrate, nickel nitrate and cadmium nitrate were procured from Sigma Aldrich. Bentonite clay was obtained as a gift sample from the department of Civil engineering, NITK Surathkal, India. Deionized and distilled water was used for the preparation of metal ion solutions with different initial feed concentrations.

4.1.2. Activation of bentonite clay

The activated bentonite clay was prepared using the procedure reported in the literature (Önal *et al.* 2007). In brief, bentonite clay (5 g) was mixed with a 7 N sulfuric acid solution (100 ml). The obtained suspension was heated to 90 ° C for 18 h under constant stirring. The reaction was carried out in a glass flask furnished with a reflux condenser in order to avoid evaporation of solvent during the experiment. After acid activation, the slurry was filtered and the filtrate was thoroughly washed with de-mineralized water until it is free from sulfate ions (tested by BaCl₂ solution). The acid activated sample was dried initially at room temperature and then at 70 ° C for 3 h.

4.1.3 Preparation of composite membrane

PEI/activated bentonite clay nanocomposite membranes were prepared via phase separation method. The detailed procedure for the membrane preparation by phase inversion method is given in chapter 3. In brief, calculated amount of activated bentonite clay (1 wt. % to 4 wt. % of PEI dosage) was mixed with the desired volume of NMP and magnetically stirred for 1.0 h at room temperature. PEI was added to premixed solution along with 5 % PEG 1000 as an invariable additive (pore forming agent) and heated to 65 °C. The obtained homogeneous solution was casted and immersed in water bath. Overviews of the experimental conditions were described in Table 4.1.

Table 4.1 Composition of casting solutions

Membrane	PEI(g)	NMP(g)	Clay(g)	PEG 1000(g)	W _{clay} *(wt %)
PBM-0	16.5	78.5	0	5	0
PBM-1	16.5	78.3	0.16	5	1
PBM-2	16.5	78.1	0.33	5	2
PBM-3	16.5	78.0	0.49	5	3
PBM-4	16.5	77.8	0.66	5	4

4.2 CHARACTERIZATION AND PERFORMANCE STUDY

The membrane hydraulic resistance (R_h) of the membrane was calculated by measuring the pure water flux of the membranes at different transmembrane pressure (TMP) (Hegde *et al.* 2013). The hydraulic resistances of the membranes (R_h) were evaluated from the slope of the plot of pure water flux versus pressure difference (ΔP) using the equation

$$R_h = \frac{\Delta P}{J_w}$$

Where ' J_w ' is the pure water flux (L/m²h), ' ΔP ' (kPa) is the pressure difference and ' R_h ' is the membrane resistance (kPa/Lm²h⁻¹).

The water uptake study was carried out as mentioned in CHAPTER 2, section 2.3.4. The performance of the membrane was tested by determining the PWF and calculated as described in CHAPTER 2, section 2.3.5.

The heavy metal ion rejection performance of all membranes was carried out by using self-constructed dead end filtration cell. The feed solutions of cadmium nitrate, nickel nitrate and copper nitrate with concentration of 250 ppm, 500 ppm and 1000 ppm were used for the metal ion rejection study. The feed solution was filled into a filtration tank and pressurized as required using a nitrogen cylinder. Then permeate was collected for a regular interval of time and the concentration of the heavy metal ion was measured using an atomic absorption spectrometer. The percentage of rejection of the membranes was determined by using the equation.

$$\%R = \left(1 - \frac{C_p}{C_f}\right) \times 100$$

Where, ' C_p ' and ' C_f ' are the concentration of permeate and feed solution respectively.

4.3 RESULTS AND DISCUSSIONS

4.3.1 Chemical composition of bentonite clay

Table 4. 2 shows the changes in the chemical composition of the bentonite clay after acid treatment. The acid activated bentonite clay exhibit significantly different physicochemical characteristics compared to their non-activated counterparts. One of these physicochemical properties is the surface area. The surface area and the porous structure of bentonite can be changed to the desired extent by acid activation. During acid treatment, the structure of the raw clay is opened and becomes porous (Didi *et al.*2009). At the same time, H^+ ion replaces the metallic ions such as Fe^{+3} , Na^+ , Mg^{+2} in the bentonite structure. This yields clay with highly active surface area.

Table 4. 2 EDX analysis results of elemental compositions for acid treated and untreated bentonite clay

Sample	Content of element (%)					
	O	Si	Al	Mg	Fe	Na
Untreated clay	63.56	20.13	9.88	1.07	2.72	2.10
Acid treated clay	68.05	27.57	3.54	-	-	-

Bentonite was subjected to EDX analysis to determine the elemental composition. From the Fig.4.5, the untreated clay consists of Na, Mg, Si, Al and other elements. After acid treatment, peak corresponding to Na and Mg disappeared in the clay. This confirms the exchange of sodium and magnesium ions with protons.

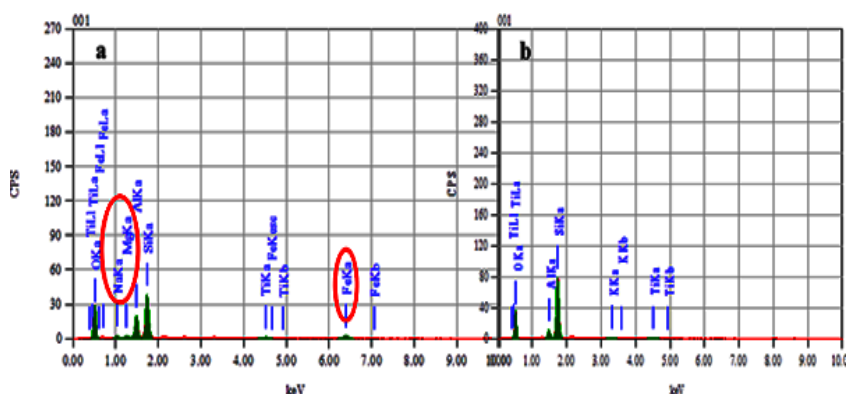


Fig.4.5 EDX analysis of bentonite clay a) before acid activation b) after acid activation

4.3.2 Porosity and contact angle

In general, the skin layer of an asymmetric membrane decides its performance and the supporting layer provides mechanical strength. The rejection and intrinsic permeation

properties are determined by the porosity and average pore size distribution of the membranes. Our experiments revealed that the addition of different amounts of inorganic material to the polymer solution affects the performance of the resulting membrane (Ma *et al.* 2012). In order to substantiate this, there was a remarkable change in the porosity and morphology of membranes, which was due to different bentonite clay dosage. The porosity of the PEI/ activated bentonite nanocomposite membranes is shown in Table 4.3. It can be observed that with the increase in bentonite content, the porosity increased from 39.2 % for PBM-0 membrane to 61.4 % for PBM-4 membrane. This change was due to the effect of the addition of a certain amount of bentonite to the membrane dope.

The hydrophilic properties and wetting characteristic of the membrane surface were analyzed by water contact angle measurements. In general, smaller the contact angle, higher is the hydrophilicity of the membrane (Barth *et al.* 2000). Membranes showed decrease in the contact angle with increase in the activated bentonite clay (Table 3.3). This may be because bentonite has the capacity to hold water molecules by being negatively charged. Hydrophilicity is enhanced with the increase in the bentonite content of the membrane.

Table 4.3 Physical properties of membranes

Membrane code	Clay (wt%)	Membrane thickness (μm)	Porosity (%)	Contact angle ($^\circ$)	PWF ($\text{L}/\text{m}^2\text{h}$)
PBM-0	0	156	39.2	79.4	138.1
PBM-1	1	162	45.1	76.1	177.9
PBM-2	2	164	49.8	74.3	186.4
PBM-3	3	158	56.5	72.6	197.7
PBM-4	4	161	61.4	69.4	210.9

4.3.3 Morphology of the membranes

It is well known that the performance of membrane is strongly influenced by surface porosity, compactness, sub-layer morphology and top layer thickness (Monticelli *et al.* 2007, Rajesh *et al.* 2011). The effect of concentration of activated clay as the additive on the membrane morphology was investigated by SEM. The presence of activated bentonite clay and uniform distribution across the membrane was confirmed by conducting elemental mapping of silicon and aluminium (Fig.4.6). Fig.4.7 represents the cross sectional image of the PEI/ activated bentonite clay composite membranes with different amount of clay dosage. All membrane has shown the typical asymmetric structure comprising of dense top skin layer and porous sublayer. The skin layer functioned as a separation layer and the

porous sublayer or support layer provided the mechanical strength. The surface morphology might be due to the instantaneous demixing of membrane casting solution and rapid precipitation of polymer matrix (Kumar *et al.* 2013).

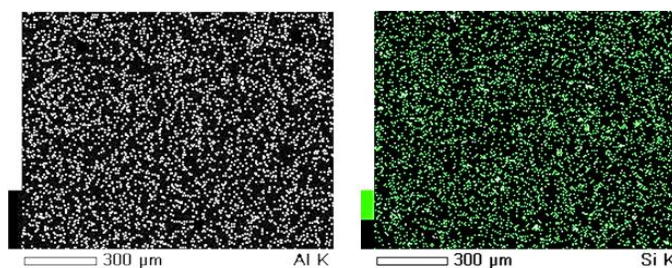


Fig.4.6 The aluminium and silicon mapping of PBM-4 membrane

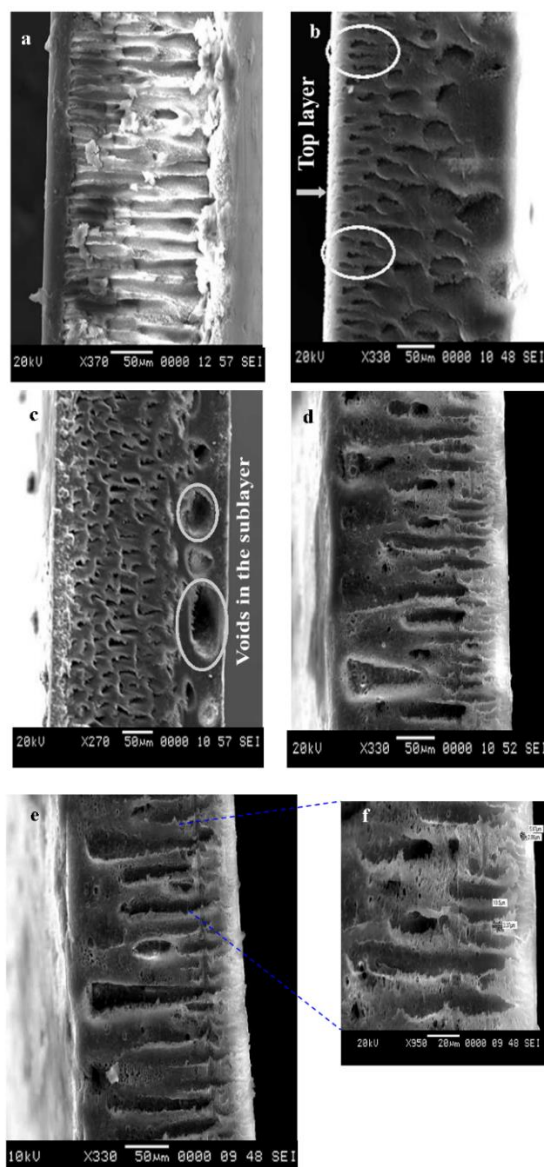


Fig.4.7 Cross sectional SEM images of a) PBM-0, b) PBM-1, c) PBM-2, d) PBM-3, e) PBM-4, and f) Magnified cross sectional image of PBM-4 membrane

From the literature, it can be noticed that the presence of activated bentonite clay in the membrane dope might have been responsible for major influence on the morphological features of the membranes. The layered silicate arrangement of the clay and polymer (PEI) are likely to form intercalated and exfoliated structures. This results in reduced interaction among polymer chains and enhances the nano-scale interaction between polymer and activated bentonite clay. Due to this, delayed demixing was taking place in the coagulation bath. On the other hand, due to the hydrophilicity of bentonite and possibility of formation of hydrogen bond between NMP and bentonite clay, the rate of non-solvent (water) inflow increases and solvent (NMP) outflow decreases (Ghaemi *et al.* 2011). Both phenomena resulted in the delay of the coagulation of polymer in the presence of bentonite clay. Consequently, the growth of the skin layer is enhanced and the formation of macrovoids in the support is improved.

4.3.4 Pure water flux

Porosity, membrane morphology and hydrophilicity are considered to be key factors which decide the flux of the membrane. PWF has a direct relationship with the porosity and the average pore size of the membrane surface. The time dependent pure water flux (0.3 MPa) of the membranes was measured and is given in Fig.4.8. Initially gradual decrease in PWF was observed for all the membranes during compaction due to mechanical deformation of the polymeric membrane matrix. The clay content has more effect on PWF of the membranes. It can be seen from Table 4.3 that the membrane with 1.0 % of clay content showed flux of $177.9 \text{ Lm}^{-2}\text{h}^{-1}$ and it was increased to $210.6 \text{ Lm}^{-2}\text{h}^{-1}$ for 4.0 % of clay dosage. The increase of PWF may be attributed to the increase of membrane porosity and hydrophilicity of the membranes. In addition to this, bentonite clay has the capacity to hold the water and membrane certainly becomes wet. Due to this phenomenon, water molecules can easily pass through the membrane matrix.

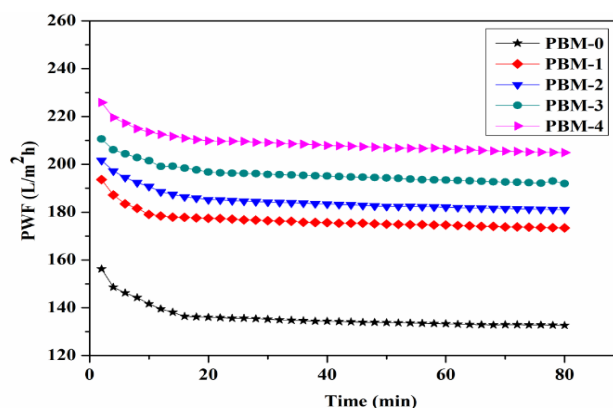


Fig.4.8 Time dependent pure water flux of membranes at 0.3 MPa TMP

4.3.5 Hydraulic resistance of membranes

The pure water flux of the membranes was measured at different transmembrane pressures (Fig.4.9) and the hydraulic resistance of the membranes were calculated as the inverse of the slope of the plots of PWF against the respective transmembrane pressure. The hydraulic resistance offered by the membranes with different amount of activated clay is shown in Table 4.4. The membrane with 1 wt. % of activated clay showed hydraulic resistance of $1.1242 \text{ kPa/Lm}^{-2}\text{h}^{-1}$ and it was observed to decline to $0.9483 \text{ kPa/Lm}^{-2}\text{h}^{-1}$ when membrane with 4 wt. % of clay content was used. The decline in the hydraulic resistance was observed with increased content of clay. This can be explained by the fact that, bentonite clay being negatively charged imparts hydrophilicity to the membranes. When surface exhibits hydrophilicity, the water molecules form weak interaction with the molecules of the surface. Due to this phenomenon membrane easily became wet and shows less resistance to the water to pass through it (Al-Rashdi *et al.* 2013). In addition to this, the presence of clay content leads to formation of pores on the membrane surface. Therefore, increase in flux was observed, thereby decreasing the membrane hydraulic resistance.

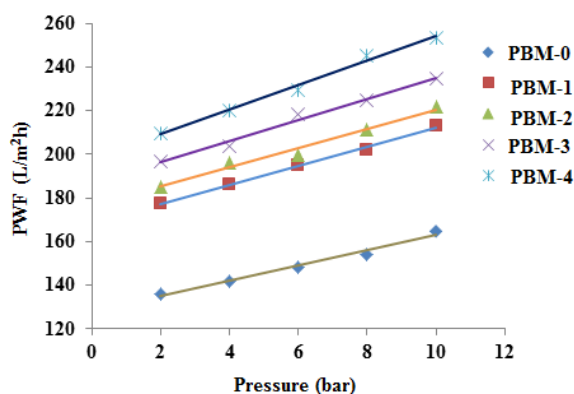


Fig.4.9 Pressure dependent pure water fluxes of membranes

Table.4.4

Hydraulics resistance of different membranes

Membrane Code	Hydraulic membrane resistance (Rh) ($\text{Kpa/Lm}^{-2}\text{h}^{-1}$)
PBM-1	1.1467
PBM-2	1.1153
PBM-3	1.0914
PBM-4	1.0914

4.3.6 Heavy metal ion rejection study

4.3.6.1 Effect of initial metal ion concentration

The prepared membranes were studied for cadmium, nickel and copper rejection performance and the rejection performance were measured at various initial feed concentrations. Fig.4.10, Fig.4.11 and Fig.4.12 shows the variation of Cd (II), Ni (II) and Cu (II) rejection of all prepared membranes with different initial feed concentrations. From the results, it was observed that the rejection of metal ion has decreased as the initial feed concentration increased. Also the rejection of metal ion has increased with the increase in bentonite content in the membrane. For the Cd (II), Ni (II) and Cu (II) ions, the rejection at feed concentration of 250 ppm was 69.3 %, 76.2 % and 82.5 % and this has dropped down to 56.8 % , 64.8 % and 71.3 % respectively at 1000 ppm feed concentration. Similar results for heavy metals and other salts were reported for NF 270 membranes by Al-Rashdi et.al (2013) and Al-Zoubi *et al.* (2007). This trend can be explained as follows, PEI is hydrophobic in nature, having insignificant interaction with metal ions, whereas bentonite is hydrophilic clay which plays a major role in rejection of heavy metal ion. The amount of rejection increases gradually with higher bentonite clay loading. At a low metal ion concentration, the ratio of metal ions to the number of available active adsorption sites is less, but as the metal ion concentration increases, the competition for adsorption sites becomes intense. As a result, the extent of adsorption comes down considerably, however the amount of metal ion adsorbed per unit mass of the adsorbent increases. Above results can be substantiated by comparing the element mapping analysis of both virgin and PBM-4 membrane after the rejection experiments (Fig.4.13). In the virgin membrane, the amount of metal ions present on the membrane surface is very less, however very high concentration of rejected heavy metal ion was present on the surface of PBM-4 membrane. Hence it can be concluded that, the presence of activated bentonite clay in the membrane matrix exhibited very high adsorption capacity of heavy metal ions.

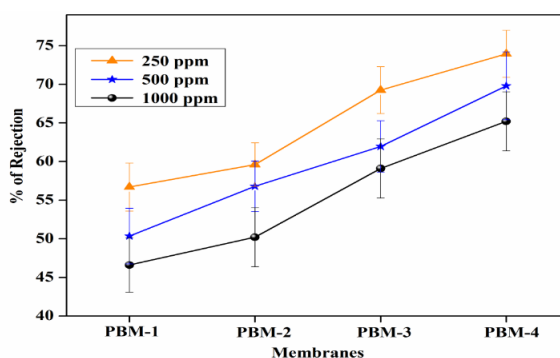


Fig.4.10 Variation of nickel rejection with different initial feed concentration (pH= 4±0.5)

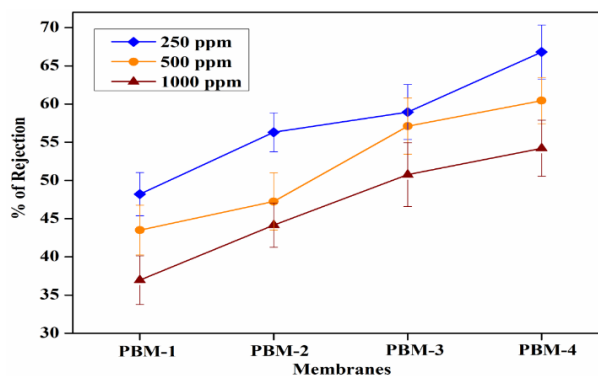


Fig.4.11 Variation of cadmium rejection with different initial feed concentration (pH= 4 ± 0.5)

The rejection increases in the order of Cd (II) < Ni (II) < Cu (II). This can be explained in terms of cation hydration capacity. Tansel *et al.* (2006) described that metal ion with smaller ionic radius tend to hold their hydration sphere (i.e. are strongly attached to water molecules) thus would be more rejection by the membrane. Since copper is comparatively smallest ion with highest positive charge density, therefore the extent of hydration is maximum in copper as compared to nickel and cadmium. Due to this, diffusion of metal ion occurs slowly and couldn't pass through the smaller diameter pores of the membranes. However, only size exclusion is not the main mechanism to explain heavy metal ion rejection. Metal deposition and charge exclusion play very significant roles which cannot be ignored.

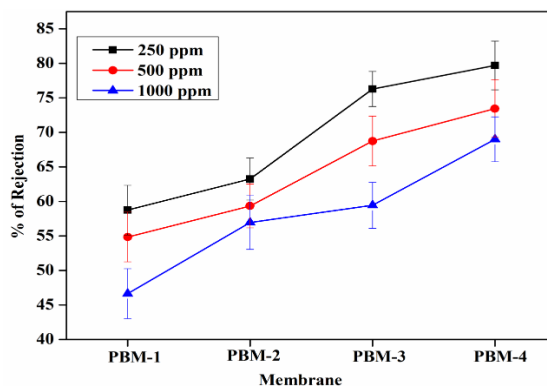


Fig.4.12 Variation of copper rejection with different initial feed concentration (pH= 4 ± 0.5)

4.3.6.2 Effect of pH on rejection of heavy metal ion

Fig.4.14 describes the effect of pH on rejection of the heavy metal ion solution showed by the PBM-4 membrane. The rejection of copper, nickel and cadmium was found to increase with increased pH of feed solution. The results indicate that pH exerts great influence on heavy metal ion rejection. At the lower pH there is a competition between the metal ions and H_3O^+ ions for active adsorption sites on bentonite clay. Since the number of

H_3O^+ ions exceeds several times that of the metal ions and the surface is most likely shielded with H_3O^+ ions, the deposition of metal ion on the membrane is found to be less (Anirudhan *et al.* 2012). When the pH increases, more and more H_3O^+ ions leave the clay surface, making the sites available to the metal ions. As pH changes, there will be change in concentration of H^+ and OH^- ions in the solution, which triggers the modification of surface functional groups as shown below.

According to above reaction, as the pH of the feed solution increases, it enhances the negative charge on the membrane surface by reacting with hydroxyl group present on the clay. Therefore, bentonite acquires higher negative charge density resulting from the spread of isomorphous substitution in octahedral and tetrahedral sheets of bentonite. That is, higher negative charged surface allows the metal ions to have more electrostatic interaction with bentonite clay (Zhu *et al.* 2014). In addition to this, when the pH of the solution is acidic, the hydration sphere of the heavy metal ions was affected by the proton, which might cause the decrease in the size of the hydration sphere of cation. There is a decrease in the rejection observed with decrease in pH of the feed solution.

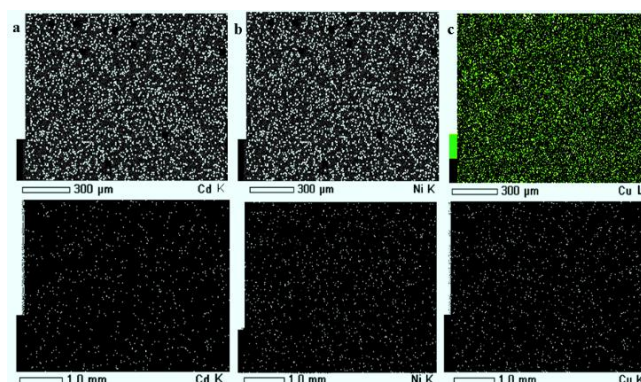


Fig.4.13 Elemental mapping of a) cadmium b) nickel c) copper after rejection study of PBM-4 and virgin membranes

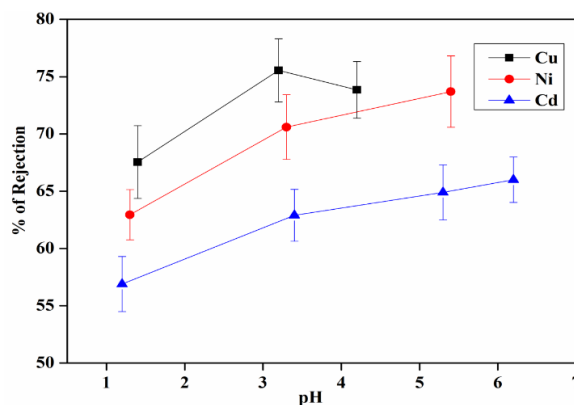


Fig.4.14 Rejection of heavy metal ions at different pH values for PBM-4 membrane

4.4 CONCLUSIONS

The uniform distribution of activated bentonite in the membrane matrix has been confirmed by elemental mapping studies. The resultant nanocomposite membranes showed enhanced porosity, permeate flux and lower membrane hydraulic resistance. The membrane showed the good rejection towards the heavy metal ions without any external chelating agent. The rejection follows the order, Cu (II) > Ni (II) > Cd (II) attributed to the adsorption capacity and extent of hydration sphere of the corresponding metal ion. The membrane with 4 wt. % clay dosage showed maximum rejection of 69.3 %, 76.2 % and 82.5 % for 250 ppm of Cd (II), Ni (II) and Cu (II) ion solutions respectively.

CHAPTER 5

FUNCTIONALIZATION OF POLYETHERIMIDE MEMBRANE WITH BENTONITE CLAY GRAFTED WITH POLY (4-STYRENESULFONATE) BRUSHES AS EFFECTIVE REMOVAL OF HAZARDOUS HUMIC ACID AND HEAVY METAL IONS

Abstract: In a continued effort to improve membrane performance and finding the better additive to enhance the antifouling and heavy metal ion rejection properties, modification of bentonite clay was carried out. In this chapter poly (4 styrenesulfonate) brushes were grafted to bentonite and attempted as a performance modifier. The hybrid nanocomposite membrane was prepared and subjected to permeation, antifouling and heavy metal ion rejection studies. The results are presented in detail.

Mixed matrix ultrafiltration membranes could be an attractive alternative for the water treatment process. These membranes utilize a polymer base with an immobilised inorganic additive in the matrix, which augments their selectivity and productivity. Predominantly cost-effectiveness, size and properties of the materials are the key factors to optimize the inorganic additives (Guillen *et al.* 2010). Panpanit *et al.* (2001) studied the influence of bentonite clay addition in UF membrane flux enhancement during the waste water treatment. This study demonstrated that the addition of bentonite clay can result in reduction of total membrane fouling. This can be due to adsorption of foulants layer on UF membrane surface. It has also been witnessed that bentonite immobilised polymer membrane matrix have highly porous surface and were able to remove heavy metal ions from aqueous solutions.

Lee and Tiwari (2012) stated that, activated bentonite clay was used to adsorb γ -picoline which is the major pyridine based hazardous effluent present in chemical industrial wastewater. The poly(epichlorohydrinedimethylamine) modified bentonite composite was used as adsorbent for the removal of anionic dyes from aqueous solution. They observed that the adsorption process follows pseudo second order kinetics and lower dye loading exhibits maximum affinity towards the polymer bentonite composite.

Unuabonah and Taubert (2014) conducted the study on antimicrobial properties of clay polymer nanocomposite (CPN) using a thin film of sodium- bentonite and poly (diallyldimethyl ammonium chloride). It was observed that this CPN exerts good resistance towards *Escherichia coli* and *salmonella typhmurimum*.

Jin *et al.* (2016) modified the bentonite with humic acid for the effective removal of 2,4-dichlorophenol and Cu (II) from aqueous solution (Fig.5.1). The batch adsorption experiments revealed that amount of sorption was 14.23 mg g^{-1} and 22.40 mg g^{-1} for 2,4-dichlorophenol and Cu(II) respectively at $30 \text{ }^\circ\text{C}$.

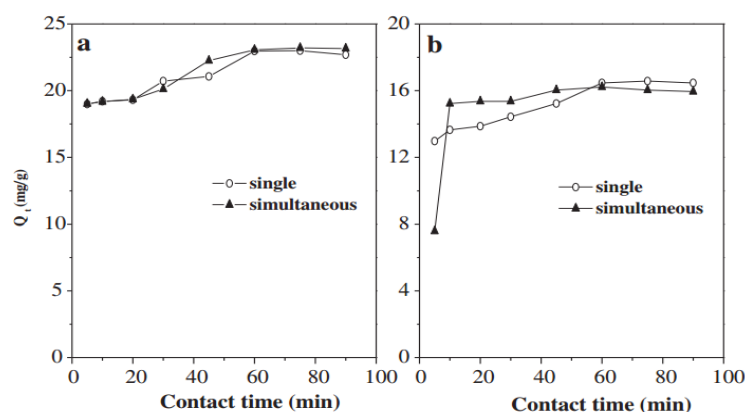


Fig.5.1 Comparison of sorption of (a) Cu (II) and (b) 2,4-dichlorophenol individually and simultaneously onto humic acid modified bentonite (Jin *et al.* 2016)

Dehghani (2017) chemically modified the bentonite using the chitosan biopolymer for the removal of hazardous arsenic (V) removal from aqueous solutions. From the experimental investigation, they stated that high adsorption capacity (122.23 mg/g) was observed with 1.5 g/L of modified bentonite dosage. Among the isotherm models, the Langmuir isotherm model was the best fit for the obtained data. The adsorption kinetics following a pseudo-second-order kinetic model was involved in the adsorption process of As (V).

In recent years, sulfonated polymer brushes grafted to nanomaterials are viewed as new type of chemical modification to improve the membrane properties. Polymer brushes are assemblies of one end tethered polymer chains at high graft density on a surface or an interface. The properties of polymer brushes are unique and more effective with even grafted polymer chains at low graft density.

Cai *et al.* (2012) reported that, PVDF membranes with covalently immobilized hyperbranched polymer brushes has shown significant improvement in the antifouling and antibacterial properties (Fig.5.2). The graft copolymers of PVDF was synthesised by using poly[2-(N,N-dimethylamino)ethyl methacrylate] as side chain, via activators generated by ATRP.

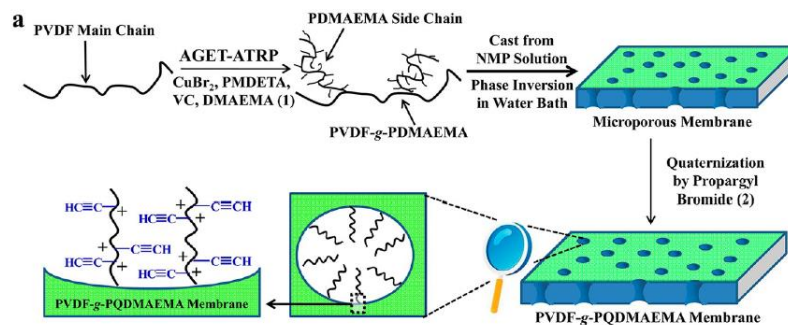


Fig.5.2 Poly (vinylidene fluoride) (PVDF) membranes with covalently immobilized hyperbranched polymers (Cai *et al.* 2012)

Zhu *et al.* (2014) described the preparation of negatively charged PES nanofiltration membrane by blending with halloysite nanotubes grafted with poly (sodium 4-styrenesulfonate) via surface-initiated ATRP (Fig.5.3). It has been stated that the degree of grafting was effectively controlled by varying the reaction time and the amount of monomers added. The results show that the hydrophilicity and permeation properties of hybrid membranes increased considerably.

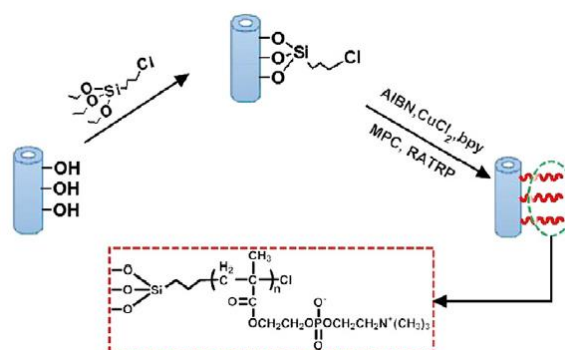


Fig.5.3 Schematic representation of preparation of HNTs-poly (NASS) (Zhu *et al.* 2014).

Kumar *et al.* (2016) employed polymer-grafted bentonite as hydrophilic additive for the fabrication of polysulfone UF membranes for wastewater treatment. For this purpose polyvinylpyrrolidone-grafted-bentonite, polyvinylacetate-grafted-bentonite and poly (1-vinylpyrrolidone-co-acrylonitrile)-grafted-bentonite was synthesized. The nanocomposite membranes were prepared via phase inversion method using different additive dosage. The modified membrane showed superior hydrophilicity, porosity, pure water permeability and antifouling ability compared to neat polysulfone membrane.

Guo *et al.* (2017) modified the bentonite poly(glycidyl methacrylate) via surface-initiated atom transfer radical polymerization. Further it was modified by tetraethylenepentamine (TEPA) through a ring opening reaction of the epoxy groups in poly(glycidyl methacrylate) to form polyamine grafted bentonite (Fig.5.4). These modified bentonite was used for the removal of negatively charged Orange I dye from the aqueous solution. The adsorption process was influenced by pH value, especially at low pH, and the maximum adsorption amount was 616.6 mg g^{-1} at pH 3.0.

In this chapter, poly (sodium 4-styrenesulfonate) was grafted onto the surface of natural bentonite clay via surface-initiated atom transfer radical polymerization. The changes in the surface morphological and topology features were observed by SEM and AFM. The resultant membranes were characterised in terms of its contact angle, porosity, water uptake capacity, permeation and antifouling ability. The heavy metal ion rejection capacity of the hybrid membranes were investigated using 1000 ppm of lead nitrate and cadmium nitrate solution.

5.1 MATERIALS AND METHODS

5.1.1. Materials

The 3-(methacryloxy)propyltrimethoxysilan (MPS), styrene (St), Sodium-p-styrenesulfonate (SS) and 2,2'- Azobisisobutyronitrile (AIBN) were obtained from Alfa Aesar. The N-methyl pyrrolidone (NMP) was procured from Merck, India.

5.1.2 Grafting of sodium 4-styrenesulfonate brushes onto bentonite clay

The grafting of sodium 4-styrenesulfonate on bentonite clay was carried out according to distillation- precipitation polymerisation method (Bai *et al.* 2014). The schematic representation of the reaction was represented in the Fig.5.4. In brief, the bentonite (3g) was dispersed into the mixture of water (90 ml), ethanol (9 ml) and aqueous solution of ammonia (7.5 ml). The resultant suspension was magnetically stirred for 24 h at room temperature. To this suspension, MPS (0.6 ml) was added drop wise and stirred for another 24 h. Then MPS modified bentonite was collected by centrifugation and dried in an oven at 50°C . MPS-modified bentonite (0.60 g), St (0.80 ml) SS (0.80 ml), and AIBN (0.032g) were dispersed into acetonitrile (160 ml) in a dried three necked RB flask. The suspension was heated and kept under boiling condition until half acetonitrile was distilled out. The product obtained was collected by centrifugation and purified by using acetonitrile. The resultant hybrid bentonite was then treated with 0.1M HCl to exchange

Na^+ ions in $-\text{SO}_3\text{Na}$ with H^+ ions. Then bentonite grafted with poly (4-styrenesulfonate) brushes was obtained after being dried in the vacuum oven at 70°C .

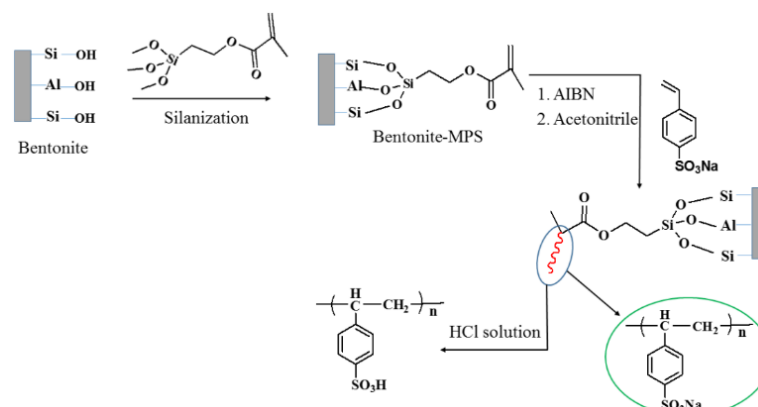


Fig.5.4 Synthetic route for the modified bentonite

5.1.3 Preparation of Membranes

The PEI/ modified bentonite nanocomposite membranes with different amount of additive concentration were prepared by immersion precipitation method (Shenvi *et al.* 2014). The detailed procedure of membrane preparation is given in chapter-2, Section 2.1.2. In brief, desired quantities of ratio of PEI, modified bentonite and PVP (pore forming agent) were dissolved in the desired volume of NMP at 60°C . The obtained homogeneous solution was casted over the glass plate and gently immersed in water bath for the phase inversion. The over view of the composition of casting solution were presented in Table-5.1.

Table 5.1 Composition of casting solutions

Membrane	PEI(g)	NMP(g)	Ben-(SPB) (g)	PVP(g)	W*(wt%)
PEM-0	16.5	78.5	0	4	0
PEM-1	16.5	78.3	0.16	4	1
PEM-2	16.5	78.1	0.33	4	2
PEM-3	16.5	78.0	0.49	4	3

* W means mass ratio of Ben-(SPB) to PEI

5.2 CHARACTERIZATION OF MODIFIED BENTONITE AND MEMBRANES

The surface modification of modified bentonite was characterized by X-ray diffraction (XRD) using $\text{Cu-K}\alpha$ radiation over the 2θ range of $20-60^\circ$ at a scan rate of 2 deg min^{-1} (Bruker AXS Diffractometer D8 powder XRD). The percentage weight loss before and after modification was carried out by TGA measurements (Parkin elmer TGA4000/pyris6 instrument) in the temperature range of $35^\circ\text{C} - 800^\circ\text{C}$. The water uptake

capacity and contact angle analysis were carried out according to the procedure given in the CHAPTER-2, Section 2.3.5. In addition to this, from the obtained WCA values, the work of adhesion or surface energy (ω_A) of the membranes could be determined as

$$\omega_A = \gamma_w (1 + \cos\theta) \quad (5.1)$$

Where, ω_A is the surface energy (mN/m), γ_w is the surface tension of water (7.2×10^{-2} N/m) and θ is the contact angle. The porosity of the resultant membrane was analysed as mentioned in the CHAPTER 2, Section 2.2.6.

The humic acid rejection properties of the resultant membranes were determined according to the procedure given in the CHAPTER-3, Section 3.2.4. The heavy metal ion rejection efficiency of the membranes were investigated by both UF and PEUF. For PEUF, 1000 ppm concentration of lead nitrate and cadmium nitrate solutions were complexed with 1% polyethyleneimine aqueous solution. The feed solution was filled into a filtration tank and pressurized as required using a nitrogen cylinder. The concentration of heavy metal ion was measured using AAS and permeate was collected for a particular interval of time. The percentage of rejection was calculated by using the equation

$$\%R = \left(1 - \frac{C_p}{C_f}\right) \times 100 \quad (5.2)$$

Where ' C_p ' and ' C_f ' concentration of permeate and feed solution respectively.

5.3 RESULTS AND DISCUSSIONS

5.3.1 FTIR analysis

The chemical modification on the bentonite clay was confirmed by taking FTIR spectra of both raw bentonite and modified bentonite (Fig.5.5). The spectrum of raw bentonite showed an absorption peak at 3407 cm^{-1} and 1635 cm^{-1} , which is due to the stretching and bending vibrations of $-\text{OH}$ functionality of absorbed water molecules on the clay surfaces. The absorption peaks at 3694 cm^{-1} and 3619 cm^{-1} are corresponding to the stretching vibrations of hydroxyl groups coordinated to the octahedral cations. The most intensive absorption peak at 998 cm^{-1} attributed to the $-\text{Si}-\text{O}$ stretching vibrations. Compared to raw bentonite, the modified bentonite exhibited new absorption peaks in the spectrum. The characteristic absorption band associated with $-\text{CH}_2$ stretching vibrations was observed at 3010 cm^{-1} , however peak intensity is low due to low molar concentration. The absorption peak corresponding to the carbonyl ($-\text{C}=\text{O}$) group was observed at 1736

cm^{-1} . Two new peaks appear at 1347 cm^{-1} and 1211 cm^{-1} and are ascribed to the stretching vibrations of the sulfonate groups. Furthermore, the intense broad peak for adsorbed water molecules on the bentonite was observed around 3422 cm^{-1} . This substantiates the presence of hydrophilic $-\text{SO}_3\text{H}$ groups, which enhance the water retention of bentonite.

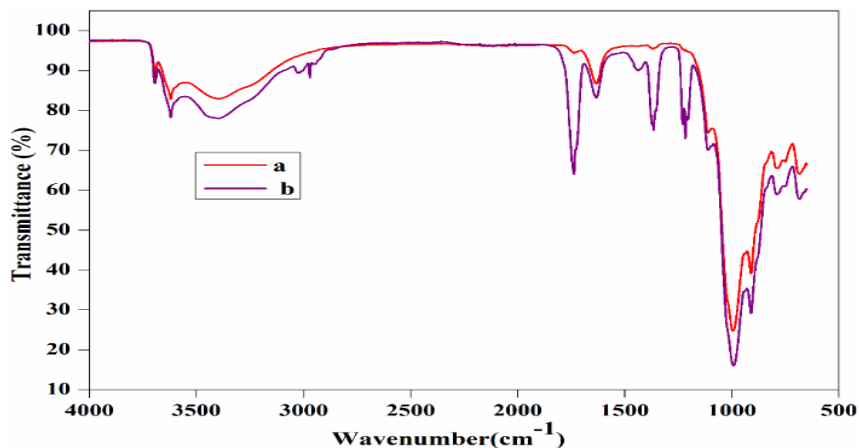


Fig.5.5 FT-IR spectrum of a) bentonite b) modified bentonite

In order to further confirm the chemical modification, EDX analysis was carried out. From the Fig 5.6, it was observed that, bentonite consists of silicon (Si), aluminium (Al) and oxygen (O) as the main elements. After chemical modification, the peaks corresponding to the carbon (C) with 26.17 % and sulphur (S) with 0.27 % appeared along with other peaks. This endorses the chemical modification on the bentonite. The elemental percentage composition of both bentonite and modified bentonite were tabulated in Table-5.2. In addition to this, TGA analysis was carried out for the confirmation of the chemical modification and resultant output has been presented in Fig.5.7. The result revealed two-stage weight loss for both bentonite and modified bentonite material. The first-stage of weight loss around $30\text{--}200^\circ \text{C}$ is mainly due to adhered water molecules in the surface and intercalations bentonite structure. The second-stage of weight loss around $350\text{--}800^\circ \text{C}$ corresponds to decomposition of the organic counterparts present in the material. However, compared to the percentage of weight loss of both the material, modified bentonite exhibited higher weight loss. This is attributed to the modified bentonite comprising of attached polyelectrolyte with $-\text{SO}_3\text{H}$ functionality which undergo decomposition at higher temperature.

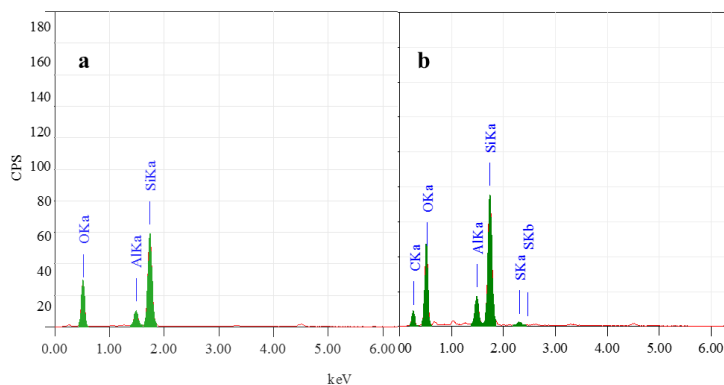


Fig 5.6 EDX analysis of a) bentonite and b) modified bentonite

Table-5.2 : The elemental composition of the bentonite and modified bentonite

Samples	Content of element (%)				
	Si	Al	O	S	C
Bentonite	27.63	4.53	67.83	-	-
Modified bentonite	18.80	3.43	51.34	0.27	26.17

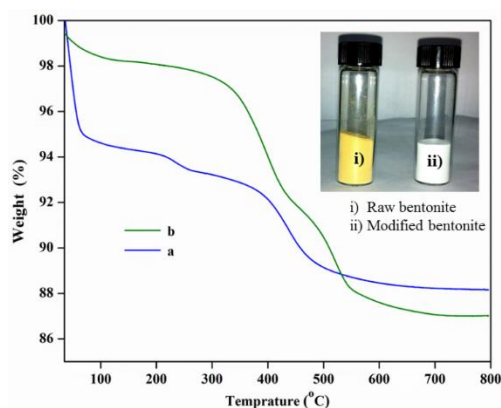


Fig.5.7 TGA analysis of a) bentonite and b) modified bentonite

Further, Fig.5.8 represents the FESEM and TEM images of the modified bentonite clay. From the images, it was observed that bentonite is having a typical layered structure comprising of aluminium and silicon as basic building unit. However, there is no significant structural changes in the bentonite observed after chemical modification of bentonite. This was further substantiated by investigating through the XRD analysis. The XRD patterns for pure and bentonite and modified bentonite nanoparticles are given in Fig.5.9. The characteristic peaks at diffraction angle, $2\theta = 20.7^\circ, 26.5^\circ, 36.3^\circ, 54.7^\circ$ corresponds to the planes (110), (210), (124) and (144) of the bentonite material. These XRD pattern are in good agreement with the standard JCPDS file (card no.01-088-0891). From the graph it can be observed that, there is neither significant change in intensity of the patterns, nor

there is shift in the peaks. This behaviour is due to no significant change in the phase structure of material after the modification.

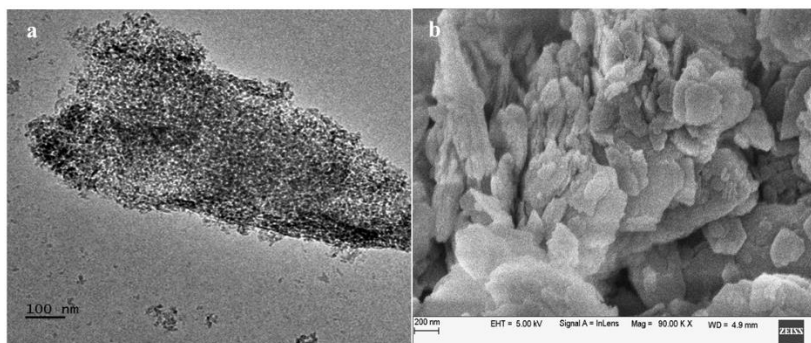


Fig.5.8 a) TEM and b) FESEM images of bentonite

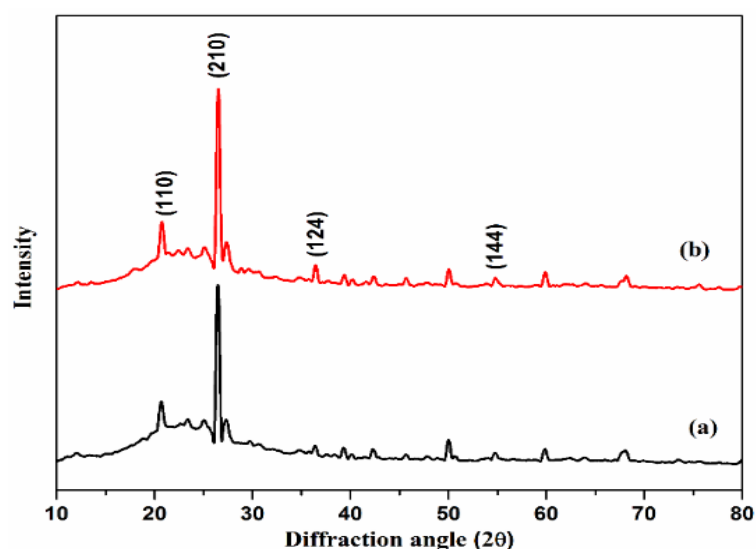


Fig.5.9 XRD analysis of a) bentonite and b) modified bentonite

5.3.2 Contact angle measurement

Fig.5.10 displays the contact angle and surface energy of the nanocomposite membranes. The decreasing trend of contact angle was observed with increased modified bentonite additive dosage. The membrane with 3 wt. % of additive had shown lowest contact angle of 63.8° , which was nearly 16° less than that of PEM-0 membrane. Further, contact angle values were used to determine the surface energy (ω_A) of the resultant membrane. The lowest ω_A of 85.2 mN/m was obtained for the PEM-0 membrane, whereas PEM-3 membrane exhibited highest ω_A value of 103.7 mN/m . These results indicate that, addition of modified bentonite to the membrane matrix could significantly improve the surface hydrophilicity.

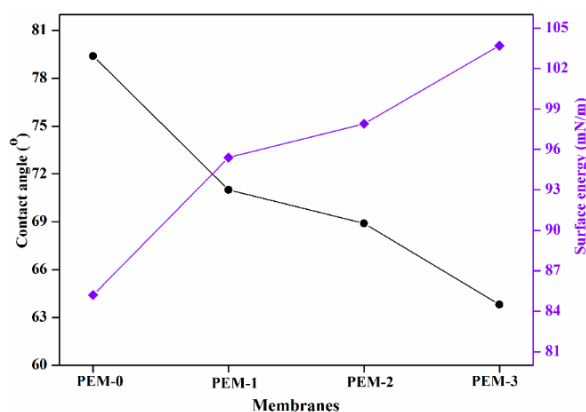


Fig.5.10 Contact angle and surface energy of the membranes

Furthermore, all membranes showed apparent decline in the contact angle with increase in the dropage. The PEM-0 membrane displayed slight decrease in the contact angle, whereas modified membranes offered noticeable change with increasing water drop age. At the water drop age of 150 sec, contact angles of the PEM-0, PEM-1, PEM-2 and PEM-3 membranes were 79°, 71°, 68° and 63° respectively (Fig.5.11). These results imply that the immobilization of modified bentonite into the membrane matrix not only improves the surface hydrophilicity but also pore hydrophilicity (Zhao *et al.* 2012).

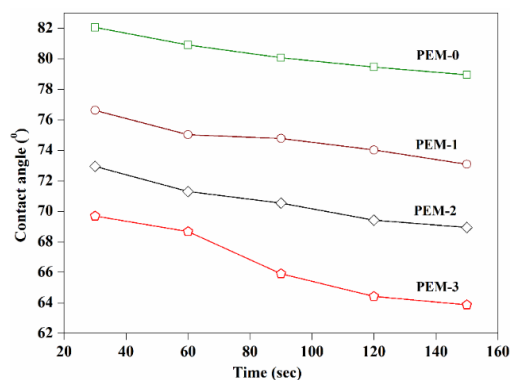


Fig.5.11 Time dependent contact angle of the membranes

5.3.3 Water uptake capacity

One more pervasive study to understand the bulk hydrophilicity of the membrane is water uptake measurement (Ganesh, *et al.* 2013). The water uptake capacities of the prepared membranes are tabulated in the Table-5.3. The results revealed that the water uptake capacity increases with increased modified bentonite content in the membrane matrix. PEM-0 membrane has shown the lower water uptake value of 34.7 %, whereas membrane with 3 wt. % of modified bentonite exhibited up to 71.3 %. This is the direct indication of increase in number of hydrophilic sites per unit area with increased modified bentonite dosage. Also from the Fig.5.6, we could observe that the PEM-3 membrane

displayed more number of macro-voids in the sublayers. This also contributes to the enhanced water uptake capacity of the membranes.

Table 5.3 Properties of the prepared membranes.

Membrane	Thickness (μm)	Porosity (%)	Water uptake (%)
PEM-0	128	32.4	34.7
PEM-1	139	42.9	48.2
PEM-2	143	53.5	65.8
PEM-3	131	62.7	71.3

5.3.4 Porosity of the membrane

The porosity of all prepared membranes were tabulated in Table-5.3. It can be observed that, the membrane with 3 wt. % of modified bentonite exhibited higher porosity up to 62.7 %, while at the same time PEM-0 showed porosity of 32.4 %. This change in the porosity could be explained on the basis of influence of modified bentonite content during the membrane formation. The addition of modified bentonite to the membrane dope enhances the influx rate of non-solvent (water) and delays the exchange process between the solvent in polymer dope and non-solvent in coagulation bath. This enhances the ratio of water content in the nascent membrane and improves the porosity. In addition, a portion of PVP was leached out of casting film during the phase inversion that acted as pore former (Kanagaraj *et al.* 2015, Zhao *et al.* 2013).

5.3.5 Membrane morphology

Fig.5.12 represents the cross-sectional SEM images of nanocomposite membrane matrix with different amount of additive dosage. All the membranes displayed asymmetric structure with dense top layer followed by porous sublayer with fully developed macropores. The proper immobilisation and uniform distribution of the additive into the membrane matrix was confirmed by elemental mapping analysis (Fig.5.13). With increase in the modified bentonite content, the number of macrovoids in the sublayer of membrane also increased. According to the literature, inclusion of hydrophilic inorganic additives and PVP into the casting solution significantly alters the morphology of resultant membranes (Zhang *et al.* 2012). The presence of PVP could accelerate the phase inversion process and thus enlarge the macrovoids, while the addition of modified bentonite could improve pore interconnection due to its migration behaviour. (Zhang *et al.* 2013, Zinadini *et al.* 2014)

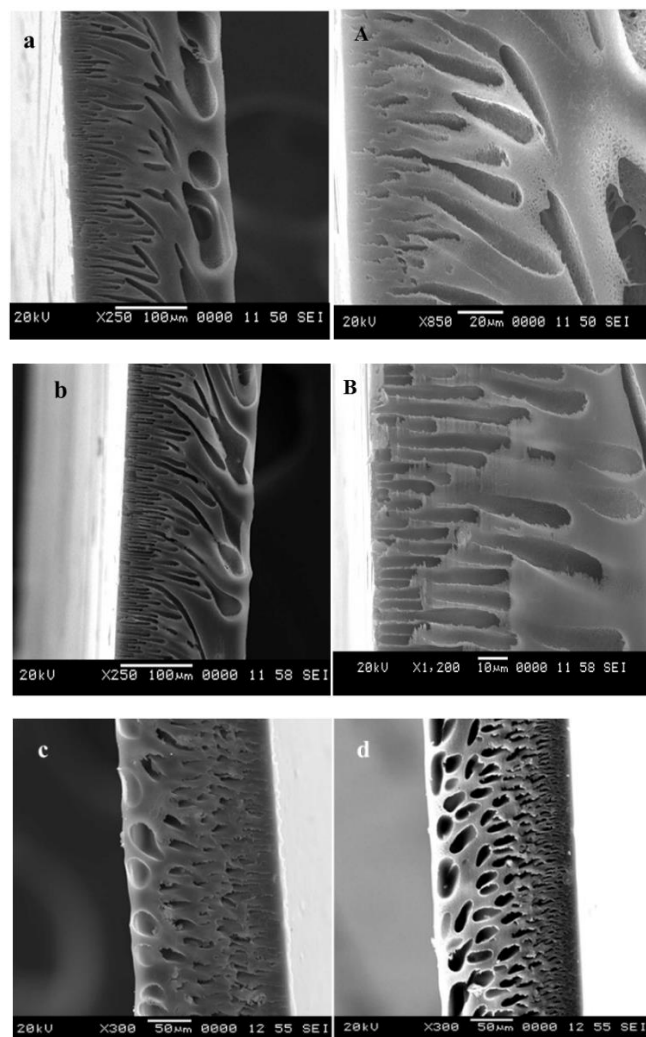


Fig.5.12 Cross-sectional SEM images of the a) PEM-0, b) PEM-1, c) PEM-2 and d) PEM-3 membranes

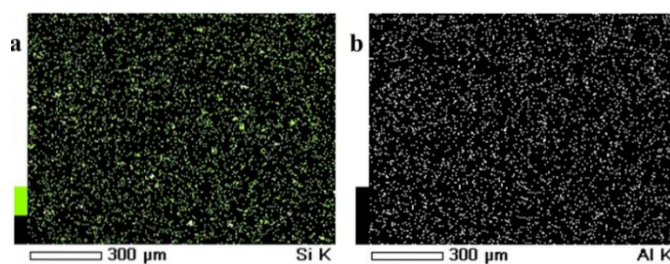


Fig.5.13 Elemental mapping of a) silicon and b) aluminium of PEM-3 membrane

Fig.5.14 displays the three dimensional AFM images of the PEI nanocomposite membranes. The roughness parameters of the membrane surfaces were also reported in terms of root mean square of Z data (Rq), mean roughness (Ra), and mean difference in the height between the highest peaks and the lowest valleys (Rz). The results of surface roughness for the prepared membranes is tabulated in Table-5.4. From the table, it was

observed that roughness parameters of all the modified membranes were higher than that of PEM-0 membrane. The PEM-0 membrane showed root mean square roughness (Rq) and mean roughness (Ra) of 7.43 nm and 5.93 nm respectively, whereas membrane with 3 wt % of modified bentonite exhibited mean roughness (Ra) and root mean square roughness (Rq) of 11.1 nm and 13.9 nm respectively. According to Zhang *et al.* (2012) membrane with higher surface roughness increases surface area and causes cavities, thus promoting permeation.

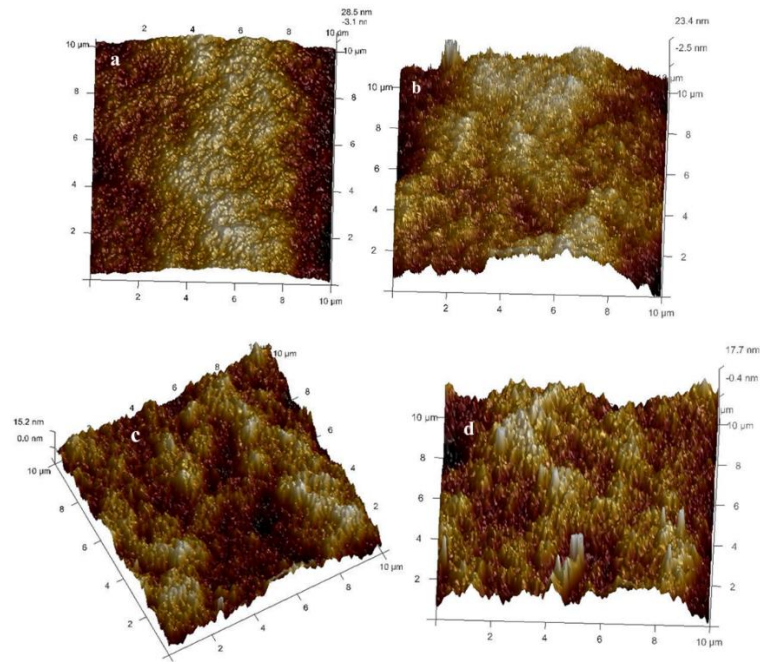


Fig.5.14 Three dimensional AFM images of a) PEM-0, b) PEM-1, c) PEM-2 and d) PEM-3 membranes

Table-5.4 Roughness parameters of the membranes

Membrane	Image surface area (μm^2)	Surface area Difference (%)	Roughness		
			Ra (nm)	Rq (nm)	$Rmax$ (nm)
PEM-0	100	0.072	5.93	7.43	67.7
PEM-1	104	1.37	7.13	9.25	99.1
PEM-2	100	0.083	8.71	10.3	108
PEM-3	102	1.62	11.1	13.9	126

5.3.6 Permeation properties

Fig.5.15 represents the time dependent pure water fluxes of the membranes with different amount of modified bentonite content. Initially, a gradual decline in PWF was observed for all the prepared membranes during compaction. This was probably due to

mechanical deformation or compression of membrane structure under the different transmembrane pressure (TMP) during the operation. Membrane with 0 wt. % of modified bentonite showed PWF of 121 L/m²h, whereas 3 wt. % of modified bentonite exhibited PWF of 211 L/m²h. The water fluxes of the PEM-1, PEM-2 and PEM-3 are 1.33, 1.52 and 1.74 times higher than that of PEM-0 membrane respectively. Here, the pure water fluxes of the nanocomposite membrane showed a similar trend that of porosity and hydrophilicity. Furthermore, the structural and morphological changes in the composite membrane when compared to PEM-0 membrane also influences the PWF. When modified bentonite content was increased from 1 wt. % to 3 wt. %, the membrane surface porosity, hydrophilicity, pore interconnection and macrovoids also increased, which significantly reduced the hydraulic resistance and thus improved membrane permeability (Li *et al.* 2009).

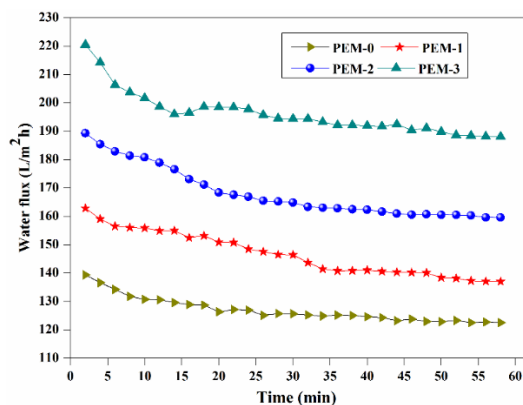


Fig.5.15 Time dependent pure water of the membranes

5.3.7 Antifouling properties

Fig.5.16 illustrates the water flux of the membranes after BSA solution filtration. It was observed that, permeability of the membranes decreased prominently when pure water was substituted by protein solution in the filtration tank, which represents the membranes fouling. After washing the membranes, the pure water flux of the PEM-0 membrane had shown a large decrease. However, the flux reduction for the modified bentonite embedded membranes was lower.

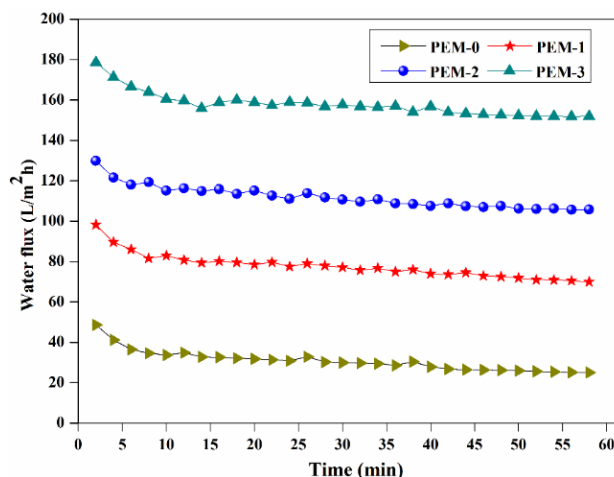


Fig.5.16 Pure water fluxes of the membranes after BSA protein solution filtration

Fig.5.17 represents the % of FRR of all the prepared membranes. Higher FRR indicates better hydraulic cleaning property of the membranes. The flux recovery ratio of the PEM-0 membrane was about 28.7 %, indicating poor self-cleaning property, while it reached up to 58.1 %, 76.5 % and 84.1 % for the PEM-1, PEM-2 and PEM-3 membranes respectively. This change in the flux recovery value of nanocomposite membranes may be attributed to modified membrane consisting of abundant number of hydrophilic functionality such as sulfonic acid ($-\text{SO}_3\text{H}$), hydroxyl ($-\text{OH}$) and carbonyl groups ($\text{C}=\text{O}$), which induces hydrophilicity to the surface, thereby minimizing strong hydrophobic–hydrophobic interactions between the foulants and membrane surface (Sotto *et al.* 2011).

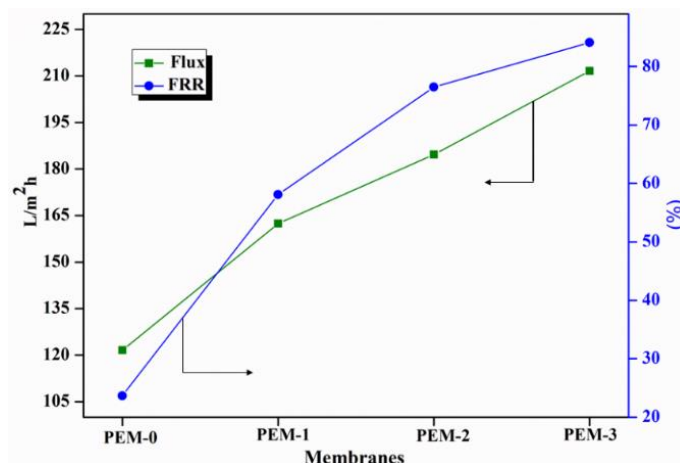


Fig.5.17 Flux recovery ratio and flux of prepared membranes

Further to examine more about the fouling behaviour, the properties such as total fouling ratio (R_t), irreversible (R_{ir}) and reversible (R_r) fouling resistance ratio were determined. The fouling nature of the modified membrane after hydraulic cleaning is

depicted in Fig.5.18. The total fouling ratio (R_t) of 92.1 % was observed for the PEM-0 membrane. PEM-3 membrane exhibited reversible fouling (R_r) up to 75.6 % with flux rate of $168.7 \text{ L m}^{-2}\text{h}^{-1}$. After modification, the irreversible fouling percentage in the total fouling drastically dropped to 41.8 %, 23.4 % and 15.8 % for PEM-1, PEM-2 and PEM-3 membranes respectively. This confirmed that the antifouling nature of hybrid membranes improved significantly.

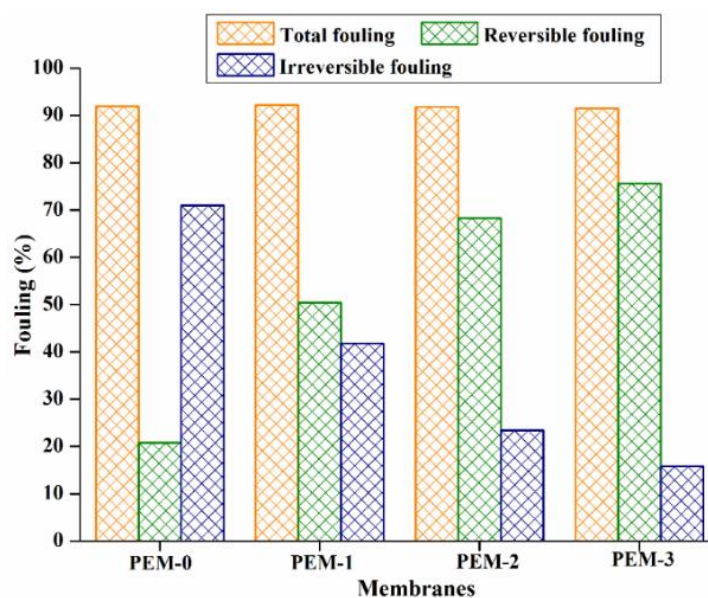


Fig.5.18 Fouling resistance behaviour of prepared membranes

5.3.8 Humic acid rejection properties

To further explore the humic acid rejection and anti-organic fouling property of modified membranes, the filtration experiments were carried out at 0.3 MPa TMP with 200 ppm humic acid solution (Fig.5.19). The flux of all the membranes decreased rapidly at the beginning of each filtration experiment, which indicates the deposition, or adsorption of humic acid molecules on the membrane surfaces. The inclusion of hydrophilic modified bentonite enhanced the relative flux indicating a higher resistance towards fouling (Fig.5.20). The membrane without additive showed $\sim 24\%$ relative to initial PWF, whereas PEM-3 membrane exhibited highest relative permeate flux of $\sim 60\%$. Fig.5.21 represents the humic acid rejection behaviour of the different membranes. From the results, it is observed that the maximum fouling resistance is offered by PEM-3 membrane with humic acid rejection efficacy of 87.6 % (Shao *et al.* 2011, Shao *et al.* 2013).

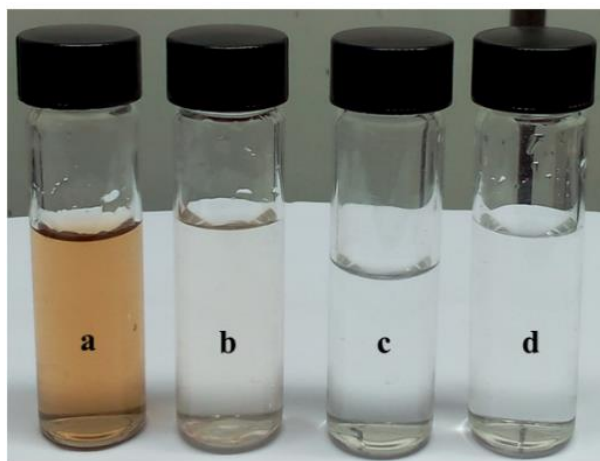


Fig.5.19 Photographic image of a) humic acid solution in the feed, b), c) and d) are permeate of PEM-1, PEM-2 and PEM-3 membranes respectively

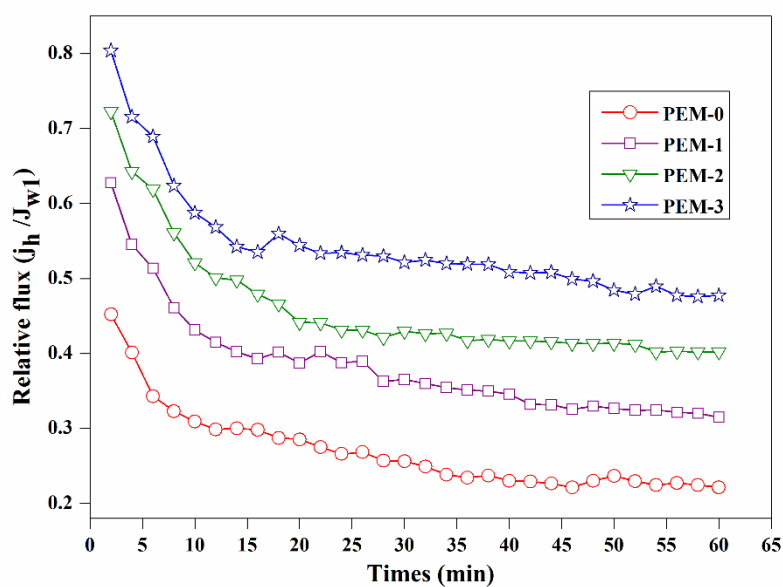


Fig.5.20 Relative flux ratio during humic acid filtration

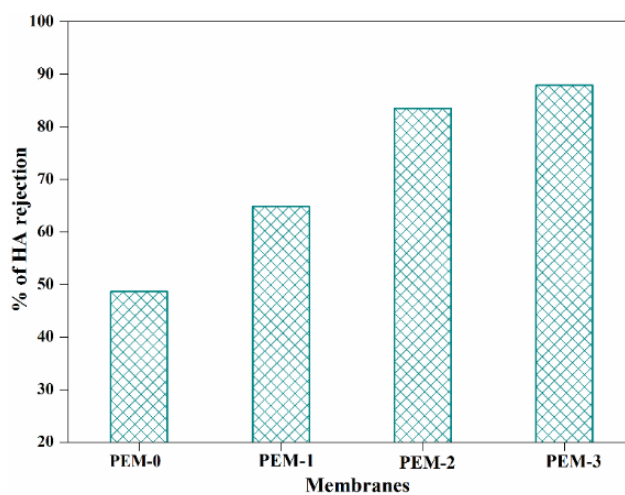


Fig.5.21 Humic acid rejected by the membranes at 0.3MPa TMP

5.3.9 Heavy metal ion rejection

UF membranes have also been exploited for the removal of toxic heavy metal ions from aqueous solutions. The heavy metal ion rejection efficiency of the hybrid membrane was investigated by both UF and PEUF process. Among the prepared membranes, the well performed membrane PEM-3, which exhibited lower contact angle, good permeability and highest FRR value was selected for the rejection studies. Fig.5.22 represents the % of heavy metal ions (Pb^{2+} and Cd^{2+}) rejected by the membrane during the PEUF and UF process. The membrane showed PEUF rejection efficacy up to 80.5 % and 74.6 % for Pb^{2+} and Cd^{2+} ions respectively. From the results, we can say that the % of rejection of the Pb^{2+} was higher than that of Cd^{2+} ions. This might be due to Pb^{2+} which forms the larger metal chelate size compared to Cd^{2+} ions as the Pb^{2+} ion has smaller size (atomic radius of Pb –180 pm) and higher electronegativity (2.33) compared to Cd^{2+} ions (atomic radius of Cd–220 pm and electronegativity of 1.69). The % rejection of Pb^{2+} and Cd^{2+} ions during the UF process was 47.3 % and 41.5 % respectively. This was probably due to heavy metal ion adsorption capacity of the modified bentonite in the mixed matrix membrane. Fig.5.23 represents the elemental mapping of the lead and cadmium on the membrane surface after the filtration experiment. This confirms the heavy metal ion adsorption capacity of the membrane. The membranes exhibited higher % of rejection during the PEUF process than the UF process (Pereira *et al.*2014).

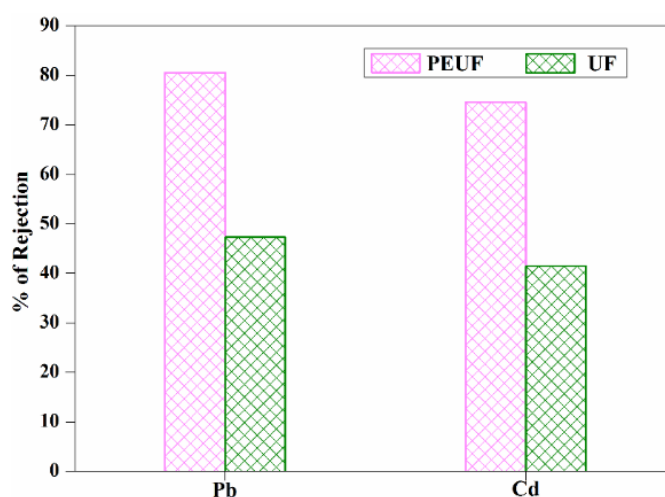


Fig.5.22 Heavy metal ion rejected by the PEM-3 membrane

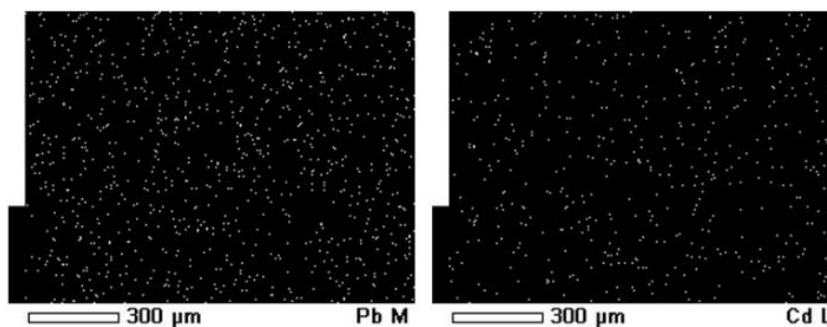


Fig.5.23 Elemental mapping of PEM-3 membrane after the heavy metal ion filtration

5.4 CONCLUSIONS

The natural bentonite clay bearing the poly (4-styrenesulfonate) brushes were synthesised by surface initiated ATRP reaction and employed as performance modifying agent. The modified bentonite brushes have significant influence on anti-organic fouling nature of the membrane. The membrane with 3 wt. % of additive dosage has shown FRR value of 84.1 % with irreversible fouling ratio of 15.8 % and reversible fouling (R_r) up to 75.6 %. The humic acid rejection study revealed that PEM-3 membrane having rejection efficiency up to 87.6 % and foulents can be easily removed by simple hydraulic cleaning. Moreover, modified membranes were also having the capacity to adsorb heavy metal ion from the aqueous solution.

CHAPTER 6

FABRICATION OF POLYDOPAMINE FUNCTIONALIZED HALLOYSITE NANOTUBE/POLYETHERIMIDE MEMBRANES FOR HEAVY METAL REMOVAL

Abstract: In this chapter, effort has been made to address the antifouling and heavy metal ion rejection nature of PEI membrane. For this purpose, halloysite nanotubes were coated with polydopamine and incorporated into the PEI membrane matrix. The contact angle, porosity, permeation and antifouling properties of hybrid membranes were studied and results are discussed in detail. In addition to this, anti-biofouling property of the membrane was also investigated.

Clay nanotubes are new prospective fillers for polymeric composites due to their large surface area, high length-to-diameter (L/D) ratio, good physicochemical properties and low cost, in particular, halloysite, a type of naturally occurring clay material with a nanotubular structure (Fig 6.1). This consists of 1:1 aluminosilicate layer with abundant Si-OH and Al-OH groups, which endow halloysite nanotubes (HNTs) with net negative charge, strong hydrophilicity and facile modification ability (Yu *et al.* 2016). Compared with other nanosized materials, naturally occurring HNTs are easily obtained and much cheaper than other nanoparticles such as carbon nanotubes (CNTs). Hence, HNTs may have the potential to replace the expensive CNTs as hydrophilic additives.

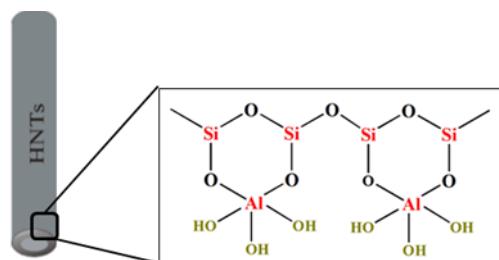


Fig 6.1 Chemical structure of halloysite nanotube

Zhang *et al.* (2012) reported preparation of poly(4-vinylpyridine) (P4VP) grafted onto the surface of HNTs via in situ polymerization, and then, silver ions were immobilized on P4VP via complex reaction (Fig.6.2). The permeation properties of the hybrid membranes were significantly superior to the pure PES membrane, especially when the modified HNTs content was 3%, the pure water flux of the membrane reached the maximum at $396.5 \text{ Lm}^{-2}\text{h}^{-1}$. Antibacterial activity of the hybrid membrane was evaluated with the viable cell count method using antibacterial rate against *Escherichia coli* (*E. coli*) and *Staphylococcus aureus* (*S. aureus*). The antibacterial rates of the hybrid membranes against *E. coli* and *S. aureus* were about 99.9% and 99.8%, respectively.

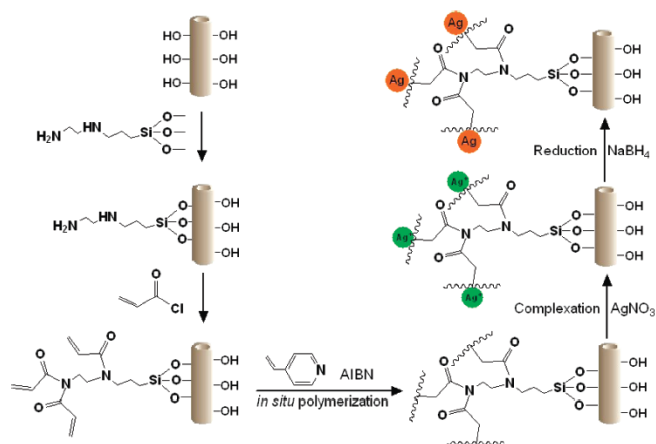


Fig.6.2 Schematic representation for the preparation of silver doped HNTs (Zhang *et al.* 2012)

Yu *et al.* (2014) studied the antifouling nature of polyethersulfone (PES) UF membrane by the inclusion of dextran grafted HNTs. The schematic representation of chemical modification of HNTs is presented in Fig.6.2. The results indicated that the surface hydrophilicity of membrane significantly improved after adding HNTs-dextran. Compared with the pristine PES membranes, the hybrid membranes possess higher flux and good antifouling properties.

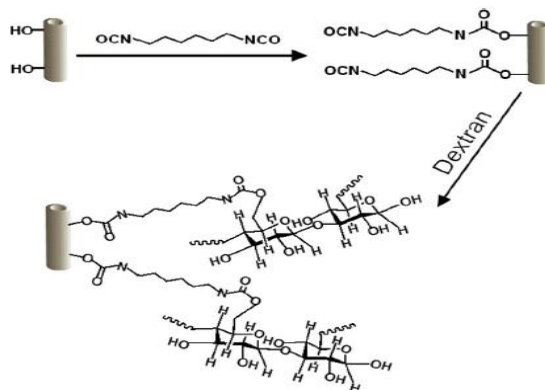


Fig.6.3 Schematic representation for the preparation of dextran grafted HNTs (Yu *et al.* 2014)

Wang *et al.* (2014) reported the fabrication of antifouling property of PES UF hybrid membrane containing HNTs grafted 2-methacryloyloxyethyl phosphorylcholine (HNTs-MPC) which was prepared via phase inversion method. The hybrid membrane was shown to be more hydrophilic with a higher pure water flux. The thickness of the thin separating layer on the top tended to decrease with the addition of HNTs-MPC. The BSA

adsorption experiment indicated that the adsorption amounts of BSA on the membrane dramatically decreased.

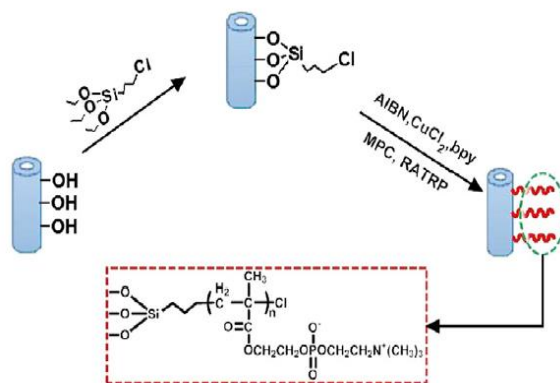


Fig. 6.4 Preparation process of HNTs-MPC via reverse atom transfer radical polymerization (Wang *et al.* 2014)

Liu *et al.* (2016) reported the preparation of sulfonated HNTs via dopamine-initiated atom transfer radical polymerization and employed as an additive to improve the membrane properties. The schematic representation of modification was given in Fig. 6.5. They stated that the sulfonated functionality on the modified HNTs significantly enhance the interaction between the additives and sulfonated poly(ether ether ketone) (SPEEK) membrane matrix, thereby greatly influencing the membrane morphology and other physicochemical properties of resultant membrane.

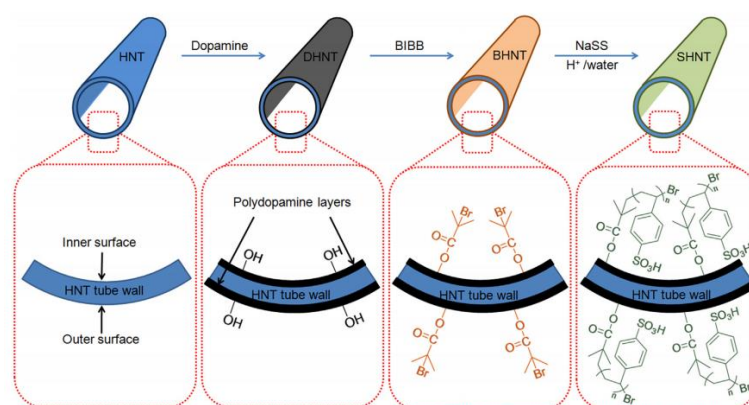


Fig. 6.5 Schematic representation of preparation of sulfonated HNTs (Liu *et al.* 2016)

Recently, Messersmith *et al.* (2007) described the facile and versatile modification technique using dopamine as a powerful modifier. Dopamine is a kind of catecholamine that contains both catechol and primary amine functional groups. Under oxidizing

conditions, dopamine is able to undergo self-polymerization in aqueous solution to give polydopamine (PDA) (Lee *et al.* 2007). Jiang *et al.* (2013) stated that, PDA could strongly adhere into many solid substrate such as TiO₂ nanoparticles, graphene oxide and clay materials. Liu *et al.* (2013) enlightened that the polar groups in PDA layer such as hydroxyl and amine groups provide the substrates with improved hydrophilicity and antifouling ability. It also enhances the interfacial interactions between nanomaterials and polymer matrixes. According to Gao *et al.* (2013) abundant functional groups of PDA functionalized graphene showed high adsorption capacities toward a wide spectrum of contaminants, including heavy metals, synthetic dyes and organic pollutants.

Shao *et al.* (2014) enhanced the UF membrane properties of PVDF membrane via self-polymerisation of dopamine and further modified it by treating with ammonium fluortitanate. The contact angle and SEM analysis showed a considerable improvement in hydrophilicity and morphology of PVDF UF membrane after the modification. The PDA layer on membrane helps in strong adhesion of TiO₂ on the membrane matrix. In addition to this, modified membrane showed enhancement in the permeation and antifouling properties. Lv *et al.* (2015) developed a new strategy of improving the nanofiltration membrane performance via deposition and crosslinking of PDA and polyethylenimine on the base hydrolysed polyacrylonitrile UF membrane. Zeta potential measurements showed that these membranes were slightly positively charged, resulting in a salt rejection sequence of MgCl₂ > CaCl₂ > MgSO₄ > Na₂SO₄ > NaCl at pH 5. The permeation and rejection efficiency of NF membranes are presented in Fig.6.6.

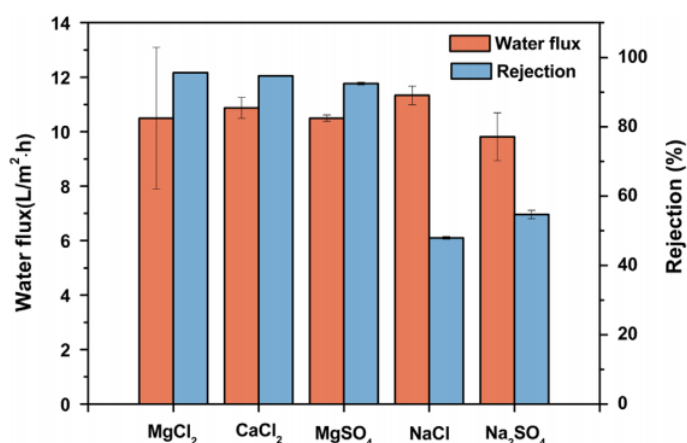


Fig.6.6 Rejection behaviour of NF membrane with different electrolyte solutions

Sianipar *et al.* (2016) reported the modification of multiwalled carbon nanotubes (MWCNTs) via PDA coating and employed it as hydrophilic additive in polysulfone UF membrane. The inclusion of 0.5 wt.% of an additive in the membrane matrix significantly improves the permeation rate with BSA protein rejection rate of 99.88 %. Tripathi *et al.* (2016) illustrated the straightforward approach to enhance the UF membrane performance and antifouling properties by incorporating PDA modified silica nanoparticles. The resultant nanocomposite membrane showed higher water flux and rejection rates compared to pristine polyacrylonitrile UF membrane.

In this chapter, well-dispersed HNTs modified with PDA was synthesised through one-step facile procedure and used as additive to modify the PEI membranes. Effect of additive on the membrane structure and performance were investigated in detail. The performance of modified membranes was studied in terms of water uptake capacity, water flux and membrane hydraulic resistance. Furthermore, antifouling, anti-biofouling and heavy metal ion rejection behavior was investigated in detail.

6.1 MATERIALS AND METHODS

6.1.1. Materials

Halloysite nanotubes and dopamine were supplied by Sigma Aldrich. Tris(hydroxymethyl)aminomethane (99%) was obtained from Alfa Aesar. BSA was procured from Central Drug House (CDH). The polyvinylpyrrolidone (PVP) was purchased from Sigma Aldrich, India.

6.1.2 Preparation of modified HNTs

The chemical modification of HNTs was carried out using reported procedure in the literature (Chao *et al.* 2013). In brief, the calculated amount of HNTs were dispersed in demineralised water using ultrasound treatment for 0.5 h to get a HNTs suspension (10 mg/mL, 50 mL). The pH value of the suspension was adjusted to alkalescence (pH 8.8) by using the base tris(hydroxymethyl)aminomethane. Afterwards, 0.2 mg/mL of dopamine powder was added into the HNTs suspension while being stirred at 30 °C. The obtained solution was continuously stirred for 6 hrs to get HNTs coated with black insoluble PDA polymer (Fig.6.7). The resulting product was collected by centrifugation and washed with distilled water repeatedly until the black filtrate became colourless.

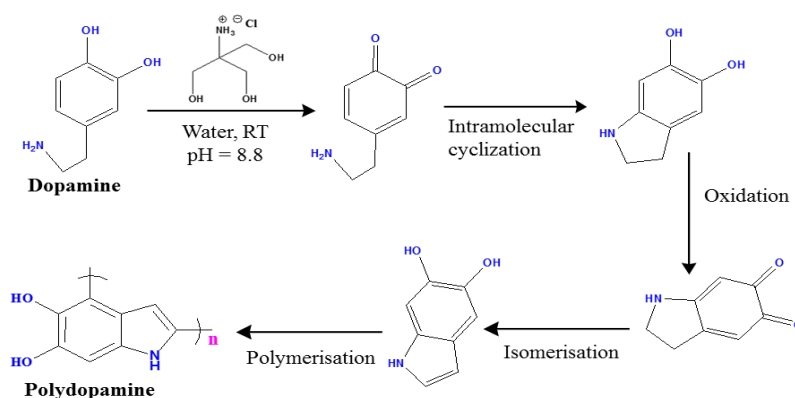


Fig.6.7 Schematic representation of polymerisation of dopamine

6.1.3. Preparation of composite membrane

PEI/MHNTs mixed matrix membranes were prepared by non-solvent induced phase separation method (Ganesh *et al.* 2013). Detailed procedure of membrane preparation via phase inversion method is given in the membrane preparation section in CHAPTER-2, Section 2.1.2. In brief, calculated amount of MHNTs (0 wt% to 4 wt% of PEI dosage) was dispersed in suitable volume of NMP solvent and stirred for 90 minutes at ambient temperature. The desired quantity of PEI (overall 20 wt% of polymer concentration mentioned in the final casting solution) was added to the above dispersed solution along with 2 % of invariable pore forming agent PVP. The obtained homogeneous casting solution was casted over a glass plate and immersed into water. Overviews of compositions of the membranes are described in Table 6.1.

Table 6.1 - Composition of the casting solution

Membrane	PEI(g)	NMP(g)	MHNTs(g)	PVP	W_{MHNTs}^* (wt%)
HMM-0	18	80	0	2	0
HMM-1	18	79.8	0.18	2	1
HMM-2	18	79.4	0.36	2	3
HMM-3	18	79.1	0.54	2	4

* W_{MHNTs} is the mass ratio of MHNTs to PEI.

6.2 CHARACTERIZATION AND PERFORMANCE STUDY

The chemical modification of the HNTs were analysed by FTIR spectrum. The FTIR spectra were recorded using Avatar 360 IR spectrophotometer in the range of 4000-500 cm^{-1} . The TEM images of HNTs and MHNTs were recorded using JEM 1230 Electron Microscope. The cross sectional SEM images of the prepared composite membranes were

recorded as per reported procedure CHAPTER-2, Section 2.2.3 The water uptake capacity and contact angle of the membrane are the important parameters to know about hydrophilic nature and analysis was carried out according to the procedure given in the CHAPTER-2, Section 2.2.4. The porosity of the prepared membranes were determined according to the procedure given in CHAPTER-2, Section 2.2.6. The membrane hydraulic resistance offered by the prepared membranes were determined by the procedure given in CHAPTER-4, Section 4.2. The permeation and antifouling properties of nanocomposite membranes were analysed according to the procedure in CHAPTER-3, Section 3.2.3. PEUF and UF experiments were carried out to analyse the heavy metal ion rejection behaviour of the prepared membranes according to the procedure given in CHAPTER 5, Section 5.2.

Antimicrobial property of the MHNTs modified membrane was investigated by inhibition of microbial growth according to the literature (Jiang *et al.* 2013). In brief, the standard cultures of three bacteria *Mycobacterium smegmatis* (MTCC 994), *Staphylococcus aureus* (MTCC3160) and *Escherichia coli* (MTCC1687) and fungi *Candida albicans* (MTCC 7253) was obtained from IMTECH, Chandigarh, India. Microbial cultures were grown in nutrient agar media and sub cultured into nutrient broth. Hundred microlitre of microbial culture (0.5 Mac Farland) was spread on the agar plate using a cotton bud. Membranes were cut into about 9 mm disc like pieces and placed on microbial mat with active surface facing the culture. The plates were incubated for 12 hours and observed for the zone of inhibition. Standard Fluconazole and Ciprofloxacin prepared at 10 mg/mL concentration was used as reference standards for fungi and bacteria respectively.

Another set of experiments were carried out to check the anti-biofouling capacity of the membranes by incubation method. In brief, membranes were cut into 1 cm x 3 cm size strips and incubated in 100 times diluted 0.5 Mac Farland microbial culture in a test tube for 12 hours. Sterile whatman filter paper strip of similar size was used as control. After 12 hours of incubation, all the strips were taken out, drained and placed on nutrient agar plates. Agar plates were observed for the microbial colonies around the membranes.

6.3 RESULTS AND DISCUSSIONS

6.3.1 TEM analysis

The representative TEM images of the pristine HNTs and MHNTs were displayed in Fig.6.8. The image Fig.6.8a reveals that the HNTs possess a tubular structure with open

end in the either side. The lengths of the HNTs varies from 150 nm to 600 nm and the thickness in the range of 30 nm to 90 nm. The change in the morphology of the MHNTs elucidated by measuring the diameters of nanotubes before and after modification from TEM images. The tubular structure of MHNTs becomes thicker than that of HNTs (Fig.6.8b). After modification, thickness of the MHNTs increased to about 15-20 nm compared to virgin HNTs. This indicates that a polydopamine polymer layer had formed on the surface of the HNTs (Chao *et al.* 2013).

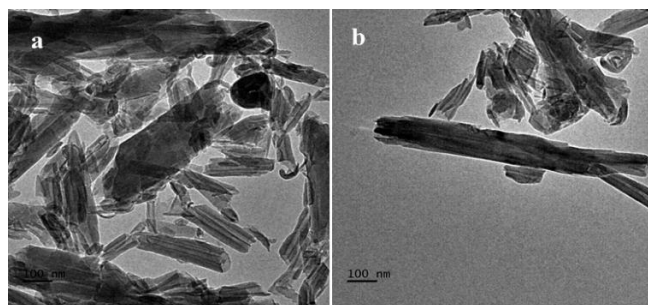


Fig.6.8 TEM images of a) HNTs and b) MHNTs

6.3.2 FTIR analysis

Fig.6.9 represents the FTIR spectra of HNTs and MHNTs. The spectrum of HNTs showed absorption peaks at 3688 cm^{-1} and 3618 cm^{-1} due to the stretching vibration of -OH groups. The peak at 913 cm^{-1} represents the bending vibration of Al-OH bond. The spectral band at 1022 cm^{-1} corresponding to the stretching vibration of Si-O bonds. After modification of HNTs, the spectrum displayed broad peak at 3422 cm^{-1} corresponding to the -OH groups of the polydopamine. Also, the peak at 3615 cm^{-1} and 3688 cm^{-1} ascribed to symmetric and asymmetric stretching vibration of -NH groups respectively. The absorption band at 1624 cm^{-1} corresponds to the carbonyl group of polydopamine. This confirms the formation of the polydopamine coating on the HNTs.

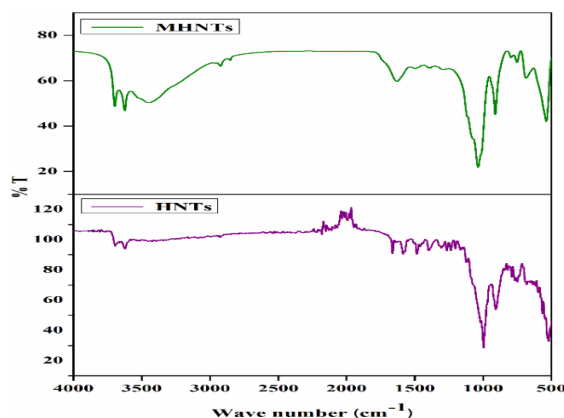


Fig.6.9 FTIR spectrum of the HNTs and MHNTs

6.3.3 Hydrophilicity of membranes

The water uptake capacity of all prepared membranes is presented in Fig.6.10. The membrane with 0 wt.% of MHNTs showed around 58.4 % of water uptake capacity and it increases as the MHNTs content increased in the membrane matrix. This is the direct indication of increase in number of hydrophilic sites in membrane matrix and also suggests towards increased macro voids in the sub-layer of the membrane (Ganesh *et al.* 2013). Generally, the water contact angle measurement is used to estimate the hydrophilicity and wetting characteristics of the membranes (Fig.6.10). The HMM-0 membrane had showed a contact angle value of about 79.1°, whereas membrane with 4 wt. % of MHNTs dosage in the membrane matrix showed contact angle of 66.3°. This implies that the hydrophilicity of the membrane surface improves significantly due to the addition of the MHNTs. The top surface photographs of prepared membranes are represented in Fig.6.11. The results illustrate that, the surface of the membrane was darker as increase in the MHNTs dosage. Therefore, hydrophilic MHNTs presented on the membrane surface were easily susceptible to wet and adsorbed by water, giving rise to lower water contact angle.

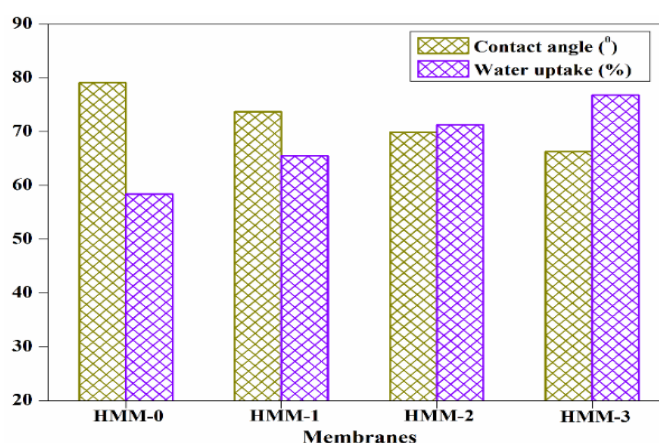


Fig.6.10 Contact angle and water uptake capacity of the membranes

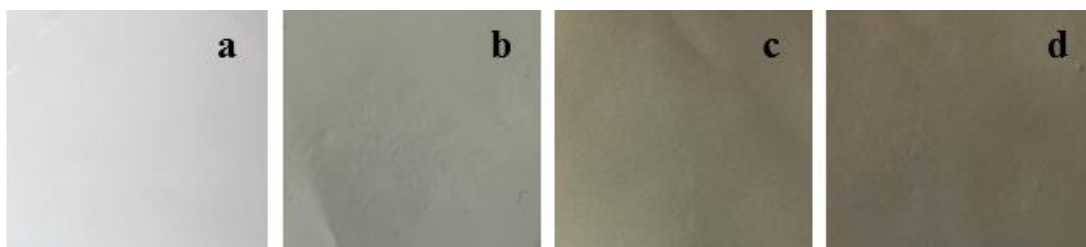


Fig.6.11 Digital photography of the top surface of a) HMM-0 b) HMM-1 c) HMM-2 and d) HMM-3 membranes

Table 6.2 Properties of the prepared membranes

Membrane Code	Membrane Thickness(μm)	Porosity (%)	Hydraulic resistance ($\text{Kpa/Lm}^{-2}\text{h}^{-1}$)
HMM-0	205	36.8	1.59
HMM-1	203	49.2	1.21
HMM-2	206	61.7	0.88
HMM-3	210	58.5	1.05

6.3.4 Porosity of the membrane

Porosity of the PEI/ MHNTs nanocomposite membranes is displayed in Table-6.2. The results revealed that, all PEI/MHNTs nanocomposite membranes have exhibited higher porosity than HMM-0 membrane. However, with an increase in MHNTs content, membrane porosity increases first and then decreases. This is due to the addition of MHNTs into the casting solution, which enhances the inflow rate of non-solvent i.e water and at the same time hinders the exchange process between solvent and non-solvent during the phase separation process. There is an enhancement in the ratio of water content in the nascent membrane, which increases the porosity. Also a portion of PVP was leached out of the casting film during the exchange of solvent–nonsolvent process and acted as a pore-former during membrane formation, which may be another reason for enhancing the membrane porosity (Abdoul Raguime *et al.* 2007).

6.3.5 Morphological study

The influence of MHNTs on the morphology of the prepared membranes were investigated by SEM analysis and the representative image is shown in Fig.6.12. All the membranes showed typical asymmetric structure with compact top layer and porous sub-layer (fully developed macropores at the bottom). With the addition of MHNTs into the casting solution, the number of macrovoids increases in bottom layer and the pore walls among macrovoids become looser with some channel-like pores (Fig.6.13). From the literature it was observed that the presence of inorganic additives in the membrane dope have significant influence on the membrane morphology (Sun *et al.* 2009). Addition of hydrophilic MHNTs additive into the casting solution alters the kinetics and thermodynamic behaviour during phase inversion process. (Li *et al.* 2007).

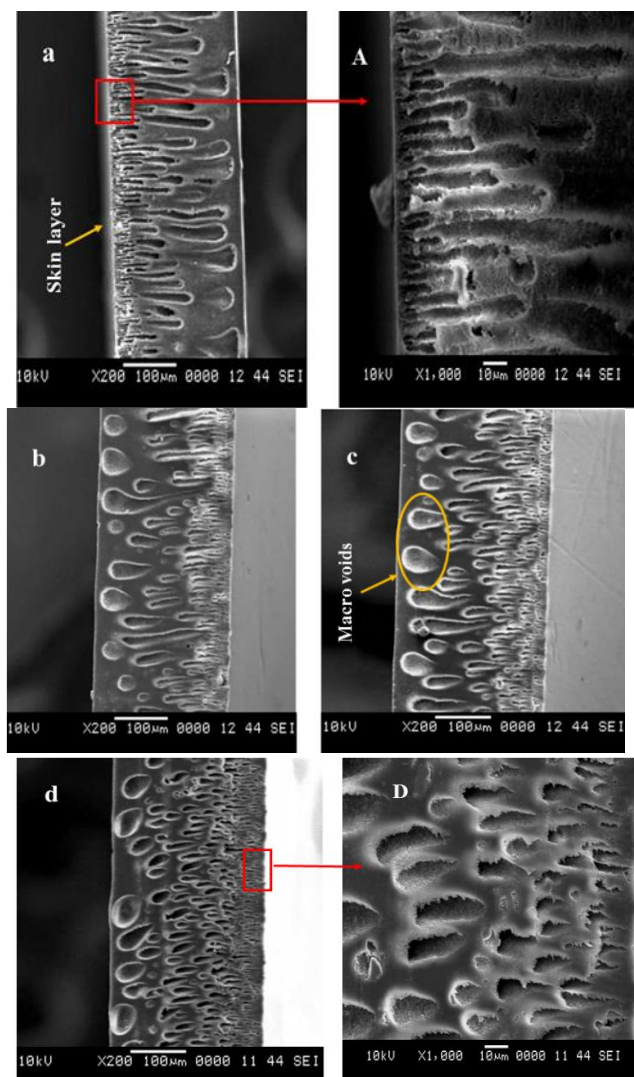


Fig.6.12 Cross sectional SEM images of the a) HMM-0, A) magnified HMM-0, b) HMM-1, c) HMM-2, d) HMM-3 and D) magnified HMM-3

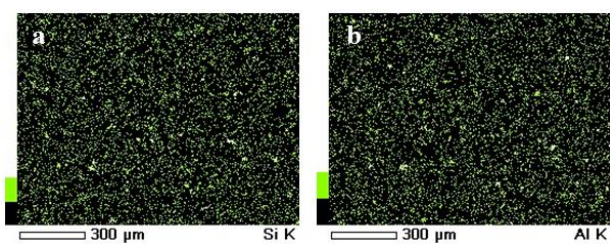


Fig.6.13 Elemental mapping of silicon and aluminium on HMM-2 membrane

6.3.6 Permeation properties

Time dependent PWF of the prepared membranes at 0.3 MPa pressure is shown in Fig.6.14. It can be observed that there is a gradual decrease in the PWF of membranes during membrane compaction. Compaction is described as a compression of membrane

structure under a transmembrane pressure (TMP) difference causing a reduction in membrane permeability. In present work, the water flux of HMM-0 membrane decreased from $149 \text{ Lm}^{-2}\text{h}^{-1}$ to $125 \text{ Lm}^{-2}\text{h}^{-1}$, whereas HMM-2 membrane exhibited flux reduction $276 \text{ Lm}^{-2}\text{h}^{-1}$ to $245 \text{ Lm}^{-2}\text{h}^{-1}$ during membrane compaction. When MHNTs content increased from 0-3 wt. %, the porosity, surface pore size, pore interconnection, macrovoids and hydrophilicity of the membrane was increased, which significantly declines the resistance of water permeating through the membranes and thus increased membrane permeability. However, higher particle concentration (4 wt. %) in the membranes matrix lead to a decrease in PWF because of the pore blockage caused by excessive particles and the pore collapse in membrane cross-section resulted from aggregation of nanoparticles.

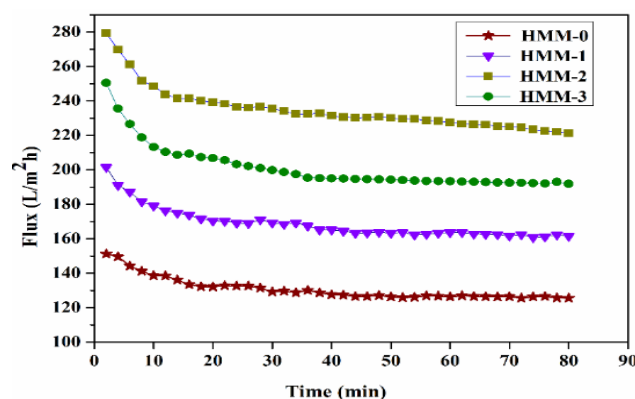


Fig 6.14 Time dependent pure water flux of the membranes

6.3.7 Membrane hydraulic resistance

PWF of the nanocomposite membranes were measured at different transmembrane pressures (Fig.6.15). The membrane hydraulic resistances (R_h) were determined as the inverse of the slope of the plots of PWF against the respective transmembrane pressures. The hydraulic resistance offered by the membranes with different amount of MHNTs are shown in Table-6.2. The membrane showed decrease in the hydraulic resistance with increase in the MHNTs content in the membrane. The HMM-0 membrane showed hydraulic resistance of $1.59 \text{ Kpa/Lm}^{-2}\text{h}^{-1}$ and it was observed to decline $0.88 \text{ Kpa/Lm}^{-2}\text{h}^{-1}$ for the HMM-2 membrane. This can be explained by the fact that, the modified membrane consist of number of hydrophilic groups to enhance the hydrophilicity.

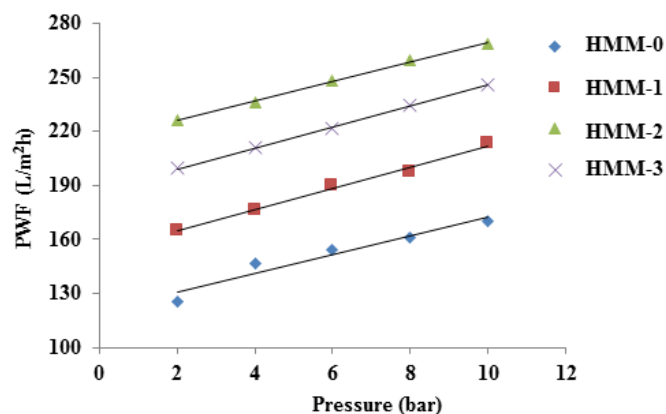


Fig.6.15 Pressure dependent pure water fluxes of membranes

6.3.8 Antifouling performance of the membrane

In current study, BSA was used as a model protein to conduct the antifouling property study of the prepared membranes. Fig.6.16 shows the flux of the prepared membranes performed at 0.3 MPa pressure in different conditions i.e. before BSA filtration, during BSA filtration and after BSA filtration. It can be seen that fluxes of all the membranes decrease rapidly during BSA ultrafiltration, which may be due to the deposition and absorption of BSA on membrane surface and pores.

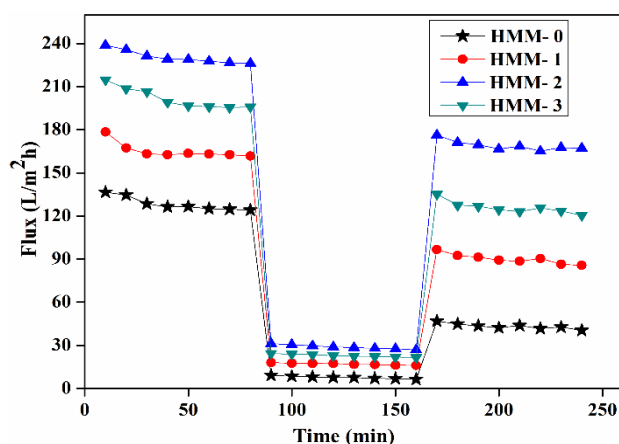


Fig.6.16 Flux versus time for membranes at 0.3 MPa during three conditions

Flux recovery ratio (FRR) of the prepared membranes are tabulated in Table-6.3. The FRR was as low as 26.6 % and total fouling ratio (R_t) of 92.1% was observed for the HMM-0 membrane. After addition of MHNTs into the membrane matrix, the overall permeation FRR of the modified membrane reached up to 74.5%. The total fouling gradually decreased from 92.1% to 86.2 % for HMM-0 and HMM-2 membrane respectively. Particularly, HMM-2 membrane exhibited reversible fouling (R_r) upto 60.7% with flux rate of $168.7 \text{ L m}^{-2}\text{h}^{-1}$. Thus, the loosely adhered or adsorbed protein molecules

on the membrane surface were easily detached by simple washing resulting in a high FRR. The results of flux decline behaviour and FRR values indicated that the modified membranes had better antifouling property as compared to HMM-0 membrane.

Table 6.3 : Filtration and antifouling performances of the membranes

Membrane code	Permeate Flux ($\text{L m}^{-2}\text{h}^{-1}$)			FRR and Fouling recovery (%)			
	J_{w1}	J_p	J_{w2}	FRR	R_t	R_r	R_{ir}
HMM-0	125.2	9.8	33.4	26.6	92.1	18.8	73.4
HMM-1	164.8	18.1	87.6	53.1	89.0	42.1	46.9
HMM-2	226.3	31.2	168.7	74.5	86.2	60.7	25.5
HMM-3	199.5	24.3	133.9	67.1	87.8	55.0	32.9

6.3.9 Heavy metal ion rejection study

In the present work, heavy metal ion rejected by the membranes were studied by both PEUF and UF experiments (Table 6.5). The HMM-3 membrane exhibited rejection of 79 % for Pb^{+2} ions and 73 % for Cd^{+2} ions respectively during the PEUF. The higher rejection of Pb^{+2} compared to Cd^{+2} was due to the ability of Pb^{+2} ion to form the larger size complex with polyethyleneimine complexing agent. Further, the % rejection of Pb^{+2} and Cd^{+2} during the normal UF (without complexing agent) were 34 % and 27 % respectively. This rejection behaviour is due to the adsorption behaviour by the membrane surface. In order to substantiate this, elemental mapping analysis of lead and cadmium were carried out on the membrane surface after the UF experiment (Fig.6.17). MHNTs inherently offers the negative charge to the membrane surface and presence of hydroxyl and amine groups on the polydopamine acts as chelating agents. Thus, positively charged lead and cadmium ions exhibit strong secondary force of interaction such as hydrogen bonding, dipolar interactions, electrostatic interactions etc. with the membrane surface (Fig.6.18). The reusability of the prepared membranes for heavy metal ion removal was investigated by treating 0.2 M nitric acid solution for 18 h. From the results, we could observe that (Table-6.4) modified membranes were able to remove almost same amount of heavy metal ion after acid treatment. This implied that modified membrane could be regenerated by simple acid treatment.

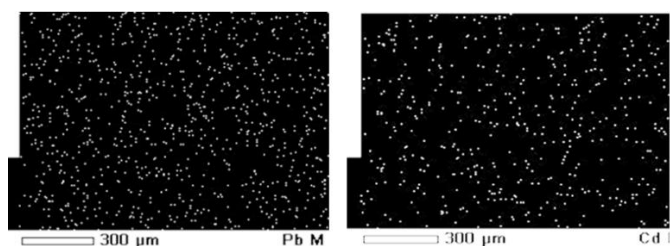


Fig.6.17 Elemental mapping of lead and cadmium after the UF experiment

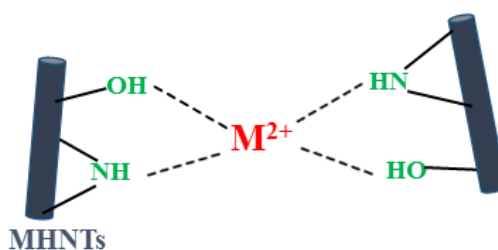


Fig.6.18 Interaction of heavy metal ion with MHNTs

Table 6.4 Reusability study for the heavy metal ion rejection

Cycles	Pb ²⁺		Cd ²⁺	
	PEUF	UF	PEUF	UF
1	79	34	73	27
2	76	31	71	25
3	74	32	69	26
4	75	33	70	25
5	76	31	68	27
6	75	32	69	25
7	76	33	68	26
8	75	33	68	25

6.3.10 Antimicrobial activity of membranes

There was a significant inhibition for *Escherichia coli*, *Mycobacterium smegmatis* and *Candida albicans* observed below the surface of the membranes, but no zone of inhibition observed around the disc for any of the microorganisms. The clear zone found below the membrane for *Escherichia coli*, *Mycobacterium smegmatis* and *Candida albicans* indicates membranes are inhibiting gram negative bacteria as well as fungi. There are few colonies grown below the membrane for *Staphylococcus aureus* indicating less inhibition for gram positive bacteria. Inhibition of *Candida albicans* below the membrane

and growth of few colonies of *Staphylococcus aureus* below the membrane are represented in the Fig.6.19. In addition to this, membrane incubation experiment showed very little or no microbial colonies around the membrane strips after 24 hours of incubation in microbial culture, whereas lot of the microbial colonies grown around the control strip (Fig.6.20).

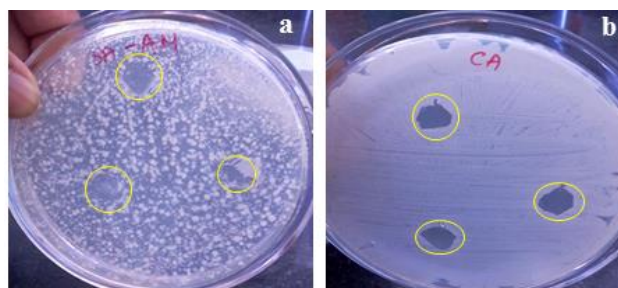


Fig.6.19 Representative agar plates showing a) few colonies of *Staphylococcus aureus*, b) complete inhibition of *Candida albicans*.

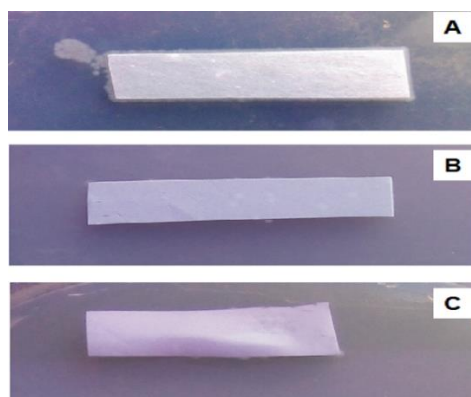


Fig.6.20 A) colonies of *Candida albicans* around the control strip and no colonies on the HMM-1 (B) and HMM-2 (C) membrane strip respectively.

6.4 CONCLUSIONS

Well dispersed hydrophilic MHNTs additives were prepared by using the facile and versatile polydopamine as modifying agent. The permeation experiments showed that the PWF of the nanocomposite membrane exhibited lower membrane hydraulic resistance ($0.88 \text{ Kpa/Lm}^{-2}\text{h}^{-1}$) compared to HMM-0 membrane ($1.59 \text{ Kpa/Lm}^{-2}\text{h}^{-1}$). The modified membrane exhibited superior antifouling behaviour with FRR of 74.5 % and reversible fouling ratio of 60.7 % for 3 wt. % of MHNTs dosage in the matrix. Also the modified membrane having the capacity to adsorb the heavy metal ion, thereby showing the rejection towards the Pb^{2+} and Cd^{2+} . Moreover, the modified membrane showed excellent resistance to microbial growth on the membrane surface.

CHAPTER 7

**FABRICATION OF POLYETHERIMIDE
NANOCOMPOSITE MEMBRANE WITH AMINE
FUNCTIONALISED HALLOYSITE NANOTUBES FOR
EFFECTIVE REMOVAL OF CATIONIC DYE EFFLUENTS**

Abstract: In this chapter, functionalised HNTs were immobilised into PEI membrane matrix with the aim of enhancing the properties and possible cationic dye rejection efficacy. The properties of fabricated nanocomposite membranes were examined in terms of porosity, hydrophilicity, surface energy, zeta potential and permeability. Further, dye rejection efficacy was determined by using rhodamine B (Rh.B) and methylene blue (MB) with different experimental parameters such as pH, initial dye concentration and contact time.

With the emergent growing rate of industries, the discharge of coloured effluents from various sources in to the water bodies is causing serious problems to human and several living organisms due to their harmful toxic effects. According to colour index, currently more than 10,000 dyes are being synthesised by the industries and approximate annual production of dye is more than 700,000 tonnes. Dye molecules find its considerable application in various fields such as plastic, paper, concrete, rubber, textile, and medicine based industries. The discharge of more than 15 % of dye solution in to the water source is of considerable attention due to its high bio-toxicity, potential mutagenic and carcinogenic effects (Ahmad *et al.* 2015, Pereira *et al.* 2016, Lin *et al.* 2016). The dispersed dye molecules into water sources, leads to blockage of sunshine from reaching the bulk of water source, thereby reduces the dissolved oxygen demand (DOD) level and also increases the biochemical oxygen demand (BOD) of the polluted water body (Karim *et al.* 2014).

For example, basic dye pigments have very high colour intensity even at trace quantities that provide colour to water, which is detrimental for sanitation and consumption purpose. Although the effects of cationic dyes such as rhodamine B (Rh.B) and methylene blue (MB) are not as dangerous as reactive or azo dyes, severe exposure to the same can lead to serious health problems. Rh.B is frequently used as a staining agent in biotechnology based laboratories and industries (Mittal and Mishra 2014). The long term exposure of these dyes may cause irritation in respiratory tract, eyes and skin in addition to carcinogenicity and neurotoxicity. One more dye, MB can instigate enhanced heart beat rate on inhalation and also ingestion through the mouth that can lead to nausea, vomiting, jaundice, quadriplegia and tissue necrosis (Guillen *et al.* 2011, Geise *et al.* 2010).

Luo *et al.* (2011) reported that HNTs were chemically modified with a silane coupling agent such as N- β -aminoethyl- γ -aminopropyl trimethoxysilane displays high affinity towards the adsorption of hazardous chemicals from the aqueous stream. The schematic representation of chromium (VI) removal by modified HNTs was given in

Fig.7.1. Modified HNTs displayed a high rate of adsorption for harmful chromium (VI) ions and reached up to 95 % of removal efficiency within 5 min.

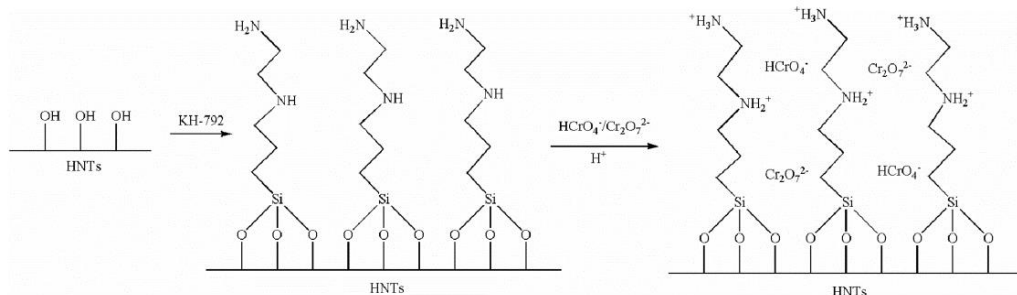


Fig.7.1 Schematic representation of adsorption of Cr (IV) to modified HNTs.

Zhao *et al.* (2013) illustrated that HNTs have high adsorption affinity towards the cationic dyes from aqueous stream. The dye removal capacity of HNTs is much higher than most of the conventional adsorbents and could be easily reused by burning after adsorption. Zhu *et al.* (2014) reported the grafting of poly (sodium 4-styrenesulfonate) on the surface of HNTs and employed it as additive to enhance polyethersulfone ultrafiltration membrane performance. The permeation properties of the hybrid membranes with 3 wt. % of modified HNTs showed higher pure water flux of 396.5 L/m²h and rejection properties significantly affected.

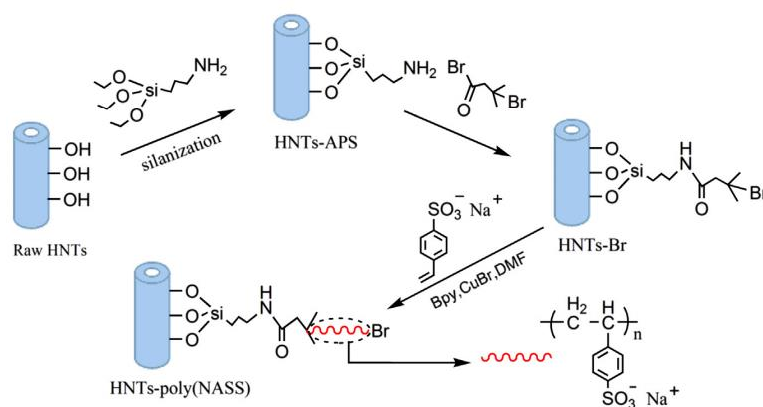


Fig. 7.2 Schematic representation of chemical modification of HNTs

In another study, Liu *et al.* (2014) also investigated the efficiency of HNTs as one of the adsorbent for the effective removal of the cationic dye molecules with high adsorption capacity and rapid adsorption rate of 113.64 mg/g for 0.1 g adsorbent dosage. Wang *et al.* (2015) reported the preparation of sulfonated HNTs and polyethersulfone nanocomposite membrane for effective removal of hazardous reactive dyes. The results

revealed that permeation properties of the hybrid membrane was enhanced considerably after adding sulfonated HNTs and exhibited maximum rejections for Reactive Black 5 dye above 90 % and Reactive Red 49 dye around 80–90 %.

Recently, Zeng *et al.* (2016) incorporated the 3-Aminopropyltriethoxysilane modified HNTs into PVDF UF membrane to improve the permeation and rejection rates. The schematic representation of modification of HNTs and PVDF membrane is shown in Fig. 7.3. The homogeneous dispersion of HNTs exhibited a lower contact angle, higher flux rate and superior antifouling properties compared to pristine PVDF membrane. Based on the literature, it is evident that HNTs can also be modified by several silane coupling agents, various surfactants, and polyelectrolytes for enhancing the performance and higher dye removal efficacy (Yuan *et al.* 2008, Zhu *et al.* 2014).

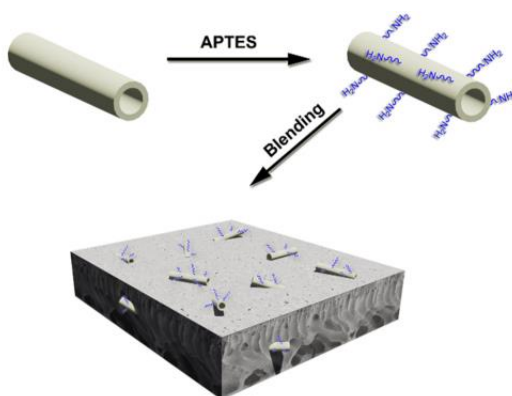


Fig.7.3. Schematic representation of chemical modification of HNTs and PVDF membrane. (Zeng *et al.* 2016)

In this chapter, HNTs were modified with N- β -(aminoethyl)- γ -aminopropyltrimethoxy silane (AEAPTMS) and modification was confirmed by FT IR, TGA, TEM and EDX analysis. The modified HNTs (MHNTs) were immobilised into the PEI membrane matrix by phase inversion method for enhanced permeation and dye rejection efficiency. The effect of MHNTs on morphology and surface roughness were explored by SEM and AFM analysis. The other membrane properties were investigated in terms of porosity, water contact angle, surface energy and zeta potential analysis. The cationic dye rejection studies were carried out with different initial dye concentration, pH, and contact time. Interaction of dye molecules with membrane surface was investigated by Langmuir and Frindlich adsorption isotherm studies.

7.1 MATERIALS AND METHODS

7.1.1 Materials

HNTs, AEAPTMS were procured from Sigma Aldrich. Polyethylene glycol ($M_w = 1000$) was purchased from Sigma. Rhodamine B (Rh.B) ($M_w \approx 479.01$ g/mol) and Methylene blue (MB) ($M_w \approx 373.9$ g/mol) was from Sigma-Aldrich Co.

7.1.2 Preparation of modified HNTs

The chemical modification of the HNTs was carried out according to the procedure in the literature (Luo *et al.* 2011). Then HNTs dispersed in a beaker containing 200 ml of toluene by using ultra-sonication at 70 °C. To the above dispersed solution, AEAPTMS was added and stirred magnetically for 24 h at 70 °C. The resultant modified HNTs (MHNTs-1) were collected by centrifugation and were washed with 400 mL of tetrahydrofuran (THF) followed by 400 mL of distilled water. The obtained MHNTs-1 was dried in oven at 95 °C. Further, dried MHNTs-1 powder was ball-milled using mixer to prevent any agglomeration among MHNTs. The set of experiment was carried out with same procedure and were designated as MHNTs-2. The schematic representation of modification of HNTs is given in Fig.7.4.

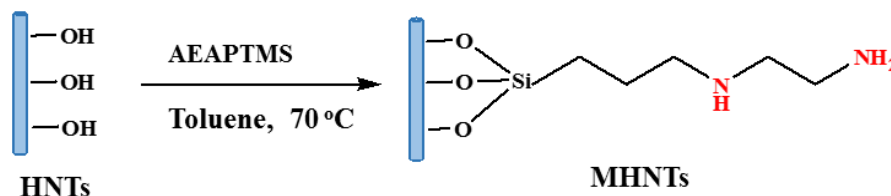


Fig.7.4 Chemical modification of HNTs by AEAPTMS

7.1.3 Membrane preparation

PEI/ MHNTs nanocomposite membranes were fabricated by immersion precipitation technique. In brief, calculated quantity of MHNTs (1 wt. % to 4 wt. % of PEI dosage) was dispersed in a desired volume of NMP solvent using ultra-sonication. To this solution PEI and PEG 1000 (invariable additive) were added and stirred magnetically for 18 h at 60 °C. Thus obtained homogeneous polymer solution was kept for 6 h at the same temperature to get rid of trapped air bubbles. The casting solution was casted over glass plate with the support of an automatic membrane casting apparatus and gently immersed in the coagulation bath for phase inversion process. The composition of casting solutions are tabulated in Table-7.1

Table 7.1 Chemical composition of the nanocomposite membrane

Membrane	PEI(g)	NMP(g)	HNTs(g)	PEG1000 (wt%)	W _{clay} *(wt%)
MHM-0	1.8	8.0	0	3	0
MHM-1	1.8	8.0	0.18	3	1
MHM-2	1.8	8.0	0.36	3	2
MHM-3	1.8	8.0	0.72	3	4

7.2 CHARACTERIZATION OF MHNTs AND MEMBRANE

The chemical modification of the HNTs were analysed by FTIR spectrum. The FTIR spectra were recorded using Avatar 360 IR spectrophotometer in the range of 4000-500 cm⁻¹. The TEM images of HNTs and MHNTs were recorded using JEM 1230 Electron Microscope. The cross sectional SEM images of the prepared composite membranes were recorded as reported procedure in CHAPTER-2, Section 2.3.2. Water uptake capacity, contact angle, surface energy and porosity analysis was carried out according to the procedure given in the CHAPTER -2, Section 2.2.4, Section 2.2.5.

7.2.1 Dye Removal Studies

The cationic dye removal efficiency and its mechanism were determined by the batch adsorption experiments. All the experiments were carried out using an orbital shaker at 28 °C and at 160 rpm with different initial concentration, pH and contact time. To study the adsorption isotherm, 0.1g of membrane was added into the 10 mL of different initial concentration of MB solution at neutral pH. After the completion of adsorption experiment, initial and final concentration of dye solution was analysed by measuring the absorbance of dye solution using ultraviolet–visible spectrophotometer. The absorbance of Rh.B and MB were determined at wavelengths 554.5 nm and 665 nm respectively. The amount of dye molecules adsorbed per unit mass of adsorbent was determined.

$$q = \frac{(C_0 - C_e)V}{m}$$

Where C_0 and C_e are the initial and equilibrium dye concentrations (mg L⁻¹), V is the volume of solution (L) and m is the mass of adsorbent (g).

From the initial (C_0) and final (C_e) dye concentration, the percentage of dye removal capacity by the nanocomposite membrane was calculated by below equation

$$\%R = \left(1 - \frac{C_e}{C_0}\right) \times 100$$

7.3 RESULTS AND DISCUSSIONS

7.3.1 Characterisation of MHNTs

The chemical modification of HNTs was confirmed by FTIR analysis and results are presented in Fig 7.5. The modified HNTs exhibited new band at 2842.1 cm^{-1} and 2929.3 cm^{-1} corresponding $-\text{CH}_2$ stretching and peak at 1481.7 cm^{-1} corresponding to $-\text{CH}_2$ deformation. The peak at 1342.9 cm^{-1} can be attributed to $-\text{SiCH}$ deformation and 1181.2 cm^{-1} corresponds to $-\text{CH}_3$ deformation. Further, peaks at 1083.1 cm^{-1} and 3357.1 cm^{-1} , 3351.9 cm^{-1} are due to HNTs surface modification by AEAPTMS due to $-\text{SiO}$ stretching, and $-\text{NH}_2$ functionality.

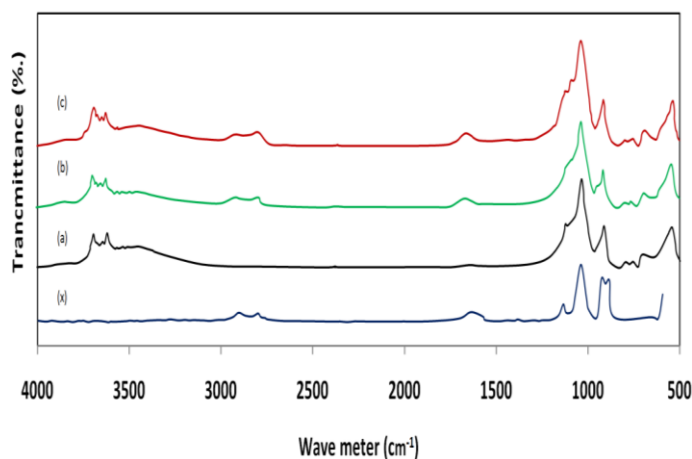


Fig 7.5. FTIR spectra of x) AEAPTMS, b) raw HNTs, c) MHNTs-1 and d) MHNTs-2

Fig 7.6 displays the representative TEM images of pristine HNTs and chemically modified HNTs. The chemical modification of HNTs is elucidated by detecting the elemental composition of the nanotubes before and after the modification. EDX analysis showed the presence of silica (Si), alumina (Al) and oxygen (O) peaks, which are the basic building blocks of HNTs. After chemical modification, extra peaks for the carbon (C) and nitrogen (N) were also observed; this further confirms the chemical modification of HNTs.

The TGA graph of the HNTs and MHNTs are presented in the Fig.7.7. The weight loss of compounds with different temperature range has been identified. First weight loss occurred at (a) $53.6\text{ }^{\circ}\text{C}$, (b) $53.9\text{ }^{\circ}\text{C}$ and (c) $53.8\text{ }^{\circ}\text{C}$ (c), was due to their adsorbed water molecules. Another weight loss was observed at (a) $286.52\text{ }^{\circ}\text{C}$, (b) $287.3\text{ }^{\circ}\text{C}$ and (c) $286.8\text{ }^{\circ}\text{C}$ concerning to the desorption of intercalated water among HNTs. Further weight loss for the three types of HNTs showed at the (507.7 (a), 508.8 (b), and 508.6 (c)) $^{\circ}\text{C}$ corresponding to the Al-OH de-hydroxylation of HNTs structure. However, M1-HNTs and M2-HNTs

have shown another different peaks at 186.3 °C (b) and 192.9 °C (c) corresponded to evaporation of adsorbed AEAPTMS, also at the 372.3 °C (b) and 359.4 °C (c) attributed to the de-composition AEAPTMS.

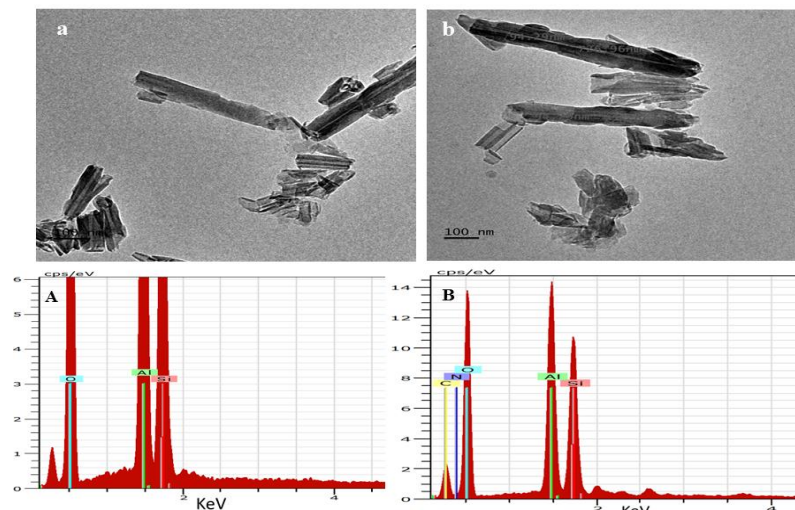


Fig.7.6. TEM and EDX analysis of a) HNTs and b) MHNTs.

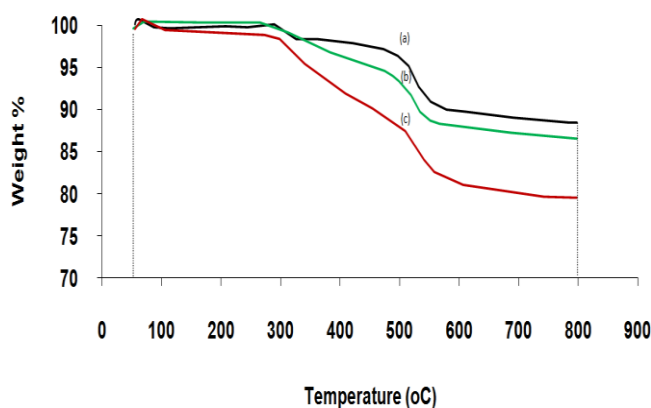


Fig.7.7 TGA analysis of HNTs and modified HNTs. a) HNTs, b) MHNTs-1 and c) MHNTs-2

7.3.2 Porosity and Contact angle of membrane

Our experimental study revealed that inclusion of hydrophilic MHNTs into casting solution showed considerable change in the performance of the resultant membrane. Variation in the porosity of nanocomposite membranes with different amount of MHNTs dosage is displayed in Table-7.2. From the results, it is noticed that MHM-0 membrane having 28.8 % porosity was increased up to 35.6 %, 49.4 % and 58.2 % for the 1 wt. %, 2 wt. % and 4 wt. % of the additive concentration respectively.

The effect of MHNTs dosage on hydrophilicity and surface energy of the nanocomposite membrane were investigated by contact angle analysis. Fig.7.8 represents the contact angle analysis of nanocomposite membranes embedded with functionalized HNTs nanomaterial. Contact angle of MHM-0 membrane was found to be 80.6° , which significantly decreases with addition of MHNTs dosage. At the drop age of 120s, contact angle values of MHM-1, MHM-2 and MHM-3 are found to be 72.5° , 69.4° and 66.8° respectively. These results indicate that inclusion of MHNTs into PEI membrane significantly improves the hydrophilicity and water wettability. Further, the decreasing trend of hydrophilicity was substantiated by calculating the surface energy and the values of these nanocomposite membranes are displayed in Fig.7.8. The lowest surface energy, 83.7 mN/m was obtained for MHM-0 membrane, whereas surface energy of 100.3 mN/m was obtained for the 4 wt. % of MHNTs dosage. This could be due to the fact that during the process of membrane formation, hydrophilic MHNTs spontaneously migrate towards the upper surface, thereby easily interacting with water molecules and enhances the hydrophilicity of the resultant membrane.

Table-7.2 Properties of prepared membranes

Membrane Code	Thickness (μm)	Porosity (%)	Flux ($\text{L/m}^2\text{h}$)
MHM-0	136	29	96
MHM-1	131	36	137
MHM-2	129	49	177
MHM-3	133	58	195

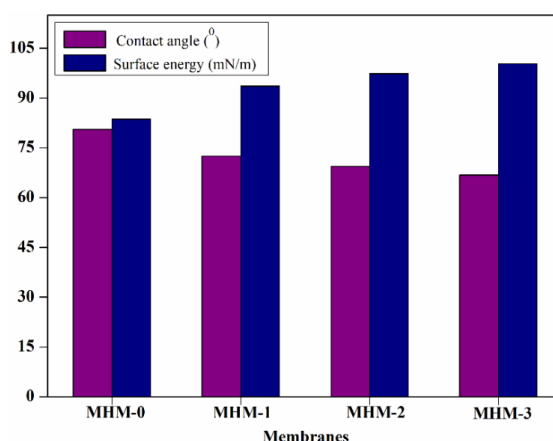


Fig.7.8 Contact angle and surface energy of the prepared membranes.

7.3.3 Zeta potential measurement

Fig.7.9 represents zeta potential values of the nanocomposite membrane as function of streaming pH, which ranges from pH 2.0 - 10.0. It was observed that the prepared membrane has shown positive zeta potential value at lower pH and negative at higher pH range. The PEI/ MHNTs nanocomposite membrane consist of $-NH$, $-NH_2$ and $-OH$ functional groups which will be protonated at lower pH leading to a positive zeta potential value (i.e positive charge). The groups will be deprotonated as pH of the stream increases, causing the membrane to become more negatively charged leading to negative zeta potential.

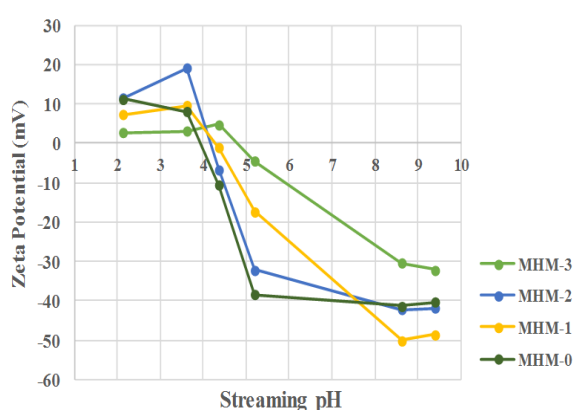


Fig.7.9 Zeta potential measurement of prepared membranes.

Moreover, pH dependent analysis helps in identifying the isoelectric point (IEP) of the membranes. The MHM-0 membrane showed net zero charge (i.e zeta potential = 0 mV) at pH~3.8. The IEP of the nanocomposite membrane reached up to pH range of 4.3-4.9 with the addition of different concentration of MHNTs nanoparticles. Most importantly, either positive charge at lower pH or negative charge at higher pH, nanocomposite membrane exhibits much higher zeta potential compared to MHM-0 membrane. Further, as the concentration of MHNTs concentration increases, zeta potential of the membrane shifts to higher value.

7.3.4 Membrane morphology

In order to explore the effect of MHNTs dosage on the membrane morphology, SEM analysis was carried out. Fig.7.10 depicts the cross section SEM images of the nanocomposite membranes. All the prepared membranes exhibited typical asymmetric structure comprising of dense skin layer and porous sublayer with macrovoids. The variation in the morphological features of the membrane depends on instantaneous

demixing or delayed demixing during membrane preparation process (De Sitter *et al.* 2014). With increasing MHNTs dosage, the number of macrovoids in the sublayer increases and becomes larger. In the current work, the variation in the morphology of resultant membrane was due to the combination of the effects of PEG and MHNTs. That is, the presence of MHNTs in the casting solution results in the formation of both well interconnected pores and large macrovoids (Shawky *et al.* 2011).

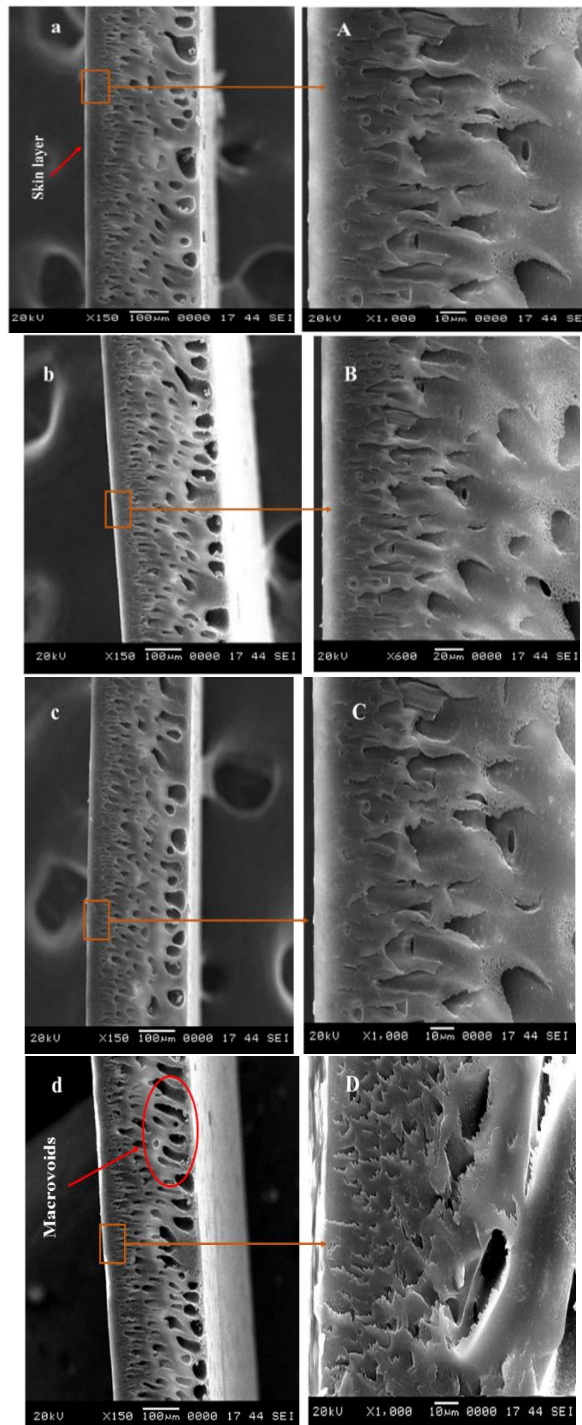


Fig.7.10 Cross sectional and magnified cross sectional SEM images of a) MHM-0, b) MHM-1, c) MHM-2, d) MHM-3 membranes

Fig.7.11 illustrates the representative three-dimensional AFM images of prepared membranes. The roughness parameters were analysed in terms of root mean square of Z data (Rq), mean roughness (Ra) and mean variation between the highest peaks and the lowest valleys (Rz) and values tabulated in Table-7.3. From the results, it was observed that addition of MHNTs has considerable influence on surface properties of resultant membrane. All roughness parameters of modified membrane were larger than MHM-0 membrane. The MHM-3 membrane exhibited maximum surface roughness with root mean square roughness of 221 nm, indicating the migration of MHNTs towards membrane surface during phase inversion process. Increased surface roughness of modified membrane favours adsorption of dye molecules.

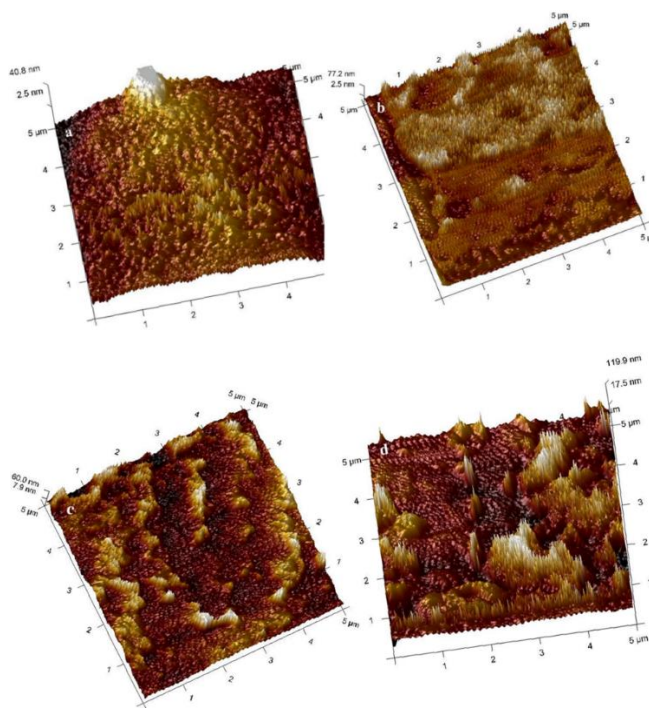


Fig.7.11 Three dimensional AFM images of a) MHM-0, b) MHM-1, c) MHM-2, d) MHM-3 membranes.

Table 7.3 Roughness parameters of the prepared membranes

Membrane	Image surface area (μm^2)	Surface area Difference (%)	Roughness		
			Ra (nm)	Rq (nm)	$Rmax$ (nm)
MHM-0	25.4	1.63	6.48	8.87	86.8
MHM-1	25.6	2.56	7.02	9.39	141
MHM-2	26.3	5.36	10.9	14.7	175
MHM-3	27.0	7.83	11.5	14.9	221

7.3.5 Permeation properties.

The time dependent PWF of prepared membranes at 0.4 MPa transmembrane pressure has been presented in Fig.7.12. During the filtration experiment, initial decline in PWF was witnessed for all the prepared membranes, which is due to the compression of membrane structure under a transmembrane pressure difference. It is interesting to note that membrane with 0 wt. % of MHNTs exhibited PWF of 96 L/m²h, which was increased up to 195 L/m²h with 4 wt. % of additive dosage. This signifies that MHNTs shows synergetic effect on permeation properties of the membranes due to its hydrophilic nature and its hollow structure. Here, PWF of nanocomposite membranes showed the similar trend of hydrophilicity.

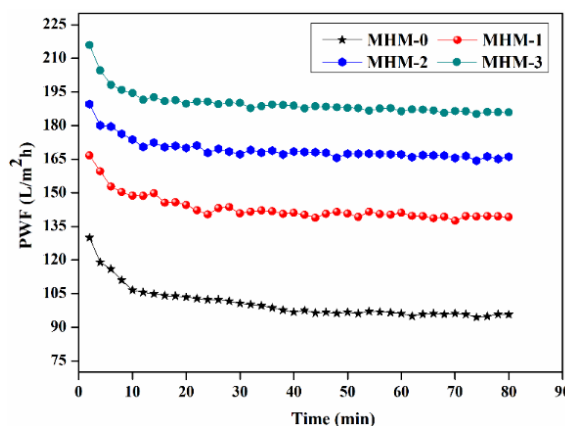


Fig.7.12 Time dependent pure water flux of the membranes.

7.3.6 Dye removal studies

The prepared nanocomposite membranes were targeted for the rejection of cationic dye removal application and also to determine the possible mechanism for the interaction of dye molecules with membrane surface. From the experimental results, it was found that

nanocomposite membranes have strong affinity towards the dye molecules and instantly adsorb over the surface. Fig.7.13 represents the naked eye detection of removal efficiency of the nanocomposite membrane after adsorption. According to the literature, adsorption of dye molecules towards the membrane surface was driven by the specific characteristic of the dye molecules such as type of charge, charge density, functional group responsible for interaction with adsorbent and affinity of dye molecules with adsorbent. These kind of driving forces leads to adsorption driven by the hydrogen bond, dispersion forces, electrostatic interaction and complexation (Al-Ghouti *et al.* 2010, Haque *et al.* 2011).

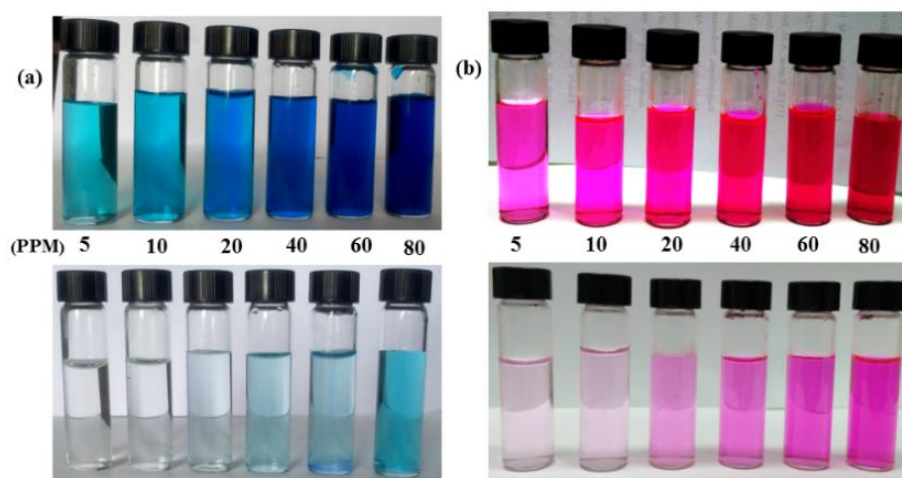


Fig.7.13 Photographic image of a) MB and b) Rh.B before adsorption and after adsorption

7.3.6.1 Effect of pH of dye solution

It is generally accepted that pH of the solution can significantly influence the surface properties of the membranes and polarity of functional groups in dye molecules. Thus, pH of the solution is an essential consideration during the dye removal process. Fig.7.14 represents the effect of pH on the dye removal efficacy of the membrane. At lower pH ($\text{pH} < \text{Pzc}$), there is competitive effect between hydrogen ions (H^+) and cationic dye molecules to interact with the active adsorption site on the membrane surface. When $\text{pH} < \text{Pzc}$, the membrane becomes more positively charged. Hence, the electrostatic repulsive interaction between cationic dye molecules and active adsorption sites on the membrane would result in reduced dye removal efficiency. In contrast, higher dye removal efficiency was observed with increased pH of the solution. This was because, at higher pH ($\text{pH} > \text{Pzc}$) the active sites get deprotonated and membrane becomes negatively charged. This intensifies the electrostatic force of interaction between cationic dye molecules and negatively charged membrane, which enhance the adsorption of dye molecules (Shenvi *et al.* 2015). Fig.7.15 represents the possible mechanism of interaction of cationic dye

molecules with membrane surface. An important observation in the case of Rh.B was that its removal efficiency was less. According to literature, above pH 4, Rh.B molecules exist in zwitterionic form in the water. Thus, presence of zwitterionic form diminishes the interaction between membrane surface and Rh.B molecule which is resulted in the decreased Rh.B rejection. At pH 2, the protons present in the solution competed with Rh.B molecules to adsorb on the active site of membrane and hence showed the less rejection (Bhattacharyya *et al.* 2014).

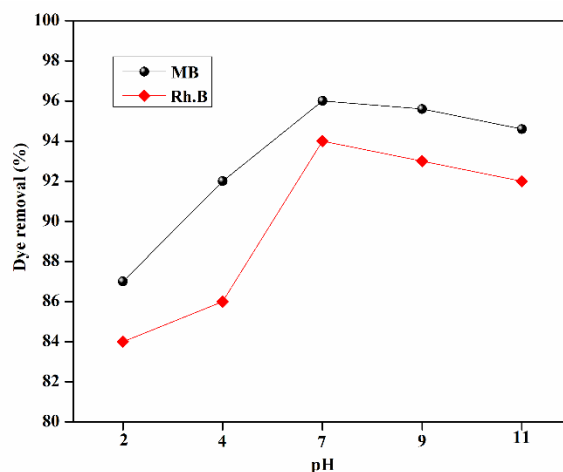


Fig.7.14 Effect of pH on the dye removal capacity.

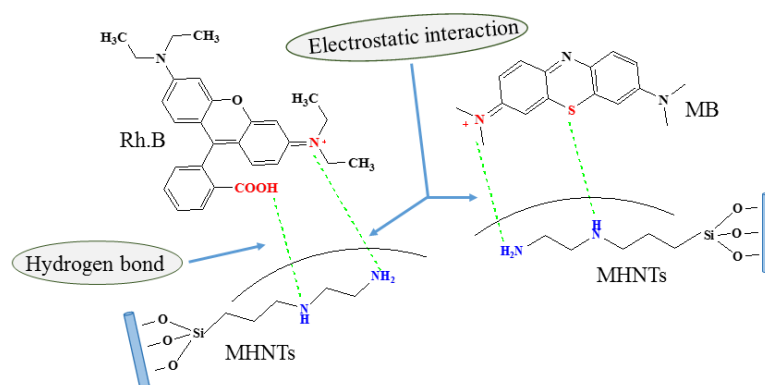


Fig.7.15 Schematic representation of mechanism of interaction of dye molecules with the MHNTs.

7.3.6.2 Effect of contact time

Fig.7.16 represents the dye removal efficiency as a function of time. The adsorption capacity and % of dye rejection MHM-3 membrane increases in the initial stage of adsorption and relatively slow increase with contact time until it reaches the equilibrium stage. In the initial stage of adsorption process, nearly 85 % of cationic dye was removed which signifies the efficacy of MHM-3 membrane. At equilibrium, 97 % and 94 % of

rejection were observed for the MB and Rh.B dye respectively. This phenomenon is attributed to the fact that during the initial stage, more number of active adsorption sites was available for the dye molecule. After a span of time, vacant sites were difficult to occupy due to repulsive force of interaction between dye molecules on the membrane and bulk of the solution (Ai *et al.* 2011). This resulted in decreased adsorption rate of the dye from the bulk solution. Constant value was attained when the amount of dye getting adsorbed onto the membrane surface was in a state of dynamic equilibrium with the amount of dye desorbed.

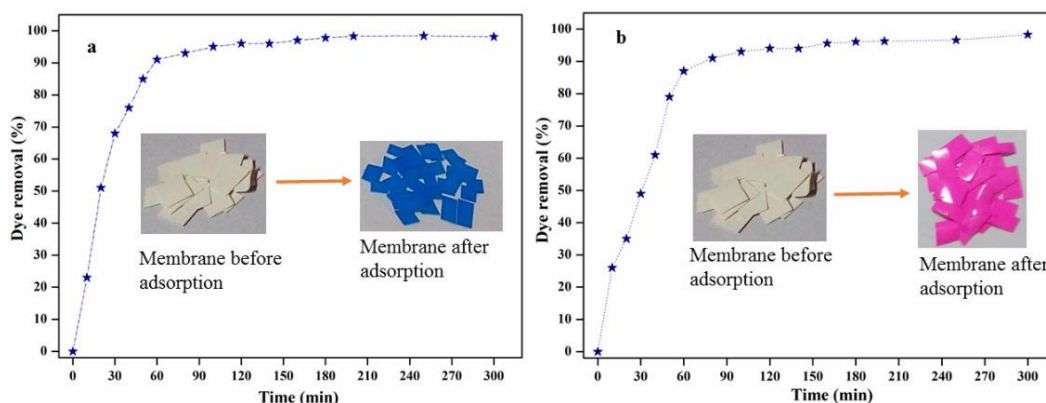


Fig.7.16 Dye removal efficiency as a function of time for a) MB and b) Rh.B (pH=7±0.5)

7.3.6.3 Adsorption Isotherms.

The adsorption isotherm study illustrates how an adsorbate interacts with adsorbent. The isotherm gives a relationship between the amount of dye adsorbed on the solid phase and the concentration of dye in solution when both phases are in equilibrium (Vadivelan and Kumar 2005, Arami *et al.* 2006). Table-8.4 represents the adsorption isotherms for MB and Rh.B onto MHM-3 membrane. The equilibrium adsorption data were analysed by Freundlich and Langmuir isotherm models.

Langmuir Isotherm. It is based on the hypothesis that all the adsorbent sites are equivalent and having equal adsorbate affinity to form monolayer. The linear equation for the Langmuir isotherm is given as

$$\frac{C_e}{q_e} = \frac{1}{bq_{max}} + \frac{C_e}{q_{max}}$$

Where ' q_e ' (mg/g) and ' C_e ' (mg/L) are the amount of dye adsorbed and concentration of the solution at equilibrium, ' b ' is the Langmuir coefficient (L/mg) connected to the affinity of binding site and ' q_{max} ' is the maximum adsorption capacity per unit mass (mg/g).

Freundlich Isotherm. This isotherm gives the empirical relation to heterogeneous system based on the hypothesis that the adsorption sites are not equivalent. The linear equation form of Freundlich isotherm is as

$$\ln q_e = \ln K_F + \frac{1}{n} \ln C_e$$

Where ' C_e ' and ' q_e ' have their usual denotation as stated above and K_F ($\text{mg}^{1-1/n} \text{L}^{1/n} \text{g}^{-1}$) and n are Freundlich coefficients related to adsorption intensity and adsorption capacity, respectively. If the reciprocal of Freundlich coefficient ($1/n$) is <1 , it is reflected as a sign of favourable adsorption process (Natarajan *et al.* 2014, Shenvi *et al.* 2015).

Table -7.4 Adsorption isotherm parameters of MB and Rh.B dyes on nanocomposite membrane

Parameters	MB	Rh.B
<i>Langmuir isotherm</i>		
q_{max} (mg/g)	19.6	20.4
b (L/mg)	0.086	0.052
R^2	0.94	0.97
<i>Freundlich Isotherm</i>		
$1/n$	0.38	0.37
K_F	1.61	1.52
R^2	0.89	0.86

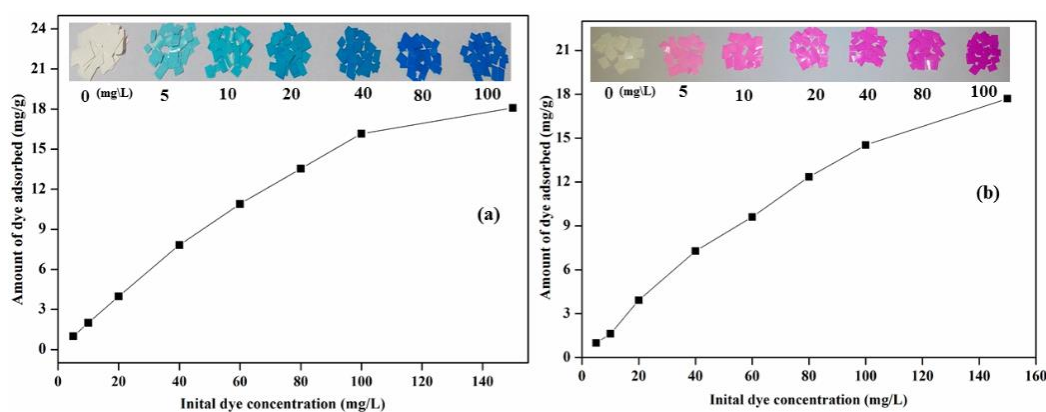


Fig.7.17 Variation in amount of a) MB and b) Rh.B dye adsorbed on the membrane.

Isotherms based on the experimental results and the parameters obtained from nonlinear regression by both models are shown in Table 7.4. From the experimental data,

R^2 value of the Langmuir and Freundlich Isotherm are 94, 97 and 89, 86 for the MB and Rh.B respectively. This indicates the Langmuir isotherm model is suitable for illustrating the adsorption equilibrium process for MB and Rh.B dye molecules onto nanocomposite membrane. From the Langmuir plot, amount of dye adsorbed (q_{max}) on the membrane surface was determined and it was found to be 20.4 mg/g and 19.6 mg/g for MB and Rh.B respectively. This outcome has been revealed in Fig.7.17. It was noticed that with an upsurge in the initial dye concentration, the amount of dye adsorbed also intensifies. The dye concentration plays a vital role in leading the mass transfer resistance of dye molecules between solid phase and the aqueous phase. The enhanced dye concentration aids as a driving force to overcome this resistance, which in turn increased the probability of collision between the dye molecules and the adsorbent, thus leading to higher adsorption (Baral *et al.* 2009, Ai *et al.* 2011)

7.4 CONCLUSIONS

Naturally occurring, low cost, environmental friendly HNTs was chemically modified and employed as additive to enhance the properties of resultant nanocomposite membrane. The proper immobilisation and uniform distribution of the additive into the membrane matrix was confirmed by elemental mapping analysis. The nanocomposite membrane prepared with 4 wt. % of MHNTs dosage showed maximum water permeation rate of 195 L/m²h. Moreover, prepared nanocomposite membrane can be effectively employed for the removal of cationic dyes such as MB and Rh.B from aqueous solution. MHM-3 membrane has the capacity to remove the dye molecules up to 97 % and 94 % for MB and Rh.B dyes respectively. Langmuir adsorption isotherm is the best model to explain the interaction between dye molecules and membrane surface. Thus, facile and efficient MHNTs modified nanocomposite membrane can be potential candidate to remove the cationic dyes from the contaminated aqueous stream.

CHAPTER 8

**EFFICIENT TREATMENT OF HAZARDOUS REACTIVE
DYE EFFLUENTS THROUGH ANTIFOULING
POLYETHERIMIDE HOLLOW FIBER MEMBRANE
EMBEDDED WITH FUNCTIONALISZD
HALLOYSITE NANOTUBES**

Abstract: A simple, efficient and scalable approach was followed for the fabrication of highly fouling resistance hollow fiber nanocomposite membranes with the aim of effective removal of reactive dyes. The naturally occurring HNTs were functionalized via facile self-polymerization of *m*-aminophenol in mild acidic condition and employed as an additive. The effect of additive on the hollow fiber nanocomposite membrane on its surface properties and performance was investigated in detail. This chapter describes the permeation and efficient treatment of hazardous reactive dye effluents.

Colour produced by the synthetic dye molecules in the aqueous stream is reflected as one of the extremely detrimental water pollutant. In addition to having harmful adverse effects, presence of colour in water is visually unpleasant and can destroy the entire ecosystem. Investigation of acute toxicity of every dye constituents is very much essential due to its harmful adverse influences on the living organisms and human health (Ahmad *et al.* 2015, Ngulube *et al.* 2017). In particular, azo dyes containing aromatic amines, which are extremely carcinogenic in nature and at the same time, they can act as an explosive after the reductive cleavage of the azo functionality (Chung 2016). Most regular carcinogens like benzidine group containing dye molecules must be treated properly before entering into the water bodies. Recently, analysis regarding the estrogenic and anti-estrogenic properties of textile dyes was reported, which further substantiate the adverse effects of synthetic dyes on living organisms (Nguyen and Juang 2013). Thus it is causing severe harmful impact on the environment.

Recently, hollow fiber (H.F) membranes have been exploited in various commercial separation applications like water treatment, dialysis, bio-separations and gas purification due to its admirable mass-transfer capacity. H.F membranes have the advantage of large surface area per unit module volume and hence exhibits improved permeation and rejection rates (Zheng *et al.* 2013, Ong *et al.* 2014, Wang *et al.* 2017).

Maurya *et al.* (2012) effectively employed polysulfone-polyvinylpyrrolidone based ultrafiltration H.F membranes for the purification of hazardous reactive dye solutions. The membrane showed the weight cut-off values in the range of 490 to 730 g/mole. The rejection rate was obtained in the range of 90 % with permeation rate of $35 \text{ Lm}^{-2}\text{h}^{-1}$. They also stated that the flux decreased slightly while the rejection remained almost the same upon increasing the dye concentration from 400 ppm to 2500 ppm in feed.

Zheng *et al.* (2013) prepared thin-film polypropylene composite H.F nanofiltration membranes. Further it was modified by using trimethylammonium substituted hydroxyethyl cellulose and crosslinking with glutaraldehyde. The resultant H.F membrane rejection efficiency of 99.2 %, 99.8 % and 99.8 % for Crystal Violet, Victoria Blue B and Brilliant Green respectively under the trans-membrane pressure (TMP) of 0.7 bar was observed. The percentage of dye rejection and water flux of the membrane is given in Fig.8.1.

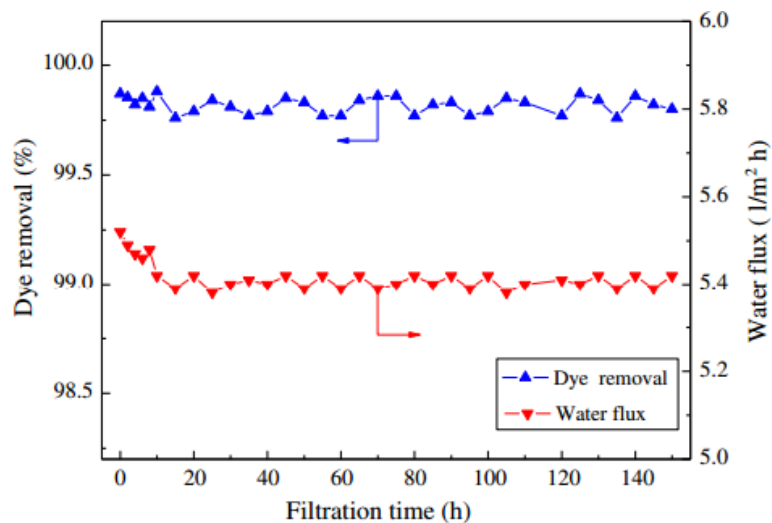


Fig.8.1 Permeation rate and dye rejection capacity of the H.F membrane. (Zheng *et al.* 2013)

Ong *et al.* (2014) illustrated the applicability and effectiveness of H.F membranes for the waste water treatment in laboratory scale and pilot scale utility. A systematic experiment was carried out to estimate the functioning of newly prepared polyamide-imide H.F nanofiltration membrane in several operational parameters such as feed pH (i.e., 3, 7, 10), solute concentration (i.e., 100, 500, 1000 ppm) and temperature (i.e., 25, 40, 50, 70°C). The results revealed that the H. F membrane has shown more than 90 % dye rejection under testing conditions. The effect of dye concentration on permeation and rejection rate of H.F membrane is given in Fig.8.2.

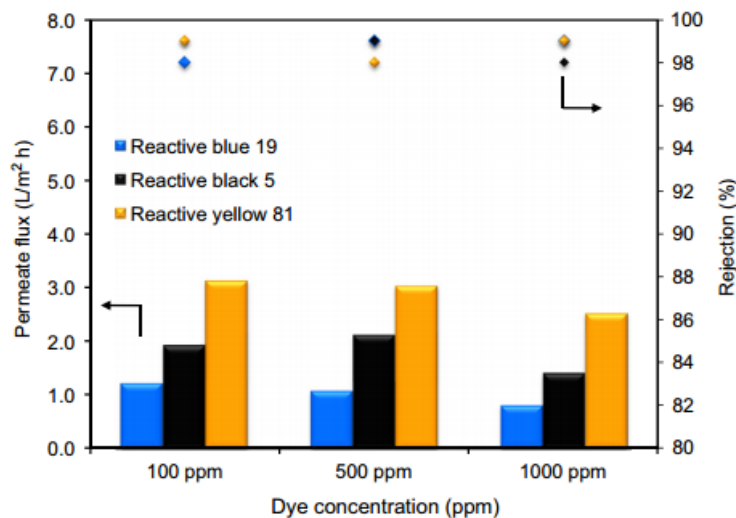


Fig.8.2 Effect of dye concentration on permeation and rejection rate of H.F membrane. (Ong *et al.* 2014)

In another study, Liu *et al.* (2015) developed the thin film composite H.F membrane via dual layer interfacial polymerization of polypiperazine amide. The properties of the H.F membrane was altered by adding the cyclic ethers such as dioxane, oxolane and trioxane. With the addition of 2 wt. % dioxane exhibited hydraulic permeation of $16.6 \text{ L m}^{-2} \text{ h}^{-1}$, a MWCO of 330 Da and a tensile strength of 10.3 MPa was observed.

In addition to this, presence of modified HNTs in the membrane matrix could enhance the hydraulic permeation and dye rejection efficiency of the membrane. Wang *et al.* (2015) reported the preparation of sulfonated HNTs and incorporated them into membrane matrix via phase inversion method. They stated that hybrid membrane showed higher rejection of more than 90 % for Reactive Black 5 and nearly 80–90 % for Reactive Red 49. Similarly, Zeng *et al.* (2016) illustrated the effect of 3- aminopropyltriethoxysilane modified HNTs in the polyvinylidene fluoride membrane for dye removal application. The resultant nanocomposite membrane exhibited more than 94.9 % dye rejection efficiency with superior water permeation rate (Fig.8.3). According to the literature, functionalized HNTs have greater efficacy and influence towards the dye removal and other waste water treatment applications (Yu *et al.* 2016, Shahamati Fard *et al.* 2016, Shu *et al.* 2016).

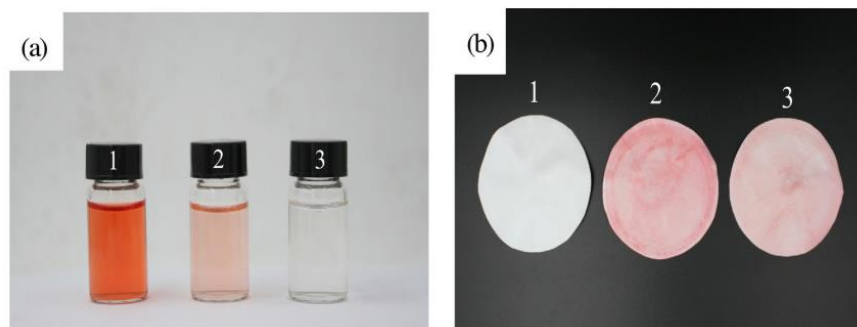


Fig.8.3 Photos of (a) solutions and (b) membranes before and after dye permeating. (Zeng *et al.* 2016).

Polyaniline based hybrid materials have been potentially examined due to their easy preparation, good processability and stability over the wide range of pH and wide application. In addition to this, polyaniline and its derivatives coated into the inorganic materials exhibited improvement in the performance of membranes due to their well dispersion and enhanced hydrophilicity (Mallick *et al.* 2006, Daraei *et al.* 2012, Pereira *et al.* 2015). Interestingly, Mallick *et al.* (2006) described the properties of poly(o-aminophenol)-palladium nanocomposite. Neelgund *et al.* (2008) illustrated preparation and characterizations of polyaniline and its alkyl derivatives modified silver nanocomposite for improvement of thermal properties. Daraei *et al.* (2012) illustrated the enhanced Cu (II) removal efficiency from the aqueous solution after the modification of polyethersulfone nanocomposite membrane with core-shell polyaniline-Fe₃O₄ nanoparticles. The resultant membrane was capable to eliminate more than 75 % of Cu (II) ions from initial low concentration feed solution (5 mg/L). Zhao *et al.* (2012) reported the synthesis of polyaniline-poly(vinylpyrrolidone) nanocomposite and employed it as performance modifying agent to polysulfone membranes. The nanocomposite membranes exhibited superior permeability and antifouling nature. Teli *et al.* (2013) reported the polyaniline modified TiO₂ nanoparticles and immobilized them into the polysulfone membrane matrix to enhance hydrophilicity, permeability and antifouling nature. The membrane with 1.5 wt. % of additive dosage resulted in higher flux recovery value of 77.6 % in comparison with pristine membrane. According to the literature, modification of inorganic nanoparticles by the polyaniline and its derivatives can prevent the agglomeration, enhance the stability and uniform dispersion into polymer matrix. These merits of polyaniline and its derivatives are beneficial for the overall enhancement in the membrane performance (Pendergast and Hoek 2011, Zhao *et al.* 2014).

In this chapter, we developed a poly(m-aminophenol) modified HNTs for the fabrication of H.F nanocomposite PEI membrane. The modified HNTs were characterized by FTIR, TEM and EDX analysis. The nanocomposite H.F membrane was characterized in terms of surface energy, porosity, equilibrium water content, hydrophilicity, morphology and elemental mapping analysis. The applicability of prepared membrane for the effective removal of hazardous reactive dyes like Reactive Red-120, Reactive Black-5 from aqueous solution under different experimental conditions was performed.

8.1 MATERIALS AND METHODS

8.1.1. Materials

PEI was procured in the form of pellets from Solvay specialty polymers. PVP, K29-32 (MW: 58,000 g/mol) was purchased from Acros Organics. BSA, m-aminophenol, reactive red 120, and reactive black 5 were obtained from Sigma Aldrich. NMP (purity > 99.5%) used as solvent, procured from Acros Organics.

8.1.2 Modification of HNTs

The chemical modification of HNTs by poly (m-aminophenol) (PHNTs) was carried out according to the oxidative polymerization method (Kar *et al.* 2010). In brief, m-aminophenol (0.5g) solution was prepared by dissolving in 2 M HCl solution. The sample of HNTs was dispersed in demineralized water (20 mg/mL, 50 mL) and sonicated for 0.5 h in order to avoid the agglomeration. These dispersed HNTs was added to the solution containing m-aminophenol and stirred for 3 h. The polymerization reaction of m-aminophenol was carried out by adding equimolar ratio of ammonium persulfate at room temperature. The final suspension was stirred for 18 h to obtain HNTs coated with water insoluble poly (m-aminophenol) polymer (Fig-8.4). Centrifugation of the reaction mixture resulted in the final product which was washed with distilled water and ethanol. The modified HNTs were dried in the oven for 80 °C for 24 h before further characterization.

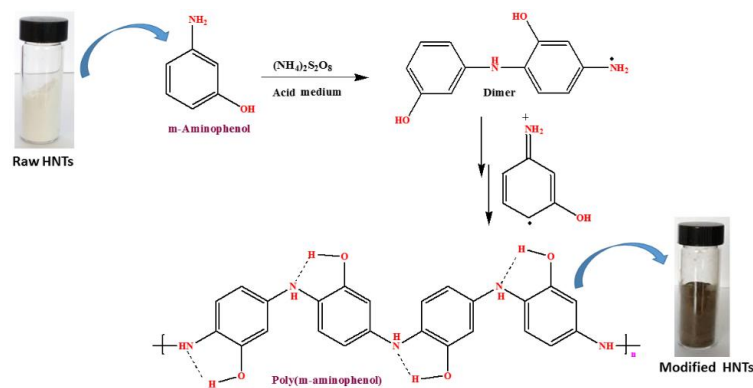


Fig.8.4. Self-polymerization of m-aminophenol over the HNTs (PHNTs)

8.1.3 Preparation of hollow fiber membranes

PEI/PHNTs mixed matrix nanocomposite H.F membrane was prepared by dry-wet spin technique at room temperature using equipment described in Fig.8.5. The non-solvent induced phase separation method was the main process to prepare the H.F membrane. To prepare the dope solution, desired quantity of PHNTs was dispersed in NMP (as solvent) and sonication was performed for 30 minutes to avoid the agglomeration of nanoparticles. To this suspension, calculated amount PEI and PVP (invariable additive) were added and magnetically stirred for 18 h at 60° C. The obtained homogeneous dope solution was sonicated for 30 minutes to remove the effect of any entrapped air bubbles. The overall composition of dope solution is described in Table 8.1

Table 8.1. Casting solution composition

Membrane	PEI(g)	NMP (g)	PVP (g)	PHNTs (g)	W_{PHNTs}^* (wt%)
PMM-0	1.8	8.0	0.2	0	0
PMM-1	1.8	7.9	0.2	0.018	1
PMM-2	1.8	7.9	0.2	0.036	2
PMM-3	1.8	7.9	0.2	0.054	3

* W_{PHNTs} is the mass ratio of PHNTs to PEI.

As illustrated in Fig.8.5, the dope solution was passed through annular region of the spinneret under nitrogen pressure. Deionized water as bore liquid was passed through the inner tube of spinneret to prepare the H.F membrane. Spinneret was placed at a certain distance from the non-solvent bath to get the dry-wet process (Kajekar *et al.* 2015). The parameters employed in the process are tabulated in the Table 8.2. Once dope solution and bore fluid meet at the tip of

the spinneret, they were guided to pass through the two coagulation baths. Finally H.F membrane was collected through the rotating roller drum. These newly prepared membranes were immersed in the non-solvent for 48 h to eliminate the residual solvent.

Table 8.2 -Spinning conditions of PEI/PHNTs H.F membranes.

Parameters	Condition
Spinneret DO/ID	1.1 mm / 0.55 mm
Spinneret Temperature (°C)	27
Dope solution	PEI/PVP/PHNTs
Bore fluid composition	DI water
Bore fluid flow rate (mL/min)	1.5
Range of air-gap distance (cm)	10
Coagulant	Water
Coagulant temperature (°C)	27
Washing bath	water
Washing bath temperature (°C)	27
Take-up speed (cm/min)	2.1

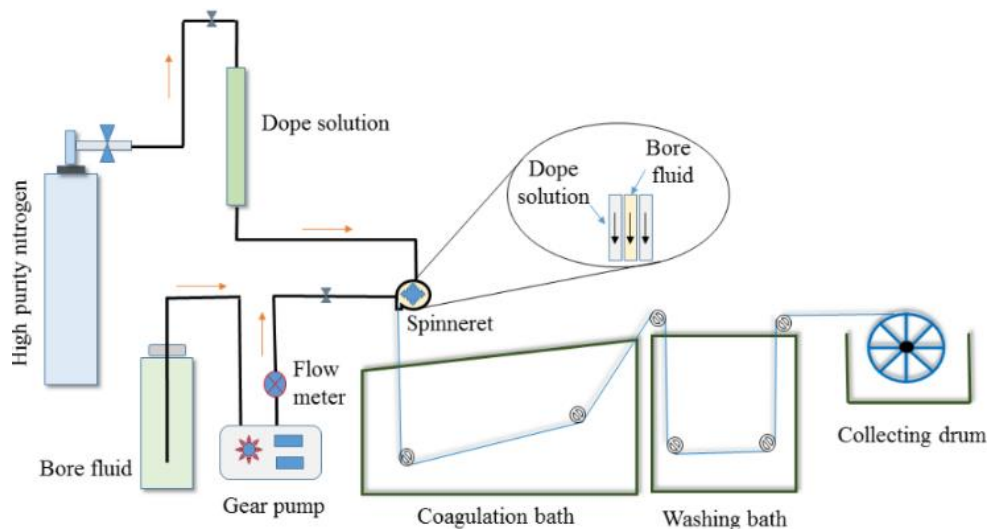


Fig.8.5 Schematic representation of the hollow fiber membrane fabrication system

8.2 CHARACTERIZATION AND PERFORMANCE STUDY

The chemical modification of the HNTs were analysed by FTIR spectrum. The TEM images of HNTs and modified HNTs were recorded using JEM 1230 Electron Microscope.

The cross sectional SEM images of the prepared H.F membranes were recorded as reported procedure in CHAPTER-2, Section 2.2.3 Water uptake capacity, contact angle, surface energy and porosity analysis was carried out according to the procedure given in the CHAPTER-2, Section 2.2.4.

8.2.1 Zeta Potential analysis

The surface charge behavior of prepared H.F membranes were determined after analyzing the streaming potentials. The zeta potential of membrane was examined in the pH range of 2.0–7.0, by using a SurPASS Electrokinetic Analyser (Anton Paar, Graz, Austria). During the study, 1 mM potassium chloride (KCl) solution was the electrolyte, 0.1 M hydrochloric acid (HCl) solution and 0.1 M sodium hydroxide (NaOH) solution were used as titration solutions.

8.2.2 Permeation analysis

Prepared nanocomposite H.F membranes were subjected for the water permeation experiments using the cross flow filtration unit (Kumar *et al.* 2013). A H.F membrane bundle containing 5 fibers with ~10 cm in length was potted over the stainless still holder. The potted modules were kept at ambient temperature for 24 h to dry the resin completely. During the experiment, modules were fitted into permeability setup and demineralized water was employed to measure the flux at 0.2 MPa pressure. The flux of the resultant membrane was calculated using the formula (4)

$$j = \frac{Q}{n\pi L D_i} \quad (4)$$

Where, ‘j’ is the permeate flux, ‘Q’ is the volumetric flow rate (ml/min), ‘n’ is the number of H.F membranes, ‘ D_i ’ is the inner diameters of H.F membranes (cm), ‘L’ is length of H.F (cm). The fouling mechanism and antifouling behavior of nanocomposite H.F membrane was determined according to the procedure given in CHAPTER -3, section 3.2.3.

8.2.3 Reactive dye rejection study

In order to determine the harmful reactive dye removal efficiency of prepared H.F nanocomposite membrane, rejection studies was carried out with different experimental conditions like pressure and operating time. After completion of filtration process, the absorbance value of feed and permeate solutions were determined with λ_{\max} of 120 nm and

592 nm for the reactive red 120 and reactive black 5 respectively. From the initial and final dye concentration, % removal capacity was calculated by using equation

$$\%R = \left(1 - \frac{C_p}{C_f}\right) \times 100$$

Where, ' C_p ' and ' C_f ' concentration of permeate and feed respectively.

8.3 RESULTS AND DISCUSSIONS

8.3.1 FTIR analysis

The chemical modification on the HNTs was confirmed by taking FTIR spectra of both raw HNTs and poly (m-aminophenol) coated HNTs. The obtained results are presented in Fig.8.6. FTIR of HNTs showed peaks at 3694 cm^{-1} and 3608 cm^{-1} corresponding to the $-\text{OH}$ stretching vibration. The absorption peak at 905 cm^{-1} is due to the Al-OH bending vibration. Characteristic observed at 1018 cm^{-1} represents the Si-O stretching vibration. After the chemical modification, the broad peak at 3437 cm^{-1} corresponds to the $-\text{OH}$ groups in the poly (m-aminophenol) and peak at 2940 cm^{-1} and 2851 cm^{-1} represents the $-\text{CH}$ stretching vibration of aromatic ring. Aromatic $-\text{C}-\text{O}$ group of the polymer was observed at 1050 cm^{-1} . The bending vibration peak at 1639 cm^{-1} corresponds to $-\text{NH}$ groups. This confirmed the modification of HNTs by the poly(m-aminophenol). Similar kind of results was reported by many of the researchers (Kar *et al.* 2010, Kar *et al.* 2011, Yuan *et al.* 2008).

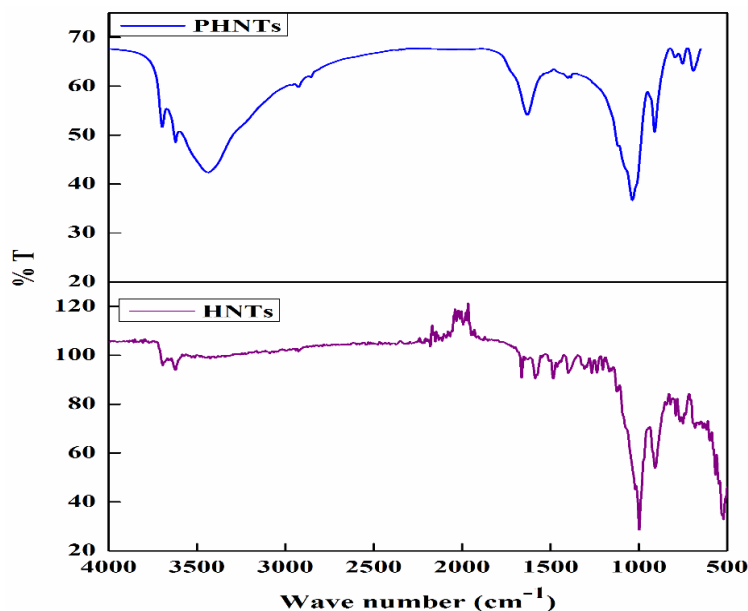


Fig.8.6 The FT IR spectrum of the HNTs and PHNTs

8.3.2 TEM analysis

The structure and elemental compositions of raw HNTs and chemically modified HNTs were examined by the TEM and EDX analysis (Fig.8.7). From the images, it was observed that HNTs are having a hollow tube like structure with an opening on either side. The length varies between 40 nm to 650 nm and the thickness between 10 nm to 90 nm. Further, these compounds were subjected to EDX analysis in order to confirm the variation in the elemental composition after chemical modification. EDX analysis showed the presence of silica (Si), alumina (Al) and oxygen (O) peaks, which are the basic building blocks of HNTs. After chemical modification, extra peaks for the carbon (C) and nitrogen (N) were also observed, this further confirms the chemical modification of HNTs.

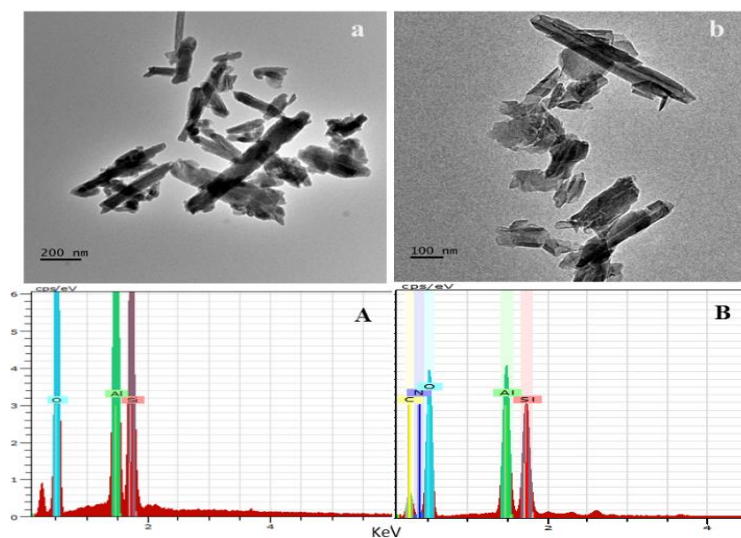


Fig.8.7 TEM and EDX analysis of a) HNTs and b) modified HNTs

8.3.3 Contact angle and surface energy analysis

The dynamic contact angle and surface energies of the prepared membranes are presented in Fig.8.8. The PMM-0 membrane exhibited highest contact angle of 79.6° , which indicates the less hydrophilic nature of the membrane, whereas contact angle decreases to 71.2° , 64.8° and 66.9° for PMM-1, PMM-2 and PMM-3 membranes respectively. The results clearly confirmed the changes in hydrophilicity of resultant membrane after incorporation of PHNTs into membrane matrix (Kanagaraj *et al.* 2015). In order to further substantiate this, surface energy of the H.F membrane was calculated by using contact angle values. The PMM-0 membrane showed least surface energy of 84.9 mN/m which increased up to 102.6 mN/m

with 2 wt. % of additive dosage. This has played an important role in evaluating permeation and fouling resistance properties of the membrane.

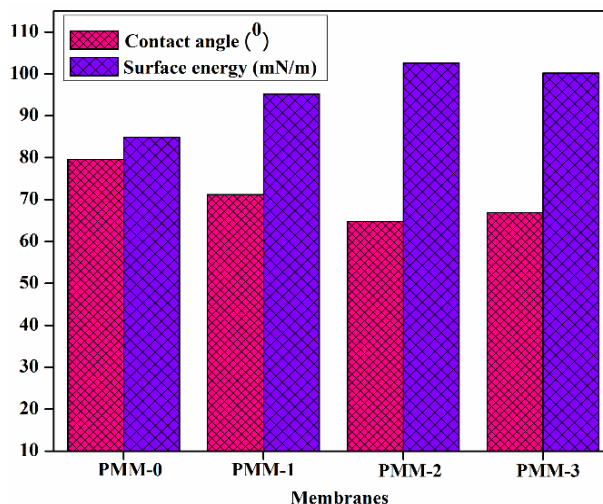


Fig.8.8 Contact angle and surface energies of the prepared membranes

8.3.4 Zeta potential analysis

The interaction of any substance at the interface of the membrane surface is related to the charge characteristics and electro-kinetic behavior (Liao *et al.* 2014). Fig.8.9 represents zeta potential results of the nanocomposite H.F membrane as function of streaming pH, which ranges from pH 2.0 - 6.0. The PMM-0 membrane showed net zero charge (i.e zeta potential = 0 mV) at pH~3.3. The IEP of the nanocomposite membrane reached up to pH range of 3.6-4.0 with the addition of different concentration of PHNTs nanoparticles. Most importantly, either positive charge at lower pH or negative charge at higher pH, nanocomposite membrane exhibits much higher zeta potential compared to PMM-0 membrane.

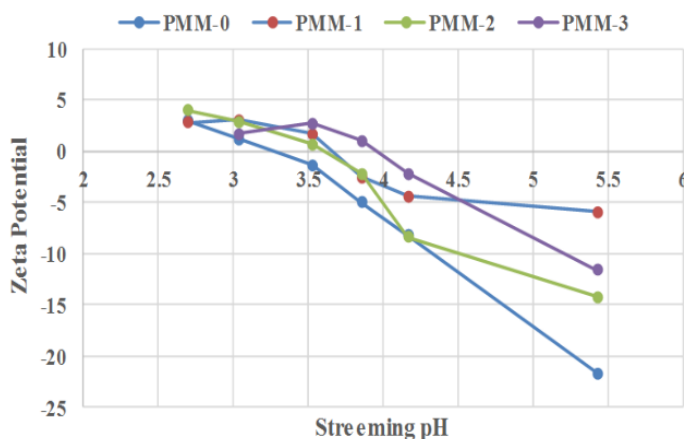


Fig.8.9 Zeta potential measurements of prepared nanocomposite H.F membrane

8.3.4 Porosity and water content

Porosity of the nanocomposite H.F membranes is presented in Fig.8.10. It was evident that the increase in PHNTs dosage improved the porosity from 40.5 % for PMM-0 membrane to 65.8 % for PMM-2 membrane with 2 wt. % of additive concentration. All of nanocomposite H.F membranes exhibited higher porosity as compared with that of virgin PEI membrane (Fig.8.10). In addition, with increase in PHNTs additive content, porosity of the membrane got enhanced initially and then reduced (Qiu *et al.* 2009). The water uptake capacity of the membranes are presented in Fig.8.10. The wettability nature of the membrane increased with enhanced hydrophilic PHNTs content as expected. As stated previously, PHNTs aided as both hydrophilic enhancer and pore former to the membrane (Chen *et al.* 2011).

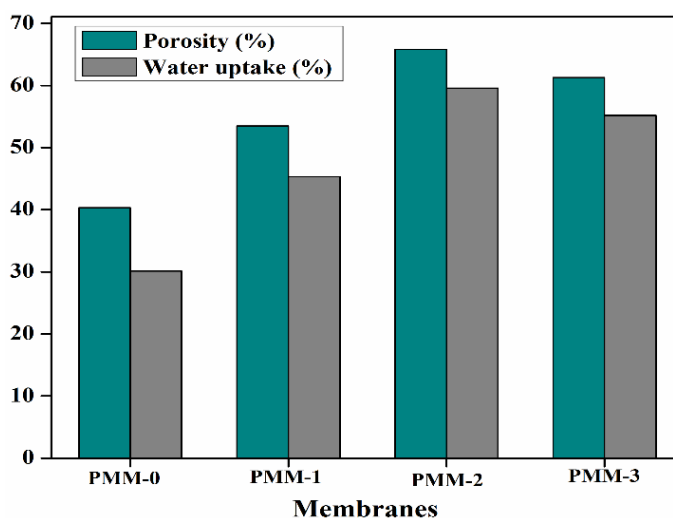


Fig.8.10 Porosity of the prepared nanocomposite hollow fiber membrane

8.3.5 Membrane morphology

The cross sectional SEM images of prepared H.F membranes are presented in the Fig.8.11. From the SEM images, it was noticed that all the nanocomposite membranes exhibited asymmetric structure with larger macro-voids in the sublayer, which is the typical morphology of ultrafiltration membrane prepared via the phase separation process (Zhao *et al.* 2011). The proper immobilization and well dispersion of PHNTs into the membrane core was confirmed by performing elemental mapping analysis and the same has been presented in Fig.8.12. The results show uniform distribution of silicon and aluminum (basic building blocks of HNTs) over entire membrane surface (Khulbe and Matsuura 2016).

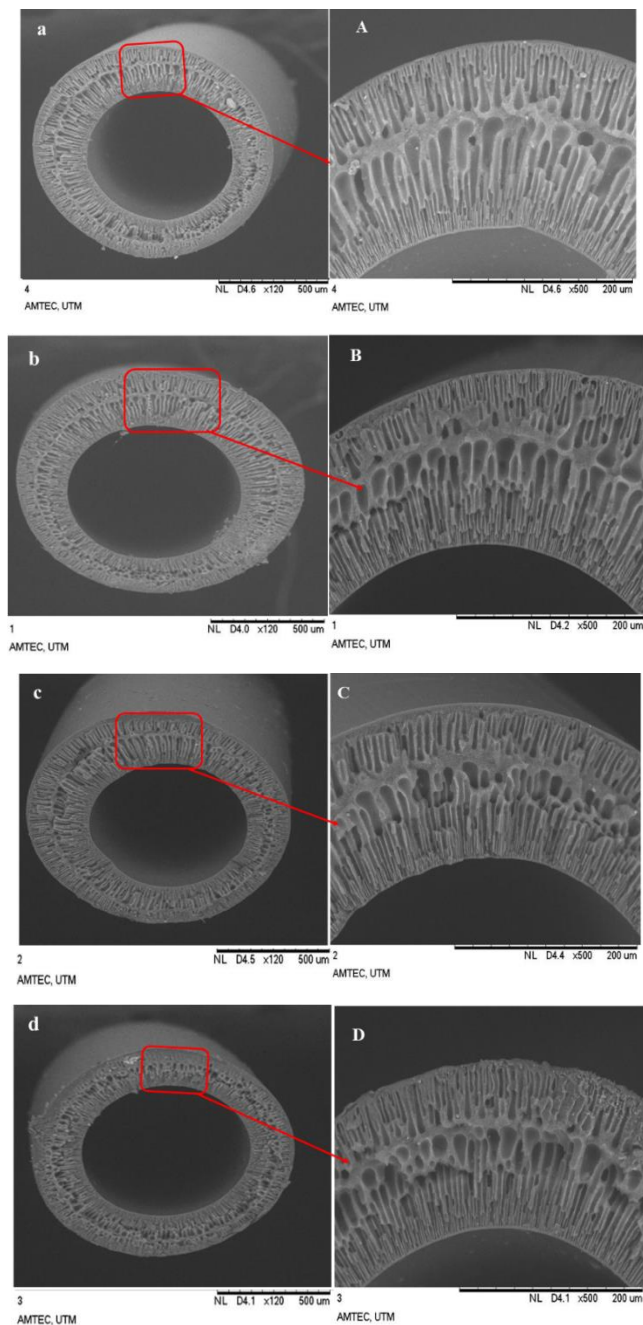


Fig.8.11 Cross sectional images of both magnified cross sectional SEM images of a) PMM-0, b) PMM-1, c) PMM-2 and PMM-3 membranes

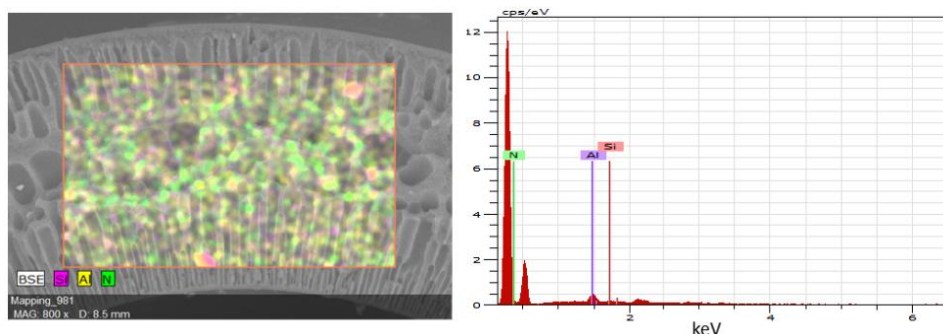


Fig.8.12 Elemental mapping analysis on cross sectional PMM-3 membrane

8.3.6 Permeation properties

Fig.8.13 represents the time dependent water flux and permeability of the membranes. The steady water flux of the PMM-0 membranes was $41 \text{ L/m}^2 \text{ h}$ and it reached up to $104.6 \text{ L/m}^2 \text{ h}$ with addition of 2 wt. % of PHNTs dosage, which indicates the synergistic effect of PHNTs on the permeation properties of nanocomposite membrane. Here, hydraulic permeability trend of nanocomposite membranes were similar to that of hydrophilicity trend (Yangali-Quintanilla *et al.* 2016). When PHNTs content increases more than 2 wt. %, flux of the membrane reduces to $92 \text{ L/m}^2 \text{ h}$. This could be due to agglomeration of nanoparticles into the pores of the membrane, which thereby increases the hydraulic resistance to water to pass through the membrane matrix.

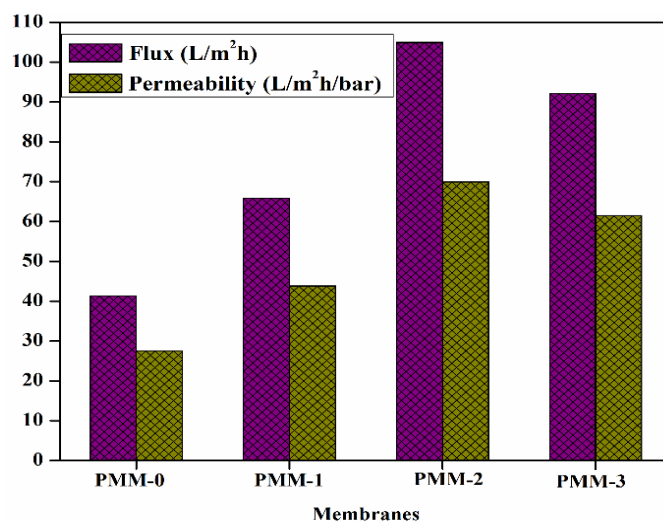


Fig.8.13 Permeation and permeability of prepared membranes

8.3.7 Antifouling properties of the membranes

Fig.8.14 represents the time dependent flux variation of the membrane before filtration, during filtration and after BSA protein filtration experiment. Flux of all the membranes

decreased, when pure water was replaced by the BSA solution in the filtration tank. The PMM-0 membrane underwent severe permeation flux decline and showed low flux recovery value compared to the nanocomposite H.F membrane. (Tang *et al.* 2017). The BSA rejection study was carried out and results are presented in Fig.8.15. All the membranes showed more than 97 % of BSA protein rejection during the filtration.

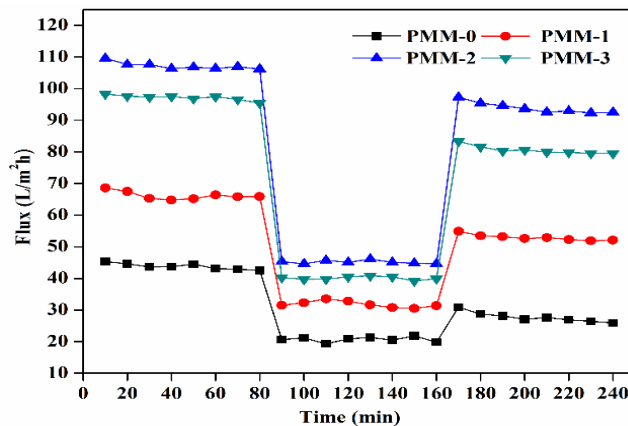


Fig.8.14 Time dependent water flux of the prepared H.F membranes with three different filtration conditions

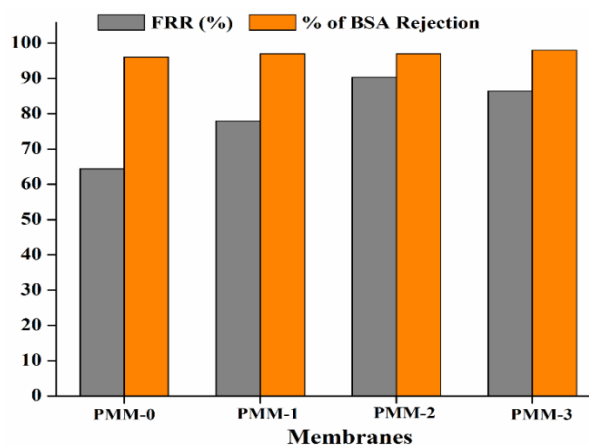


Fig.8.15 FRR and BSA protein rejection of nanocomposite H.F membranes

Total fouling phenomena of prepared nanocomposite H.F membranes are presented in Fig.8.16. The PMM-0 membrane underwent drastic flux decline and low flux recovery value of 64.4 % with other parameters like R_t , R_r , and R_{ir} were 71.6 %, 36.1 % and 35.5 % respectively. The anti-fouling nature of the nanocomposite H.F membrane drastically improved by the addition of PHNTs into membrane matrix. The inclusion of 2 wt. % of PHNTs

the FRR, R_t , R_r , and R_{ir} values reached up to 90.3 % , 61.6 % , 51.9 % and 9.6 % respectively. (Cai *et al.* 2016).

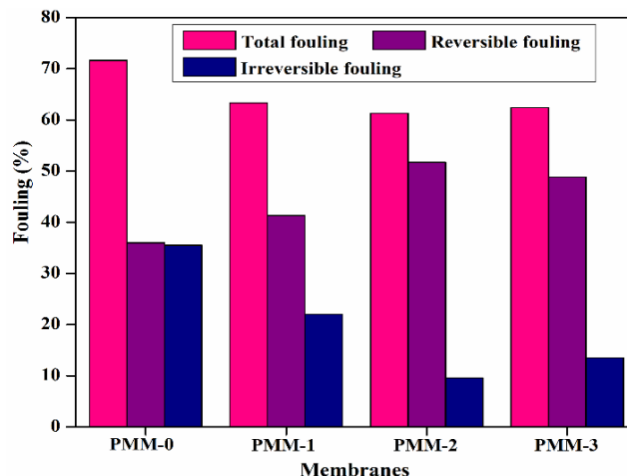


Fig.8.16 Total fouling phenomena of prepared nanocomposite H.F membranes

8.3.8 Reactive dye rejection.

The newly prepared H.F nanocomposite membranes were targeted for the removal of hazardous reactive dye application. For the dye rejection studies, well performed PMM-2 membrane was preferred due to the superior hydrophilicity, porosity, permeation and other properties. The filtration results showed that the H.F membranes have strong affinity towards the removal of dye molecules and permeate appears to be almost colorless. Fig.8.17 represents the naked eye detection of removal efficiency of reactive red 102 and reactive black 5 dyes with four cycles of experiment.

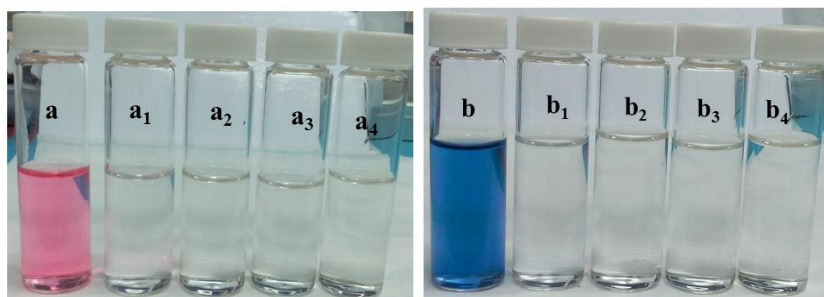


Fig.8.17 Photographic image of a) reactive red 120, b) reactive black 5 dye before and after dye rejection ($\text{pH } 7 \pm 0.5$)

The membrane with 2 wt. % of the PHNTs dosage showed more than 97 % and 94 % for the Reactive Red-120 and Reactive Black-5 dyes respectively. The increased dye rejection capacity of hybrid membrane is attributed to the presence of abundant polar functional groups

on the membrane surface and it can easily interact with the dye molecules through various secondary force of interactions. According to the literature, dye removal mechanism depends on various parameters like, the nature of dye, structure, charge density, surface chemistry of membrane as well as the specific interactions between the membrane surface and dye molecules (Liu *et al.* 2011, Xianchu *et al.* 2006, Duan *et al.* 2012, Liu *et al.* 2012).

8.3.8.1 The effect of pressure

In order to explore the effect of different transmembrane pressure on flux and dye rejection properties of nanocomposite H.F membrane, permeation experiment was carried out using different reactive dye solution. In case of pressure driven filtration process, higher transmembrane pressure gives higher permeation flux. During the experiment, PWF of the nanocomposite membrane was linearly varied with pressure. Interesting fact was that the permeate flux of reactive dye solution was not in linear proportion to the change of transmembrane pressure. According to the He *et al.* (2008), during mass transport, increasing operating pressure results in the formation of solute layer on membrane surface. This will reduce the transport rate of component with increased operating pressure (He *et al.* 2008). Therefore, very high pressure is not necessary for a high permeate flux. Fig.8.18 illustrates the effect of pressure on reactive dye rejection efficacy of the membrane.

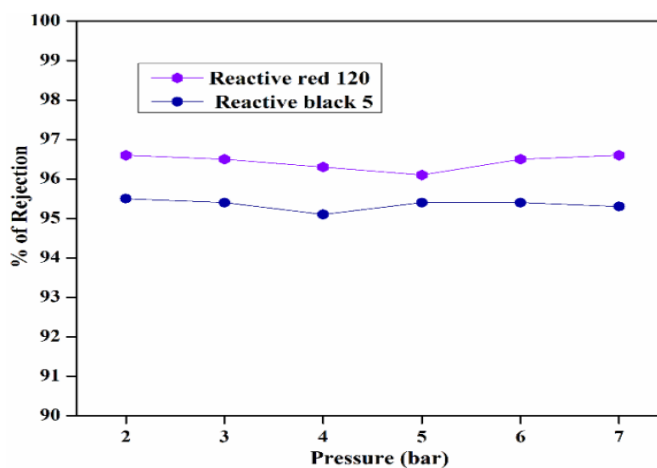


Fig.8.18 Effect of transmembrane pressure on the rejection of reactive dyes

8.3.8.2 Effect of operating time

Fig.8.19 represents the time dependent reactive dye permeate flux of H.F membrane. It was observed that permeate flux of the hybrid membrane was decreased with prolonged operating time. The initial permeate flow rate of reactive dye solution for PMM-2 membrane

was 103 L/m²h and it decreased up to 83 L/m²h and 78 L/m²h for Reactive Red-120 and Reactive Black-5 dyes respectively. These phenomena were ascribed to the fact that the reactive dye molecules accumulation on membrane surface intensified with enhanced operating time. The resultant gel layer developed by the rejected dyes molecules on membrane surface also offers an additional resistance to permeate flux. Therefore, permeation rate was reduced and dye rejections got enhanced as the operating time protracted. (Wu *et al.* 2007).

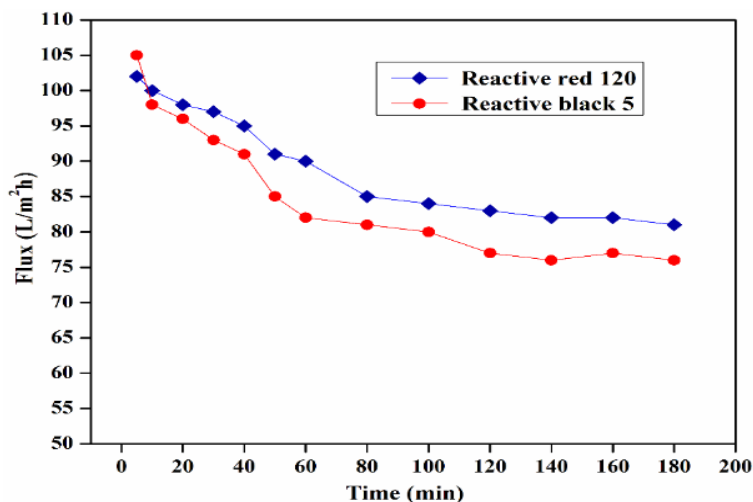


Fig.8.19 Time dependent flux study of reactive dye solutions

8.4. CONCLUSIONS

The naturally occurring HNTs were modified with poly (m-aminophenol) under mild acidic environment by oxidative polymerization method and were confirmed by FTIR, TEM and EDX analysis. The nanocomposite H.F membrane was fabricated by dry-wet spin technique with different additive dosage. The uniform dispersion and proper inclusion of PHNTs into the membrane core was confirmed by the elemental mapping analysis. The membrane physical properties such as, hydrophilicity (64.8°), surface energy (102.6 mN/m) and porosity (65.8 %) significantly improved by the addition 2 wt. % PHNTs concentration. The permeation experiments illustrate superior water flux of 104.9 Lm⁻¹h⁻¹ and only 9.6 % of irreversible fouling with more than 90.3 % of flux recovery by the simple water washing. Moreover, nanocomposite H.F membrane showed very good rejection of 97 % and 94 % for the hazardous reactive red 102 and reactive black 5 dyes respectively.

CHAPTER 9

**PREPARATION AND CHARACTERIZATION OF
FUNCTIONALIZED IRON OXIDE NANOPARTICLES
INCORPORATED POLYETHERIMIDE HOLLOW FIBER
MEMBRANE FOR HUMIC ACID REJECTION
APPLICATION**

Abstract: *In this chapter, well dispersed functionalized Fe₂O₃ nanoparticles were used to fabricate the nanocomposite hollow fiber membrane with enhanced surface and anti-biofouling properties. The nanocomposite membrane exhibited relatively higher normalized flux and rejection during the filtration of hazardous humic acid under different parameters. In addition to this, presence of functionalized Fe₂O₃ nanoparticles in the membrane significantly inhibits the growth of bacteria and other microorganisms resulting in enhanced anti-biofouling property.*

Hollow fiber (H.F) membrane based separation technology have been extensively employed for the production of hygienic drinking water, food industry, dialysis, biomedical and other applications (Quintanilla *et al.* 2016, Zhao *et al.* 2017). However, membrane fouling and biofouling is one of the major inherent drawback during the filtration process. This diminishes the separation performance and shortens the service life of membrane modules, which is a key factor for limiting the advancements of membrane technologies (Wang *et al.* 2017). More interestingly various investigation of MF and UF process proved that natural organic matter (NOM) present in the lake, river and ground water are considered as one of the predominant hazardous material and major foulants during membrane separation processes (Yuan and Zydney 2000, Shao *et al.* 2011, Cheng *et al.* 2016,).

Hamid *et al.* (2011) prepared titanium dioxide incorporated polysulfone H.F membrane for better removal of NOM and mitigation of fouling during the filtration process. The inclusion of 2 wt. % hydrophilic TiO₂ offered more than 91 % NOM removal capacity and exhibited lower fouling resistance as a result of less interaction with membrane surfaces. Shao *et al.* (2011) stated that, flux decline and extent of fouling during filtration of humic substances depends on the electrostatic interaction between membrane surface (pores) and foulants. Moreover, feed solution including metal ion concentration, pH and ionic strength, crosslinking between the humic substances strongly influence the permeation rate decline and rejection efficacy of charged membrane.

Zhao *et al.* (2013) reported the poly(N-isopropylacrylamide) brushes grafted with ZrO₂ incorporated H.F membrane for humic acid removal applications. Modified H.F membrane showed considerable improvement in hydrophilicity, hydraulic permeation and antifouling properties. During the filtration of humic acid solution, they observed the decline in adsorption fouling and higher rejection rate. Moreover, addition of Ca²⁺ ions into humic acid feed solution

reduces the electrostatic exclusion and enhances the fouling propensity. The schematic representation of humic acid adsorption a) without and b) with Ca^{2+} are given in Fig.9.1

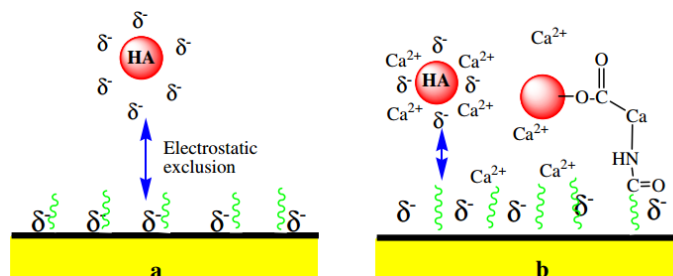


Fig.9.1 Schematic representation of humic acid adsorption a) without and b) with Ca^{2+} (Zhao *et al.* 2013)

Wang *et al.* (2015) developed an antifouling poly(vinyl butyral) H.F membrane incorporated MWCNTs U.F membrane for humic acid removal applications. The results indicate that the membrane properties such as morphology, porosity, hydrophilicity, and permeation rate evidently improved in the presence of MWCNTs. With addition of 0.6 wt.% of MWCNTs, humic acid rejection was enhanced to 94.7 ± 2.4 % with FRR value of 98.3%.

Kumar *et al.* (2016) reported charged polysulfone with higher hydrophilic nature and graphene oxide- titanium dioxide (GO-TiO₂) nanocomposite hybrid membranes for NOM (Humic acid) removal applications. The schematic representation of preparation of GO-TiO₂ nanocomposite is given in Fig.9.2. After the inclusion of GO-TiO₂ nanocomposite, fouling resistance characteristic of hybrid membrane improved significantly against the humic acid solutions. Membrane with 5 wt.% of GO-TiO₂ nanocomposite loading exhibited enhanced irreversible fouling due to humic acid and lower irreversible fouling ratio of 3.2 %.

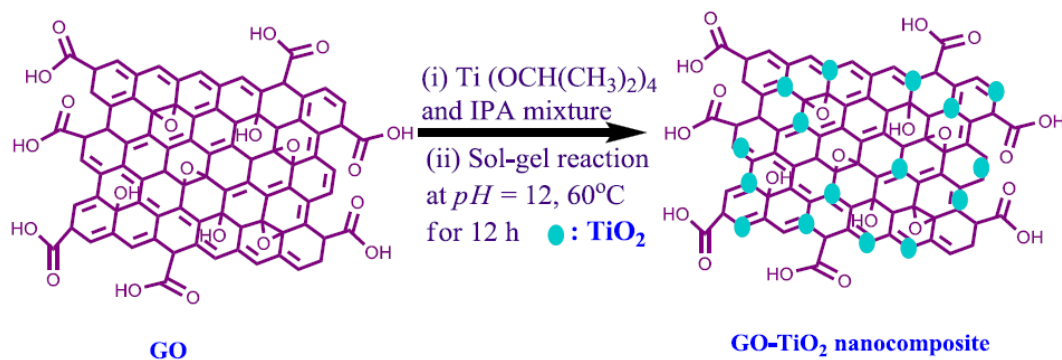


Fig.9.2 Schematic representation of preparation of GO-TiO₂ nanocomposite (Kumar *et al.* 2016)

Koutahzadeh *et al.* (2017) extensively studied the effect of UV/H₂O₂ pretreatment on humic acid fouling of polysulfone/TiO₂—and polysulfone/MWCNTs nanocomposite membrane. These nanocomposite membranes showed flux decline of just 10 % with 95% FRR%. This was due to UV/H₂O₂ pretreatment which changed the physicochemical properties of humic acid, by the super-micrometer size range (>1 μm) aggregates to a bimodal distribution of two submicrometer size ranges <1 μm (10–100 nm and 100–1000 nm). The oxidative pretreatment of humic acid feed improves the separation efficacy of the H.F membrane (Fig.9.3).

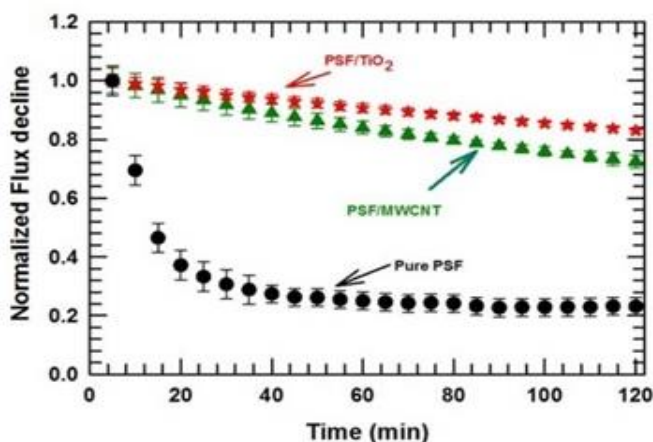


Fig.9.3 Normalized flux decline during the humic acid filtration (Koutahzadeh *et al.* 2017)

A number of inorganic nanomaterials like graphene oxide (GO), zeolite, ZnO, TiO₂, SiO₂, carbon nanotubes (CNTs) have been employed for the fabrication of nanocomposite membrane to improve the physicochemical properties and performance (Hamid *et al.* 2011, Wang *et al.* 2015, Simeonidis *et al.* 2016, Kumar *et al.* 2016, Ahmad *et al.* 2017). Among them, iron oxide (Fe₂O₃) nanoparticles have been extensively studied due to their structural flexibility, adsorption properties, excellent abrasiveness, cost-effectiveness, and chemical properties (Al-Hobaib *et al.* 2016, Zhang *et al.* 2017). Earlier, Lee *et al.* (2008) reported the antibacterial properties of zero-valent iron nanoparticles (nano-Fe⁰) against the *Escherichia coli*. The interaction of iron with intracellular oxygen caused oxidative stress mediated inactivation for *E. coli*. Prucek *et al.* (2011) demonstrated the antifungal and antibacterial activity of γ -Fe₂O₃@Ag magnetic nanocomposite with average particle size of about 70 nm. These nanocomposites showed significant antimicrobial activity against tested microorganism colonies. The minimum inhibition concentrations (MIC) of 1.9 mg/L to 31.3 mg/L showed

four candida species and 15.6 mg/L to 125 mg/L for the bacterial strains. Daraei *et al.* (2012) prepared modified iron oxide nanoparticles and incorporated them into polyethersulfone membrane matrix to enhance the surface properties, permeation and rejection behavior. Shinde *et al.* (2012) reported the applicability of modified iron oxide in the poly(propylene) flat sheet membrane for effective removal of hazardous metal ions from the waste water. In addition to this, antimicrobial activity of Fe₂O₃ nanoparticles is well known as it exhibits strong antimicrobial properties against number of viruses and bacteria. Durmus *et al.* (2013) also reported the enhanced anti-biofouling resistance activity of iron oxide nanoparticles in presence of metabolites.

In this chapter, Fe₂O₃ nanoparticles were modified by using N-(phosphonomethyl)iminodiacetic acid. The effect of modified Fe₂O₃ nanoparticles on H.F membrane properties were investigated. Cross flow filtration was employed to determine pure water permeation, reversible and irreversible fouling resistance properties. The removal of humic acid and influence on relative flux were investigated in detail in terms of feed solution pH and ionic strength. In addition to this, anti-biofouling properties were analyzed against *E. coli* and other microorganisms.

9.1. MATERIALS AND METHODS

9.1.1 Materials

Polyvinylpyrrolidone (PVP) K29-32 (MW: 58,000 g/mol) was obtained from Acros Organics. Bovine serum albumin (BSA), N (phosphonomethyl)iminodiacetic acid hydrate, iron (II,III) nanoparticle < 80 nm were purchased from Sigma Aldrich. Humic acid was obtained from HIMEDIA chemicals. NMP of purity > 99.5% used as solvent, procured from Acros Organics.

9.1.2 Modification of iron oxide nanoparticles

The chemical modification of Fe₂O₃ nanoparticles was carried out according to the procedure reported by Sen *et al.* (2014) using phosphonate grafting agent. The schematic representation of chemical modification is presented in Fig.9.4. In brief, Fe₂O₃ nanoparticles were dispersed in the ultrapure water and ultra-sonicated for about 30 min in order to avoid agglomeration of nanoparticles. Resultant suspension was maintained around pH 10 by the addition of 0.1M sodium hydroxide solution. In the next step, equimolar concentration (1:1

molar ratio) of N-(phosphonomethyl)iminodiacetic acid hydrate (PMIDA) was added to above suspension and magnetically stirred for 18 h at ambient temperature. The obtained modified iron oxide nanoparticles were collected by centrifugation followed by washing with water and neutralization dilute hydrochloric acid (HCl) solution. Finally, washed with ethanol and dried in vacuum oven at 75 ° C for about 15 h.

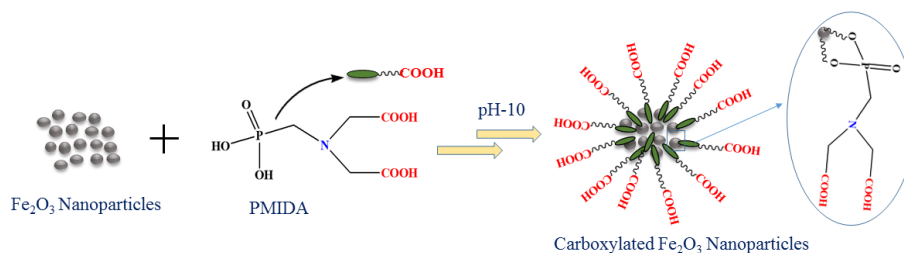


Fig. 9.4 Schematic representation of chemical modification of Fe_2O_3 nanoparticles

Surface modification of Fe_2O_3 nanoparticles was characterized by X-ray diffraction (XRD) using $\text{Cu-K}\alpha$ radiation over the 2θ range of $20\text{--}60^\circ$ at a scan rate of 2 deg min^{-1} (Bruker AXS Diffractometer D8 powder XRD). The changes in the functional groups after modification was confirmed by FTIR spectroscopy. In order to investigate the elemental composition of nanoparticles before and after modification, EDX analysis was carried out. The particle size and nature of charge density was determined by particle size layer (Horiba sz 100 nanoparticle size).

9.1.3 Preparation of hollow fiber membrane

The modified iron oxide immobilized PEI nanocomposite H.F membrane was prepared by dry-wet method using the phase inversion technique (Khulbe *et al.* 2016). The overview of dope solution compositions and spinning conditions are presented in Table-9.1 and Table 9.2. To prepare the dope solution, calculated amount of modified Fe_2O_3 nanoparticles was dispersed in NMP solvent and ultra-sonicated for 30 minutes to avoid the agglomeration of nanoparticles. To this suspension, desired amount PEI and PVP were added and magnetically stirred for 24 h at 60°C to obtain homogeneous polymer solution. The resultant solution was degasified before spinning the H.F membrane. The detailed procedure for the preparation of H.F membrane is given in CHAPTER -7, section 7.1.3.

Table 9.1 Composition of casting solution.

Membrane	PEI(g)	NMP (g)	PVP (g)	MIONPs(g)	W_{MIONPs}^* (wt%)
IOM-0	1.8	8.0	0.2	0	0
IOM-1	1.8	7.9	0.2	0.009	0.5
IOM-2	1.8	7.9	0.2	0.018	1.0
IOM-3	1.8	7.9	0.2	0.027	1.5

* W_{MIONPs} is the mass ratio of MIONPs to PEI.

Table 9.2 Spinning parameters of nanocomposite H.F membranes.

Parameters	Condition
Spinneret DO/ID	1.1 mm / 0.55 mm
Spinneret Temperature (°C)	27
Dope solution	PEI/PVP/MIONPs*
Bore fluid composition	DI water
Bore fluid flow rate (mL/min)	1.5
Range of air-gap distance (cm)	10
Coagulant	Water
Coagulant temperature (°C)	27
Washing bath	water
Washing bath temperature (°C)	27
Take-up speed (cm/min)	2.1

* MIONPs - modified Fe₂O₃ nanoparticles.

9.2 CHARACTERIZATION OF NANOCOMPOSITE HOLLOW FIBER MEMBRANE

9.2.1 Membrane characterization

To investigate the effect of modified iron oxide nanoparticles on PEI H.F nanocomposite membrane morphology, SEM analysis was carried out. The charge characteristic of pristine and modified membrane was analyzed by SurPASS electrokinetic analyzer (Anton Paar, Graz, Austria). Anti-biofouling properties of prepared membrane was determined by using *Mycobacterium smegmatis* (MTCC 994), *Staphylococcus aureus* (MTCC3160) and *Escherichia coli* (MTCC1687) and fungi *Candida albicans* (MTCC 7253)

microbial stains. Further, permeation and antifouling analysis of the membranes were carried out according to the procedure given in CHAPTER 7, section 7.2.2. The humic acid rejection was studied according the procedure given in CHAPTER 3, section 3.2.4.

9.3. RESULTS AND DISCUSSIONS

9.3.1 Characterization of iron oxide nanoparticles

The changes in functional groups after the modification of iron oxide nanoparticles were confirmed by FTIR analysis and obtained spectrum is presented in Fig. 9.5. The strong adsorption band at 580 cm^{-1} corresponds to Fe–O vibration, which is characteristic peak of iron oxide nanoparticles. The broad peak around 3300 cm^{-1} indicates the presence of –OH functionality in the nanoparticles. After modification with N-(phosphonomethyl)iminodiacetic acid, the strong peak at 1480 cm^{-1} represents the –P=O and M–P–O groups superimposed on one another and broad peak around 3400 cm^{-1} represents the –OH group of carboxylic acids. The typical carbonyl group adsorption band was observed around 1735 cm^{-1} and confirms the incorporation of phosphonate grafting agent into nanoparticles (Sahoo *et al.* 2011, Sen *et al.* 2014). Fig.9.6 shows the XRD patterns for pure Fe_3O_4 and PMIDA conjugated Fe_3O_4 nanoparticles. The characteristic peaks were observed at $2\theta = 30^\circ, 35^\circ, 43^\circ, 53^\circ, 57^\circ,$ and 63° for Fe_3O_4 nanoparticles, which were marked by their indices (220), (311), (400), (422), (511), and (440). Similar kind of peaks were also observed for modified Fe_3O_4 nanoparticles. This revealed that the surface modification and conjugation of the Fe_3O_4 nanoparticles did not lead to their phase change. These XRD patterns were matched with the standard JCPDS file (card no. 10- 0319). In addition to this, particle size analysis and FESEM confirms the modified Fe_2O_3 nanoparticles having the average particle size distribution around 60 nm to 80 nm and experimental results are presented in Fig.9.7.

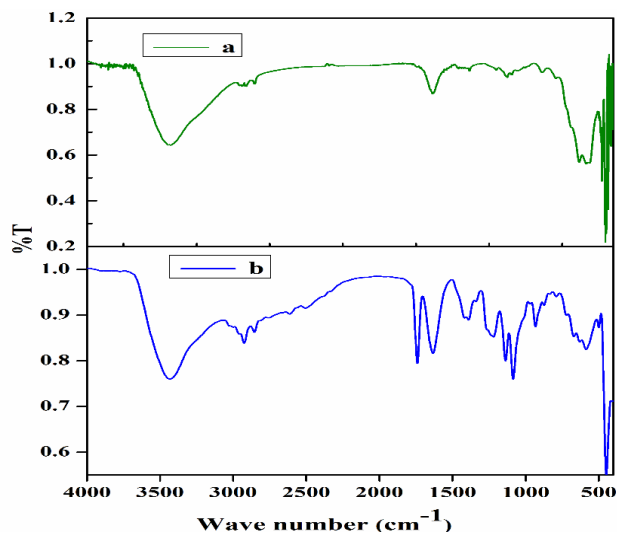


Fig .9.5 FTIR spectrum of a) Fe₂O₃ nanoparticles and b) modified Fe₂O₃ nanoparticles.

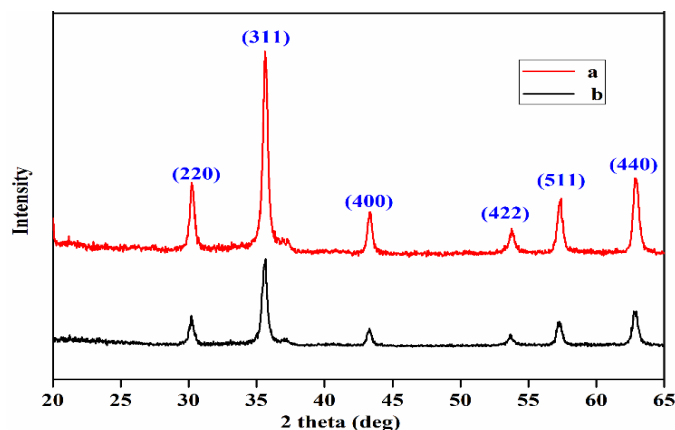


Fig.9.6 X-ray diffraction patterns of a) Fe₂O₃ nanoparticles and b) modified Fe₂O₃ nanoparticles

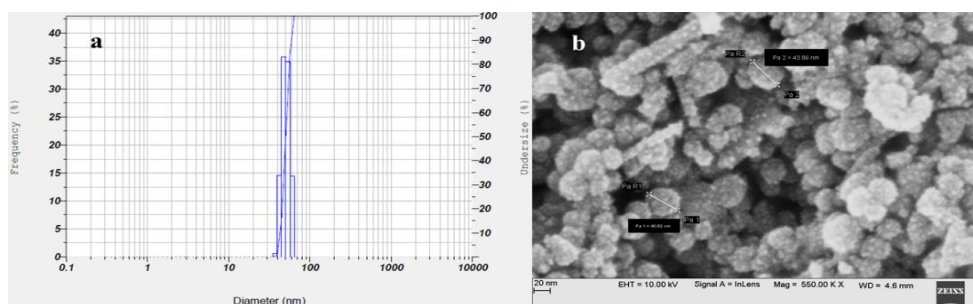


Fig.9.7 a) Average particle size distribution and b) FESEM images of modified Fe₂O₃ nanoparticles

The elemental composition of unmodified and modified iron oxide nanoparticles were determined by EDX analysis and results are presented in Fig.9.8. The unmodified Fe₂O₃ nanoparticles showed presence of iron (Fe) and oxygen (O) as the prominent elements. After

the chemical modification along with these elements, presence of carbon (C) and phosphorous (P) confirmed the chemical modification. In addition to this, negative charge density of particles were analyzed by zeta potential analysis (Fig.9.9). The Fe₂O₃ nanoparticles showed zeta potential of -57.8 and after modification it was up to -67.7, due to the presence abundant number of -OH, -C=O, -COOH and -P=O functional groups. These analyses further confirmed the chemical modification of Fe₂O₃ nanoparticles.

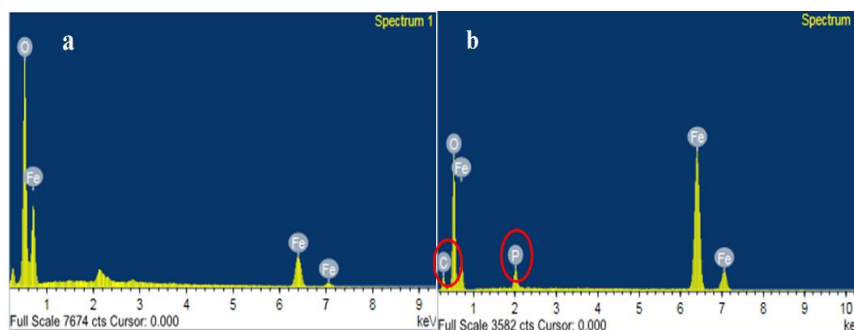


Fig.9.8 EDX analysis of a) Fe₂O₃ nanoparticles and b) modified Fe₂O₃ nanoparticles

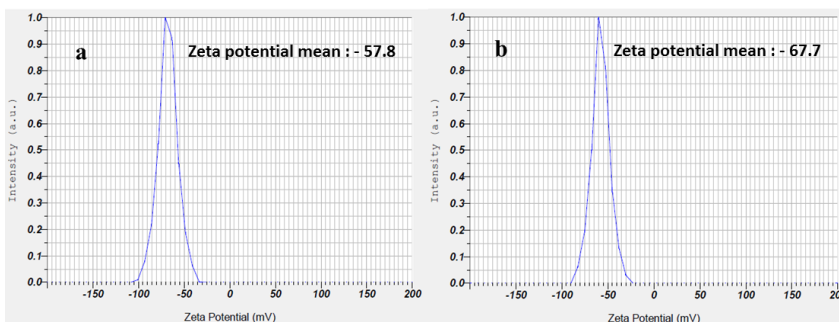


Fig.9.9 Zeta potential analysis of a) Fe₂O₃ nanoparticles and b) modified Fe₂O₃ nanoparticles (P^H = 7 ± 0.5)

9.3.2 Membrane morphology and properties

Fig.9.10 represent the cross sectional SEM images of pristine and modified nanocomposite H.F membrane. The addition of various dosage of hydrophilic modified Fe₂O₃ nanoparticles into the casting solution has synergistic influence on resultant membrane morphology. From the images, it was observed that, finger like projection with dense skin layer and macrovoids in sublayer, which is the typical morphology of UF membrane prepared via the phase separation process. The modified iron oxide nanoparticles, concentration of additive dosage and change in spinning parameters like air gap distance will have major impact on morphological structure and physico-chemical properties of resultant hybrid membranes,

which was confirmed by analyzing porosity, surface energy, charge density and hydrophilicity behavior.

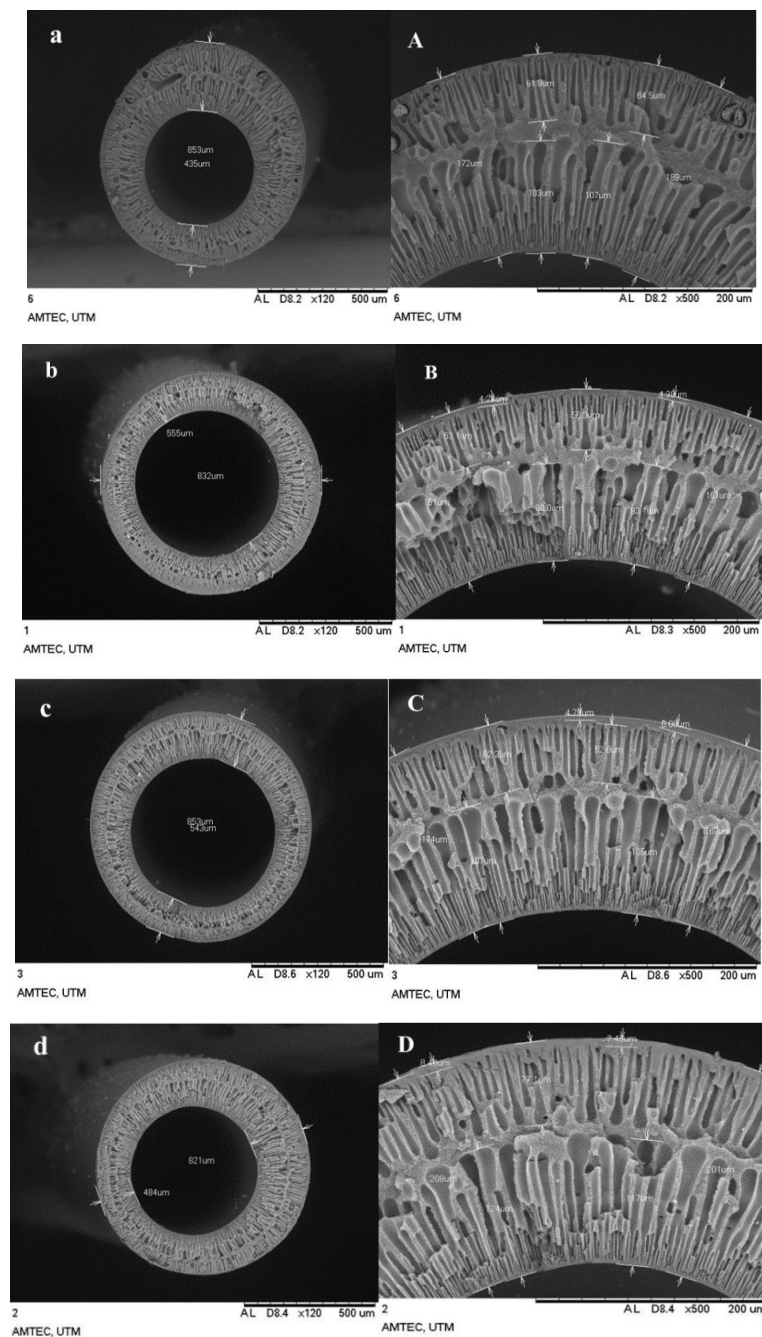


Fig.9.10 SEM images of the a) IOM-0, b) IOM-1, c) IOM-2 and d) IOM-3 H.F membranes.

Table 9.3 represents the summarized experimental results of water uptake capacity, porosity and surface energy of prepared nanocomposite H.F membranes. Among all membranes, IOM-0 membrane showed lower porosity of 41.8 % and water uptake capacity of

39.2 % due to reasonably hydrophobic nature compared to hybrid nanocomposite H.F membrane. The membrane with 1.5 wt. % showed highest water adsorption capacity of 61.7 %, due to presence of macrovoids in sublayer and abundant hydrophilic functional groups in the membrane matrix increases the water binding capacity (Zhang *et al.* 2013). The dynamic contact angle and surface energies of the prepared membranes are presented in the Fig.9.11. Contact angle values of prepared H.F nanocomposite membranes also showed a similar trend as obtained for water uptake capacity. The results clearly confirmed the changes in hydrophilicity of resultant membrane after incorporation of modified iron oxide nanoparticles into membrane matrix. In order to further substantiate this, surface energy of the H.F membrane was calculated by using contact angle values. The IOM-0 membrane showed least surface energy of 84.8 mN/m and increased up to 106.7 mN/m with 1.5 wt % of additive dosage.

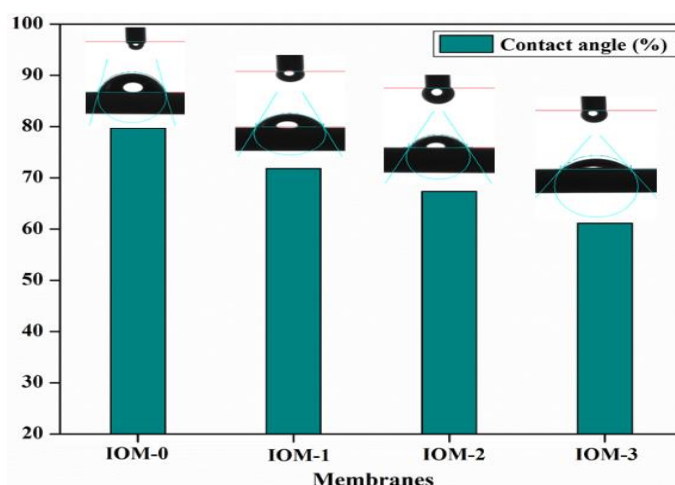


Fig.9.11 Contact angle analysis of prepared membranes

Table 9.3 Physical properties of the prepared nanocomposite H.F membranes.

Membrane	Porosity (%)	Water uptake (%)	Flux (L/m ² h)	Surface energy (mN/m)
IOM-0	41.8	39.2	45.6	84.8
IOM-1	56.3	48.3	76.8	94.4
IOM-2	59.7	56.4	98.1	99.7
IOM-3	64.5	61.7	124.7	106.7

9.3.3 Zeta potential analysis

Fig.9.12 represents zeta potential results of the nanocomposite H.F membrane as function of streaming potential, ranges from pH 2.0 - 9.0. The interaction of any substance at the interface of the membrane surface depends on electro-kinetic behavior and charge characteristics (Li *et al.* 2017). The IOM-0 membrane showed the zeta potential value of -51.6 mV and after the inclusion of 1.5 wt. % of iron oxide nanoparticles, value increased to -63.23 mV. The pH dependent measurements help in identifying the isoelectric point (IEP) of the H.F membranes. The IOM-0 membrane showed net zero charge (i.e zeta potential = 0 mV) at pH~ 3.2. The IEP of the nanocomposite membrane reached up to pH range of ~ 4.8 with the addition of 1.5 wt.% of iron oxide nanoparticles.

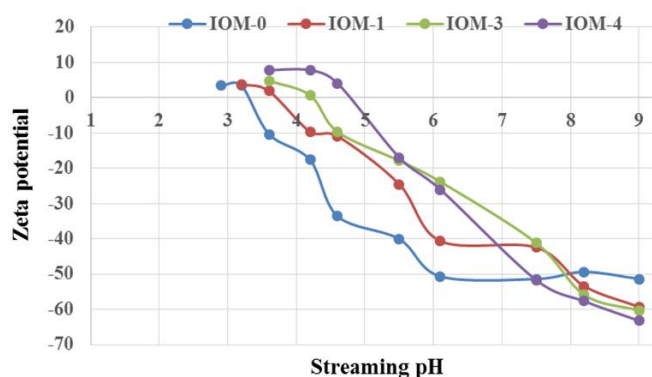


Fig.9.12 Zeta potential analysis of prepared nanocomposite hollow fiber membrane.

9.3.4 Permeations and antifouling study

The pure water flux of prepared membrane are presented in Table-9.3. The water permeability increased significantly with nanocomposite H.F membrane compared to pristine PEI membrane. The IOM-0 membrane offered higher membrane hydraulic resistance with comparatively lower water flux of 45 L/m²h. After modification, i.e membrane immobilized with 1.5 wt. % of hydrophilic additive, the membrane hydraulic resistance reduced and flux value reached to 124 L/m²h (Geng *et al.* 2017). Fig.9.13 represents the fouling behavior under dynamic filtration process through pure water filtration, protein filtration and followed by water filtration after hydraulic cleaning. The IOM-0 membrane underwent drastic flux decline and low flux recovery value of 63.8 % with other parameters like R_t , R_r , and R_{ir} , were 61.8 %, 25.6% and 36.1% respectively. After the inclusion of 1.5 wt. % of modified iron oxide

nanoparticles, the FRR, R_t , R_r , and R_{ir} values reached up to 91.2% , 51.9%, 43.2% and 8.7% respectively (Fig.9.14).

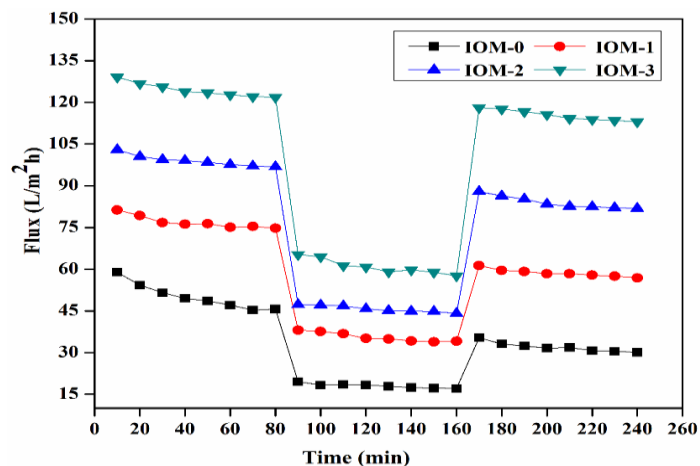


Fig.9.13 Time dependent water flux at different filtration environments

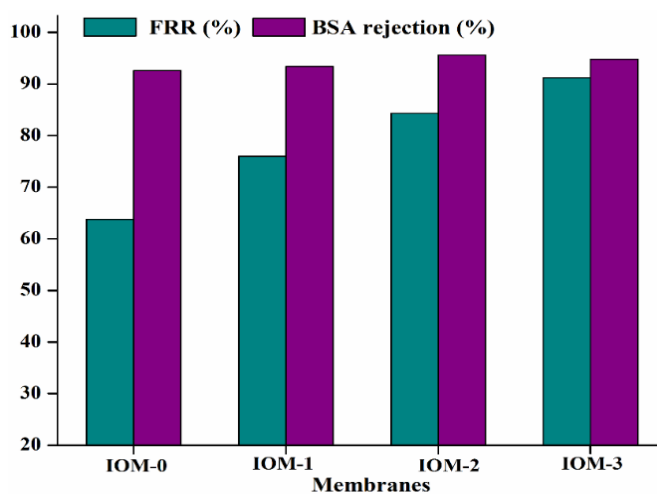


Fig.9.14 FRR and BSA protein rejection of prepared membranes

9.3.5 Anti-biofouling properties of membrane

Anti-biofouling nature of prepared nanocomposite H.F membrane was investigated by inhibition of microbial growth according to the procedure given in CHAPTER 6, Section 6.2. Fig.9.15 represents the control and membranes in nutrient agar plates after the incubation. These results showed that the control i.e whatman filter paper strip displayed microbial growth in agar plates, whereas no microbial growth was observed in case of nanocomposite IOM-3 H.F membrane. This illustrates the potential resistance towards the microbial growth on the membrane surface over the prolonged period. This was substantiated as follows; presence of

iron oxide nanoparticles in the membrane matrix are able to mitigate the microbial contaminant in drinking water (Cho *et al.* 1999, Park *et al.* 2005). This was due to the presence of iron oxide nanoparticles in skin layer of the membrane which can predominantly destroy the cell membrane or lose their cellular regularity of microorganism thereby reducing the microbial growth.

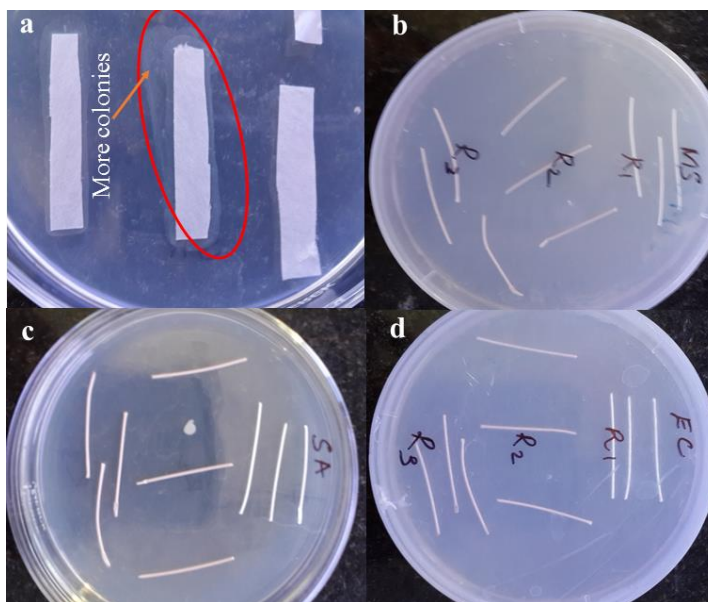


Fig.9.15 Biofouling analysis a) microbial growth on whatman filter paper strip (as control), and membrane incubated with b) *Mycobacterium smegmatis*, c) *Staphylococcus aureus* d) *Escherichia coli* colonies.

9.3.6 Humic acid removal study

The filtration experiments were carried out at 0.3 MPa transmembrane pressure with 100 ppm humic acid solution and rejection profile which is presented Fig.9.16. The flux of all the membranes decreased rapidly at the beginning of each experiment due to the deposition or adsorption of humic acid molecules on the membrane surfaces. It was interesting to note that, humic acid rejection coefficient (R) of the modified H.F membrane with 1.5 wt. % additive dosage increased to 0.94 compared to unmodified membrane with $R > 0.76$ under the same experimental condition. This indicates that, modified iron oxide has synergistic influence on effective membrane performance (Tang *et al.* 2007).

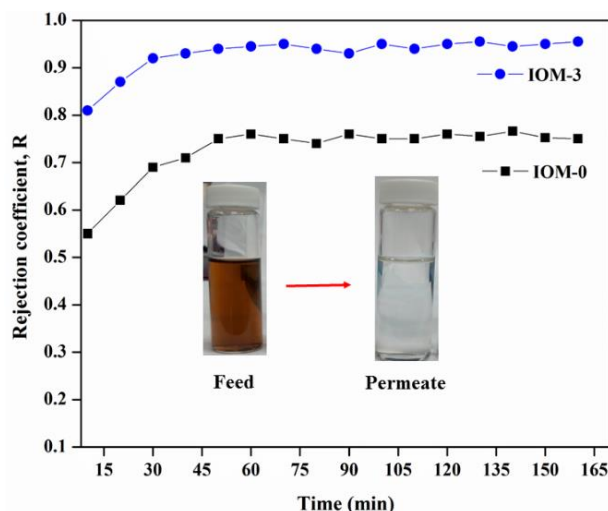


Fig.9.16 Humic acid rejection coefficients of the hollow fiber membranes ($\text{pH}=7\pm 0.3$)

9.3.6.1 Relative flux rate

Fig.9.17 shows the relative hydraulic permeation rate (J_h/J_{w1}) during the time dependent filtration experiment through modified and unmodified H.F membranes. Initial decline in relative flux was observed for all membranes in which 65 % flux decline was obtained for IOM-0 membrane whereas only 19 % was obtained for IOM-3 membrane. It is well known that the main mechanism for reducing flux value during the filtration was due to interactions between humic acid and water molecule with membrane matrix. As mentioned above, modified membrane showed lower contact angle and higher zeta potential as compared to IOM-0 membrane. (Shao *et al.* 2011). Where J_h humic acid flux and J_{w1} pure water flux.

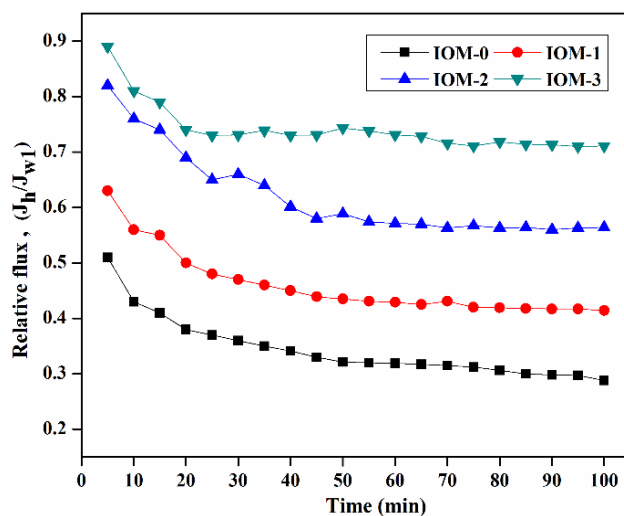


Fig.9.17 Time dependent relative flux of prepared membranes

9.3.6.5 Effect of feed solution pH

Fig.9.18 represent the relative flux during the filtration experiment with feed solution pH of 3 and 8 respectively. It was observed that the initial flux decline was more rapid at pH 3 compared to feed solution of pH 8 for both modified and unmodified H.F membrane. The decline in the relative flux ratio at 30 min filtration time is 36 % at pH 3 whereas 29 % was observed at pH \approx 8 under same experimental condition for IOM -3 membrane. These results indicate the synergistic effect of pH of feed solution on permeation behavior of H.F membrane (Katsoufidou *et al.* 2005).

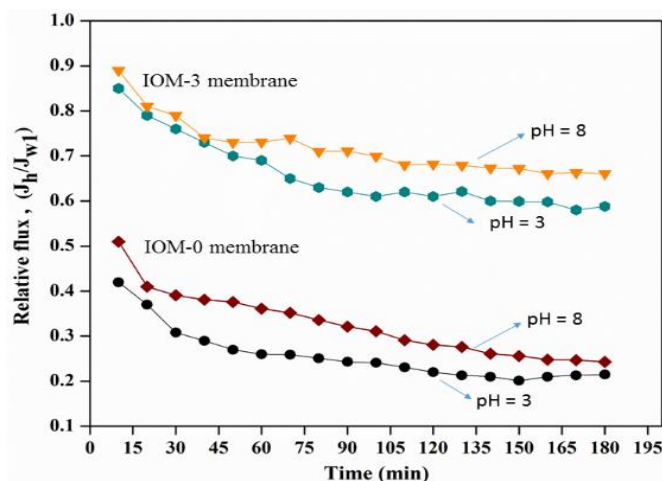


Fig.9.18 Effect of feed solution pH on normalized permeation rate

9.3.6.3 Effect of ionic strength

The concentration of ionic strength has significant influence on permeation properties of both pristine and modified H.F membranes. Fig.9.19 illustrate the variation in relative permeation rate of IOM-0 and IOM-3 H.F membranes. It was observed that, the IOM-0 membrane exhibited relative flux coefficient of 0.48, 0.35, 0.23 for humic acid solution with 10 mM, 50 mM and 100 mM of sodium chloride concentration respectively. After the modification of H.F membrane, relative flux was considerably high as compared to unmodified membrane. However, as the concentration of ionic strength in humic acid feed solution increases to 10 mM, 50 mM and 100 mM, relative flux decreases to 0.76, 0.68, 0.59 respectively.

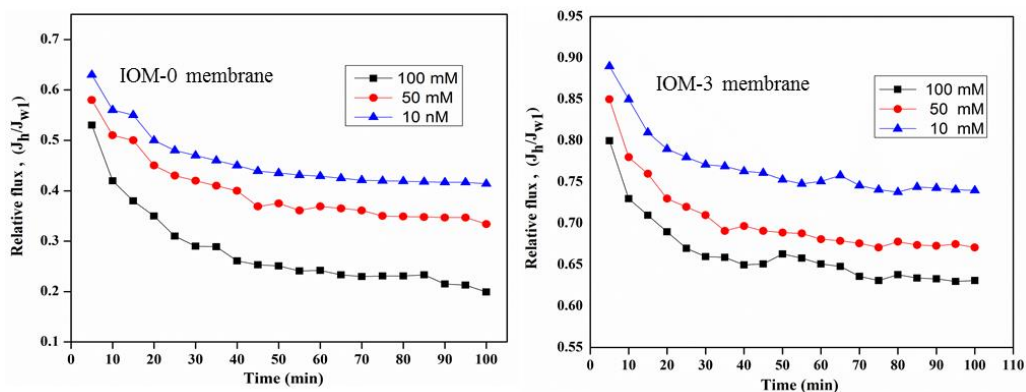


Fig.9.19 Effect of ionic strength of feed solution on normalized hydraulic permeation

9.4. CONCLUSIONS

The functionalization and fabrication of PEI nanocomposite H.F membrane was carried out by incorporating the carboxylated Fe_2O_3 nanoparticles by using phase inversion technique. The favorable properties like higher hydrophilicity, water uptake capacity, surface energy and porosity was observed with inclusion of 1.5 wt. % of additive dosage. The permeation experiments illustrates superior water flux of $124 \text{ Lm}^{-1}\text{h}^{-1}$ and only 8.7 % of irreversible fouling with more than 91.2 % of flux recovery by the simple water washing. The prepared membrane exhibited relatively higher rejection and normalized flux during the filtration of NOM with different environment such as feed solution pH, ionic strength. The presence of modified Fe_2O_3 nanoparticles in the membrane significantly inhibits the growth of *Escherichia coli*, *Staphylococcus aureus* and other microorganisms on the membrane surface, resulting in enhanced anti-biofouling property.

CHAPTER 10
SUMMARY AND CONCLUSIONS

Abstract

This chapter summarizes the entire work in brief and draws a comparison between in house synthesized membranes in terms of their properties and performance. It also lists the major conclusions drawn from the work.

10.1 SUMMARY OF THE WORK

- ✓ A total of thirty three membranes (8 series) with different compositions were prepared in this research work.
- ✓ Among the thirty three membranes, twenty five were flat sheet membranes and eight were hollow fiber membranes.
- ✓ Different organic and inorganic additives such as ascorbic acid, citric acid, maleic acid, PIAM, bentonite, HNTs and iron oxide nanoparticles were used as additive. The above mentioned inorganic nanoparticles were chemically modified and incorporated into membrane matrix.
- ✓ Both flat sheet and hollow fiber membranes were prepared by phase inversion method using water as non-solvent in the coagulation bath.
- ✓ The morphology and roughness parameters of the prepared membranes were studied using SEM and AFM.
- ✓ The performance of the prepared membranes was evaluated by investigating the hydraulic permeation, surface hydrophilicity, porosity, membrane hydraulic resistance, water uptake capacity, antifouling and anti-biofouling study.
- ✓ The prepared membranes were subjected to water purification with respect to heavy metal ion rejection, humic acid rejection and dye removal.

From the experimental investigations following important results were obtained.

1. The membrane modified with 80:20 ratio of PEI:hydrolyzed PIAM provides FRR value of 73% with sodium sulfate rejection of 76 %.
2. The addition of citric acid, ascorbic acid and melic acid considerably alter the membrane morphology with decreasing surface roughness. The citric

acid incorporated membrane showed PWF of $242.3 \text{ L m}^{-2}\text{h}^{-1}$ with FRR of 72 % and having humic acid rejection efficiency up to 86 %.

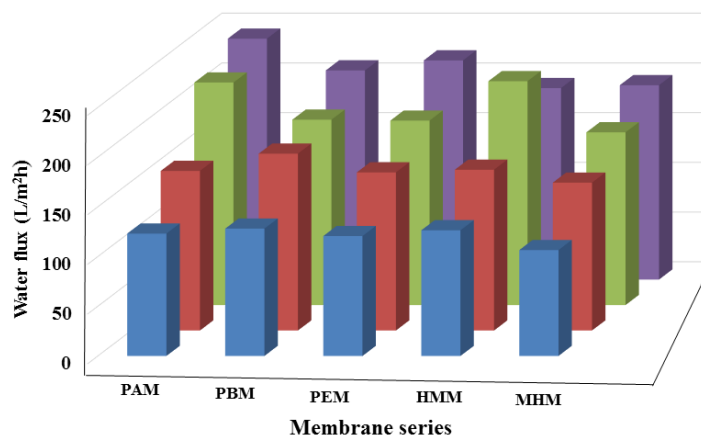
3. The membrane with 4 wt. % activated bentonite dosage showed maximum rejection of 69.3 %, 76.2 % and 82.5 % for 250 ppm of Cd (II), Ni (II) and Cu (II) ion solutions respectively.
4. The membrane with 3 wt. % bentonite clay bearing the poly (4-styrenesulfonate) brushes showed the FRR value of 84.1 % with irreversible fouling ratio of 15.8 % and reversible fouling upto 75.6 %. In addition to this, membrane exhibited rejection efficacy upto 80.5 % and 74.6 % for Pb^{2+} and Cd^{2+} ions respectively during PEUF.
5. The presence of 3 wt. % polydopamine modified HNTs in the membrane showed FRR of 74.5 % and reversible fouling ratio of 60.7 %. The HMM-3 membrane exhibited rejection of 79 % (Pb^{+2}), and 73 % (Cd^{+2}) respectively during the PEUF. Moreover, HMM-3 membrane showed excellent resistance to microbial growth on the membrane surface.
6. The hollow fiber membrane PMM-2, exhibited the water flux of $104.9 \text{ L m}^{-2}\text{h}^{-1}$ and only 9.6 % of irreversible fouling with more than 90.3 % of flux recovery. Also showed rejection of 97 % and 94 % for the hazardous reactive red 102 and reactive black 5 dyes respectively.
7. The membrane MHM-3, showed the rejection capacity of 97 % and 94 % for MB and Rh.B dyes respectively.
8. The hollow fiber membrane IOM-3, showed water flux of $124 \text{ L m}^{-2}\text{h}^{-1}$ and only 8.7 % of irreversible fouling with more than 91.2 % of flux recovery.

The performance of all the prepared membranes in terms of PWF, contact angle and antifouling ability are compared below. The eight series of membranes are named as follows

Table 7.1 Prepared membrane series

Membrane series name	Membranes
PM	PM-1, PM-2, PM-3, PM-4
PAM	PAM-0, PAM-1, PAM-2, PAM-3
PBM	PBM-0, PBM-1, PBM-2, PBM-3, PBM-4
PEM	PEM-0, PEM-1, PEM-2, PEM-3
HMM	HMM-0, HMM-1, HMM-2, HMM-3
MHM	MHM-0, MHM-1, MHM-2, MHM-3
PMM	PMM-0, PMM-1, PMM-2, PMM-3
IOM	IOM-0, IOM-1, IOM-2, IOM-3

Fig.10.1 and Fig.10.2 shows the PWF of prepared membranes flat sheet and H.F membranes. From the experimental results it was observed that, flat sheet PEI membrane with 4 wt. % of activated bentonite showed higher water permeation value. The H.F membrane with 1.5 wt. % of modified iron oxide nanoparticles exhibited higher flux. The membrane with hydrophilic inorganic additives has significant influence on physicochemical properties of the membrane, thereby alters the hydraulic permeation behavior. (Where in PBM series PBM-0, PBM -1, PBM-2 and PBM-4).

**Fig.10.1** Pure water flux of (L/m²h) of prepared flat sheet membranes

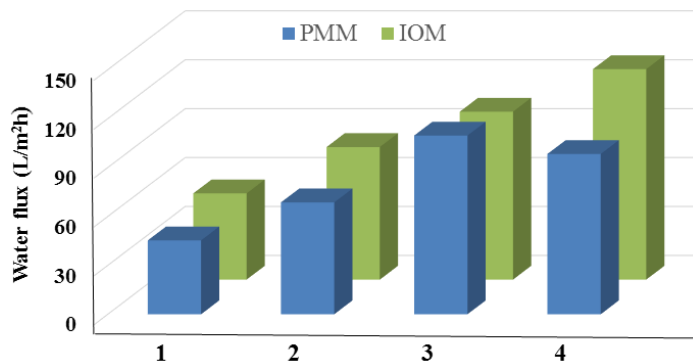


Fig.10.2 Pure water flux of (L/m²h) of prepared hollow fiber membranes

Fig.10.3 represents the contact angle of all prepared membranes. In water treatment applications, contact angle of the membrane place a vital role in permeability and performance. The hydrophilic organic and inorganic additives in to the membrane matrix significantly increase the hydrophilicity. The lowest contact angle was shown by PM-3 membrane of PM series, containing 80:20 PEI:hydrolysed PIAM blend ratio. (Where in PBM series PBM-0, PBM -1, PBM-2 and PBM-4).

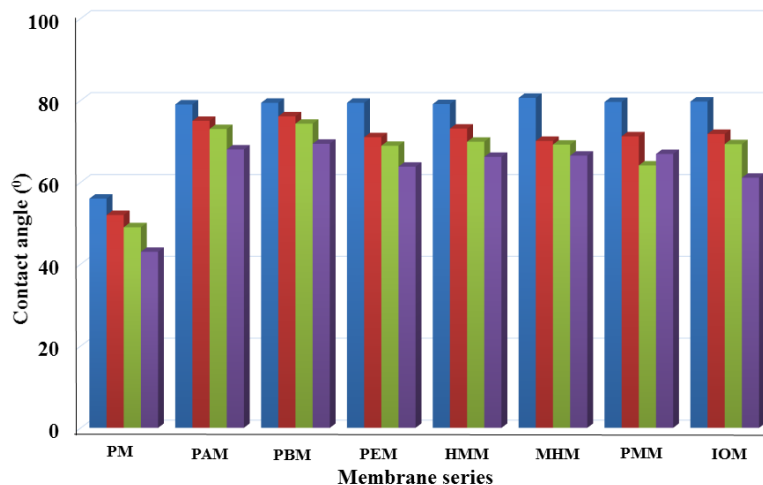


Fig.10.3 Contact angles (in degrees) of prepared membranes.

The antifouling ability of the membranes was studied by measuring the % FRR values for the membranes. Fig.10.4 represents the FRR of prepared membranes. All the membrane series showed an increasing trend in the % FRR values by the addition both organic and inorganic hydrophilic additives into the PEI membrane. Among all prepared membrane H.F

membrane with 1.5 wt. % modified iron oxide nanoparticles showed the maximum FRR of 92 %. (Where in PBM series PBM-0, PBM -1, PBM-2 and PBM-4).

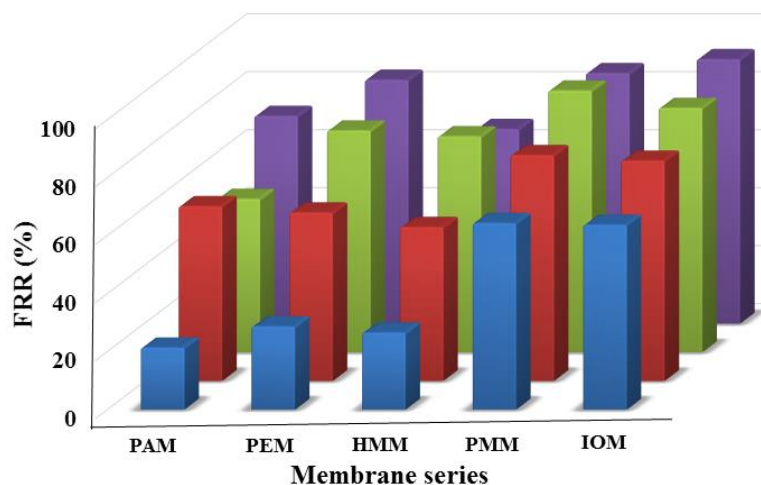


Fig.10.4 FRR values of prepared membranes

10.2 CONCLUSIONS

The major conclusions of the present work are listed below

- The addition of polycarboxylic acid i.e. citric acid alters the membrane morphology and considerably improve antifouling and humic rejection properties.
- The activated bentonite, HNTs and Fe_2O_3 nanoparticles can significantly improve the hydrophilicity, porosity, hydraulic permeation, antifouling and anti-biofouling properties
- There exists threshold content for the nanomaterials in the membranes beyond which the nanomaterials agglomerate in the membranes
- The change in spinning parameters during hollow fiber membrane fabrication brings about change in membrane morphology and performance.
- The well performed membranes in this research work can be used for the heavy metal ion removal and dye removal from aqueous solutions under suitable conditions

The nanocomposite flat sheet and hollow fiber membranes prepared in this work can be subjected to further studies of heavy metal ion removal and removal of other hazardous dyes.

Also the different nanomaterials and the nanocomposites prepared in this work can serve as a guiding path for preparing new membranes with novel applications.

REFERENCES

REFERENCES

Ahmad, A., Abdulkarim, A., Shafie, Z. M. and Ooi, B. (2017). "Fouling evaluation of PES/ZnO mixed matrix hollow fiber membrane." *Desalination*, 40(3),53-63.

Ahmad, A., Mohd-Setapar, S. H., Chuong, C. S., Khatoon, A., Wani, W. A., Kumar, R. and Rafatullah, M. (2015). "Recent advances in new generation dye removal technologies: novel search for approaches to reprocess wastewater." *RSC Advances*, 5(39), 30801-30818.

Ai, L., Li, M. and Li, L. (2011). "Adsorption of methylene blue from aqueous solution with activated carbon/cobalt ferrite/alginate composite beads: kinetics, isotherms, and thermodynamics." *J. Chem. Eng. Data*, 56(8), 3475-3483.

Ai, L., Zhang, C., Liao, F., Wang, Y., Li, M., Meng, L. and Jiang, J. (2011). "Removal of methylene blue from aqueous solution with magnetite loaded multi-wall carbon nanotube: kinetic, isotherm and mechanism analysis." *J. Hazard. Mater.*, 198(282-290).

Albrecht, W., Schauer, J., Weigel, T., Richau, K., Groth, T. and Lendlein, A. (2007). "Modification of poly (ether imide) membranes with brominated polyvinylpyrrolidone." *J. Membr. Sci*, 291(1), 10-18.

Albrecht, W., Seifert, B., Weigel, T., Schossig, M., Holländer, A., Groth, T. and Hilke, R. (2003). "Amination of Poly (ether imide) Membranes Using Di-and Multivalent Amines." *Macromol. Chem. Phys.*, 204(3), 510-521.

Alexandre, B., Langevin, D., Médéric, P., Aubry, T., Couderc, H., Nguyen, Q., Saiter, A. and Marais, S. (2009). "Water barrier properties of polyamide 12/montmorillonite nanocomposite membranes: structure and volume fraction effects." *J. Membr. Sci.*, 328(1), 186-204.

Al-Ghouti, M. A., Li, J., Salamh, Y., Al-Laqtah, N., Walker, G. and Ahmad, M. N. (2010). "Adsorption mechanisms of removing heavy metals and dyes from aqueous solution using date pits solid adsorbent." *J. Hazard. Mater.*, 176(1), 510-520.

Al-Rashdi, B., Johnson, D. and Hilal, N. (2013). "Removal of heavy metal ions by nanofiltration." *Desalination*, 31(5), 2-17.

- Al-Zoubi, H., Hilal, N., Darwish, N. and Mohammad, A. (2007). "Rejection and modelling of sulphate and potassium salts by nanofiltration membranes: neural network and Spiegler–Kedem model." *Desalination*, 206(1), 42-60.
- Anirudhan, T., Bringle, C. and Radhakrishnan, P. (2012). "Heavy metal interactions with phosphatic clay: Kinetic and equilibrium studies." *Chem. Eng. J. (Lausanne)*, 200(149-157).
- Arami, M., Limaee, N. Y. and Mahmoodi, N. M. (2006). "Investigation on the adsorption capability of egg shell membrane towards model textile dyes." *Chemosphere*, 65(11), 1999-2008.
- Azimi, A., Azari, A., Rezakazemi, M. and Ansarpour, M. (2016). "Removal of Heavy Metals from Industrial Wastewaters: A Review." *ChemBioEng Reviews*,
- Bai, H., Zhang, H., He, Y., Liu, J., Zhang, B. and Wang, J. (2014). "Enhanced proton conduction of chitosan membrane enabled by halloysite nanotubes bearing sulfonate polyelectrolyte brushes." *J. Membr. Sci.*, 454, 220-232.
- Baker, R. W. (2004). "Membrane technology and applications." *John Wiley & Sons Ltd*, England.
- Bakeri, G., Ismail, A. F., Shariaty-Niassar, M. and Matsuura, T. (2010). "Effect of polymer concentration on the structure and performance of polyetherimide hollow fiber membranes." *J. Membr. Sci.*, 363(1), 103-111.
- Bakeri, G., Ismail, A., Rahimnejad, M. and Matsuura, T. (2014). "Analysis of Polyetherimide/N-Methyl-2-Pyrrolidone/nonsolvent phase separation behavior." *J. Polym. Res*, 21(4), 1-7.
- Baral, S., Das, N., Chaudhury, G. R. and Das, S. (2009). "A preliminary study on the adsorptive removal of Cr (VI) using seaweed, *Hydrilla verticillata*." *J. Hazard. Mater.*, 171(1), 358-369.
- Barth, C., Goncalves, M., Pires, A., Roeder, J. and Wolf, B. (2000). "Asymmetric polysulfone and polyethersulfone membranes: effects of thermodynamic conditions during formation on their performance." *J. Membr. Sci.*, 169(2), 287-299.

- Bereket, G., Arog, A. Z. and Özel, M. Z. (1997). "Removal of Pb (II), Cd (II), Cu (II), and Zn (II) from aqueous solutions by adsorption on bentonite." *J. Colloid Interface Sci.*, 187(2), 338-343.
- Bhattacharyya, K. G., SenGupta, S. and Sarma, G. K. (2014). "Interactions of the dye, Rhodamine B with kaolinite and montmorillonite in water." *Appl. Clay Sci.*, 9(9),7-17.
- Bohnhoff, G. L. and Shackelford, C. D. (2013). "Improving membrane performance via bentonite polymer nanocomposite." *Appl. Clay Sci.*, 86(83-98).
- Bowen, W. R., Cheng, S. Y., Doneva, T. A. and Oatley, D. L. (2005). "Manufacture and characterisation of polyetherimide/sulfonated poly (ether ether ketone) blend membranes." *J. Membr. Sci.*, 250(1), 1-10.
- Bruni, L. and Bandini, S. (2008). "The role of the electrolyte on the mechanism of charge formation in polyamide nanofiltration membranes." *J. Membr. Sci.*, 308(1), 136-151.
- Cai, T., Li, X., Wan, C. and Chung, T.-S. (2016). "Zwitterionic polymers grafted poly (ether sulfone) hollow fiber membranes and their antifouling behaviors for osmotic power generation." *J. Membr. Sci.*, 49(7)142-152.
- Cai, T., Yang, W. J., Neoh, K.-G. and Kang, E.-T. (2012). "Poly (vinylidene fluoride) membranes with hyperbranched antifouling and antibacterial polymer brushes." *Ind. Eng. Chem. Res.*, 51(49), 15962-15973.
- Chao, C., Liu, J., Wang, J., Zhang, Y., Zhang, B., Zhang, Y., Xiang, X. and Chen, R. (2013). "Surface modification of halloysite nanotubes with dopamine for enzyme immobilization." *ACS Appl. Mater. Interfaces*, 5(21), 10559-10564.
- Chen, J., Li, J., Zhan, X., Han, X. and Chen, C. (2010). "Effect of PEG additives on properties and morphologies of polyetherimide membranes prepared by phase inversion." *Front. Chem. Eng. Chin.*, 4(3), 300-306.

- Chen, W., Su, Y., Peng, J., Zhao, X., Jiang, Z., Dong, Y., Zhang, Y., Liang, Y. and Liu, J. (2011). "Efficient wastewater treatment by membranes through constructing tunable antifouling membrane surfaces." *Environ. Sci. Technol.*, 45(15), 6545-6552.
- Chen, Z., Deng, M., Chen, Y., He, G., Wu, M. and Wang, J. (2004). "Preparation and performance of cellulose acetate/polyethyleneimine blend microfiltration membranes and their applications." *J. Membr. Sci.*, 235, 73-86.
- Cheng, C., Li, S., Zhao, W., Wei, Q., Nie, S., Sun, S. and Zhao, C. (2012). "The hydrodynamic permeability and surface property of polyethersulfone ultrafiltration membranes with mussel-inspired polydopamine coatings." *J. Membr. Sci.*, 41(7)228-236.
- Childress, A. E. and Elimelech, M. (2000). "Relating nanofiltration membrane performance to membrane charge (electrokinetic) characteristics." *Environ. Sci. Technol.*, 34(17), 3710-3716.
- Chinpa, W., Quémener, D., Bèche, E., Jiraratananon, R. and Deratani, A. (2010). "Preparation of poly (etherimide) based ultrafiltration membrane with low fouling property by surface modification with poly (ethylene glycol)." *J. Membr. Sci.*, 365(1), 89-97.
- Choudalakis, G. and Gotsis, A. (2009). "Permeability of polymer/clay nanocomposites: a review." *Eur. Polym. J.*, 45(4), 967-984.
- Chuang, W.-Y., Young, T.-H. and Chiu, W.-Y. (2000). "The effect of acetic acid on the structure and filtration properties of poly (vinyl alcohol) membranes." *J. Membr. Sci.*, 172(1), 241-251.
- Chung, K.-T. (2016). "Azo dyes and human health: A review." *J. Environ. Sci. Health., Part C*, 34(4), 233-261.
- Daraei, P., Madaeni, S. S., Ghaemi, N., Salehi, E., Khadivi, M. A., Moradian, R. and Astinchap, B. (2012). "Novel polyethersulfone nanocomposite membrane prepared by PANI/Fe₃O₄ nanoparticles with enhanced performance for Cu (II) removal from water." *J. Membr. Sci.*, 41(5), 250-259.

- De Sitter, K., Dotremont, C., Genné, I. and Stoops, L. (2014). "The use of nanoparticles as alternative pore former for the production of more sustainable polyethersulfone ultrafiltration membranes." *J. Membr. Sci.*, 47(1),168-178.
- Dehghani, M. H., Zarei, A., Mesdaghinia, A., Nabizadeh, R., Alimohammadi, M. and Afsharnia, M. (2017). "Response surface modeling, isotherm, thermodynamic and optimization study of arsenic (V) removal from aqueous solutions using modified bentonite-chitosan (MBC)." *Korean J. Chem. Eng.*, 34(3), 757-767.
- Didi, M., Makhoukhi, B., Azzouz, A. and Villemin, D. (2009). "Colza oil bleaching through optimized acid activation of bentonite. A comparative study." *Appl. Clay Sci.*, 42(3), 336-344.
- Duan, J., Liu, R., Chen, T., Zhang, B. and Liu, J. (2012). "Halloysite nanotube-Fe₃O₄ composite for removal of methyl violet from aqueous solutions." *Desalination*, 29(3),46-52.
- Eren, E., Afsin, B. and Onal, Y. (2009). "Removal of lead ions by acid activated and manganese oxide-coated bentonite." *J. Hazard. Mater.*, 161(2), 677-685.
- Fan, L., Harris, J. L., Roddick, F. A. and Booker, N. A. (2001). "Influence of the characteristics of natural organic matter on the fouling of microfiltration membranes." *Water Res.*, 35(18), 4455-4463.
- Fu, F. and Wang, Q. (2011). "Removal of heavy metal ions from wastewaters: a review." *J. Environ. Manage.*, 92(3), 407-418.
- Ganesh, B. M., Isloor, A. M. and Ismail, A. F. (2013). "Enhanced hydrophilicity and salt rejection study of graphene oxide-polysulfone mixed matrix membrane." *Desalination*, 313, 199-207.
- Gao, C.-Y., Li, A., Feng, L.-X., Yi, X.-S. and Shen, J.-C. (2000). "Factors controlling surface morphology of porous polystyrene membranes prepared by thermally induced phase separation." *Polym. Int.*, 49, 323-328.

Geise, G. M., Lee, H. S., Miller, D. J., Freeman, B. D., McGrath, J. E. and Paul, D. R. (2010). "Water purification by membranes: the role of polymer science." *J. Polym. Sci., Part B: Polym. Phys.*, 48(15), 1685-1718.

Ghaemi, N., Madaeni, S. S., Alizadeh, A., Daraei, P., Badieh, M. M. S., Falsafi, M. and Vatanpour, V. (2012). "Fabrication and modification of polysulfone nanofiltration membrane using organic acids: Morphology, characterization and performance in removal of xenobiotics." *Sep. Purif. Technol.*, 96, 214-228.

Govardhan, B., Chandrasekhar, S. and Sridhar, S. (2017). "Purification of surface water using novel hollow fiber membranes prepared from polyetherimide/polyethersulfone blends." *Journal of Environmental Chemical Engineering*, 5(1), 1068-1078.

Guillen, G. R., Farrell, T. P., Kaner, R. B. and Hoek, E. M. (2010). "Pore-structure, hydrophilicity, and particle filtration characteristics of polyaniline-polysulfone ultrafiltration membranes." *J. Mater. Chem.*, 20 (22), 4621-4628.

Guillen, G. R., Pan, Y., Li, M. and Hoek, E. M. (2011). "Preparation and characterization of membranes formed by nonsolvent induced phase separation: a review." *Ind. Eng. Chem. Res.*, 50(7), 3798-3817.

Guo, W., Sun, N., Du, Y., Wang, L. and Pei, M. (2017). "Preparation of polyamine grafted bentonite by surface-initiated atom transfer radical polymerization for efficient adsorption of Orange I from aqueous solution." *New J. Chem.*, 41(9), 3352-3357.

Hadjesfandiari, N., Yu, K., Mei, Y. and Kizhakkedathu, J. N. (2014). "Polymer brush-based approaches for the development of infection-resistant surfaces." *J. Mater. Chem. B*, 2(31), 4968-4978.

Hamid, N., Ismail, A. F., Matsuura, T., Zularisam, A., Lau, W., Yuliwati, E. and Abdullah, M. (2011). "Morphological and separation performance study of polysulfone/titanium dioxide (PSF/TiO₂) ultrafiltration membranes for humic acid removal." *Desalination*, 273(1), 85-92.

- Haque, E., Jun, J. W. and Jhung, S. H. (2011). "Adsorptive removal of methyl orange and methylene blue from aqueous solution with a metal-organic framework material, iron terephthalate (MOF-235)." *J. Hazard. Mater.*, 185(1), 507-511.
- Harsha, N., Kalyani, S., Rao, V. B. and Sridhar, S. (2015). "Synthesis and Characterization of Polyion Complex Membranes Made of Aminated Polyetherimide and Sulfonated Polyethersulfone for Fuel Cell Applications." *J. Fuel Cell Sci. Technol.*, 12(6), 061004.
- He, Y., Li, G., Wang, H., Zhao, J., Su, H. and Huang, Q. (2008). "Effect of operating conditions on separation performance of reactive dye solution with membrane process." *J. Membr. Sci.*, 321(2), 183-189.
- Hebbar, R. S., Isloor, A. M. and Ismail, A. (2014). "Preparation and evaluation of heavy metal rejection properties of polyetherimide/porous activated bentonite clay nanocomposite membrane." *RSC Advances*, 4(88), 47240-47248.
- Hebbar, R. S., Isloor, A. M. and Ismail, A. (2014). "Preparation and evaluation of heavy metal rejection properties of polyetherimide/porous activated bentonite clay nanocomposite membrane." *RSC Advances*, 4(88), 47240-47248.
- Hegde, C., Isloor, A. M., Padaki, M. and Fun, H.-K. (2013). "Synthesis and performance characterization of PS-PPEES nanoporous membranes with nonwoven porous support." *Arabian Journal of Chemistry*, 6(3), 319-326.
- Heydari, A., Khoshnood, H., Sheibani, H. and Doostan, F. (2016). "Polymerization of β -cyclodextrin in the presence of bentonite clay to produce polymer nanocomposites for removal of heavy metals from drinking water." *Polym. Adv. Technol.*,
- Hilal, N., Al-Zoubi, H., Darwish, N., Mohamma, A. and Arabi, M. A. (2004). "A comprehensive review of nanofiltration membranes: treatment, pretreatment, modelling, and atomic force microscopy." *Desalination*, 170(3), 281-308.
- Hołda, A. K., De Roeck, M., Hendrix, K. and Vankelecom, I. F. J. (2013). "The influence of polymer purity and molecular weight on the synthesis of integrally skinned polysulfone membranes." *J. Membr. Sci.*, 446, 113-120.

Huisman, I. H., Prádanos, P. and Hernández, A. (2000). "The effect of protein–protein and protein–membrane interactions on membrane fouling in ultrafiltration." *J. Membr. Sci.*, 179(1), 79-90.

Hwang, J. R., Koo, S.-H., Kim, J.-H., Higuchi, A. and Tak, T.-M. (1996). "Effects of casting solution composition on performance of poly(ether sulfone) membrane." *J. Appl. Polym. Sci.*, 60, 1343-1348.

Hwang, L.-L., Tseng, H.-H. and Chen, J.-C. (2011). "Fabrication of polyphenylsulfone/polyetherimide blend membranes for ultrafiltration applications: The effects of blending ratio on membrane properties and humic acid removal performance." *J. Membr. Sci.*, 384(1), 72-81.

Jansen, J. C., Macchione, M. and Drioli, E. (2005). "High flux asymmetric gas separation membranes of modified poly(ether ether ketone) prepared by the dry phase inversion technique." *J. Membr. Sci.*, 255, 167-180.

Jiang, J., Zhu, L., Zhu, L., Zhang, H., Zhu, B. and Xu, Y. (2013). "Antifouling and Antimicrobial Polymer Membranes Based on Bioinspired Polydopamine and Strong Hydrogen-Bonded Poly (N-vinyl pyrrolidone)." *ACS Appl. Mater. Interfaces*, 5(24), 12895-12904.

Jin, X., Zheng, M., Sarkar, B., Naidu, R. and Chen, Z. (2016). "Characterization of bentonite modified with humic acid for the removal of Cu (II) and 2, 4-dichlorophenol from aqueous solution." *Appl. Clay Sci.*, 134(89-94).

Jose, T., George, S. C., Maria, H. J., Wilson, R. and Thomas, S. (2014). "Effect of bentonite clay on the mechanical, thermal, and pervaporation performance of the poly (vinyl alcohol) nanocomposite membranes." *Ind. Eng. Chem. Res.*, 53(43), 16820-16831.

Jung, B. (2004). "Preparation of hydrophilic polyacrylonitrile blend membranes for ultrafiltration." *J. Membr. Sci.*, 229, 129-136.

- Kajekar, A. J., Dodamani, B., Isloor, A. M., Karim, Z. A., Cheer, N. B., Ismail, A. and Shilton, S. J. (2015). "Preparation and characterization of novel PSf/PVP/PANI-nanofiber nanocomposite hollow fiber ultrafiltration membranes and their possible applications for hazardous dye rejection." *Desalination*, 365(117-125).
- Kanagaraj, P., Nagendran, A., Rana, D., Matsuura, T., Neelakandan, S. and Malarvizhi, K. (2015). "Effects of polyvinylpyrrolidone on the permeation and fouling-resistance properties of polyetherimide ultrafiltration membranes." *Ind. Eng. Chem. Res.*, 54(17), 4832-4838.
- Kanagaraj, P., Nagendran, A., Rana, D., Matsuura, T., Neelakandan, S., Karthikkumar, T. and Muthumeenal, A. (2015). "Influence of N-phthaloyl chitosan on poly (ether imide) ultrafiltration membranes and its application in biomolecules and toxic heavy metal ion separation and their antifouling properties." *Appl. Surf. Sci.*, 329, 165-173.
- Kar, P., Behera, A. K., Adhikari, B. and Pradhan, N. C. (2010). "Optimization for the chemical synthesis of conducting poly (m-aminophenol) in HCl using ammonium persulfate." *High Perform. Polym.*, 22(4), 428-441.
- Kar, P., Pradhan, N. C. and Adhikari, B. (2011). "Doping of processable conducting poly (m-aminophenol) with silver nanoparticles." *Polym. Adv. Technol.*, 22(6), 1060-1066.
- Karim, Z., Mathew, A. P., Grahn, M., Mouzon, J. and Oksman, K. (2014). "Nanoporous membranes with cellulose nanocrystals as functional entity in chitosan: removal of dyes from water." *Carbohydr. Polym.*, 112(668-676).
- Katsikogianni, M. and Missirlis, Y. (2004). "Concise review of mechanisms of bacterial adhesion to biomaterials and of techniques used in estimating bacteria-material interactions." *Eur Cell Mater*, 8,37-57.
- Khin, M. M., Nair, A. S., Babu, V. J., Murugan, R. and Ramakrishna, S. (2012). "A review on nanomaterials for environmental remediation." *Energy & Environmental Science*, 5(8), 8075-8109.

Khulbe, K. C. and Matsuura, T. (2016). "Recent progress in polymeric hollow-fibre membrane preparation and applications." *Membrane Technology*, 2016(7), 7-13.

Khulbe, K. C. and Matsuura, T. (2016). "Recent progress in polymeric hollow-fibre membrane preparation and applications." *Membrane Technology*, 2016(7), 7-13.

Kim, I. C. and Lee, K. H. (2003). "Effect of various additives on pore size of polysulfone membrane by phase-inversion process." *J. Appl. Polym. Sci.*, 89(9), 2562-2566.

Kim, I. C., Yoon, H. G. and Lee, K. H. (2002). "Formation of integrally skinned asymmetric polyetherimide nanofiltration membranes by phase inversion process." *J. Appl. Polym. Sci.*, 84(6), 1300-1307.

Kim, S.-G. and Lee, K.-H. (2009). "Effects of chemical transition of polyetherimide membranes having an integrally skinned asymmetric structure." *Curr. Appl Phys*, 9(2), 51-55.

Kiran, S. A., Arthanareeswaran, G., Thuyavan, Y. L. and Ismail, A. (2015). "Influence of bentonite in polymer membranes for effective treatment of car wash effluent to protect the ecosystem." *Ecotoxicol. Environ. Saf.*, 12(1),186-192.

Koutahzadeh, N., Esfahani, M. R., Stretz, H. A. and Arce, P. E. (2016). "Investigation of UV/H₂O₂ pretreatment effects on humic acid fouling on polysulfone/titanium dioxide—And polysulfone/multiwall carbon nanotube—Nanocomposite ultrafiltration membranes." *Environ. Prog. Sustainable Energy*,

Kumar, R., Isloor, A. M., Ismail, A. F. and Matsuura, T. (2013). "Performance improvement of polysulfone ultrafiltration membrane using N-succinyl chitosan as additive." *Desalination*, 318, 1-8.

Kumar, R., Isloor, A. M., Ismail, A. F., Rashid, S. A. and Matsuura, T. (2013). "Polysulfone–Chitosan blend ultrafiltration membranes: preparation, characterization, permeation and antifouling properties." *RSC Advances*, 3(21), 7855-7861.

- Kumar, R., Ismail, A. F., Kassim, M. A. and Isloor, A. M. (2013). "Modification of PSf/PIAM membrane for improved desalination applications using Chitosan coagulation media." *Desalination*, 31(7), 108-115.
- Kumar, S., Mandal, A. and Guria, C. (2016). "Synthesis, characterization and performance studies of polysulfone and polysulfone/polymer-grafted bentonite based ultrafiltration membranes for the efficient separation of oil field oily wastewater." *Process Saf. Environ. Prot.*, 10(2), 214-228.
- Lee, E. K., Chen, V. and Fane, A. (2008). "Natural organic matter (NOM) fouling in low pressure membrane filtration—effect of membranes and operation modes." *Desalination*, 218(1), 257-270.
- Lee, H., Dellatore, S. M., Miller, W. M. and Messersmith, P. B. (2007). "Mussel-inspired surface chemistry for multifunctional coatings." *science*, 318(5849), 426-430.
- Lee, S. M. and Tiwari, D. (2012). "Organo and inorgano-organo-modified clays in the remediation of aqueous solutions: an overview." *Appl. Clay Sci.*, 5(9), 84-102.
- Li, J. B., Zhu, J. W. and Zheng, M. S. (2007). "Morphologies and properties of poly (phthalazinone ether sulfone ketone) matrix ultrafiltration membranes with entrapped TiO₂ nanoparticles." *J. Appl. Polym. Sci.*, 103(6), 3623-3629.
- Li, J.-H., Xu, Y.-Y., Zhu, L.-P., Wang, J.-H. and Du, C.-H. (2009). "Fabrication and characterization of a novel TiO₂ nanoparticle self-assembly membrane with improved fouling resistance." *J. Membr. Sci.*, 326(2), 659-666.
- Li, N., Xiao, C., An, S. and Hu, X. (2010). "Preparation and properties of PVDF/PVA hollow fiber membranes." *Desalination*, 250, 530-537.
- Liao, Y., Farrell, T. P., Guillen, G. R., Li, M., Temple, J. A., Li, X.-G., Hoek, E. M. and Kaner, R. B. (2014). "Highly dispersible polypyrrole nanospheres for advanced nanocomposite ultrafiltration membranes." *Materials Horizons*, 1(1), 58-64.

- Lin, J., Ye, W., Baltaru, M.-C., Tang, Y. P., Bernstein, N. J., Gao, P., Balta, S., Vlad, M., Volodin, A. and Sotto, A. (2016). "Tight ultrafiltration membranes for enhanced separation of dyes and Na₂SO₄ during textile wastewater treatment." *J. Membr. Sci.*, 51(4), 217-228.
- Liu, L., Wan, Y., Xie, Y., Zhai, R., Zhang, B. and Liu, J. (2012). "The removal of dye from aqueous solution using alginate-halloysite nanotube beads." *Chem. Eng. J.*, 18(7), 210-216.
- Liu, R., Zhang, B., Mei, D., Zhang, H. and Liu, J. (2011). "Adsorption of methyl violet from aqueous solution by halloysite nanotubes." *Desalination*, 268(1), 111-116.
- Liu, S., Wang, L., Ding, Y., Liu, B., Han, X. and Song, Y. (2014). "Novel sulfonated poly (ether ether ketone)/polyetherimide acid-base blend membranes for vanadium redox flow battery applications." *Electrochim. Acta*, 130(90-96).
- Liu, T.-Y., Bian, L.-X., Yuan, H.-G., Pang, B., Lin, Y.-K., Tong, Y., Van der Bruggen, B. and Wang, X.-L. (2015). "Fabrication of a high-flux thin film composite hollow fiber nanofiltration membrane for wastewater treatment." *J. Membr. Sci.*, 478(25-36).
- Liu, X., He, S., Song, G., Jia, H., Shi, Z., Liu, S., Zhang, L., Lin, J. and Nazarenko, S. (2016). "Proton conductivity improvement of sulfonated poly (ether ether ketone) nanocomposite membranes with sulfonated halloysite nanotubes prepared via dopamine-initiated atom transfer radical polymerization." *J. Membr. Sci.*, 504(206-219).
- Liu, Y., Jiang, X., Li, B., Zhang, X., Liu, T., Yan, X., Ding, J., Cai, Q. and Zhang, J. (2014). "Halloysite nanotubes@ reduced graphene oxide composite for removal of dyes from water and as supercapacitors." *J. Mater. Chem A*, 2(12), 4264-4269.
- Lonsdale, H. (1982). "The growth of membrane technology." *J. Membr. Sci.*, 10(2), 81-181.
- Lopes, T. D., Riegel-Vidotti, I. C., Grein, A., Tischer, C. A. and de Sousa Faria-Tischer, P. C. (2014). "Bacterial cellulose and hyaluronic acid hybrid membranes: production and characterization." *Int. J. Biol. Macromol.*, 67(401-408).

- Luo, P., Zhang, J.-s., Zhang, B., Wang, J.-h., Zhao, Y.-f. and Liu, J.-d. (2011). "Preparation and characterization of silane coupling agent modified halloysite for Cr (VI) removal." *Ind. Eng. Chem. Res.*, 50(17), 10246-10252.
- Lv, Y., Yang, H.-C., Liang, H.-Q., Wan, L.-S. and Xu, Z.-K. (2015). "Nanofiltration membranes via co-deposition of polydopamine/polyethylenimine followed by cross-linking." *J. Membr. Sci.*, 476(50-58).
- Ma, Y., Shi, F., Wang, Z., Wu, M., Ma, J. and Gao, C. (2012). "Preparation and characterization of PSf/clay nanocomposite membranes with PEG 400 as a pore forming additive." *Desalination*, 28(6), 131-137.
- Mallick, K., Witcomb, M., Dinsmore, A. and Scurrrell, M. (2006). "Preparation of highly dispersed Pd-nanoparticles in poly-(o-aminophenol) needles: An 'intimate composite material'." *J. Mater. Sci.*, 41(6), 1733-1737.
- Manohar, D., Noeline, B. and Anirudhan, T. (2006). "Adsorption performance of Al-pillared bentonite clay for the removal of cobalt (II) from aqueous phase." *Appl. Clay Sci.*, 31(3), 194-206.
- Mansourizadeh, A., Jazebizadeh, M., Vaseghi, M. and Aghili, A. (2016). "A comparative study on the structure of developed porous PVDF and PEI hollow fiber membrane contactors for CO₂ absorption." *J. Polym. Res.*, 23(1), 1-10.
- Maurya, S., Parashuram, K., Singh, P., Ray, P. and Reddy, A. (2012). "Preparation of polysulfone–polyamide thin film composite hollow fiber nanofiltration membranes and their performance in the treatment of aqueous dye solutions." *Desalination*, 30(4), 11-19.
- McKelvey, S. A. and Koros, W. J. (1996). "Phase separation, vitrification, and the manifestation of macrovoids in polymeric asymmetric membranes." *J. Membr. Sci.*, 112(1), 29-39.
- Messersmith, P. B, Lee, H., Dellatore, S. M., and Miller, W. M. (2007). "Mussel-inspired surface chemistry for multifunctional coatings." *science*, 318(5849), 426-430.

Miller, D. J., Araujo, P. A., Correia, P. B., Ramsey, M. M., Kruithof, J. C., van Loosdrecht, M., Freeman, B. D., Paul, D. R., Whiteley, M. and Vrouwenvelder, J. S. (2012). "Short-term adhesion and long-term biofouling testing of polydopamine and poly (ethylene glycol) surface modifications of membranes and feed spacers for biofouling control." *Water Res.*, 46(12), 3737-3753.

Mittal, H. and Mishra, S. B. (2014). "Gum ghatti and Fe₃O₄ magnetic nanoparticles based nanocomposites for the effective adsorption of rhodamine B." *Carbohydr. Polym.*, 101(1255-1264).

Monticelli, O., Bottino, A., Scandale, I., Capannelli, G. and Russo, S. (2007). "Preparation and properties of polysulfone–clay composite membranes." *J. Appl. Polym. Sci.*, 103(6), 3637-3644.

Mukherjee, R., Bhunia, P. and De, S. (2016). "Impact of graphene oxide on removal of heavy metals using mixed matrix membrane." *Chem. Eng. J.*, 292(284-297).

Mulder, M. (1996). "Membrane Processes." Basic Principles of Membrane Technology Second Edition *Kluwer Academic Publishers, Netherlands*, 280-412.

Nagendran, A., Vijayalakshmi, A., Arockiasamy, D. L., Shobana, K. and Mohan, D. (2008). "Toxic metal ion separation by cellulose acetate/sulfonated poly (ether imide) blend membranes: effect of polymer composition and additive." *J. Hazard. Mater*, 155(3), 477-485.

Natarajan, T. S., Bajaj, H. C. and Tayade, R. J. (2014). "Preferential adsorption behavior of methylene blue dye onto surface hydroxyl group enriched TiO₂ nanotube and its photocatalytic regeneration." *J. Colloid Interface Sci.*, 433(104-114).

Neelgund, G. M., Hrehorova, E., Joyce, M. and Bliznyuk, V. (2008). "Synthesis and characterization of polyaniline derivative and silver nanoparticle composites." *Polym. Int.*, 57(10), 1083-1089.

- Ngulube, T., Gumbo, J. R., Masindi, V. and Maity, A. (2017). "An update on synthetic dyes adsorption onto clay based minerals: A state-of-art review." *Journal of Environmental Management*, 191(35-57).
- Nguyen, T. A. and Juang, R.-S. (2013). "Treatment of waters and wastewaters containing sulfur dyes: A review." *Chem. Eng. J.*, 219(109-117).
- Önal, M. and Sarıkaya, Y. (2007). "Preparation and characterization of acid-activated bentonite powders." *Powder Technol.*, 172(1), 14-18.
- Ong, Y. K., Li, F. Y., Sun, S.-P., Zhao, B.-W., Liang, C.-Z. and Chung, T.-S. (2014). "Nanofiltration hollow fiber membranes for textile wastewater treatment: Lab-scale and pilot-scale studies." *Chem. Eng. Sci.*, 114(51-57).
- Padaki, M., Isloor, A. M., Belavadi, G. and Prabhu, K. N. (2011). "Preparation, characterization and performance study of poly (isobutylene-alt-maleic anhydride)[PIAM] and polysulfone [PSf] composite membranes before and after alkali treatment." *Ind. Eng. Chem. Res.*, 50(11), 6528-6534.
- Park, H. G., Kim, T. W., Chae, M. Y. and Yoo, I.-K. (2007). "Activated carbon-containing alginate adsorbent for the simultaneous removal of heavy metals and toxic organics." *Process Biochem. (Amsterdam, Neth.)*, 42(10), 1371-1377.
- Park, N., Kwon, B., Kim, I. S. and Cho, J. (2005). "Biofouling potential of various NF membranes with respect to bacteria and their soluble microbial products (SMP): characterizations, flux decline, and transport parameters." *J. Membr. Sci.*, 258(1), 43-54.
- Pereira, V. R., Isloor, A. M., Al Ahmed, A. and Ismail, A. (2015). "Preparation, characterization and the effect of PANI coated TiO₂ nanocomposites on the performance of polysulfone ultrafiltration membranes." *New J. Chem.*,
- Pereira, V. R., Isloor, A. M., Al Ahmed, A. and Ismail, A. (2015). "Preparation, characterization and the effect of PANI coated TiO₂ nanocomposites on the performance of polysulfone ultrafiltration membranes." *New J. Chem.*, 39(1), 703-712.

- Pereira, V. R., Isloor, A. M., Zulhairun, A., Subramaniam, M., Lau, W. and Ismail, A. (2016). "Preparation of polysulfone-based PANI–TiO₂ nanocomposite hollow fiber membranes for industrial dye rejection applications." *RSC Advances*, 6(102), 99764-99773.
- Peterson, R., Greenberg, A., Bond, L. and Krantz, W. (1998). "Use of ultrasonic TDR for real-time noninvasive measurement of compressive strain during membrane compaction." *Desalination*, 116(2), 115-122.
- Pradas, E. G., Sánchez, M. V., Cruz, F. C., Viciano, M. S. and Pérez, M. F. (1994). "Adsorption of cadmium and zinc from aqueous solution on natural and activated bentonite." *J. Chem. Technol. Biotechnol.*, 59(3), 289-295.
- Rahimpour, A., Madaeni, S. S. and Mansourpanah, Y. (2010). "Nano-porous polyethersulfone (PES) membranes modified by acrylic acid (AA) and 2-hydroxyethylmethacrylate (HEMA) as additives in the gelation media." *J. Membr. Sci.*, 364(1), 380-388.
- Rajesh, S., Jayalakshmi, A., Senthilkumar, S., Sankar, H. S. H. and Mohan, D. R. (2011). "Performance Evaluation of Poly(amide-imide) Incorporated Cellulose Acetate Ultrafiltration Membranes in the Separation of Proteins and Its Fouling Propensity by AFM Imaging." *Ind. Eng. Chem. Res.*, 50(24), 14016-14029.
- Rajesh, S., Shobana, K. H., Anitharaj, S. and Mohan, D. R. (2011). "Preparation, morphology, performance, and hydrophilicity studies of poly (amide-imide) incorporated cellulose acetate ultrafiltration membranes." *Ind. Eng. Chem. Res.*, 50(9), 5550-5564.
- Rana, D. and Matsuura, T. (2010). "Surface modifications for antifouling membranes." *Chem. Rev. (Washington, DC, U. S.)*, 110(4), 2448-2471.
- Rana, D. and Matsuura, T. (2010). "Surface modifications for antifouling membranes." *Chem. Rev.* 110, 2448-2471.
- Ren, J., Zhou, J. and Deng, M. (2010). "Morphology transition of asymmetric polyetherimide flat sheet membranes with different thickness by wet phase-inversion process." *Sep. Purif. Technol.*, 74(1), 119-129.

Ross, C. S. and Shannon, E. V. (1926). "the minerals of bentonite and related clays and their physical properties1." *J. Am. Ceram. Soc.*, 9(2), 77-96

Sen Gupta, S. and Bhattacharyya, K. G. (2008). "Immobilization of Pb (II), Cd (II) and Ni (II) ions on kaolinite and montmorillonite surfaces from aqueous medium." *Journal of environmental management*, 87(1), 46-58.

Senthilkumar, S., Rajesh, S., Jayalakshmi, A. and Mohan, D. (2013). "Biocompatibility and separation performance of carboxylated poly (ether–imide) incorporated polyacrylonitrile membranes." *Sep. Purif. Technol.*, 107(2) 97-309.

Senthilkumar, S., Rajesh, S., Jayalakshmi, A. and Mohan, D. (2013). "Biocompatibility and separation performance of carboxylated poly (ether–imide) incorporated polyacrylonitrile membranes." *Sep. Purif. Technol.*, 107(2) 97-309.

Shahamati Fard, F., Akbari, S., Pajootan, E. and Arami, M. (2016). "Enhanced acidic dye adsorption onto the dendrimer-based modified halloysite nanotubes." *Desalin. Water Treat.*, 1-18.

Shannon, M. A., Bohn, P. W., Elimelech, M., Georgiadis, J. G., Marinas, B. J. and Mayes, A. M. (2008). "Science and technology for water purification in the coming decades." *Nature*, 452, 301-310.

Shao, J., Hou, J. and Song, H. (2011). "Comparison of humic acid rejection and flux decline during filtration with negatively charged and uncharged ultrafiltration membranes." *Water Res.*, 45(2), 473-482.

Sharma, N. and Purkait, M. (2016). "Enantiomeric and racemic effect of tartaric acid on polysulfone membrane during crystal violet dye removal by MEUF process." *J. Water Process Eng.*, 10(104-112).

Shawky, H. A., Chae, S.-R., Lin, S. and Wiesner, M. R. (2011). "Synthesis and characterization of a carbon nanotube/polymer nanocomposite membrane for water treatment." *Desalination*, 272(1), 46-50.

Shen, L. Q., Xu, Z. K., Yang, Q., Sun, H. L., Wang, S. Y. and Xu, Y. Y. (2004). "Preparation and characterization of sulfonated polyetherimide/polyetherimide blend membranes." *J. Appl. Polym. Sci.*, 92(3), 1709-1715.

Shen, L.-Q., Xu, Z.-K., Liu, Z.-M. and Xu, Y.-Y. (2003). "Ultrafiltration hollow fiber membranes of sulfonated polyetherimide/polyetherimide blends: preparation, morphologies and anti-fouling properties." *J. Membr. Sci.*, 218(1), 279-293.

Shenvi, S. S., Isloor, A. M., Ismail, A. F., Shilton, S. J. and Al Ahmed, A. (2015). "Humic acid based biopolymeric membrane for effective removal of methylene blue and rhodamine B." *Ind. Eng. Chem. Res.*, 54(18), 4965-4975.

Shenvi, S., Ismail, A. and Isloor, A. M. (2014). "Enhanced Permeation Performance of Cellulose Acetate Ultrafiltration Membranes by Incorporation of Sulfonated Poly (1, 4-phenylene ether ether sulfone) and Poly (styrene-co-maleic anhydride)." *Ind. Eng. Chem. Res.*, 53(35), 13820-13827.

Shu, Y. C., Chuang, F. S., Tsen, W. C., Chow, J. D., Gong, C. and Wen, S. (2008). "Sulfonated poly (ether imide) and poly (ether sulfone) blends for direct methanol fuel cells. I. Sulfonation of PEI and characterization of the products." *J. Appl. Polym. Sci.*, 107(5), 2963-2969.

Shu, Y. C., Chuang, F. S., Tsen, W. C., Chow, J. D., Gong, C. and Wen, S. (2008). "Sulfonated poly (ether imide) and poly (ether sulfone) blends for direct methanol fuel cells. I. Sulfonation of PEI and characterization of the products." *J. Appl. Polym. Sci.*, 107(5), 2963-2969.

Shu, Z., Chen, Y., Zhou, J., Li, T., Sheng, Z., Tao, C. and Wang, Y. (2016). "Preparation of halloysite-derived mesoporous silica nanotube with enlarged specific surface area for enhanced dye adsorption." *Appl. Clay Sci.*,

Singh, R. (2006). "Hybrid Membrane Systems for Water Purification: Technology, Systems Design and Operations." Elsevier Science & Technology Books.

- Sultan, A. S., Al-Ahmed, A. and Javaid Zaidi, S. (2011). "Reduced viscosity, rheology and morphological properties of sulfonated poly (ether ether ketone): Polyetherimide blends." *Eur. Polym. J.*, 47(12), 2295-2302.
- Sumisha, A., Arthanareeswaran, G., Ismail, A. F., Kumar, D. P. and Shankar, M. V. (2015). "Functionalized titanate nanotube–polyetherimide nanocomposite membrane for improved salt rejection under low pressure nanofiltration." *RSC Advances*, 5(49), 39464-39473.
- Sun, H., Liu, S., Ge, B., Xing, L. and Chen, H. (2007). "Cellulose nitrate membrane formation via phase separation induced by penetration of nonsolvent from vapor phase." *J. Membr. Sci.*, 295, 2-10.
- Sun, M., Su, Y., Mu, C. and Jiang, Z. (2009). "Improved antifouling property of PES ultrafiltration membranes using additive of silica–PVP nanocomposite." *Ind. Eng. Chem. Res.*, 49(2), 790-796.
- Swier, S., Shaw, M. T. and Weiss, R. (2006). "Morphology control of sulfonated poly (ether ketone ketone) poly (ether imide) blends and their use in proton-exchange membranes." *J. Membr. Sci.*, 270(1), 22-31.
- Tang, Y. P., Cai, T., Loh, D., O'Brien, G. S. and Chung, T. S. (2017). "Construction of antifouling lumen surface on a poly (vinylidene fluoride) hollow fiber membrane via a zwitterionic graft copolymerization strategy." *Sep. Purif. Technol.*, 17(6), 294-305.
- Tansel, B., Sager, J., Rector, T., Garland, J., Strayer, R. F., Levine, L., Roberts, M., Hummerick, M. and Bauer, J. (2006). "Significance of hydrated radius and hydration shells on ionic permeability during nanofiltration in dead end and cross flow modes." *Sep. Purif. Technol.*, 51(1), 40-47.
- Teli, S. B., Molina, S., Sotto, A., Calvo, E. G. a. and Abajob, J. d. (2013). "Fouling resistant polysulfone–PANI/TiO₂ ultrafiltration nanocomposite membranes." *Ind. Eng. Chem. Res.*, 52(27), 9470-9479.

Tripathi, B. P., Dubey, N. C., Subair, R., Choudhury, S. and Stamm, M. (2016). "Enhanced hydrophilic and antifouling polyacrylonitrile membrane with polydopamine modified silica nanoparticles." *RSC Advances*, 6(6), 4448-4457.

Ulbricht, M. (2006). "Advanced functional polymer membranes." *Polymer*, 47, 2217-2262.

Unuabonah, E. I. and Taubert, A. (2014). "Clay-polymer nanocomposites (CPNs): Adsorbents of the future for water treatment." *Appl. Clay Sci.*, 99(83-92).

Vadivelan, V. and Kumar, K. V. (2005). "Equilibrium, kinetics, mechanism, and process design for the sorption of methylene blue onto rice husk." *J. Colloid Interface Sci.*, 286(1), 90-100.

Vatanpour, V., Madaeni, S. S., Moradian, R., Zinadini, S. and Astinchap, B. (2011). "Fabrication and characterization of novel antifouling nanofiltration membrane prepared from oxidized multiwalled carbon nanotube/polyethersulfone nanocomposite." *J. Membr. Sci.*, 375(1), 284-294.

Waheed, S., Ahmad, A., Khan, S. M., Gul, S.-E., Jamil, T., Islam, A. and Hussain, T. (2014). "Synthesis, characterization, permeation and antibacterial properties of cellulose acetate/polyethylene glycol membranes modified with chitosan." *Desalination*, 351, 59-69.

Wandera, D., Wickramasinghe, S. R. and Husson, S. M. (2011). "Modification and characterization of ultrafiltration membranes for treatment of produced water." *J. Membr. Sci.*, 373(1), 178-188.

Wang, D. K., Elma, M., Motuzas, J., Hou, W.-C., Xie, F. and Zhang, X. (2017). "Rational design and synthesis of molecular-sieving, photocatalytic, hollow fiber membranes for advanced water treatment applications." *J. Membr. Sci.*, 524(163-173).

Wang, D., Li, K. and Teo, W. (1999). "Phase separation in polyetherimide/solvent/nonsolvent systems and membrane formation." *J. Appl. Polym. Sci.*, 71(11), 1789-1796.

- Wang, D.-X., Su, M., Yu, Z.-Y., Wang, X.-L., Ando, M. and Shintani, T. (2005). "Separation performance of a nanofiltration membrane influenced by species and concentration of ions." *Desalination*, 175(2), 219-225.
- Wang, J., Lang, W.-Z., Xu, H.-P., Zhang, X. and Guo, Y.-J. (2015). "Improved poly (vinyl butyral) hollow fiber membranes by embedding multi-walled carbon nanotube for the ultrafiltrations of bovine serum albumin and humic acid." *Chem. Eng. J.*, 260(90-98).
- Wang, Y., Zhu, J., Dong, G., Zhang, Y., Guo, N. and Liu, J. (2015). "Sulfonated halloysite nanotubes/polyethersulfone nanocomposite membrane for efficient dye purification." *Sep. Purif. Technol.*, 150, 243-251.
- Wang, Z., Wang, H., Liu, J. and Zhang, Y. (2014). "Preparation and antifouling property of polyethersulfone ultrafiltration hybrid membrane containing halloysite nanotubes grafted with MPC via RATRP method." *Desalination*, 344, 313-320.
- Wu, L., Sun, J., Lv, Z. and Chen, Y. (2016). "In-situ preparation of poly (ether imide)/amino functionalized silica mixed matrix membranes for application in enzyme separation." *Materials & Design*, 92(610-620).
- Wu, T., Mohammad, A. W., Jahim, J. M. and Anuar, N. (2007). "Palm oil mill effluent (POME) treatment and bioresources recovery using ultrafiltration membrane: effect of pressure on membrane fouling." *Biochem. Eng. J.*, 35(3), 309-317.
- Xianchu, L., Xiuyun, C., Aiping, W. and Feiyu, K. (2006). "Microstructure and Photocatalytic Decomposition of Methylene Blue by TiO₂-Mounted Halloysite, a Natural Tubular Mineral." *Acta Geologica Sinica (English Edition)*, 80(2), 278-284.
- Xu, J. and Xu, Z.-L. (2002). "Poly(vinyl chloride) (PVC) hollow fiber ultrafiltration membranes prepared from PVC/additives/solvent." *J. Membr. Sci.*, 208, 203-212.
- Xu, Z.-K., Shen, L.-Q., Yang, Q., Liu, F., Wang, S.-Y. and Xu, Y.-Y. (2003). "Ultrafiltration hollow fiber membranes from poly(ether imide): preparation, morphologies and properties." *J. Membr. Sci.*, 223, 105-118.

Yangali-Quintanilla, V. A., Holm, A. H., Birkner, M., Stoltze, H. W. C., Ulbricht, M. and Zheng, X. (2016). "A fast and reliable approach to benchmark low pressure hollow fibre filtration membranes for water purification." *J. Membr. Sci.*, 49(9), 515-525.

Yu, H., Zhang, Y., Sun, X., Liu, J. and Zhang, H. (2014). "Improving the antifouling property of polyethersulfone ultrafiltration membrane by incorporation of dextran grafted halloysite nanotubes." *Chem. Eng. J. (Lausanne)*, 237(322-328).

Yu, L., Wang, H., Zhang, Y., Zhang, B. and Liu, J. (2016). "Recent advances in halloysite nanotube derived composites for water treatment." *Environmental Science: Nano*,

Yuan, P., Southon, P. D., Liu, Z., Green, M. E., Hook, J. M., Antill, S. J. and Kepert, C. J. (2008). "Functionalization of halloysite clay nanotubes by grafting with γ -aminopropyltriethoxysilane." *J. Phys. Chem C*, 112(40), 15742-15751.

Zanetti, M., Lomakin, S. and Camino, G. (2000). "Polymer layered silicate nanocomposites." *Macromol. Mater. Eng.*, 279(1), 1-9.

Zeng, G., He, Y., Zhan, Y., Zhang, L., Shi, H. and Yu, Z. (2016). "Preparation of a novel poly(vinylidene fluoride) ultrafiltration membrane by incorporation of 3-aminopropyltriethoxysilane-grafted halloysite nanotubes for oil/water separation." *Ind. Eng. Chem. Res.*, 55(6), 1760-1767.

Zhang, G., Lu, S., Zhang, L., Meng, Q., Shen, C. and Zhang, J. (2013). "Novel polysulfone hybrid ultrafiltration membrane prepared with TiO_2 -g-HEMA and its antifouling characteristics." *J. Membr. Sci.*, 436, 163-173.

Zhang, J., Zhang, Y., Chen, Y., Du, L., Zhang, B., Zhang, H., Liu, J. and Wang, K. (2012). "Preparation and characterization of novel polyethersulfone hybrid ultrafiltration membranes bending with modified halloysite nanotubes loaded with silver nanoparticles." *Ind. Eng. Chem. Res.*, 51(7), 3081-309.

Zhao, S., Wang, Z., Wang, J. and Wang, S. (2014). "Poly (ether sulfone)/polyaniline nanocomposite membranes: effect of nanofiber size on membrane morphology and properties." *Ind. Eng. Chem. Res.*, 53(28), 11468-11477.

Zhao, S., Wang, Z., Wei, X., Zhao, B., Wang, J., Yang, S. and Wang, S. (2012). "Performance improvement of polysulfone ultrafiltration membrane using well-dispersed polyaniline–poly (vinylpyrrolidone) nanocomposite as the additive." *Ind. Eng. Chem. Res.*, 51(12), 4661-4672.

Zhao, W., He, C., Wang, H., Su, B., Sun, S. and Zhao, C. (2011). "Improved antifouling property of polyethersulfone hollow fiber membranes using additive of poly (ethylene glycol) methyl ether-b-poly (styrene) copolymers." *Ind. Eng. Chem. Res.*, 50(6), 3295-3303.

Zhao, Y., Abdullayev, E., Vasiliev, A. and Lvov, Y. (2013). "Halloysite nanotubule clay for efficient water purification." *J. Colloid Interface Sci.*, 406(121-129).

Zhao, Y., Xu, Z., Shan, M., Min, C., Zhou, B., Li, Y., Li, B., Liu, L. and Qian, X. (2013). "Effect of graphite oxide and multi-walled carbon nanotubes on the microstructure and performance of PVDF membranes." *Sep. Purif. Technol.*, 103 78-83.

Zhao, Y., Zhou, S., Li, M., Xue, A., Zhang, Y., Wang, J. and Xing, W. (2013). "Humic acid removal and easy-cleanability using temperature-responsive ZrO₂ tubular membranes grafted with poly (N-isopropylacrylamide) brush chains." *Water Res.*, 47(7), 2375-2386.

Zheng, Y., Yao, G., Cheng, Q., Yu, S., Liu, M. and Gao, C. (2013). "Positively charged thin-film composite hollow fiber nanofiltration membrane for the removal of cationic dyes through submerged filtration." *Desalination*, 32(8),42-50.

Zhu, J., Guo, N., Zhang, Y., Yu, L. and Liu, J. (2014). "Preparation and characterization of negatively charged PES nanofiltration membrane by blending with halloysite nanotubes grafted with poly (sodium 4-styrenesulfonate) via surface-initiated ATRP." *J. Membr. Sci.*, 465, 91-99.

Zhu, L.-J., Zhu, L.-P., Jiang, J.-H., Yi, Z., Zhao, Y.-F., Zhu, B.-K. and Xu, Y.-Y. (2014). "Hydrophilic and anti-fouling polyethersulfone ultrafiltration membranes with poly (2-hydroxyethyl methacrylate) grafted silica nanoparticles as additive." *J. Membr. Sci.*, 45(1), 157-168.

Zhu, W.-P., Sun, S.-P., Gao, J., Fu, F.-J. and Chung, T.-S. (2014). "Dual-layer polybenzimidazole/polyethersulfone (PBI/PES) nanofiltration (NF) hollow fiber membranes for heavy metals removal from wastewater." *J. Membr. Sci.*, 456(117-127).

Zinadini, S., Zinatizadeh, A. A., Rahimi, M., Vatanpour, V. and Zangeneh, H. (2014). "Preparation of a novel antifouling mixed matrix PES membrane by embedding graphene oxide nanoplates." *J. Membr. Sci.*, 453, 292-301.

Bio-data**Raghavendra Seetarama Hebbar**Email: rs.hebbar27@gmail.com

LIST OF PUBLICATIONS

1. R.S. Hebbar, A.M. Isloor, A. Ismail, "Preparation and evaluation of heavy metal rejection properties of polyetherimide/porous activated bentonite clay nanocomposite membrane", *RSC Adv.*, 4 (2014) 47240-47248. (*impact factor-3.28*)
2. R.S. Hebbar, A.M. Isloor, A. Ismail, "Preparation of antifouling polyetherimide/hydrolysed PIAM blend nanofiltration membranes for salt rejection applications", *RSC Adv.*, 4 (2014) 55773-55780. (*impact factor- 3.28*)
3. R.S. Hebbar, A.M. Isloor, A. Ismail, S.J. Shilton, A. Obaid, H.-K. Fun, "Probing the morphology and anti-organic fouling behaviour of a polyetherimide membrane modified with hydrophilic organic acids as additives", *New J. Chem.*, 39 (2015), 6141-6150. (*impact factor- 3.27*)
4. R.S. Hebbar, A.M. Isloor, A. Ismail, K. Ananda, "Fabrication of antifouling, antimicrobial, well dispersed polydopamine functionalized halloysite nanotube-polyetherimide mixed matrix membranes for the heavy metal removal application", *J. Mater. Chem. A*, 2016, 4, 764-774 (*impact factor-8.26*)
5. R.S. Hebbar, Arun M Isloor, A.K. Zulhairun, Mohd. Sohaimi Abdullah and A.F. Ismail, "Efficient treatment of hazardous reactive dye effluents through antifouling polyetherimide hollow fiber membrane embedded with functionalized halloysite nanotubes" *Journal of Taiwan Institute of Chemical Engineers*. 2017, 72, 244–252 (*impact factor-2.8*)
6. R.S. Hebbar, Arun M Isloor and A.F. Ismail, "Fabrication of novel hollow fiber membrane decorated with functionalized Fe₂O₃ nanoparticles: Towards sustainable water treatment and biofouling control" *New J. Chem.*, 2017, 41, 4197-4211 (*impact factor-3.27*)
7. Raghavendra S. Hebbar, Arun M. Isloor, Inamuddin, and Abdullah M. Asiri "Carbon nanotube and graphene based advanced membrane materials for desalination" *Environ. Chem. Lett.*, 2017, accepted, (*impact factor-3.59*)

8. R.S. Hebbar, A.M. Isloor, A. Ismail, "High flux, anti-irreversible fouling, polyetherimide based ultrafiltration membrane by novel derivative of polyvinyl pyrrolidone as performance modifier." Communicated (April 2017) to *Ind. Eng. Chem. Res.*,
9. Raghavendra S. Hebbar, Arun M Isloor, A.K. Zulhairun, Mohd. Sohaimi Abdullah and A.F. Ismail, "Fabrication of amine functionalized halloysite nanotubes immobilized into Polyetherimide membrane for the efficient removal of hazardous dyes from wastewater and its mechanism" communicated (April 2017) to *Sep. Purif. Technol.*,
10. Raghavendra S. Hebbar, Arun M Isloor and A.F. Ismail, "Functionalisation of polyetherimide membrane with Bentonite clay grafted with poly (4-styrenesulfonate) brushes as effective removal of hazardous humic acid and heavy metal ions" communicated (May 2017) *J. Mem. Sci.*

LIST OF BOOK CHAPTERS

1. R.S. Hebbar, A.M. Isloor, A. Ismail, "Contact Angle Measurements." **Elsevier** publication, DOI- 10.1016/B978-0-444-63776-5.00012-7
2. R.S. Hebbar, A.M. Isloor, Abdul Wahab, "Functional Cellulose and chitosan based materials for membrane applications." **Accepted by Springer on May 2017.**
3. R.S. Hebbar and A.M. Isloor "Desalination by Forward osmosis" manuscript under preparation

LIST OF CONFERENCES ATTENDED

1. R.S. Hebbar, A.M. Isloor, "Preparation and evaluation of heavy metal ion rejection properties of polyetherimide/activated bentonite clay nanocomposite membrane", 13th Eurasia Conference on Chemical Sciences (EuAsC2S-13) Indian Institute of Science, Bangalore, India from Dec 14-18th, 2014.
2. R.S. Hebbar, A.M. Isloor, A.F. Ismail, "Effect of organic acid additive on the morphology and antiorganic fouling behaviour of the polyetherimide membrane", 10th Mid-year CRSI Symposium in chemistry, National institute of technology Trichy, July 23-25, 2015.

3. R.S. Hebbar, A.M. Isloor, "Probing the effect of immobilized Activated Bentonite Clay on Polyetherimide Membrane Matrix for heavy metal ion rejection", International Conference on Membrane based separations (MEMSEP 2015), The Maharaja Sayajirao University of Baroda, Gujrath, 21-23 March 2015.
4. R.S. Hebbar, A.M. Isloor, "Fabrication and characterisation of activated bentonite clay incorporated polyetherimide mixed matrix membrane for heavy metal ions removal application." National seminar on recent advances in chemical sciences (RACS-15), ST Agnes College (Autonomous), Mangalore, Dec 17-18, 2015, page 26.
5. R.S. Hebbar, B. Garudachari, A.M. Isloor, "Preparation, characterisation and performance studies of polyetherimide ultrafiltration membrane modified by novel hydrophilic derivative of polyvinyl pyrrolidone." International conferences on advances in chemical engineering (ICACE-2015), NITK surathkal, Mangalore, Dec 20-22, 2015, page, 99.
6. R.S. Hebbar, A.M. Isloor, "Preparation and characterisation of well dispersed polydopamine modified halloysite nanotube immobilized polyetherimide membrane for heavy metal ion rejection" An international conference on recent advancements in materials and chemical sciences-2016, Bhundelkhand University Jhansi, March 2-5, 2016, **(Best paper award)**
7. R.S. Hebbar, A.M. Isloor, "Fabrication of antifouling, antimicrobial, well dispersed polydopamine functionalized halloysite nanotube-polyetherimide mixed matrix membranes wastewater treatment." An international conference on applied polymer science and technology (APST-2016), VIT University, Vellore, October 24-26, 2016.

Educational Qualification

1. M. Sc. Chemistry, National Institute of Technology, Surathkal, 8.24 (CGPA) (2012)
2. B.Sc Chemistry, Sahyadri Science College (Autonomous), Shimoga, 83.2% (2010)

Additional Qualification and achievements

1. Visited Advanced Membrane Technology Research Center (AMTEC), Universiti Teknologi Malaysia, Malaysia to carry out a part of research work.
2. Conducted labs for B. Tech and M.Sc students for more than three years of Ph. D. tenure.
3. Handled instruments such as FTIR spectrophotometer, UV-visible spectrophotometer, contact angle analyzer and Surpas Zeta potential analyzer.
4. Worked as a research associate in the area of Synthetic Organic Chemistry at Apotex Pharamchem India PVT. Ltd, Bangalore, India, from June 2012 to July 2013.

Personal details

Address for correspondence	C/o shreedhar Hebbar Mudkere, Marukeri (Po), Bhatkal (Ta) Karnataka -
Email/Contact number	rs.hebbar27@gmail.com 07259465974
Date of birth	27/04/1989
Sex	Male
Nationality	Indian
Languages known	Kannada, English, Hindi, Telugu
References Dr. Arun M. Isloor Associate Professor Dept. of Chemistry, NITK-Surathkal, Mangalore Phone no: +91-9448523990 Email: isloor@yahoo.com	Prof. Dr. Ahmad Fauzi Ismail Director Advanced membrane research centre (AMTEC) Universiti Teknologi Malaysia- 81310 Tel: +60197775545 /+6075535807 Email: afauzi@utm.my